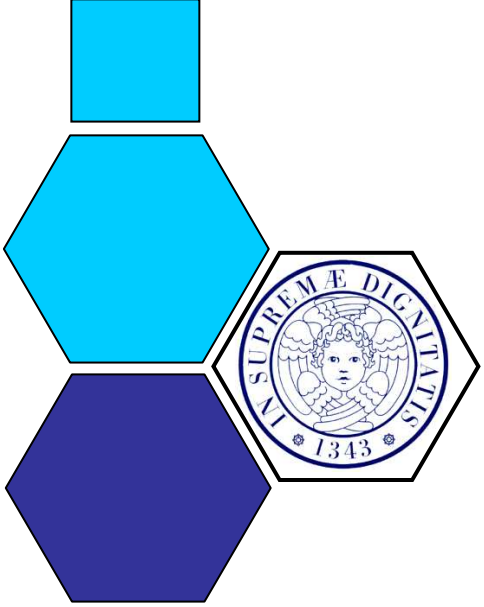

University of Pisa

Ph.D. course of
Mechanical Engineering

Mechanical aspects of the analysis of the Divertor of the ITER machine

Scientific sector: ING-IND/14

Author:
Elio D'Agata

Tutors:
Prof. Ing. L. Bertini (DIMNP, Pisa)

Ing. G. Sannazzaro (ITER, Garching)

III "Ciclo"

Years 2007

1. Introduction

ITER, in the past was the acronimous of International Thermonuclear Experimental Reactor and now means from the Latin "the way" to find a solution for the production of energy in the world. ITER is a tokamak (**TO**roidalnaja **KA**mera **MA**gnitnaja **Ka**tushka, it is a Russian acronimous that means toroidal chamber magnetic coil), a magnetic confinement fusion experimental reactor, planned to be built in France and designed to show the scientific and technological feasibility of a full-scale fusion power reactor.

In ITER and many other so-called magnetic confinement reactors, the plasma, a gas of charged particles, is confined via magnetic fields. A charged particle, when crossing a magnetic field, does not escape if left unperturbed. It simply spins around the magnetic field, in Larmor gyrorotation. The particle may move along the magnetic field unopposed by the field, but if the field is wrapped into a toroidal or doughnut shape, it is then confined.

The 2001 design fulfilled the overall programmatic objective of ITER i.e. to demonstrate the scientific and technological feasibility of fusion energy for peaceful purpose. ITER would achieve this by demonstrating an amplification energy factor of 10 and extended burn of deuterium-tritium plasma, by demonstrating technologies essential to a reactor in an integrated system and by performing integrating testing of high heat flux components under a nuclear environment. It is to be added that ITER is still an experiment and a lot of things will be tested, discovered and proved within the ITER project. One of the ITER components that will be subjected to intensive studies, testing and development is the divertor. The main function of the divertor system is to exhaust the major part of the alpha particle power as well as helium and impurities from the plasma. As the main interface component under normal operation between the plasma and material surfaces, it must tolerate high heat and electro magnetics load while at the same time providing neutron shielding for the vacuum vessel and magnet coils in the vicinity of the divertor.

The research activity of this Ph.D. has been focalized mainly on two topics that represent "the pillars" of the entire work.

The first topic concerns the methodology and a possible approach to the problem of set up the acceptance criteria for the tiles of CFC (Carbon Fibre Composite) of the divertor at the start of life of the ITER machine. In the ITER divertor design there are ~$5x10^4$ CFC to Cu alloy-tube monoblock joints of pure Cu subjected to high heat flux. An extensive Non-Destructive Examination (NDE) of the joints will be carried out, but this NDE is complicated by the geometry, by the nature of the materials and the processes used in manufacture. Hence, a few defects are likely to escape detection and be installed in the divertor. A thermographic method (SATIR) [11], [12] has been suggested to investigate the Cu-CFC joint quality. A study on the reliability and the applicability of this method as well as a possible statistical approach to the definition of the acceptance criteria are addressed in this thesis.

The second topic is the developing of a user-friendly software, inside a commercial, certificated and very well documented finite element code like ANSYS, able to evaluate the evolution of the erosion in the CFC tiles of the divertor. The divertor is one of the most challenging components of the ITER machine. It consists essentially of two parts: the plasma-facing components (PFCs) and a massive support structure called the cassette body (CB). The PFCs are actively-cooled thermal shields that can sustain the heat and

particle fluxes during normal and transient operations as well as during disruption events. The evaluation of the speed of erosion of the CFC (Carbon Fibre Composite) tiles is very important to evaluate the longevity of those components. The erosion of carbon exposed to a flux of particles is a very complex process and the code considers 3 different kinds of erosion (the word “erosion” here is used generically to indicate a loss of material from a carbon surface). The first is the sublimation of the carbon at high temperature and low pressure. The second is the physical erosion. When particles hit a carbon tile surface, they remove a certain amount of material. The third is chemical erosion. Hydrogen has a strong chemical affinity for carbon, and when hydrogen atoms (or isotopes of hydrogen) strike carbon atoms they can trigger a chemical reaction to form clusters of C_xH_x that are released from the surface.

2. General aspect of the ITER fusion reactor

ITER is an international tokamak (magnetic confinement fusion) experiment, planned to be built in France and designed to show the scientific and technological feasibility of a full-scale fusion power reactor. It builds upon research conducted on devices such as TFTR, JET, JT-60, and T-15, and will be considerably larger than any of them. The program is anticipated to last for 30 years (10 years for construction, and 20 years of operation) and cost approximately €10 billion. After many years of deliberation, the participants announced in June, 2005 that ITER will be built in Cadarache, France. Currently there are seven national and supranational parties participating in the ITER program: China, Europe, India, Japan, South Korea, Russia, and USA.

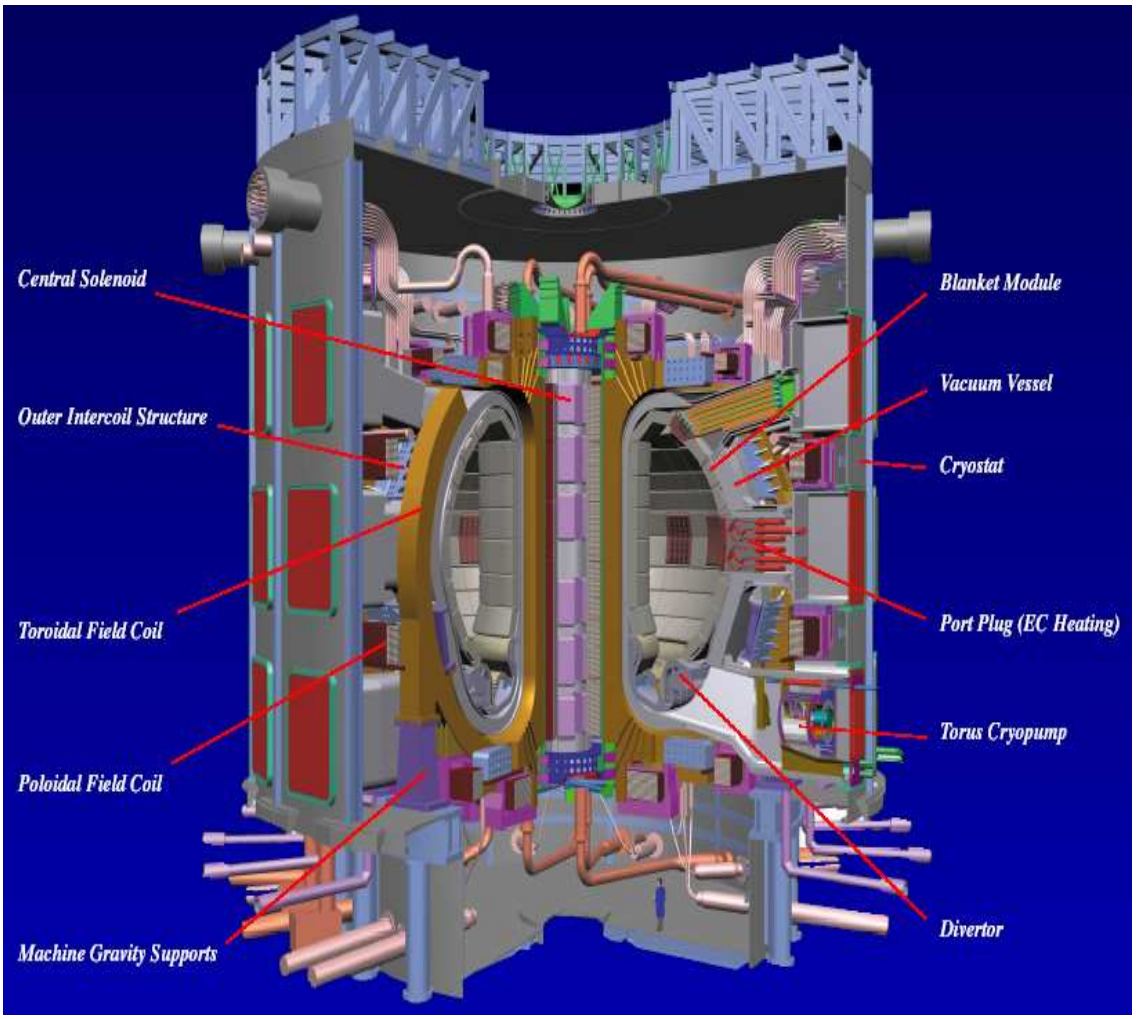

Fig. 2.1. The ITER machine.

ITER is designed to produce approximately 500 MW of fusion power sustained for up to 500 seconds (compared to JET's peak of 16 MW for less than a second). ITER will not generate electrical power for a public grid.

ITER is intended to be an experimental step between today's studies of plasma physics and future electricity-producing fusion power plants. It is technically ready to start construction and the first plasma operation is expected in 2016.

2.1 Objectives

ITER has a number of specific objectives, all concerned with developing a viable fusion power reactor:
1) To produce momentarily ten times more thermal energy from fusion heating than is supplied by auxiliary heating (a Q value of 10).
2) To produce a steady-state plasma with a Q value of greater than 5.
3) To maintain a fusion pulse for up to eight minutes.
4) To develop technologies and processes needed for a fusion power plant, including superconducting magnets (pioneered on the Russian T-15) and remote handling (maintenance by robot).
5) To verify tritium breeding concepts.

2.2 Reactor overview

When deuterium and tritium fuse, two nuclei come together to form a helium nucleus (an alpha particle), and a high energy neutron.

$$^{2}_{1}\mathrm{H} + ^{3}_{1}\mathrm{H} \rightarrow ^{4}_{2}\mathrm{He} + ^{1}_{0}\mathrm{n} + 17.6\ \mathrm{MeV}$$

While in fact nearly all stable isotopes lower on the periodic table than iron will fuse with some other isotope and release energy, deuterium and tritium are by far the most attractive for energy generation as they require the lowest temperatures to join and produce energy.
All proto and mid-life stars release and radiate enormous quantities of energy via fusion processes. In terms of fuel efficiency, the deuterium tritium process releases roughly three times as much energy as a uranium 235 fission event, and millions of times more energy than a chemical reaction such as the burning of coal. It is the goal of a fusion power plant to cause enough fusion events to release enough energy to be an economical source of electricity.
The activation energy for fusion is so high because the protons in each nucleus will tend to strongly repel one another, as they each have the same positive charge. A heuristic for estimating reaction rates is that nuclei must be able to get within 1 femtometer (1×10^{-15} meter) of each other, where the nuclei are increasingly likely to undergo quantum tunneling past the electrostatic barrier and the turning point where Strong nuclear force and the electrostatic force are equally balanced, allowing them to fuse. In ITER, this distance of approach is made possible by high temperatures. High temperatures give the nuclei enough energy to overcome their electrostatic repulsion. For deuterium and tritium, the optimal reaction rates occur at temperatures on the order of 100,000,000 K. The plasma is heated to a high temperature by ohmic heating (running a current through

the plasma). Additional heating is applied using neutral beams (which cross magnetic field lines without a net deflection and will not cause a large electromagnetic disruption) and radio-frequency (RF) or microwave heating.

In ITER and many other so-called magnetic confinement reactors, the plasma, a gas of charged particles, is confined via magnetic fields. A charged particle, when crossing a magnetic field, does not escape if left unperturbed. It simply spins around the magnetic field, in Larmor gyrorotation. The particle may move along the magnetic field unopposed by the field, but if the field is wrapped into a toroidal or doughnut shape, it is then confined.

A solid confinement vessel is also needed, both to shield the magnets and other equipment from high temperatures and energetic photons and particles, and to maintain a near-vacuum for the plasma to populate. The containment vessel is subjected to an extraordinarily hostile environment, where electrons, ions, photons, alpha particles, and neutrons constantly bombard the surface and degrade the structure. The material must be designed to stand-up to this environment for long enough so that an entire powerplant would be economical. Tests of such materials will be done by ITER.

Once fusion has begun, high energy neutrons will radiate from the reactive regions of the plasma, crossing magnetic field lines easily due to charge neutrality. Since it is the neutrons that receive the majority of the energy, they will be ITER's primary source of energy output. Ideally, alpha particles will expend their energy in the plasma, further heating it.

Beyond the inner wall of the containment vessel one of several test blanket modules are to be placed. These modules are designed to slow and absorb neutrons in a reliable and efficient manner, limiting damage to the rest of the structure, and breeding tritium from lithium and the incoming neutrons for fuel. Energy absorbed from the fast neutrons is extracted and passed onto the primary coolant. This energy would then be used to power an electricity generating turbine in a real power plant, however in ITER this is not of scientific interest, and will simply be released.

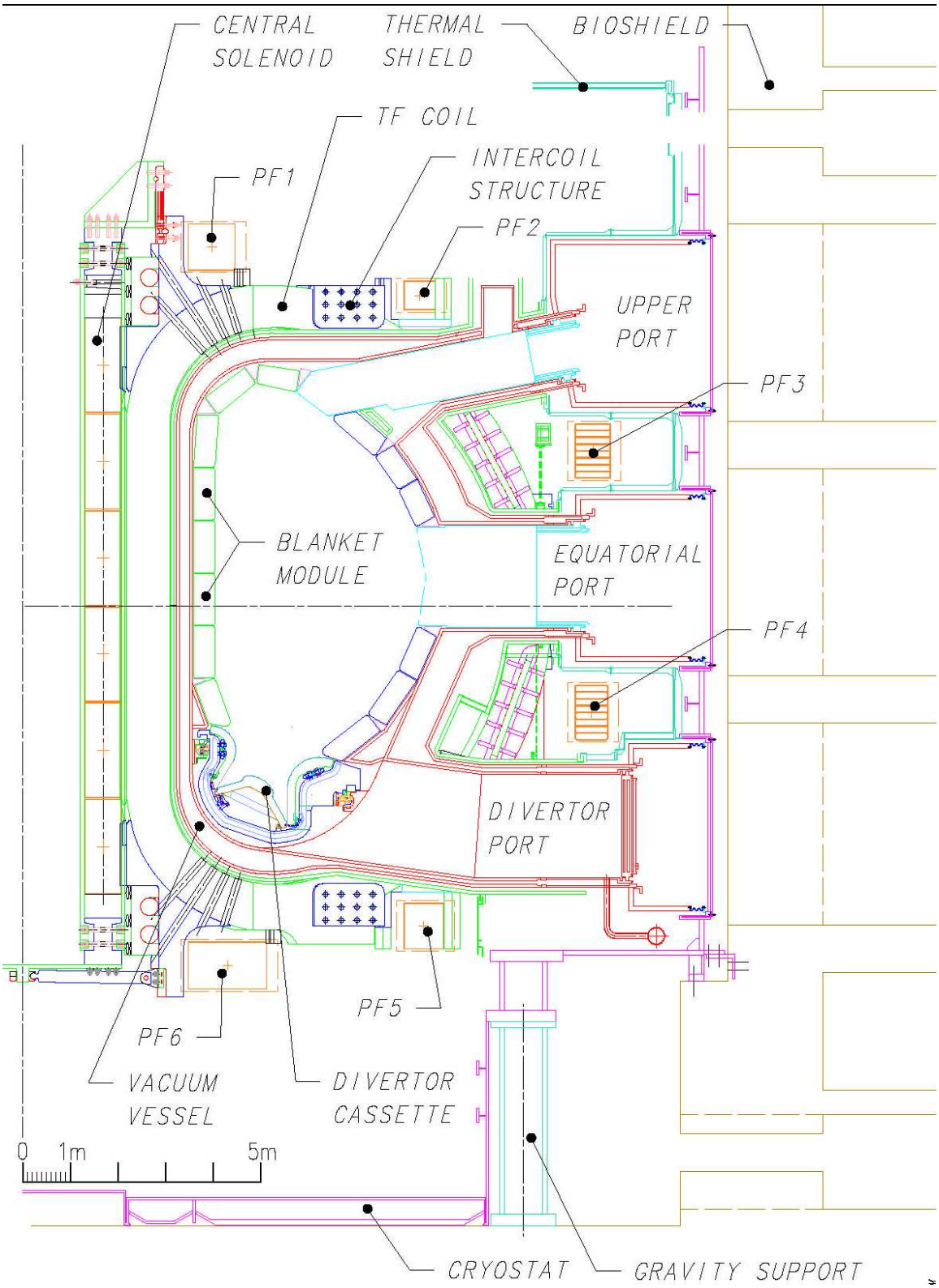

Fig. 2.2.1 ITER cross-section

Below is shown a table with the main plasma parameters and dimension.

Total Fusion Power 500 MW *(700 MW)*
Q — fusion power/additional heating power ≥ 10
Average 14MeV neutron wall loading 0.57 MW/m^2 *(0.8 MW/m^2)*
Plasma inductive burn time ≥ 400 s
Plasma major radius (R) 6.2 m
Plasma minor radius (a) 2.0 m
Plasma current (I_p) 15 MA *(17 MA [(1)])*
Vertical elongation @95% flux surface/separatrix (κ_{95}) 1.70/1.85
Triangularity @95% flux surface/separatrix (δ_{95}) 0.33/0.49
Safety factor @95% flux surface (q_{95}) 3.0
Toroidal field @6.2 m radius (B_T) 5.3 T
Plasma volume 837 m^3
Plasma surface 678 m^2
Installed auxiliary heating/current drive power 73 MW [(2)]

Table 2.2.1 Main plasma parameters and dimension

(1) The machine is capable of a plasma current up to 17 MA, with the parameters shown in parentheses) within some limitations over some other parameters (e.g., pulse length).
(2) A total plasma heating power up to 110 MW may be installed in subsequent operation phases.

From an engineer point of view, ITER is done of several main systems. Below is reported a short description of the main systems:

1) Magnets

The plasma is confined and shaped by a combination of magnetic fields from five origins: 18 toroidal field coils (TFC), 6 poloidal field coils (PFC), the central solenoid (CS), the correction coils and plasma currents. The nested magnetic surfaces are able to confine a plasma pressure equivalent to a few atmospheres, with a density 10^6 times smaller than in the atmosphere (n = $10^{20}/m^3$, T ≈ 10 keV). Aiming in ITER at steady-state operation, all the coils are superconducting: copper coils would require too large an electric power to be acceptable for ITER as well as for a future reactor.

2) Vacuum vessel

The vacuum vessel is a component with multiple functions, namely it:

- provides a boundary consistent with the generation and maintenance of a high quality vacuum, necessary for limiting impurity influx into the plasma;
- supports the in-vessel components and their resultant mechanical loads;
- participates in shielding against neutrons, and in removing the corresponding power during a pulse, and moreover in removing the decay heat of all in-vessel components in case of there being no other coolant available;
- provides a continuous conductive shell for plasma MagnetoHydroDynamic stabilisation with a toroidal one turn resistance of ~8μΩ;
- provides all access to the plasma through ports, for diagnostics, heating systems, pumping, water piping, etc.;
- provides the first confinement barrier for tritium and activated dust with a very high reliability.

All these functions are central to the operation of ITER and thus require a very robust mechanical design analyses for stresses in all possible normal and off-normal conditions. The vessel is built with two shells linked by ribs and fitted with nuclear radiation

shielding material, and ferromagnetic inserts in the shadow of the TF coils to reduce the TF ripple value.

3) Blanket

The basic function of the blanket system is to provide the main thermal and nuclear shielding to the vessel and external machine components. The design allows for the conversion of the outboard region from a shielding blanket to a breeding blanket for the tritium production in a later stage of operation.

The basic concept of the blanket system is a modular configuration with a mechanical attachment system. The blanket modules (BMs) are attached to the vacuum vessel (VV).

The ITER blanket module design is aimed of minimising, (a) the cost, (b) the radioactive waste, and (c) electromagnetic (EM) loads due to disruptions/VDEs (vertical displacement events). The module configuration consists of a shield block supporting four separable first wall (FW) panels.

4) Divertor

A more detailed description of the divertor, object of this work, will be done in the next chapter.

5) Additional heating and current drive

A combination of radio-frequency at the ion cyclotron (IC), electron cyclotron (EC), and lower hybrid (LH) mode resonant frequencies of plasma charged particles, and 1 MeV negative ions, are used for plasma heating and currrent drive. Each has their particular merits. The best mix of heating systems will therefore have to be worked out during ITER operation. The initial setup will involve two neutral beams and electron and ion cyclotron systems, but the radio-frequency systems are designed in exchangeable modular units (20 MW/port) to allow various mixes to be tried, and three neutral beams can be accommodated on the machine. A heating power in excess of 110 MW is thus attainable.

6) Diagnostic system

Plasma and first wall diagnostic systems are installed at various locations in ITER. The components of these systems are integrated within the ITER vacuum vessel, in in-vessel components, vacuum vessel ports and port interspaces, and outside the vacuum in the biological shield, in the tokamak pit access cells, transport galleries, and dedicated diagnostic area at all levels.

Plasma diagnostics fall into three categories:

- those necessary for machine protection or basic control;
- those needed for advanced performance control;
- those desirable for physics studies.

They are further segregated into a startup set, and those that can be added later for Deuterium Tritium (DT) operation.

7) Vacuum pumping & fuelling

The Vacuum Pumping System provides for the vacuum pumping of all primary vacuum systems of the torus and cryostat during all phases of operation and the leak testing of all systems and components that form the primary vacuum and cryostat boundaries.

The primary functions of the ITER fuelling systems are:

- to inject DT fuel and other impurity gases into the vacuum vessel at the required fuelling rate and response time to maintain fusion power at the required level;

- to inject tritium rich or other hydrogenic pellets into the vacuum vessel at the required fuelling rate and response time using a centrifuge type pellet injector;
- to inject impurity gas(es) using puffing valves and impurity solid pellet(s) using a mechanical type injector into the vacuum vessel for machine protection;

8) Cryostat and thermal shield

The main functions of the ITER cryostat are to provide the vacuum insulation environment for the operation of the superconducting coils and to provide the second boundary for the confinement of the radioactive inventory inside the ITER vacuum vessel (VV). The thermal shields comprise the vacuum vessel thermal shield (VVTS), which interposes between the VV and the cold magnet structures, the cryostat thermal shield (CTS), which is mounted alongside the walls of the cryostat (bottom, cylinder and upper head), thereby preventing direct line of sight from the room temperature cryostat walls to the cold structures, the transition thermal shields (TTS) that enclose the port connecting ducts and service lines that are routed between the cryostat walls and the VV, and the support thermal shields (STS) that enwrap the VV gravity supports and machine gravity supports. The STS thermal anchors in the VV and machine supports limit the heat load to cold structures due to conduction through the support structures.

3. The divertor of the ITER machine

3.1 General description

The divertor is one of the most challenging components of the ITER machine being an experimental component of an experimental machine. The main function of the divertor system is to exhaust the major part of the alpha particle power as well as helium and impurities from the plasma. As the main interface component under normal operation between the plasma and material surfaces, it must tolerate high heat and electro magnetics load while at the same time providing neutron shielding for the vacuum vessel and magnet coils in the vicinity of the divertor.
Given the uncertainties in the plasma physics extrapolation, and thus the component durability, the design provides a system for rapid replacement and refurbishment. A remote maintenance concept has been developed, which promises to allow the exchange of a complete divertor system to be performed in ~ 6 months.
The geometry of the divertor is based on simulations obtained using the B2-EIRENE [47] Monte Carlo code and by extrapolation from results from tokamak experiments [1]. The reference configuration for the ITER divertor is a vertical target/baffle with an open private flux region and a dome below the X-point (Fig. 3.1.1, 3.1.2 and 3.1.3). The divertor is segmented into 54 parts or cassettes. Each divertor cassette comprises a cassette body (see fig 3.1.3), which supports the Plasma Facing Components (PFCs), and an inner and outer vertical target (VT) and a private region PFC. Each inner and outer vertical target is split into two toroidal halves, while the private region PFC is a single unit. The vertical target is inclined so as to intercept the magnetic field lines of the separatrix at an acute angle, giving deep inboard and outboard channels in which to establish a partially detached plasma regime. In this regime, while the plasma remains attached in the outer region of the scrape-off layer (SOL), the plasma is detached from the PFCs in the region near the separatrix causing the power profile to broaden and power to be radiated to other surfaces.

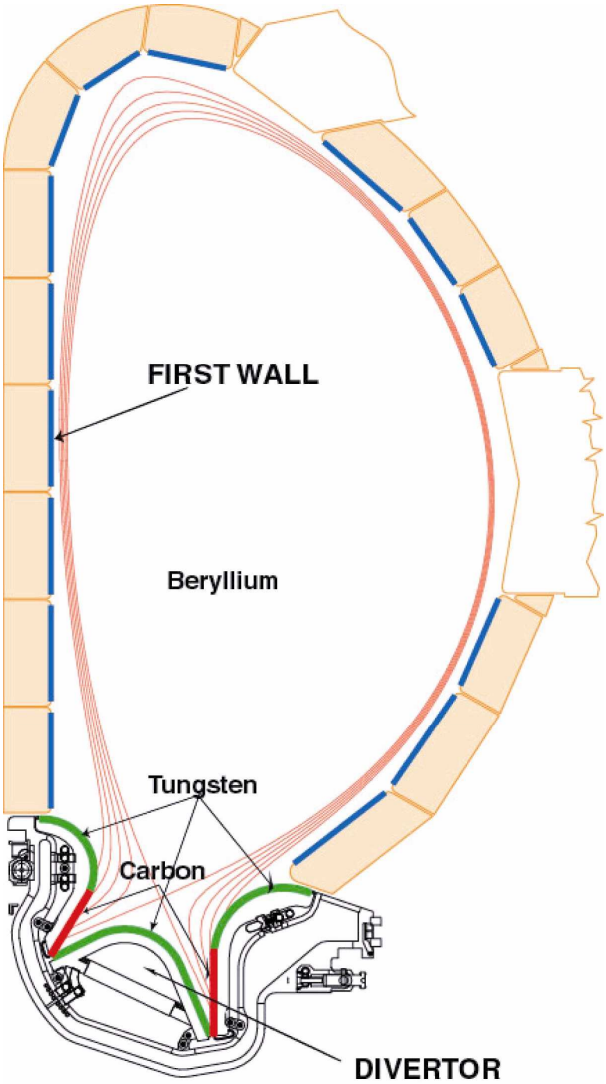

Fig. 3.1.1 The material used in the divertor.

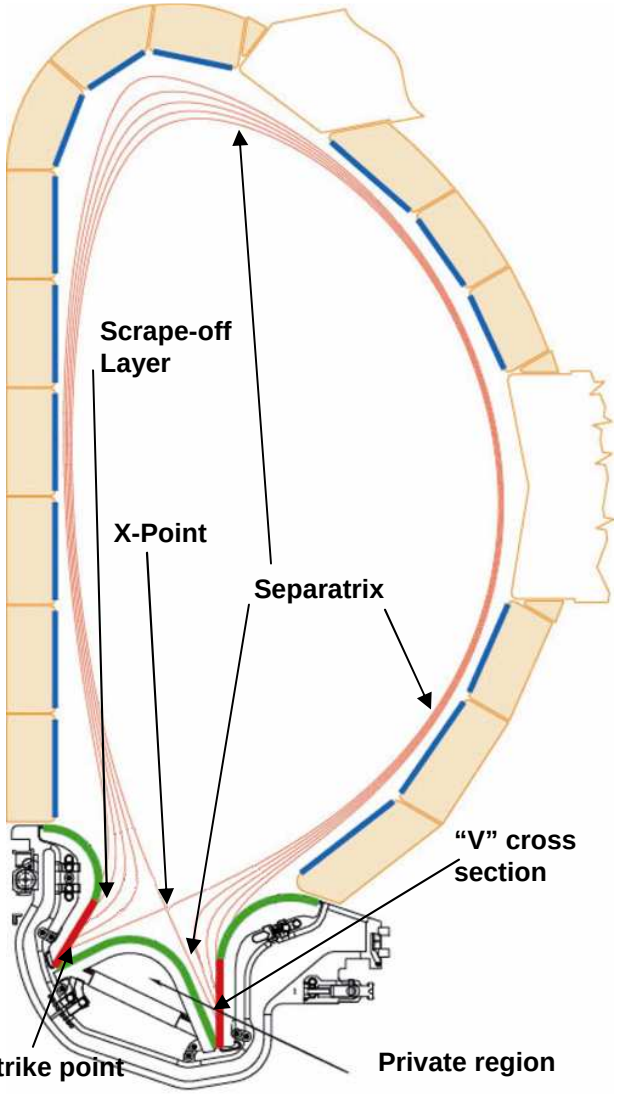

Fig. 3.1.2 The regions defined by divertor

Together with the lower end of each vertical target, a neutral particle reflector plate forms a "V" cross-section that confines neutral hydrogenic particles in the divertor channels and aids partial plasma detachment. According to code simulations [9] partial plasma detachment will occur and a maximum incident heat flux on the vertical targets of < 10 MWm^{-2} is to be expected. For steady-state scenarios up to 136 MW of thermal power is delivered via the SOL to the targets.

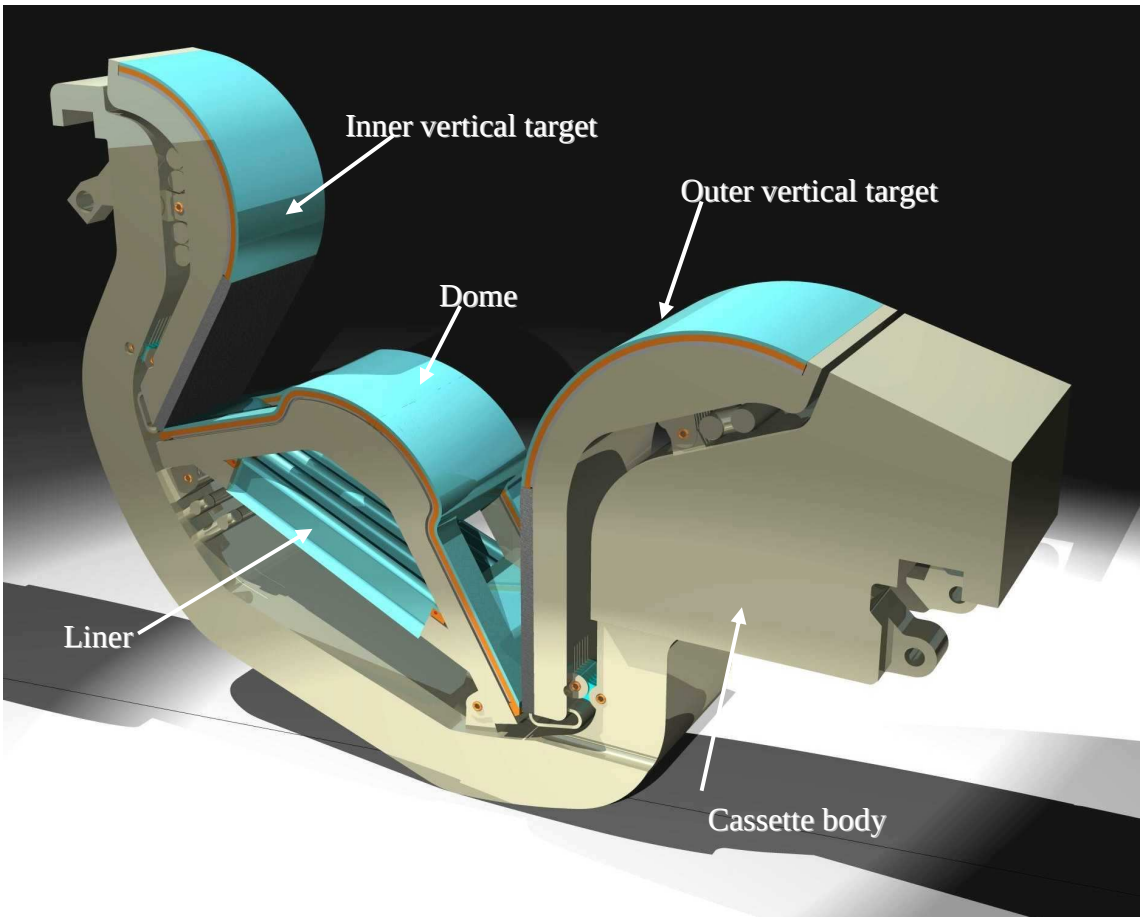

Fig. 3.1.3 The components of the divertor of the ITER machine

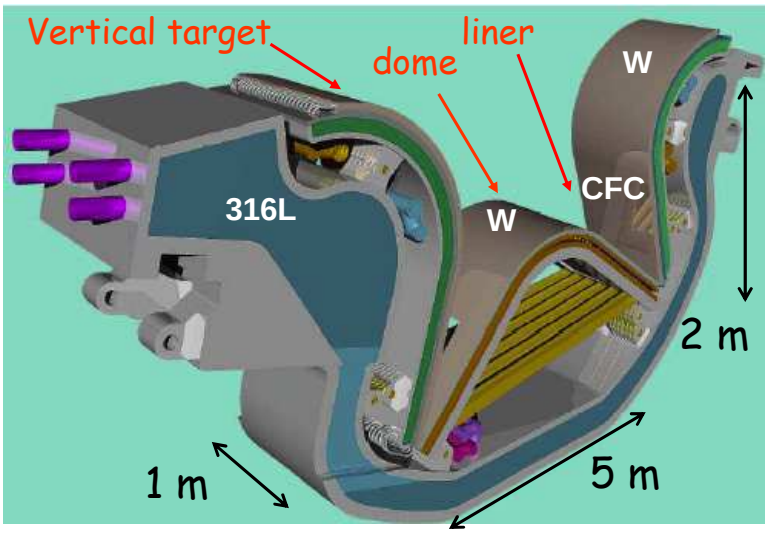

Fig. 3.1.4 The main materials and dimension of the ITER divertor.

The final configuration of the divertor is showed below:

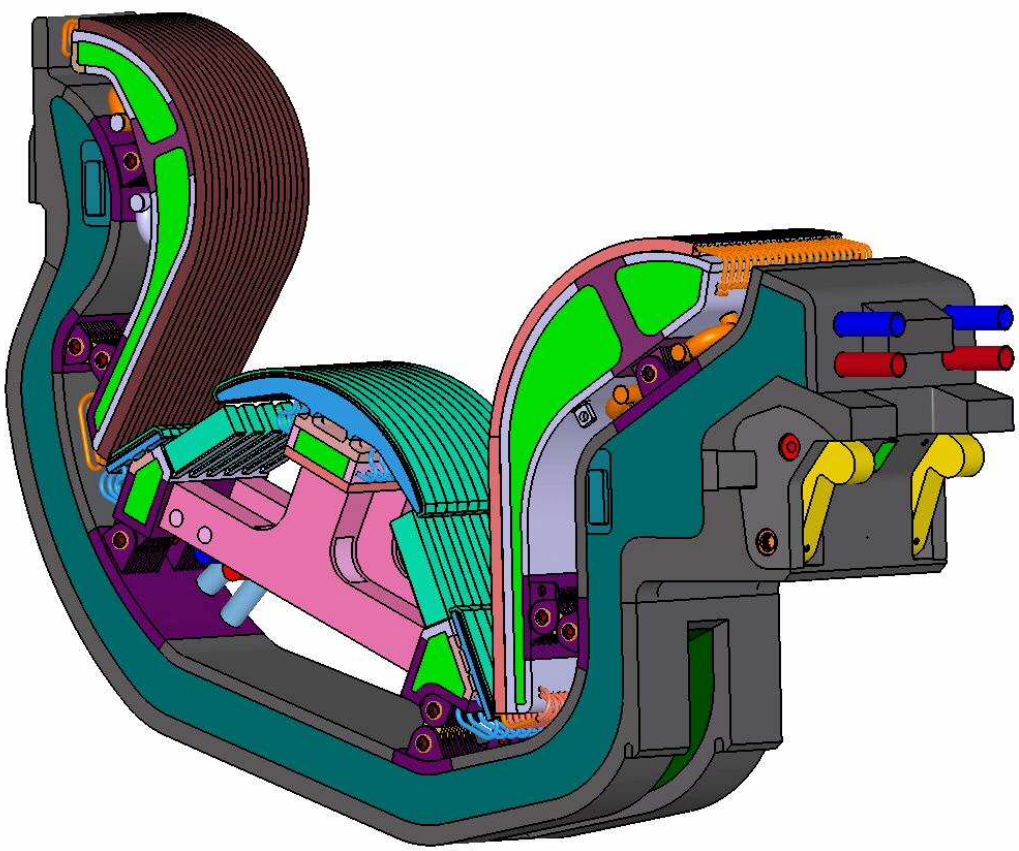

Fig. 3.1.5 The final configuration of the divertor of the ITER machine

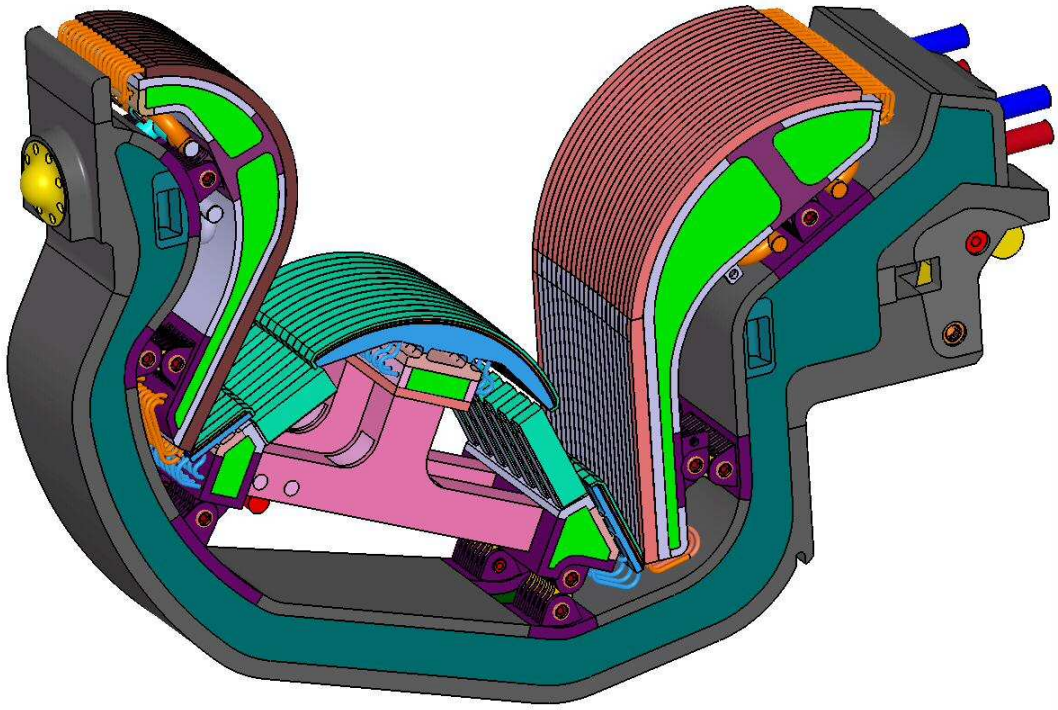

Fig.3.1.6 The final configuration of the divertor of the ITER machine

3.2 The cassette body

The cassette body that supports the Plasma Facing Components (PFCs) is designed to withstand the electromagnetic forces, provide shielding for the vacuum vessel and coils, and incorporates internal coolant channels, which cool the cassette body and act as manifolds for the PFC coolant. Each cassette body is fabricated from 316LN-IG (Low Nitrogen – ITER Grade) stainless steel and is 3.5 m long, ~ 2 m high and 0.4 to 0.8 m wide, and weighs ~ 5.7 tonnes. The thickness of the cassette body is 240mm, which allows the divertor channel depths to be maximized and is the minimum compatible with fulfilling all the above functions (see fig. 3.2.1). The minimum thickness of 240 mm includes a 40mm front plate, a 60mm back plate and these together with the connecting side plates and internal structure represent 65% of the cassette volume.

Although the 35% water volume is above the optimum range of 10 –30% for shielding the coils and VV, the helium generation in the VV field joint is less than the 1appm limit specified for the end-of-life of the machine. The VV, cassette and divertor PFCs combine to provide sufficient nuclear shielding of the Toroidal Field Coils (TFC). The local power density on the TFC system is one order of magnitude less than the limit (the limit being 1 $mWcm^{-3}$ in the conductor and 2 mWm^{-3} in the casing). The integrated nuclear heating of the lower TFCs is <1 kW, which compares favourably with the 17 kW allowed for the TFC system as a whole.

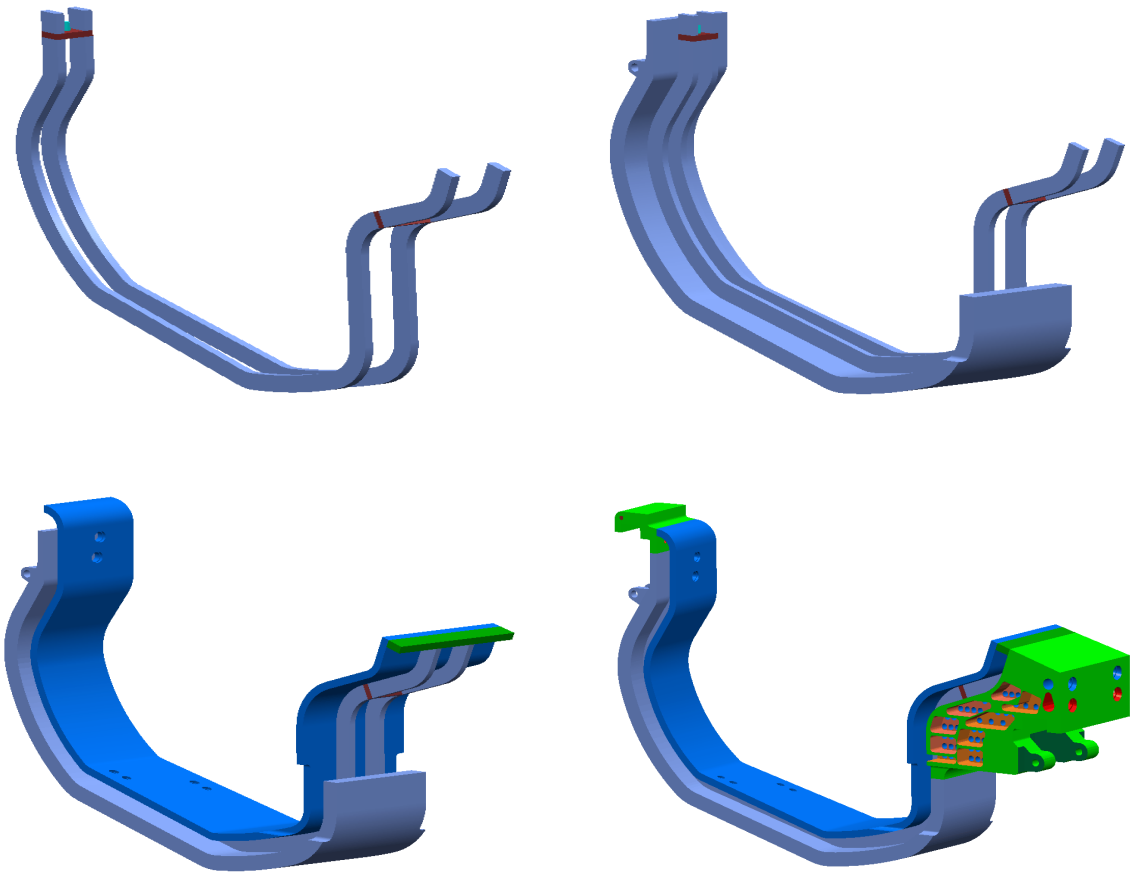

Fig. 3.2.1. Internal structure of the cassette body

Within the cassette structure there are coolant channels that run the full length of the cassette from outboard to inboard, and these channels act as manifolds for supplying water to the PFCs. In order to minimise distortion of the cassette (warping) the coolant channels are arranged symmetrically about the toroidal mid plane (see fig. 3.2.2).
The cassette is attached to the toroidal support rails (see fig. 3.2.3) that are integrated into the VV. The inboard support allows rotation in all directions and the outboard support allows rotation around the toroidal axis only, while toroidal and poloidal translation is blocked by the supports, and radial displacements are resisted by the spring effect of the cassette pressing against the vessel.
The supports have no locking mechanism and instead the cassette is pre-loaded against the inner and outer walls of the VV the cassette acting as a spring to maintain contact with the vessel walls. The pre-load is 30t and deflects the cassette body by 15mm an amount sufficient to ensure contact with the inner rail is maintained under the worst loading conditions. All the cassettes are a similar shape with the exception of those incorporating the in-vessel viewing probes (diagnostic components), which are modified in the upper outboard region of the cassette to allow insertion of the probe into the main chamber.

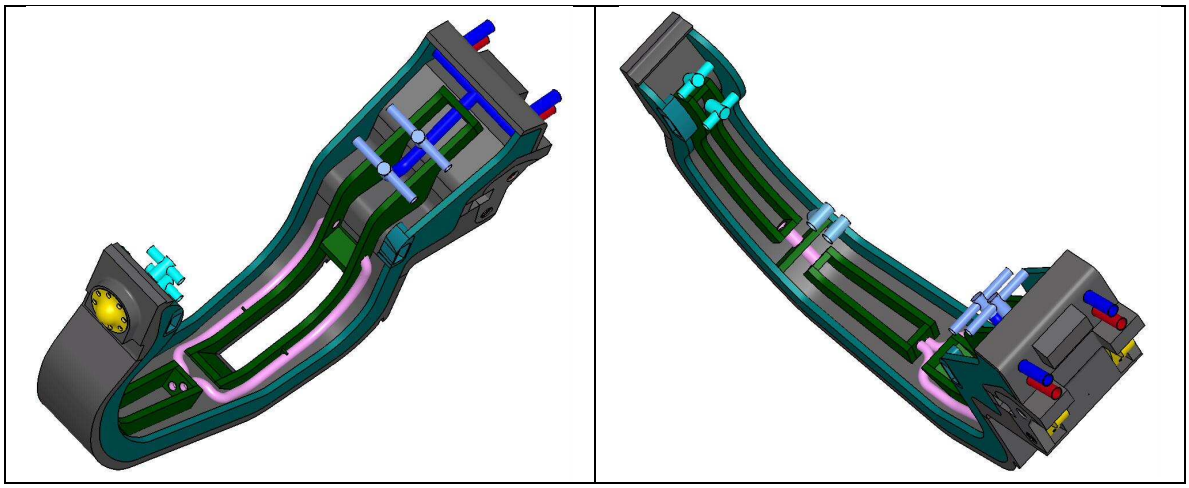

Fig. 3.2.2. Internal cooling channel inside the cassette body.

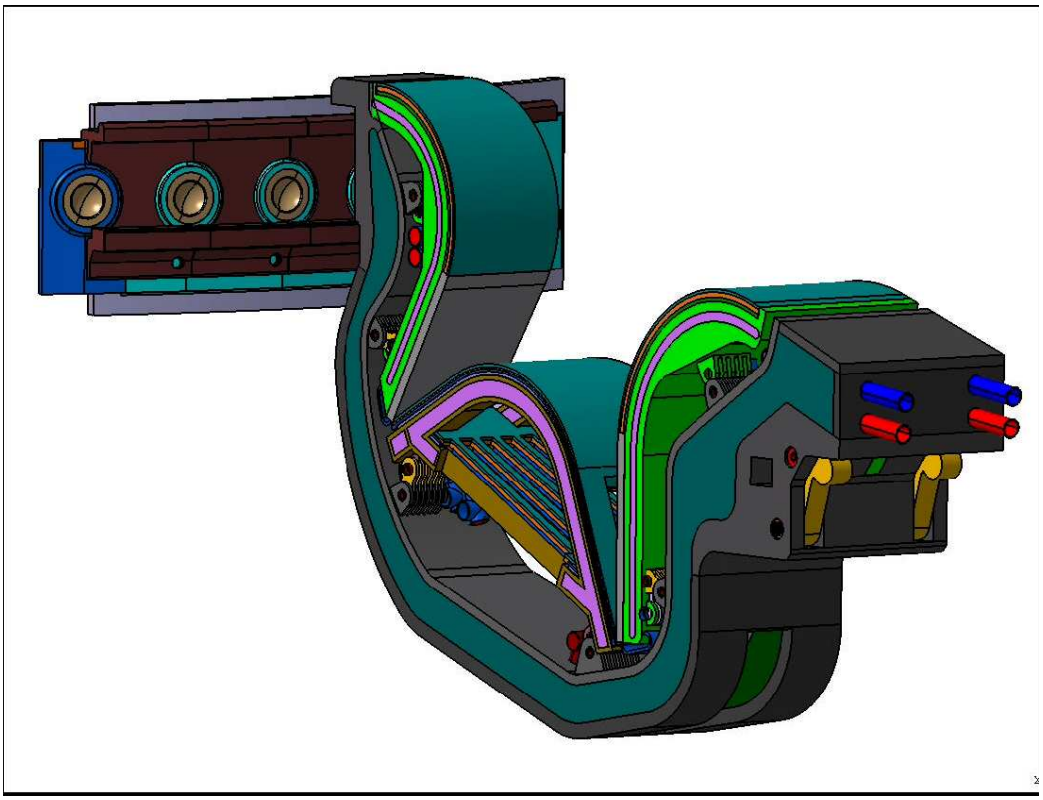

Fig. 3.2.3 Attachment of the divertor to the inner side of the Vacuum Vessel.

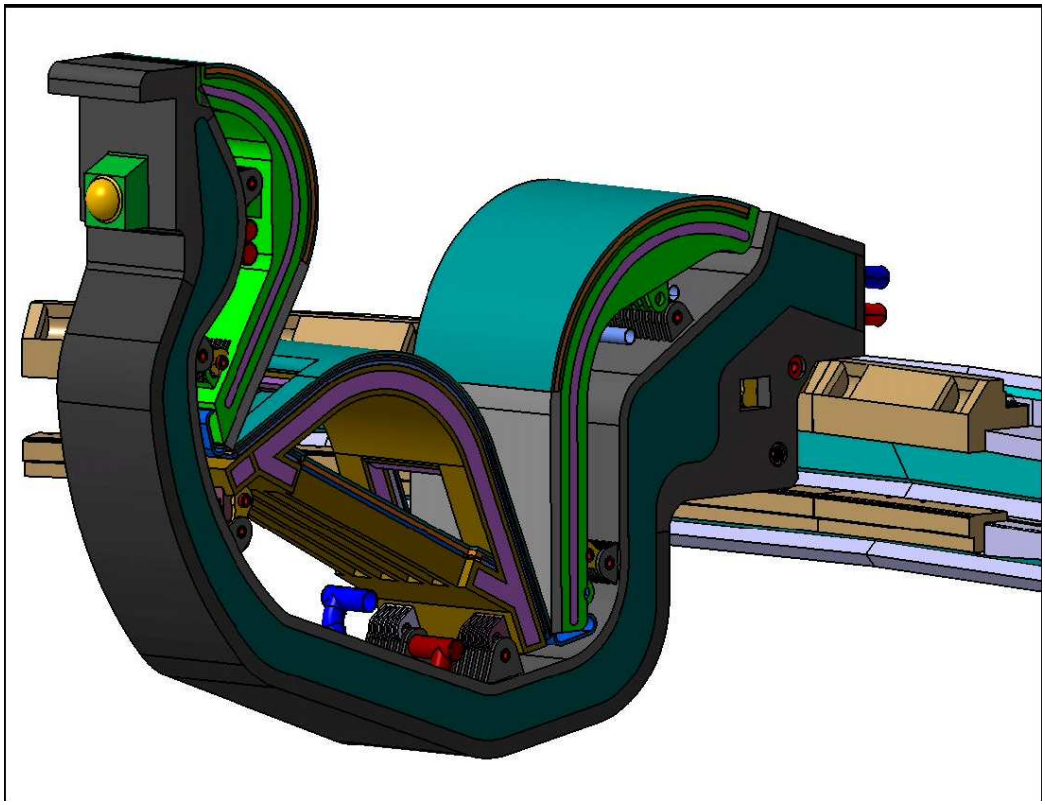

Fig. 3.2.4Attachment of the divertor to the outer side of the Vacuum Vessel.

3.3 The vertical target

Each cassette carries four vertical targets, two inner vertical targets and two outer vertical targets. The inner targets are ~ 1.7 m high x 0.25 m wide, and weighs 0.6 t. The outer targets are ~ 2.2 m high 0.35m wide, and weighs 1.0 t.
Each vertical target is based on a number of thin poloidal elements (see fig. 3.3.1) ~ 28 mm width; 11 elements for each outboard half vertical target and 8 for each inboard half. The upper part of the element is clad with W and the lower part with Carbon Fiber Composite (CFC), see fig. 3.1.1.

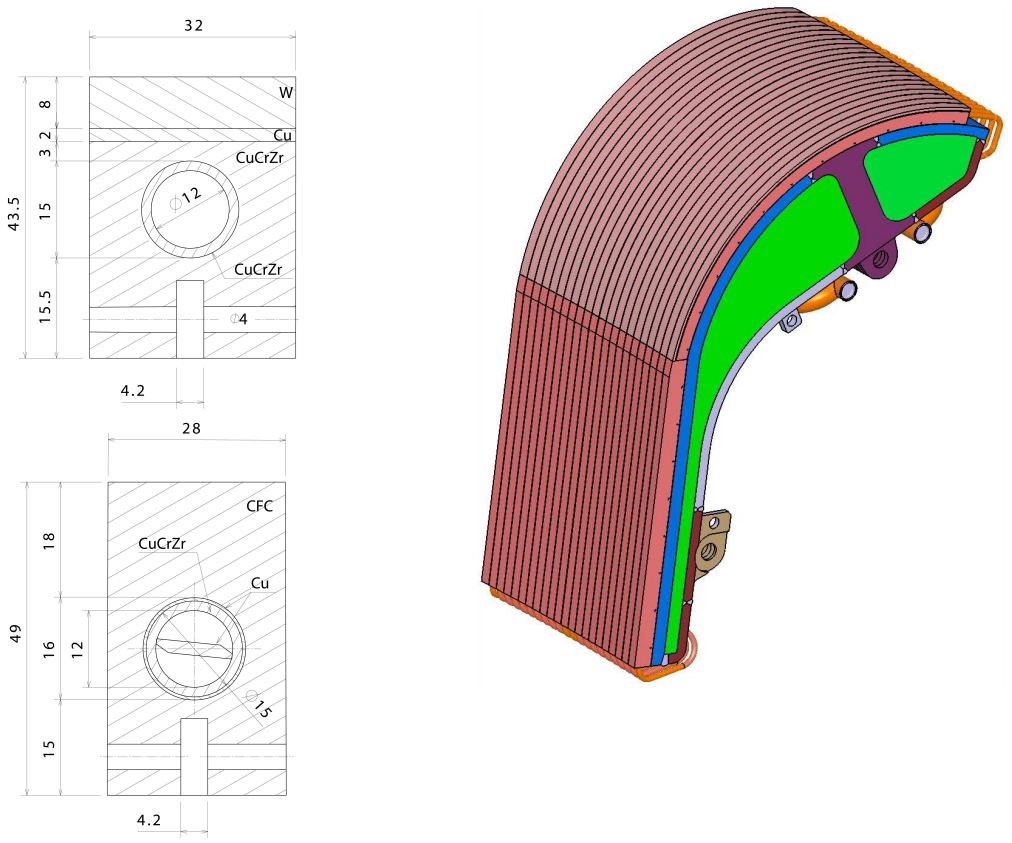

Fig.3.3.1 A section of the poloidal elements – The tiles.

All the PFCs are constructed using a similar range of manufacturing techniques, demonstrated to be viable by R&D, and all the armoured parts of the PFCs with high heat flux capability are fabrications of similar poloidal slices. This approach is intended to simplify manufacture and minimise costs, as it allows the critical fabrication steps, particularly those involving the armour-to-heat-sink joints, to be performed and tested on small units. Furthermore, a poloidal flow arrangement, rather than toroidal, better distributes the heat to the coolant. After testing the poloidal slices are assembled onto the strong back, a stainless steel box structure that supports the plasma-facing elements, acts as coolant a manifold and contributes to the neutron shielding (see fig. 3.3.2).

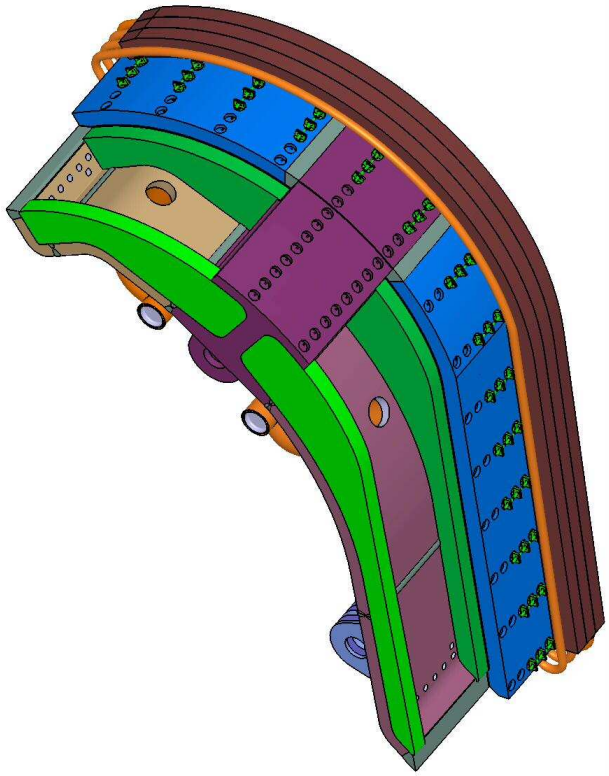

Fig. 3.3.2 Section of a Vertical target

A pair of attachments is used to fasten each target to the cassette body (see fig 3.3.3).

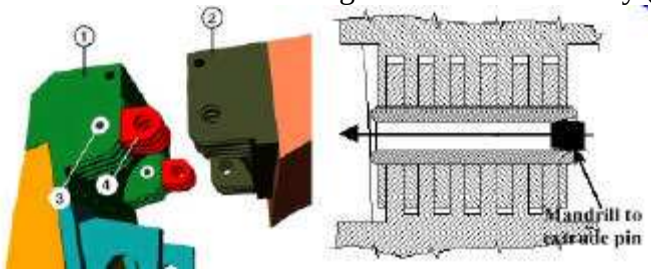

Fig.3.3.3 *.1. PFC, 2. Cassette body, 3. Extruded pin in PFC, 4. Alloy 718 links*

The poloidal expansion of the target is accommodated by the lower support, which allows both rotation around a toroidal axis and poloidal translation, and the upper support, which is adjacent to the cassette to target coolant connections and allows only rotation. The supports are sized to sustain the electro-magnetic loads induced by eddy currents in the target. The nominal gap between the poloidal elements of vertical targets is 0.5mm and is maintained to reduce electro-magnetic loads.

The lower part of the vertical target is clad with CFC and the upper baffle part with tungsten. The vertical target intercepts the SOL on its lower CFC end and is inclined with respect to the field lines. Inclining the target produces a deep divertor channel, which the B2-EIRENE code predicts will result in a SOL plasma partially detached from the target, thus reducing the peak heat flux to the target to ~10 MWm^{-2}.

A start-of-life armour thickness of 20mm and 10mm above the heat sink tube are proposed for CFC and tungsten respectively. However, the target is rated for 20 MWm^{-2}.

Although the anticipated surface heat flux on the target has been evaluated using the B2-EIRENE code, which predicts a partial detachment of the plasma, a check is made on the maximum heat flux should there be no detachment (slow transient).
At start-of-life when the CFC armour is ~20mm thick a very high heat flux (>25MWm^{-2}) will cause ablation of the carbon and even if this does not terminate the plasma, the effective heat flux into the target will be kept to ~20MWm^{-2}, thus avoiding a burn-out of the coolant channel.
The feasibility of building PFCs capable of sustaining the heat flux demanded of this component has been demonstrated by R&D using near full-scale mock-ups (see Fig 3.3.4). However, with upwards of 50,000 monoblocks and 100,000 tungsten tiles in a divertor, R&D effort is still needed to demonstrate high component reliability.

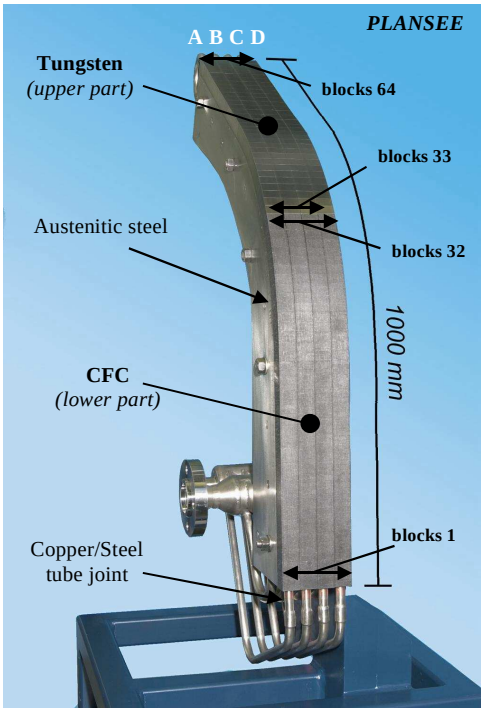

Fig. 3.3.4. European prototype with CFC & W armour.

3.4 The dome and private region

The dome and inner and outer neutral particle reflector plates of the private flux region PFCs are clad with tungsten tile armour that is attached using a similar technique as used for the upper parts of the vertical targets. The dome is supported on four posts that are protected with a combination of tungsten tile armour (surfaces facing the divertor channels) and radiatively cooled tungsten plates. As part of the PFCs a semi-transparent liner clad also with radiatively cooled tiles is suspended above the cassette body. In this way an open duct is formed beneath the dome connecting the inner and outer channels of the divertor that is clad completely in radiatively cooled tungsten plates. This allows the surfaces of the duct to be maintained at temperatures > 350 °C for the majority of the 400s discharge. The open duct allows free re-circulation of neutrals from the inboard to the outboard private flux region and their re-ionisation in the outer divertor plasma. The

dome protects the neutral particle reflector plates from the separatrix under all operating scenarios, avoiding the need for the plates to have the high heat flux capability needed in the lower vertical target and allowing the private region PFC to have only tungsten armour.

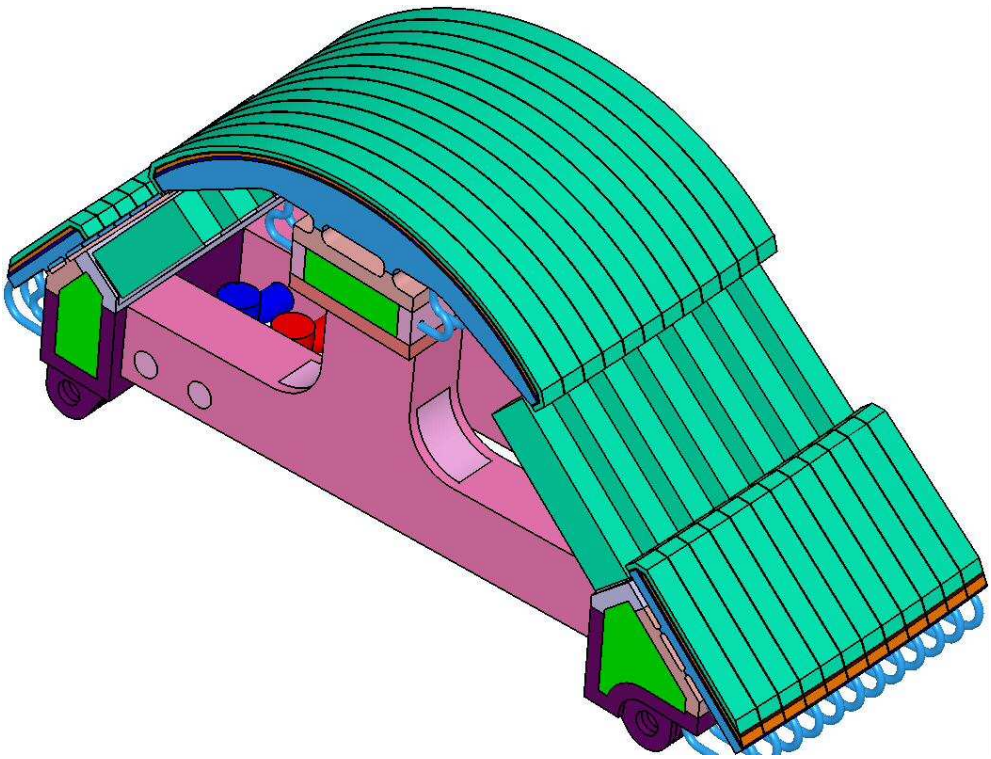

Fig. 3.4.1. The dome of the ITER divertor armoured with tungsten

The figure below show the internal structure of the dome:

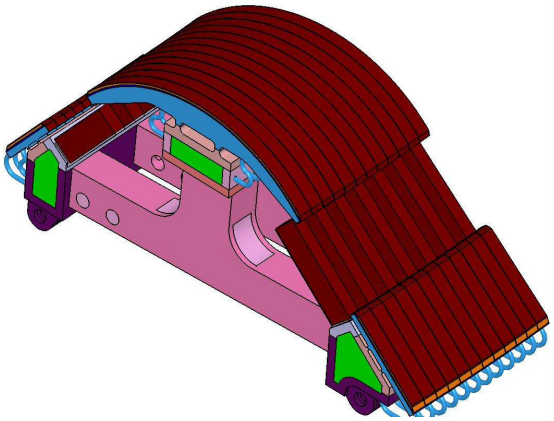

The Pure Cu layer below the W

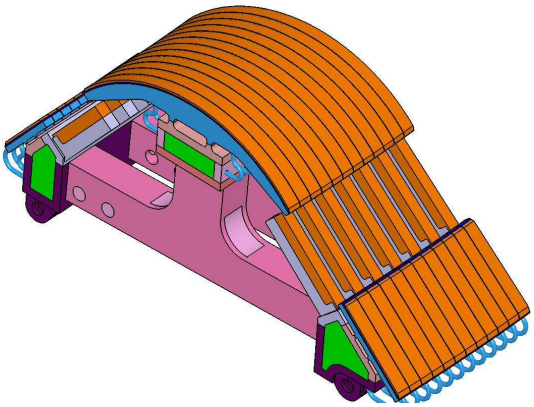

The heat sink CuCrZr below the Pure Cu

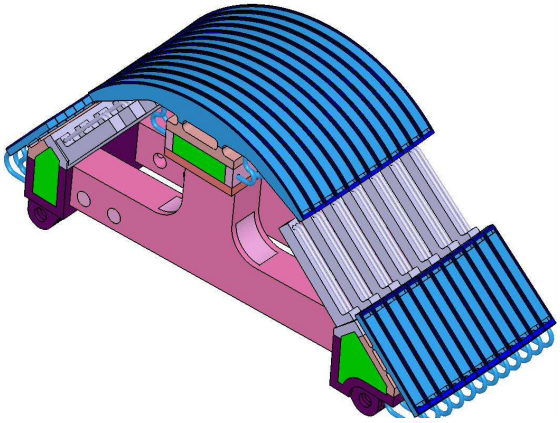

The structure SS 316(L)N-IG below the CuCrZr heat sink

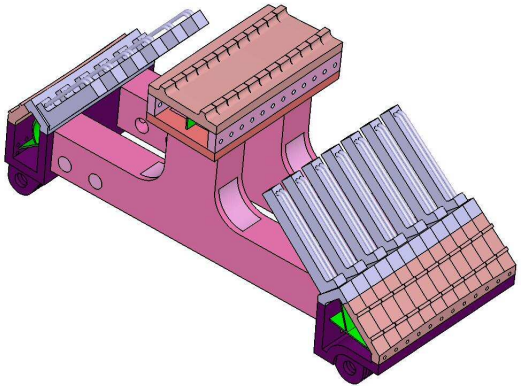

The support structure and tubes of SS 316(L)N-IG

Fig. 3.4.2. The internal structure of the dome.

4. Definition of the acceptance criteria for the CFC tiles of the divertor

4.1 Background

4.1.1 General consideration

The last period has seen impressive progress made in the development of both Carbon Fiber Composite (CFC) to Cu and tungsten to Cu joints that are not reliant on the use of silver, an element that transmutes under neutron bombardment to the element cadmium, which is unacceptable. An extensive range of CFC to Cu joints were tested as part of a design by experiment approach [2], supported by analysis in identifying manufacturing options such as tile size, optimisation of manufacturing cycle to minimise residual stresses etc.

Fig. 4.1.1.1. Design analysed for the plasma exposed wall of the ITER divertor.

The monoblock geometry has been selected as reference for the CFC armour to be used in conjunction with Active Metal Casting (AMC®) for the joint and a CuCrZr heat sink. In this combination the CFC/Cu joint provides joints of repeatable quality capable of sustaining the 20 MWm^{-2} heat flux incident on the target surface. The CFC monoblock has been shown to be a robust design for the CFC armour, and in tests the European Parties [3] built prototype has survived 2000 cycles at 20 MWm^{-2}, plus a few critical heat flux tests in excess of 30 MWm^{-2} (see fig. 4.1.1.2).

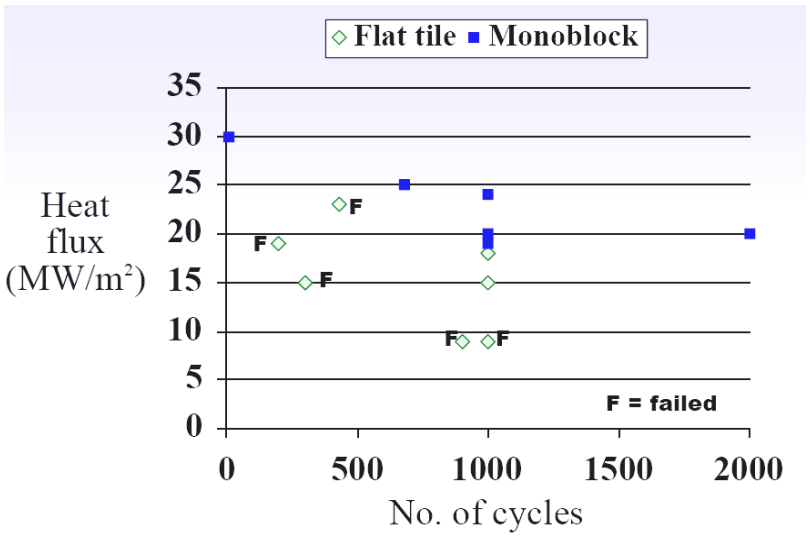

Fig. 4.1.1.2 Some results of high heat flux tests of the CFC/Cu actively cooled mock-ups [16].

The monoblock is still preferred over the less expensive flat tile design, because of concerns over the observed tendency for flat tiles to suddenly and totally detach, although recent results [4] with flat tiles with a hypervapotron heat sink as opposed to a Cu monoblock heat sink have showed no failures up to heat flux of 27 MWm^{-2}. Loss of a single tile might be tolerated, but what is not acceptable is a possible cascade failure, whereby the loss of a tile causes the heat load to the tile downstream in the Scrape-off Layer to be doubled causing it to detach, and so on. The monoblock is resistant to a cascade failure, whereas it is postulated that flat tile geometry could fail in this manner. For the AMC® joint the bore of the CFC monoblocks are lined with a pure Cu layer cast onto a laser textured and Ti-metallised surface. The laser-texturing helps the keying of the Cu into the CFC and the Ti coating aids wetting of the CFC surface. The pure Cu in the bore of the monoblocks are machined to size prior to them being low temperature HIP-ed (~ 500°C) to a CuCrZr tube. The HIP (Hot Isostatic Pressure) process gives the lowest residual manufacturing stresses, but other options such as fast-brazing or conventional brazing followed by a fast quench could be cheaper alternatives and their viability is being investigated by R&D.
Because the final design of the tiles has not been approved, the studies conducted in this thesis want to be just a way to show how to proceed in the definition of the acceptance criteria for the CFC tiles installed in the machine. In fact studies conducted in this thesis refer only to the start-of -life of the tiles.
The figure 4.1.1.3 shows the dimension of the most recent design of the monoblock.

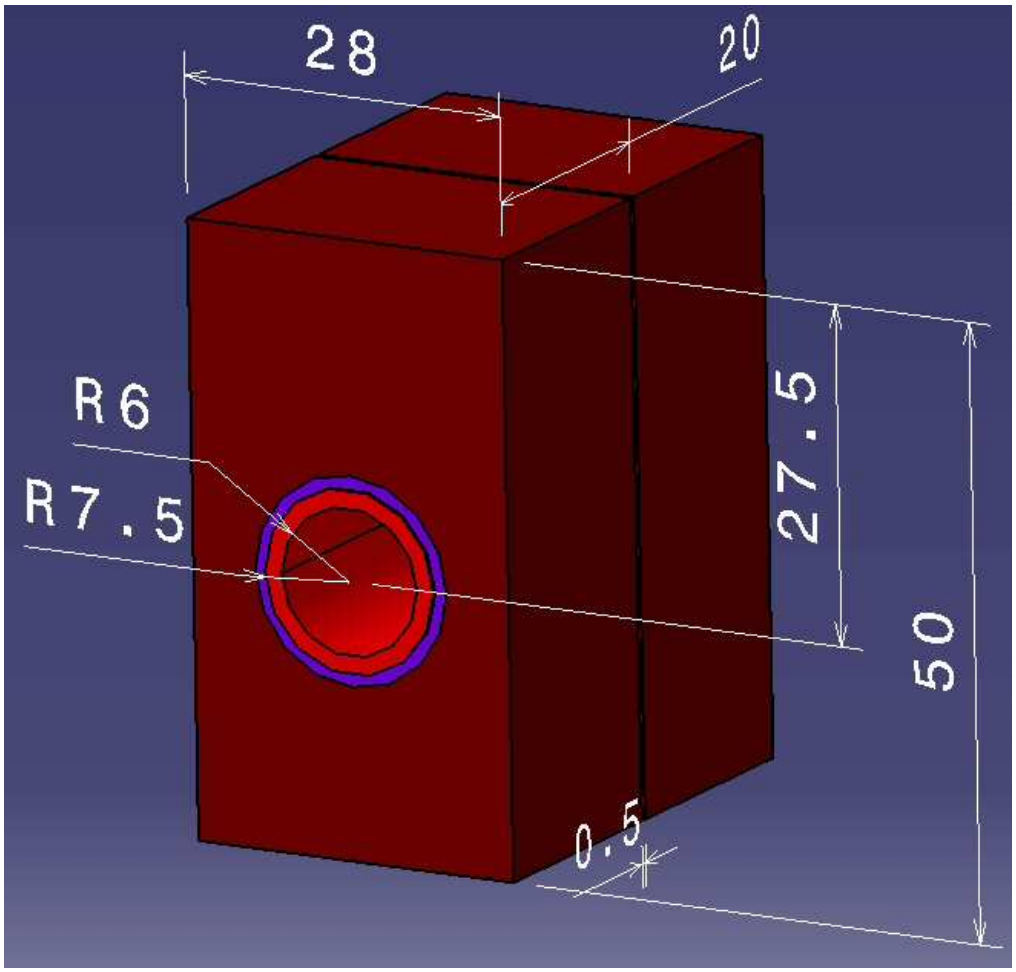

Fig. 4.1.1.3 The dimension of the monoblock [mm].

There has been an evolution in the design of the monoblock in term of geometry and material properties employed in the last years also thank to the studies reported in this work. Some preliminary studies presented in this thesis refer to the previous design of the monoblock. This circumstance could be very useful to understand the evolution of the design.

4.1.2 The CFC/Cu joining technology

The active metal casting (AMC®) process has been developed by Plansee GmbH (see figure 4.1.2.1 and 4.1.2.2). The process is summarized in the following:

- Drilling of a hole in the CFC block
- Laser conditioning or texturing of the bore. This laser conditioning cuts thin conical holes into the surface of the CFC in order to provide a good key for the cast copper (see fig. 4.1.2.3)
- The next operation is to sputter or evaporate a ~50 μm titanium coating onto the laser-conditioned surface. This acts as a wetting agent for the copper.
- Oxygen free high conductivity copper is then vacuum cast into the bore of CFC block.

• The final operation is to machine the cast copper, including the bore to suit the CuCrZr tube and the other surfaces of the CFC.

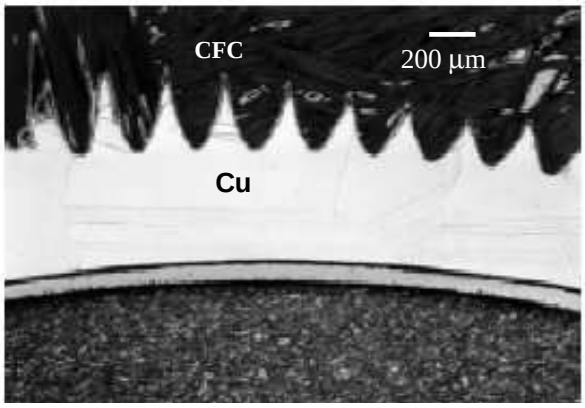

4.1.2.1 The interface between CFC and Cu.

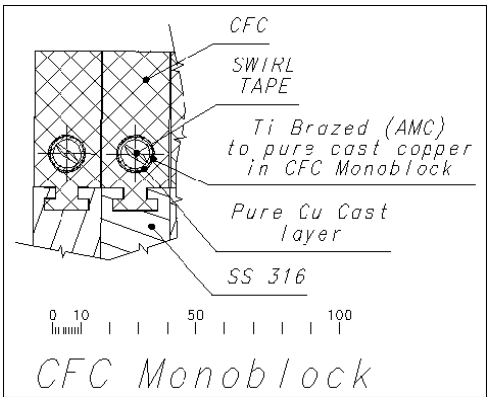

4.1.2.2 A section of the poloidal elements – The tiles.

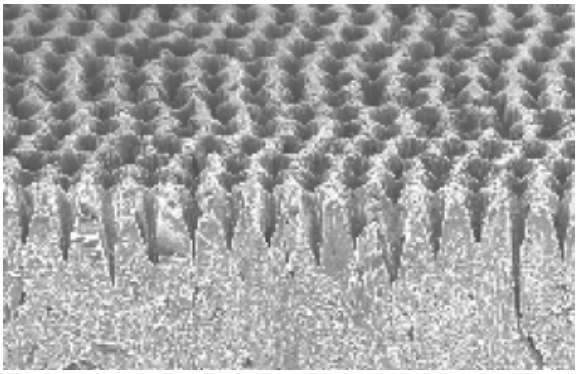

Fig. 4.1.2.3 Laser structuring of CFC surface in AMC® process

The monoblock tile is then ready to be joined to the CuCrZr tube. A straight CuCrZr tube is prepared for the monoblocks. At each end of the copper tube there is a transition between copper and stainless steel. This is accomplished by using a short length of nickel tube EB welded to the CuCrZr at one end and the other end welded to a short straight length of stainless steel tube.

The monoblocks are then threaded onto the CuCrZr tube. Each monoblock butts up to its neighbour leaving no gap between individual monoblocks. At this stage this assembly is be canned and HIP-ed. The HIP-ing process takes place at 500°C, 100MPa for 3 hrs and also acts as the hardening process for the CuCrZr.

The Hot Isostatic Pressure process is particularly suitable for large surfaces to be joined and complex geometries. It allows high quality junction that is necessary for a good heat transfer through the interface.

After removing the can the joints are examined as follows;

- full visual inspection to identify surface defects;
- check geometry;
- ultrasonic examination of the pure Cu to CuCrZr joint using an in-bore probe;

- vacuum leak test to < 10^{-9}Pam^{3}s^{-1};
- thermographic examination of the surfaces of the monoblock when exposed to alternating pulses of hot and cold water passed through the heat sink tube (this is the SATIR test developed by CEA[5]).

4.1.3 The reason to have a well defined acceptance criteria for the CFC to cooling channel joint

In the divertor design there are ~5x10^4 CFC to Cu-tube monoblock joints subjected to high heat flux. A large R&D has focused on developing repeatable and reliable joints, and robust and relatively homogeneous CFC material. Extensive **N**on-**D**estructive **E**xamination (NDE) of the joints will be carried out, but this NDE is complicated by the geometry and by the nature of the materials and processes used in manufacture. Hence, a few defects are likely to escape detection and be installed in the divertor. A thermographic method (SATIR) has been suggested to investigate the Cu-CFC joint quality. A study on the reliability, the possibility and the final use of this method are addressed in this chapter.
A target of this chapter is to investigate whether or not the defects in the joints, that might prejudice normal operation of the machine, can be identified using SATIR technique. Another target is to find a possible way to use this method to set-up an acceptance criterion for the monoblock that have to be installed in the divertor of the ITER machine.

4.2 The SATIR method

An infrared thermography test bed named SATIR [11], [12] (Station d' Acquisition et de Traitement InfraRouge) has been developed by CEA in order to evaluate the manufacturing process quality of actively water-cooled plasma facing components (PFCs) before their installation in TORE SUPRA (a French tokamak device). The infrared thermography allows to characterise the bond between CFC armour tile and metallic heat sink and is becoming more and more a valuable tool for detecting cracks and failures. It is a complementary and necessary non-destructive testing method which gives a global information about the soundness of the heat path thus being a fast and economical way to assess the acceptability of a CFC armoured component prior to its installation into a fusion machine.
Within the on-going work on acceptance criteria, SATIR inspection has been identified as the basis test to decide upon the final acceptance of the divertor PFCs.
The transient infrared thermography applied for the non-destructive inspection of PFCs is based on forcing a heat flux through the component in a path, which crosses the interfaces between the cooling water and the armour. Cold water (5 °C) is sent to the monoblocks, suddenly the temperature of the water is increased to 95 °C, past a certain time the temperature of the water is decreased again to 5 °C (see fig. 4.2.1).

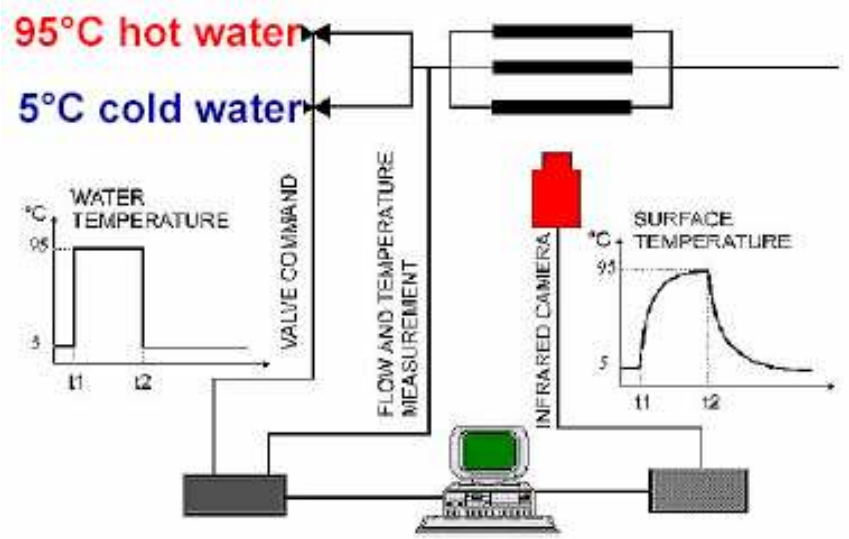

Fig. 4.2.1 Scheme of the SATIR test.

The principle is based on the comparison of the surface temperature evolution of the inspected component with that of a "defect-free" reference one. Defects are detected by a slower temperature surface response.

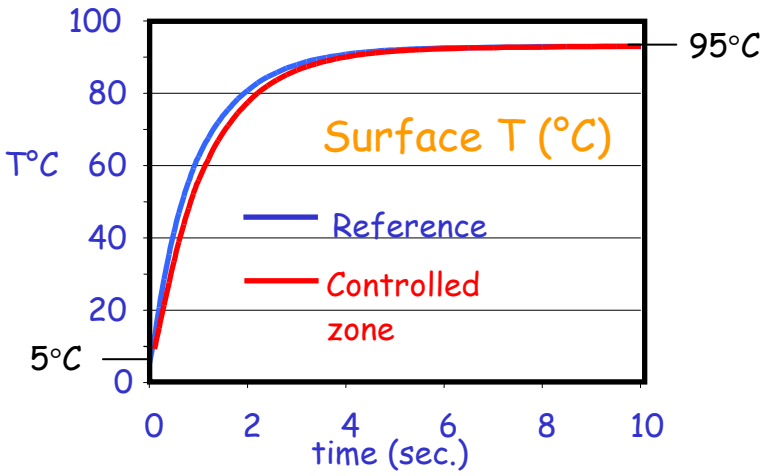

Fig. 4.2.2 The comparison of the temperature, in a certain point, between a reference tile and a tile to test

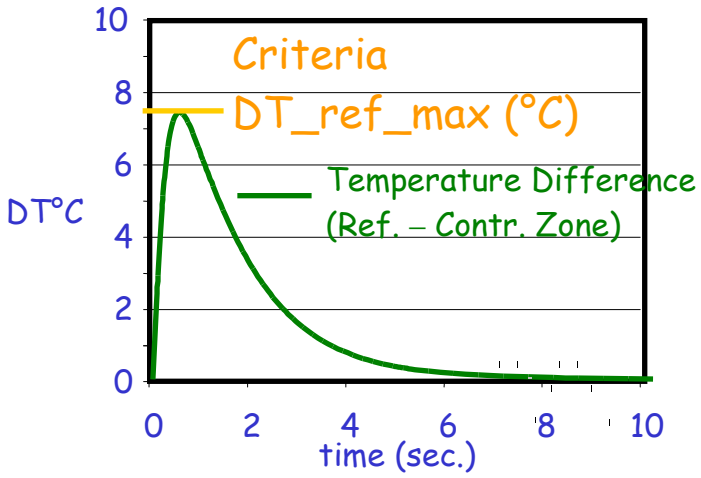

Fig. 4.2.3 The difference of the temperature vs time of a checked with a reference tile.

The armour surface temperature is observed by means of an infrared camera. The thermographic film is digitalised and saved on a hard disk. Then infrared data acquisitions are analysed by specific software.
In order to increase the defect detection capability of the SATIR test bed, several possibilities have been considered and assessed and some of them already implemented. In particular the installation in 2003 of a digital infrared camera and the improving of the thermal signal processing, has led to a considerable improvement of the performances. However, the ITER divertor PFCs pose new challenges for the following reasons:
The CFC thickness is 2-3 times higher (say 18-20 mm) than any existing components manufactured or being manufactured so far either within the ITER project or within domestic projects. Therefore, the sensitivity of the technique, which depends on the armour thickness, is lowered.
Within the planned activities to identify suitable acceptance criteria for the ITER divertor, more than 100 mock-ups with artificial defects shall be SATIR tested starting from summer 2006, before and after their high heat flux testing. This non-destructive testing has to be completed with a tight time schedule.
The number of units to be tested during the procurement of the ITER divertor will be 2-3 times higher (more than 2000) than that of any fusion machine which is existing or under construction. Therefore, the total time required to test all the units increases accordingly.
In order to increase the sensitivity to speed up the process of the test have been respectively foreseen two main improvements:

- increase the heat transfer coefficient by mean of increasing the velocity of the water to 12 m/sec and the ΔT from 5-95 °C to 5-200 °C.
- Use only the descendent part of the comparison say from 200 to 5 °C. In fact, during the descending period the $\Delta Tref$ is higher then during the ascending period (represented in fig. 4.2.2). Because at high temperature the heat transfer coefficient is higher that at lower temperature.

Below some picture of the SATIR test:

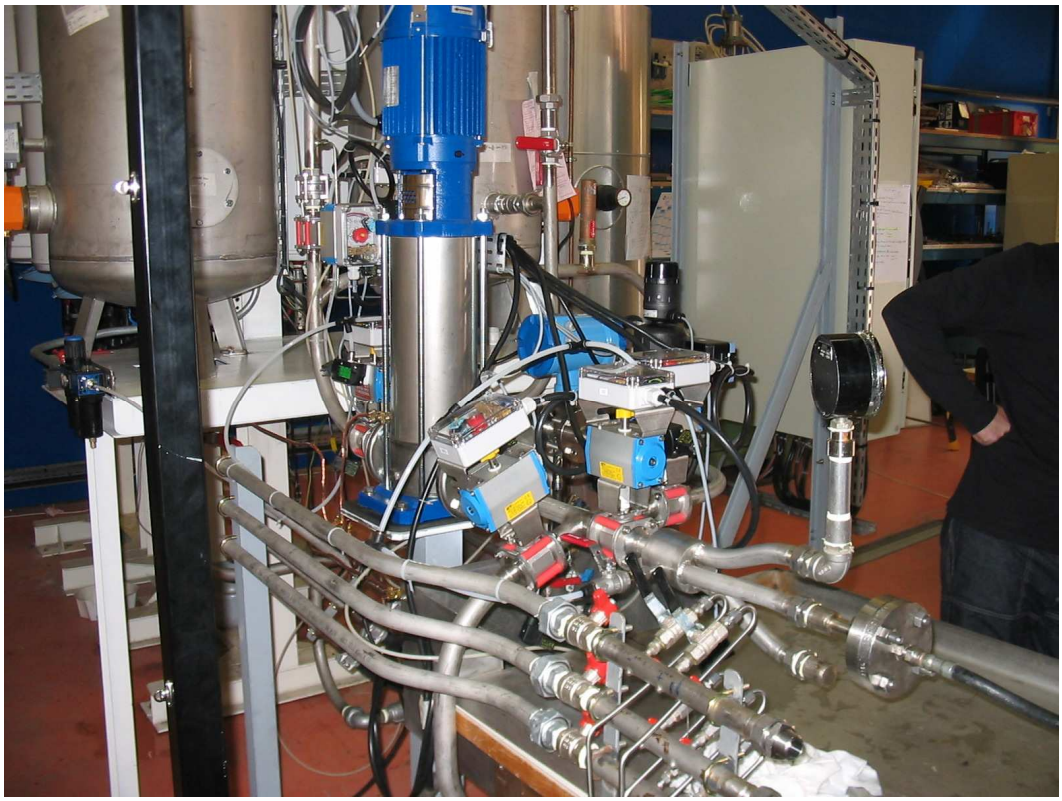

Fig. 4.2.4 SATIR test water loop control system.

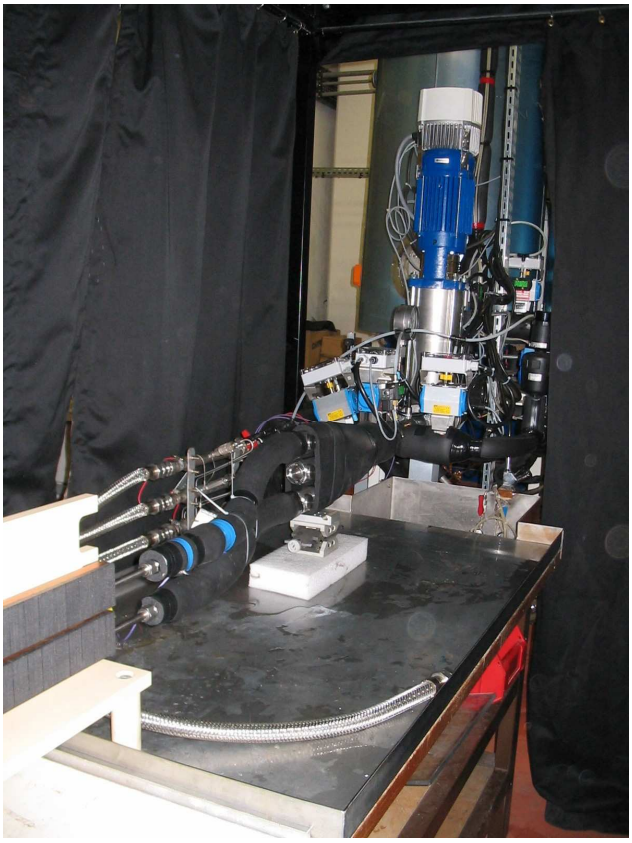

Fig. 4.2.5 SATIR test, place to test the components.

4.3 Some preliminary analyses on the detachment of the cooling channel from the monoblock

4.3.1 General considerations

In the ITER divertor the vertical targets that intercept the plasma **S**crape-**O**ff-**L**ayer (SOL) are subjected to intense heat flux. If the SOL were intercepted at normal incidence the heat flux would be ~190 MWm^{-2}. However, the targets are inclined so that the heat flux is ~10MWm^{-2}, making water cooling of the target feasible and reducing target erosion so as to provide an acceptable armour lifetime. Each target is armoured with two armour materials. **C**arbon **F**ibre **C**omposite (CFC) in the region of the SOL strike point, because it ablates rather than melts making it suitable for plasma transients. Tungsten on the upper part of the target where tungsten's low sputter-yield will mean there will be virtually no erosion during normal operation. This thesis concentrates on CFC armour, and in particular, the armour at the strike point where the heat flux is most intense. A parametric study has been done to verify the dependence of the **W**all **H**eat **F**lux (WHF) against the thickness of the cooling channel of the monoblock.
This paragraph focuses on the impact of a single defective tile at the start of life, i.e. tile thickness ~ 20mm.

4.3.2 The model

The ANSYS model shown in fig.4.3.2.1 has been used to analyse the effect of changing the thickness of the copper tube and to preliminary assess the effect of the detachment of the copper tube from its monoblock. The monoblock has been modeled as it is, with the cooling channel of CuCrZr (in green) and with the layer of pure copper (in blue) to join the Cu alloy to the CFC. The conductivity of some elements of the model (in red) is changed in order to simulate the detachment between the cooling channel and the tile; the thickness of these elements is 0.5 mm. The height, the width and the depth of the monoblock are respectively 38, 24 and 24 mm. Starting from a cooling channel with an inner diameter of 10 mm and an outer diameter of 11 mm, the outer diameter has been gradually increased up to 13 to study the influence on local heat flux. Eventually, an increasing of the thickness of the layer of the pure copper has been analysed. The thickness of the pure copper layer has been gradually increased from 0.5 mm to 1.5 mm. The gap between adjacent monoblocks is 0.5 mm. Nominally the outer diameter of the CuCrZr tube is 12 mm (1 mm thick) and the pure copper layer is 0.5 mm thick. Hence, to verify which kind of detachment is more dangerous from a CHF point of view, it has been assumed that the cooling channel has its nominally dimension, an outer diameter of 12 mm and an inner diameter of 10 mm.

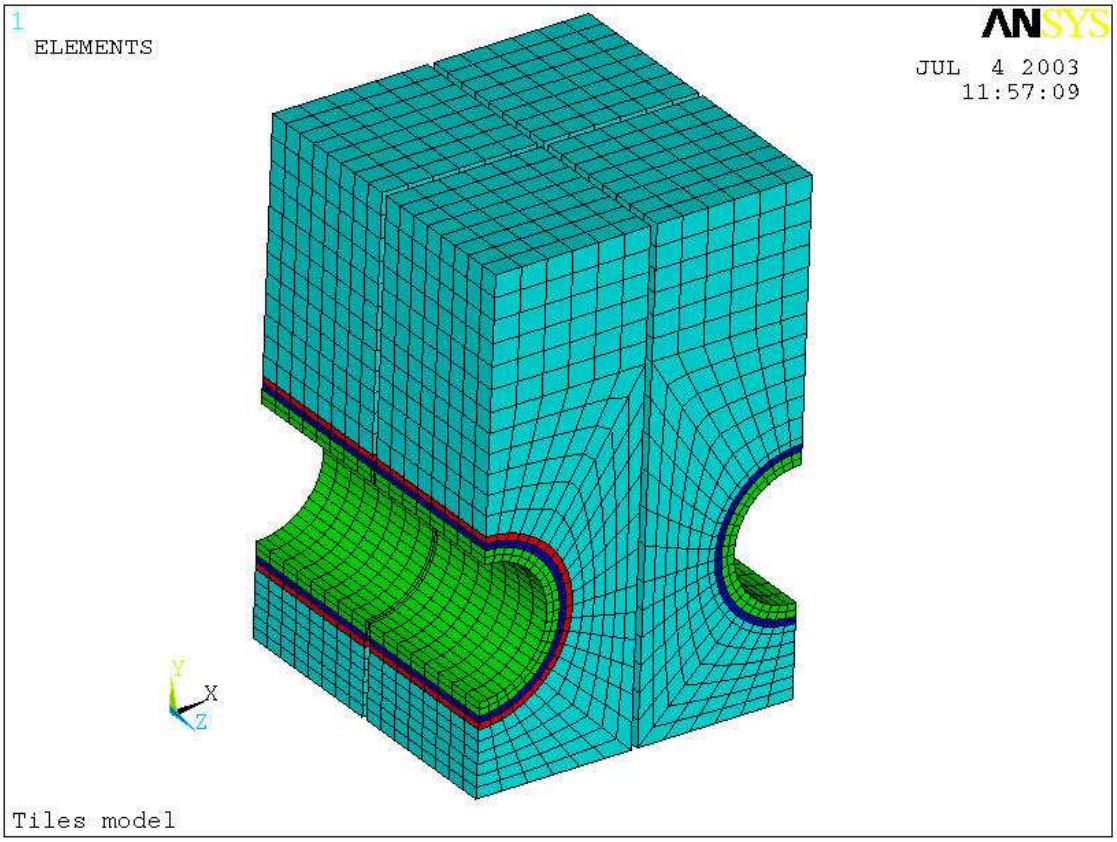

Fig. 4.3.2.1 3D Model of the tile of the PFC

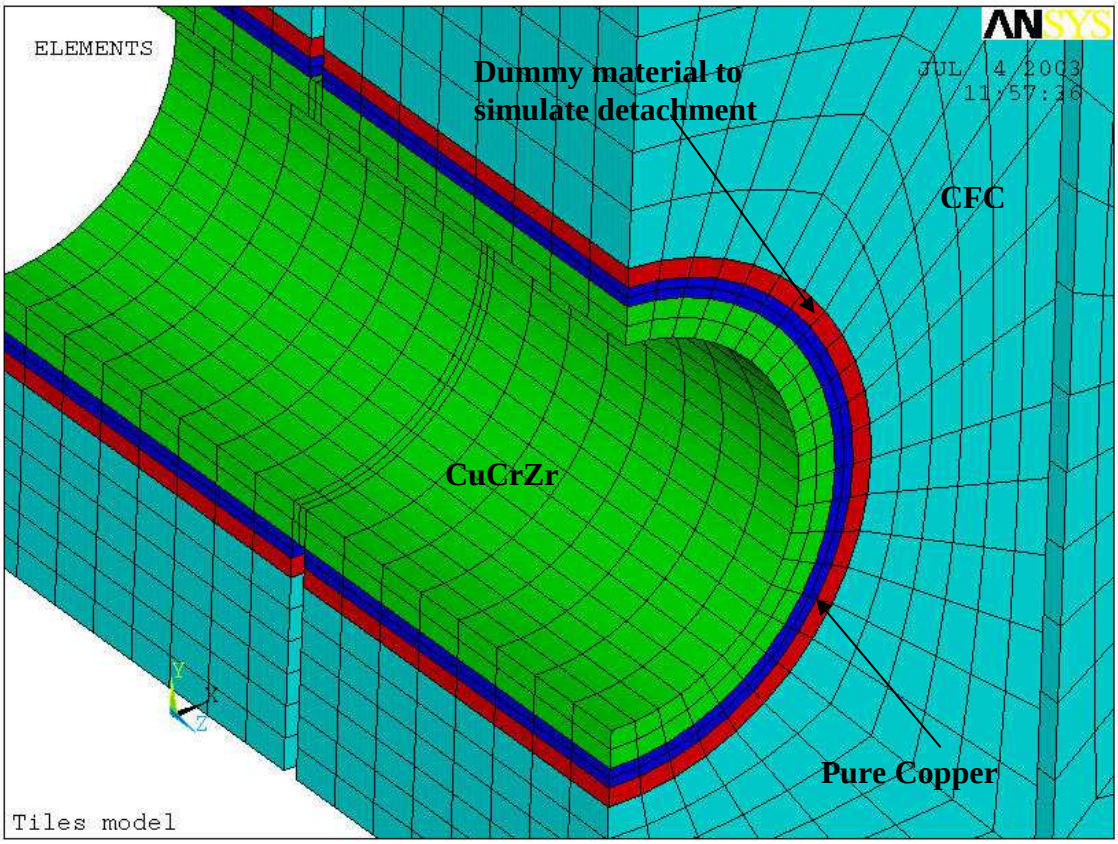

Fig. 4.3.2.2 3D Model of the tile of the PFC, particular.

4.3.3 The material properties

The materials used are **C**arbon **F**ibre **C**omposite (CFC) for the tile, an alloy of copper, CuCrZr for the cooling tube, pure copper Oxygen free for the layer that join the cooling channel to the CFC and a "dummy" material implemented into the FE model to simulate detachment. After a study of the database of the several values of the thermal conductivities the minimum possible values, temperature dependent material properties have been used and are summarised in the tables 4.3.3.1, 4.3.3.2 and 4.3.3.3.
Note that the CFC is orthotropic and the values of the conductivity at 3500 °C have been extrapolated.

CFC SEP NB31	T=100 °C	T=800 °C	T=1500 °C	T=3500 °C
Thermal conductivity along horizontal direction [W/mm*K]	0.117	0.057	0.050	0.050
Thermal conductivity along vertical direction [W/mm*K]	0.279	0.135	0.115	0.080
Thermal conductivity along axial direction [W/mm*K]	0.105	0.055	0.046	0.045
Density [Kg/mm^3]	1.958e-6	-	-	-

Table 4.3.3.1 Material property of CFC SEP NB31 (previously called N312C)

CuCrZr copper	T=20 °C	T=200 °C	T=500 °C	T=700 °C
Thermal conductivity [W/mm*K]	0.320	0.320	0.320	0.320
Density [Kg/mm^3]	8.86e-6	-	-	-

Table 4.3.3.2 Material property of CuCrZr Copper

Pure Copper Oxygen free	T=20 °C	T=250 °C	T=500 °C	T=800 °C
Thermal conductivity [W/mm*K]	0.390	0.378	0.364	0.345
Density [Kg/mm^3]	8.95e-6	8.81e-6	8.67e-6	8.49e-6

Table 4.3.3.3 Material property of pure Copper Oxygen free

Degradation in the quality of the CFC-Cu joint has been modelled by changing the conductivity of some elements. In the FE model a "dummy" material (shown in red in fig. 4.3.2.2) with a low conductivity (see Table 4.3.3.4) has been used to simulate detachment. The "*High*" thermal conductivity of the dummy material corresponds to a well-attached monoblock. To simulate local detachment of the joint the thermal conductivity of the dummy material is set to "*Low*" (insulation).
For the "Low" conductivity a conservative value of 0.0013 $Wmm^{-1}K^{-1}$ has been chosen acting over a length of 0.5 mm. It comes from consideration of the thermal contact resistivity [6]. There are a lot of mathematical models to calculate a thermal contact resistivity but, all these models have been developed for specific applications and normally they are supported by experimental data. To verify the acceptability of the assumption, a check was carried out on the worst configuration, deselecting the dummy material in order to simulate a real detachment (improbable) [7]. The results confirmed that the assumption of a thermal conductivity of 0.0013 $Wmm^{-1}K^{-1}$ for 0.5 mm is very conservative.

Temperature		100 °C	800 °C	1500 °C	3500 °C
Thermal conductivity					
High (CFC-no detachment)	$Wmm^{-1}K^{-1}$	.105÷.279	.055÷.135	.046÷.115	.045÷.080
Low	$Wmm^{-1}K^{-1}$	.0013	.0013	.0013	.0013
Density	$Kg\ mm^{3}$	1.958e-6	1.958e-6	1.958e-6	1.958e-6

Table 4.3.3.4 Material property of the dummy material.

4.3.4 Loading and boundary conditions

The heat, on the surfaces of the tile, is due to radiation and to the incident particle flux (see fig. 4.3.4.1).

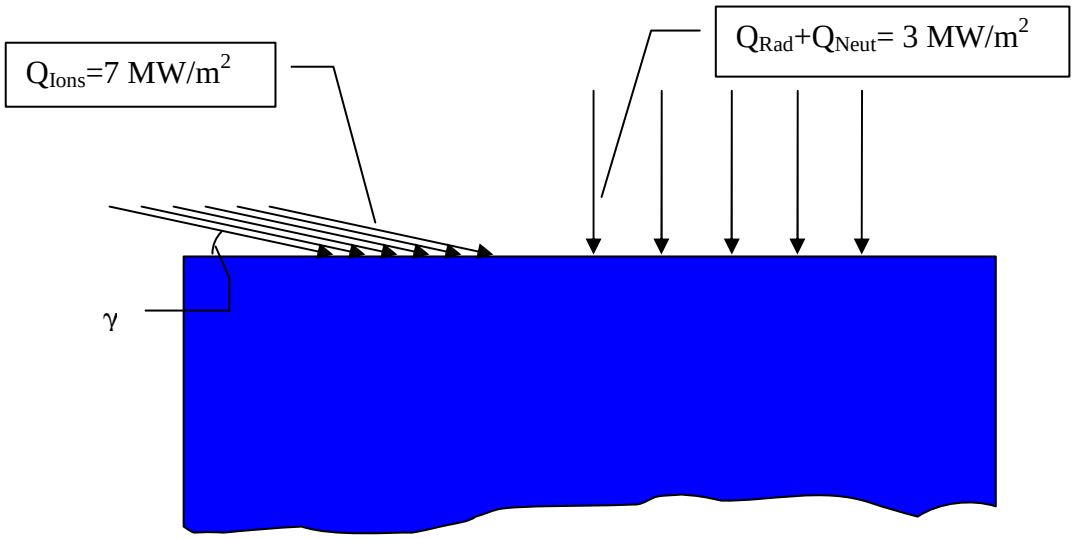

Fig. 4.3.4.1 Distribution of the heat on the surface of the tiles.

As shown in the above figure, the ion flux is not perpendicular to the surface of the tiles. It has been calculated, with consideration about the magnetic field direction, that this angle is ≈ 3 degree [8].

Considering as reference the **O**uter **V**ertical **T**arget (OVT), the contribution due to the neutrals is almost zero (see fig 4.3.4.1). Therefore, it has been assumed that the power delivered to the surfaces of the tile, at the initial condition, is:

- 3 MW/m^2 due to radiation;
- 7 MW/m^2 due to ions;
- 0 MW/m^2 due to neutrals.

The total heat flux on the surface is 10 MWm^{-2}.

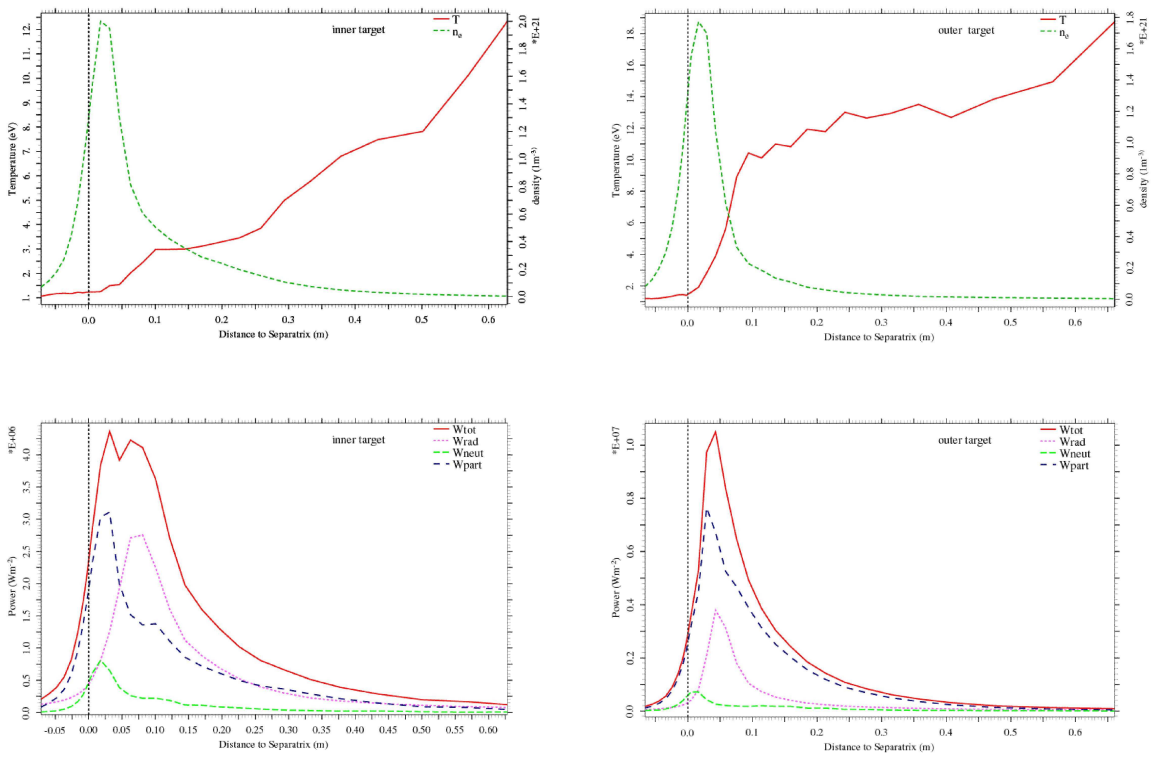

Fig. 4.3.4.1. Distribution of the power on the surface of the tiles (from B2-EIRENE code)[9].

A quarter of a monoblock with its 3 neighbors monoblocks has been modeled. Hence, the model has 4 planes of symmetry, one per each lateral side. Figure 4.3.2.1 shows the model used. Convective heat transfer has been applied to the cooling channel and the heat transfer coefficient has been calculated (function of the temperature) using the EUPITER 4.2 [10] code. It is assumed that the tube includes a swirl tape, which acts as a turbulence promoter. The twist ratio of the tape is 2 (180° twist in 2 internal pipe diameters). Table 4.3.4.1 shows the input data used to find the heat transfer coefficient. Table 4.3.4.2 shows the output data of the EUPITER 4.2 code.

Geometry data	Flow inner diameter [mm]	Tape thickness average [mm]	Tape twist ratio	Surface roughness [mm]
	10	1.65	2	3e-3

	Pressure [MPa]	Temperature [°C]	Velocity [m/s]
Inlet water conditions	3.8	120	9

Table 4.3.4.1 Input data for the EUPITER 4.2 code

Temperature [°C]	Heat Transf. Coeff. [MW/(m^2*K)]		Temperature [°C]	Heat Transf. Coeff. [MW/(m^2*K)]
120	0.08226		308	0.13215
138	0.08346		310	0.13798
156	0.08449		313	0.14396
183	0.08570		315	0.15009
200	0.08633		317	0.15634
217	0.08685		319	0.16271
234	0.08728		321	0.16918
251	0.08764		323	0.17575
280	0.09391		325	0.18241
289	0.10141		327	0.18914
306	0.12782		330	0.19939

Table 4.3.4.2. Heat transfer coefficient function of temperature calculated by EUPITER 4.2.

The CHF calculated by EUPITER 4.2 is 35 MWm^{-2}.
Radiation between adjacent monoblocks is taken into account. A radiation heating condition between the four modelled monoblocks has been implemented. Moreover, radiation from the plasma facing top surface of the monoblock is also taken into account. The emissivity of the CFC is 0.8 and the temperature of the surrounding environment has been fixed at 550 °C. The analysis is conservative because it does not take into account the heat lost by evaporative cooling of the CFC.

4.3.5 Results & discussions

The calculations referred to in this chapter are steady state. Three scenarios have been analysed.

A) Normal condition, with no joint defects in order to have a reference in terms of temperature distribution and thermal flux distribution in the tiles.
B) With several kinds of detachment, in order to establish the worst detachment allowable in terms of position and amplitude.
C) With the condition used in option B), changing the thickness of the cooling channel, in order to determine the influence of the thickness of the tube on the WHF when the tile is damaged (detached)

4.3.5.1 Nominal case for Well-attached Tile (case A)

A preliminary analysis to verify the loading and boundary options in the normal condition has been carried out. The fig 4.3.5.1.1 shows the distribution of the temperature and fig 4.3.5.1.2 and 4.3.5.1.3 the heat flux distribution for the steady-state condition with the nominal load as described in the previous paragraphs and without detachment of the cooling channel.

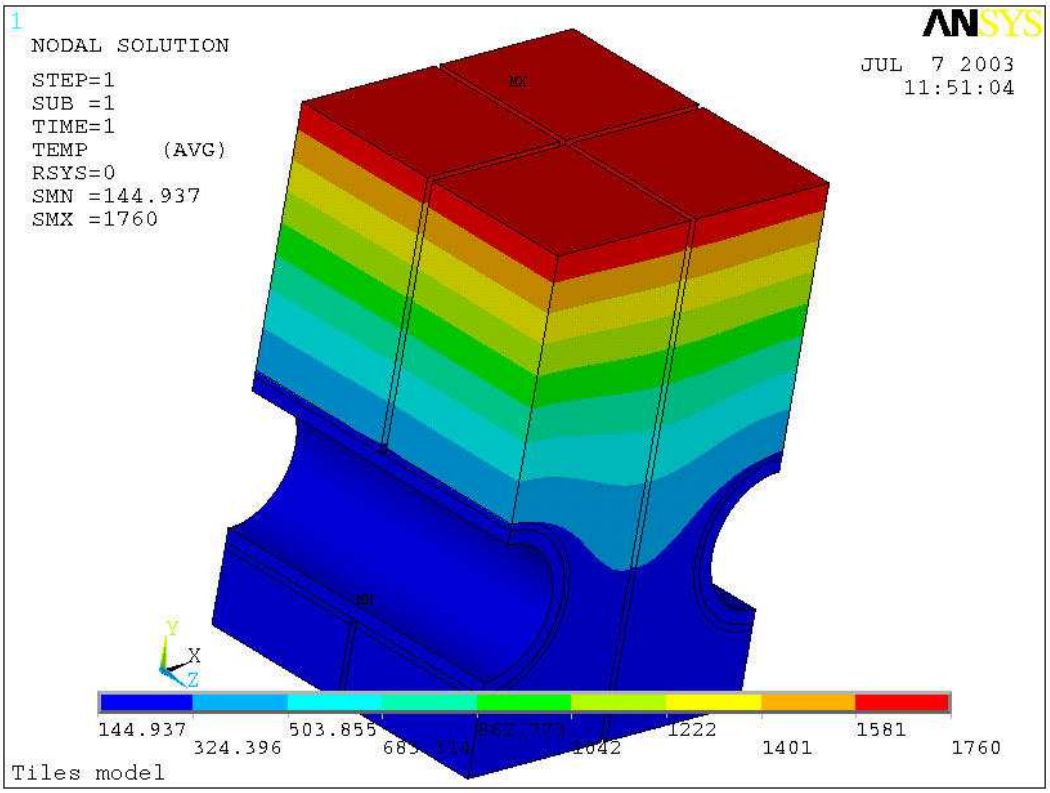

Fig. 4.3.5.1.1 Temperature distribution [°C] in nominal condition.

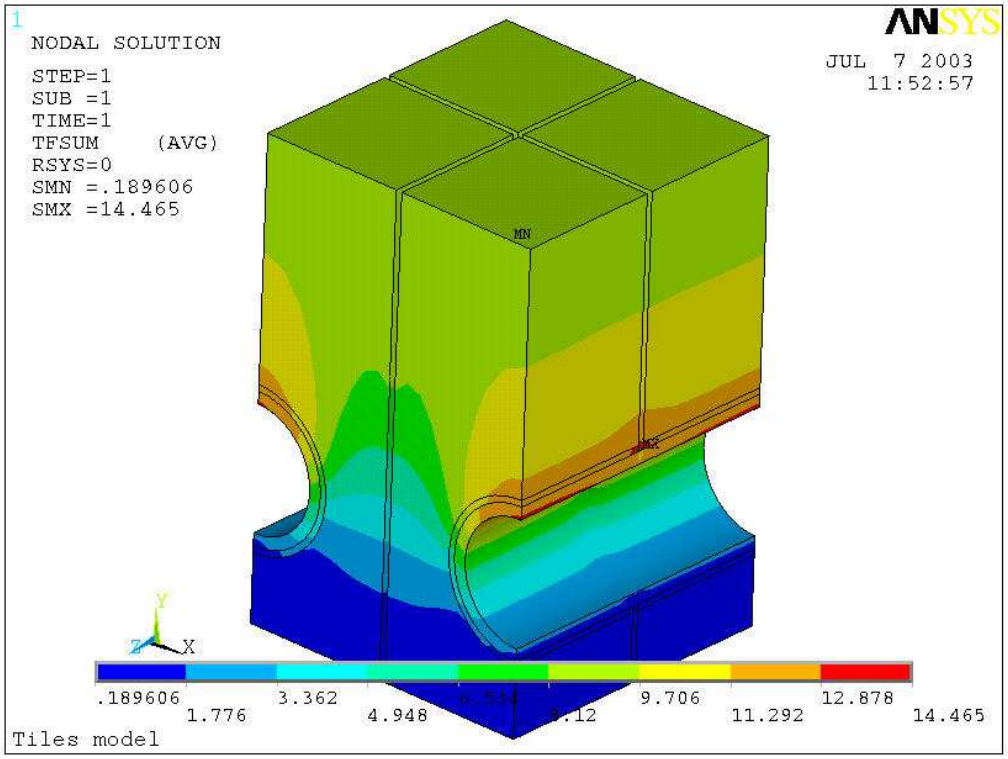

Fig 4.3.5.1.2 Thermal flux distribution [MW/m^2] in nominal condition.

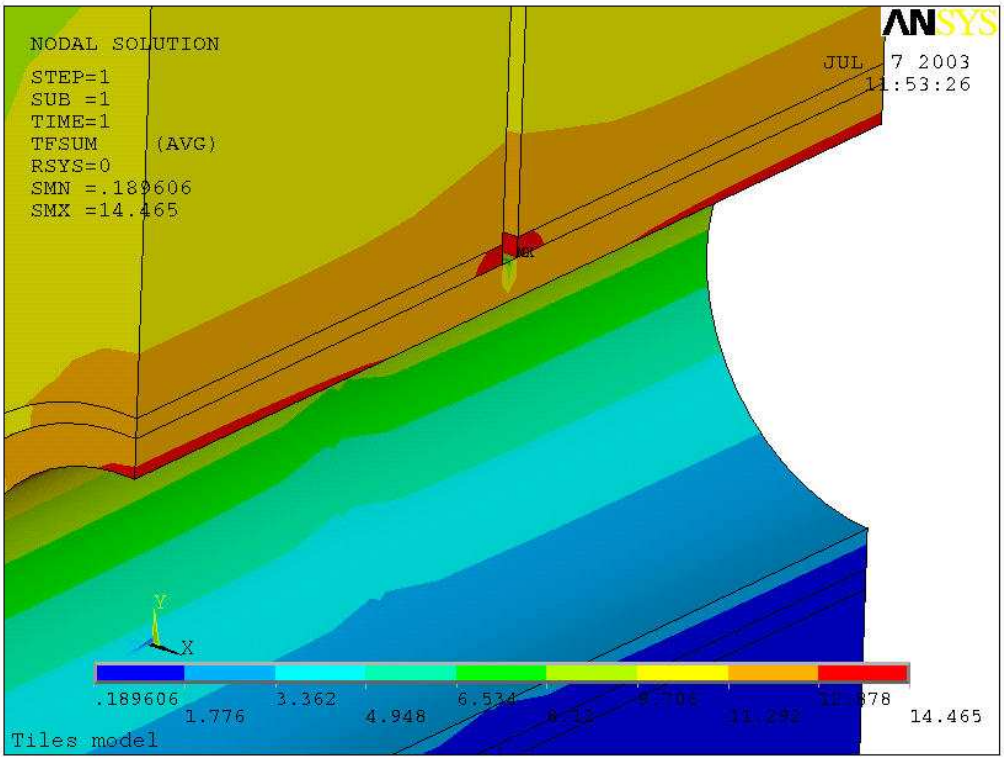

Fig 4.3.5.1.3 Thermal flux distribution [MW/m^2] in nominal condition.

Note that there is a good agreement in the distribution of the temperature between the 3D and 2D [7] analysis.

4.3.5.2 Effect on Wall Critical Heat Flux (WCHF) of Joint Defect (case B)

A degraded joint is likely to be caused by local circumferential defects either in the joint itself or in the CFC adjacent to the joint, while elsewhere, good thermal contact is maintained. A number of analyses were performed with a 2D model [7] in an attempt to establish the angular value of good contact between the Cu tube and the tile that causes the CHF limit to be reached at the tube to coolant boundary. The 2D analyses show that even with a contact of only 18° (a length of ≈ 2 mm) at 12 o'clock the heat flux at the coolant interface is less than the CHF.
This report starts from the values found in the previous 2D analyses. Axially, is most probable to have a defect in the edge where the cooling pipe comes out from the monoblock. This will give localised peaking of the heat flux at the tube to coolant interface, and in the worst case scenario it is postulated that the ~ 35MWm^{-2} CHF limit could be exceeded.
The detachment has been modelled using the dummy material (see chap. 4.3.3). It is supposed that the detachment is localised between the pure copper layer and the CFC on the CFC. The EUPITER 4.2 code was used to establish the CHF limit. The picture below shows the temperature distribution and the thermal flux distribution of the tiles when the contact between the monoblock and the cooling pipe is 30° (a horizontal of ≈ 3.5 mm)

per 3 mm in axial direction. It has been supposed that the axial detachment start from the external side of the monoblock hence, 3 mm of axial attachment are in the middle of the monoblocks (see fig. 3.2.3).

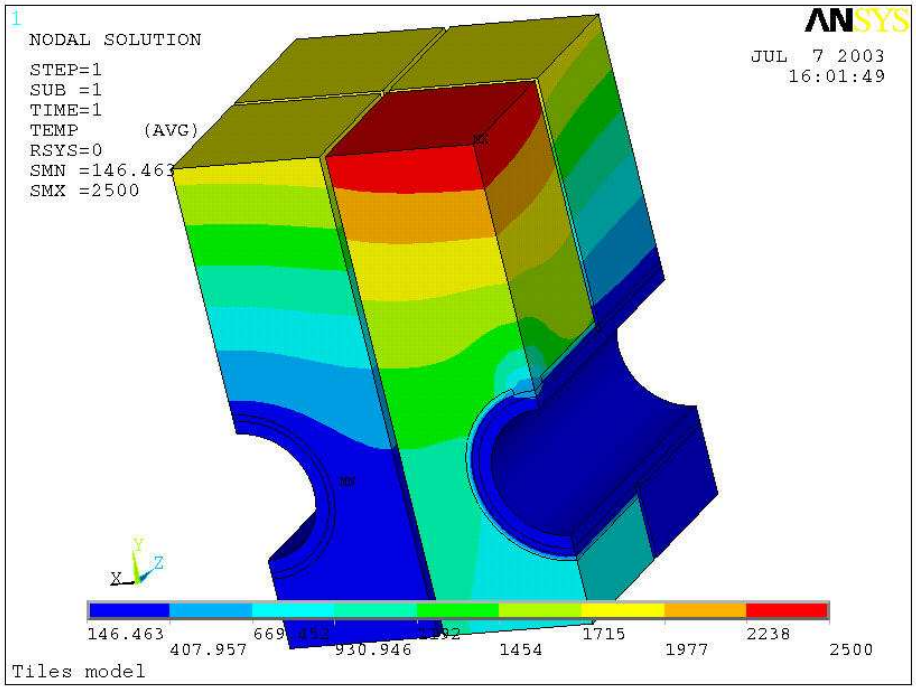

Fig. 4.3.5.2.1 Temperature distribution with the tile attached in the middle, at the top of the cooling channel

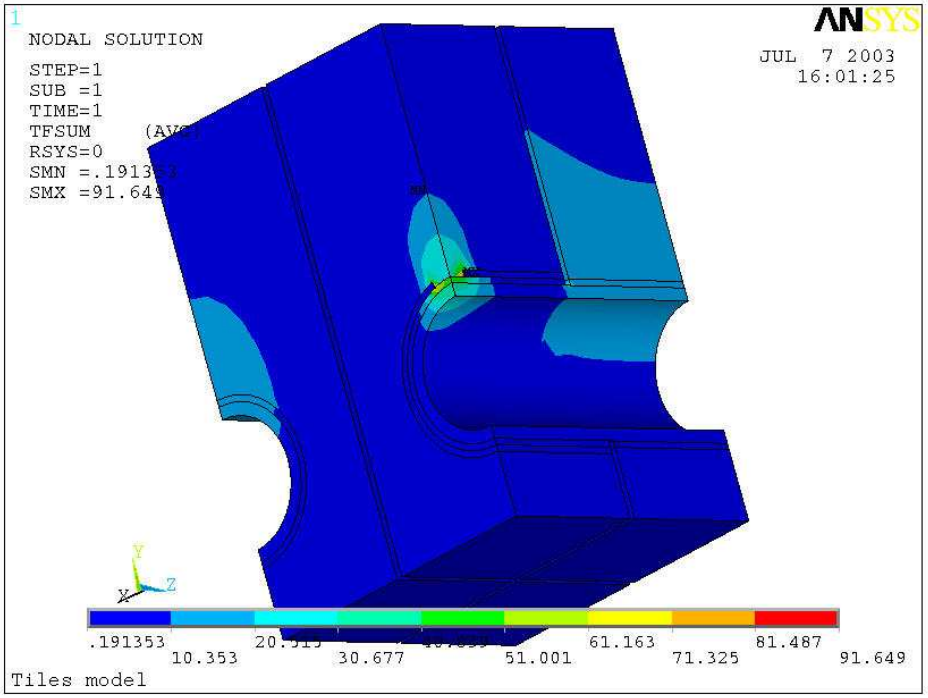

Fig. 4.3.5.2.2 Thermal flux distribution [MW/m^2] with the tile attached in the middle, at the top of the cooling channel.

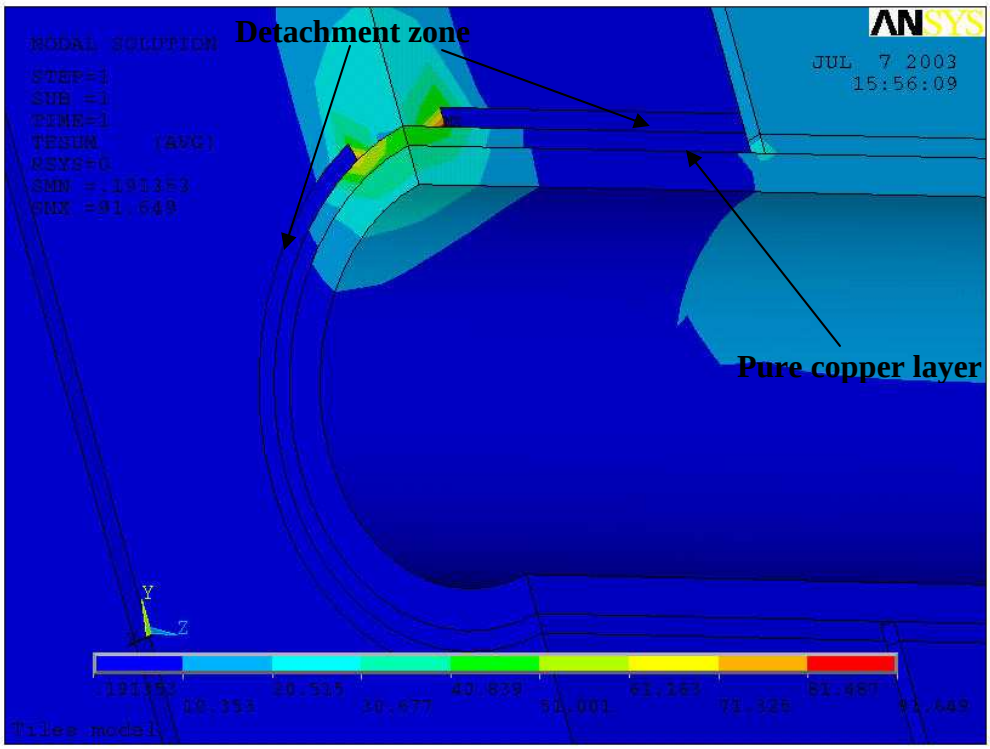

Fig. 4.3.5.2.3. Detail of the thermal flux distribution when the tile is attached in the middle, at the top, of the cooling channel. The heat flux at the coolant interface is ≈30 MW/m^2, < CHF (35 MW/m^2).

4.3.5.3 Studies on the influence of the thickness of the cooling pipe in the heat flux when the monoblock is partially detached from its cooling channel (case C)

Analyses have been carried out looking at the effect that changes in wall thickness have on the heat flux (WHF- Wall Heat Flux) in the damaged tile, in particular, in the region of the copper tube to coolant interface. All the other parameters have been frozen in order to have a direct indication of the heat flux variation with the thickness of the copper tube. The analysis has been done in two steps. In the first step it has been increased the thickness of the cooling channel of CuCrZr from 0.5 mm to 1.5 mm. In the second step it has been increased the layer of the pure copper from 0.5 mm to 1.5 mm. Fig. 4.3.5.3.1 shows the behaviour of the heat flux on the copper tube near the water where the flux is largest, at 12 o'clock in the middle of the monoblock.

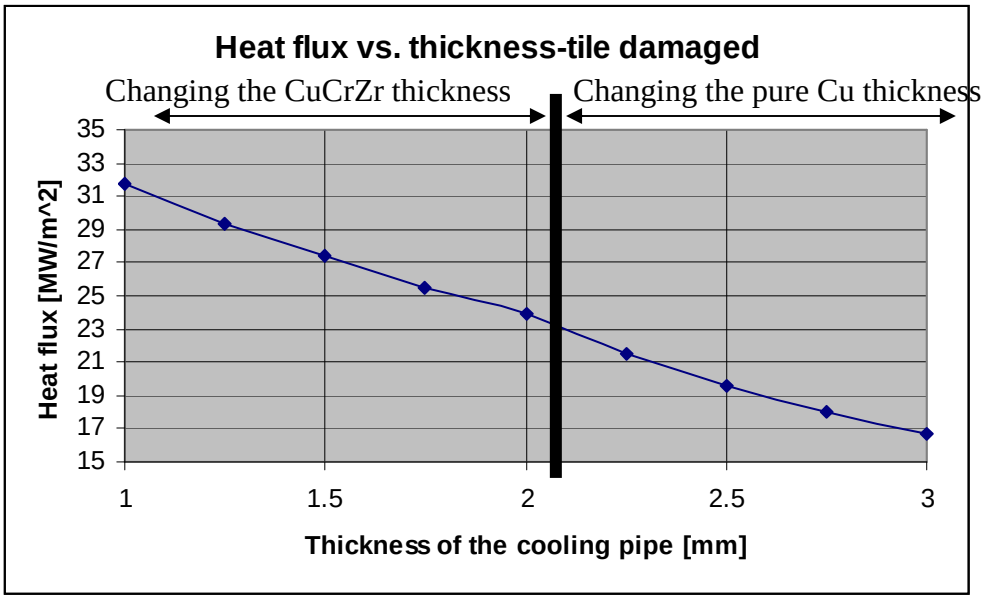

Fig. 4.3.5.3.1 Behaviour of the heat flux in the copper tube versus the thickness of the cooling pipe when a tile is detached. On the right side when is changed the CuCrZr pipe thickness, on the left side when is changed the pure Cu layer thickness.

The following pictures show the temperature distribution and the thermal flux distribution when the thickness of the pure copper tube is 0.5 mm and the thickness of the CuCrZr is 0.5 mm.

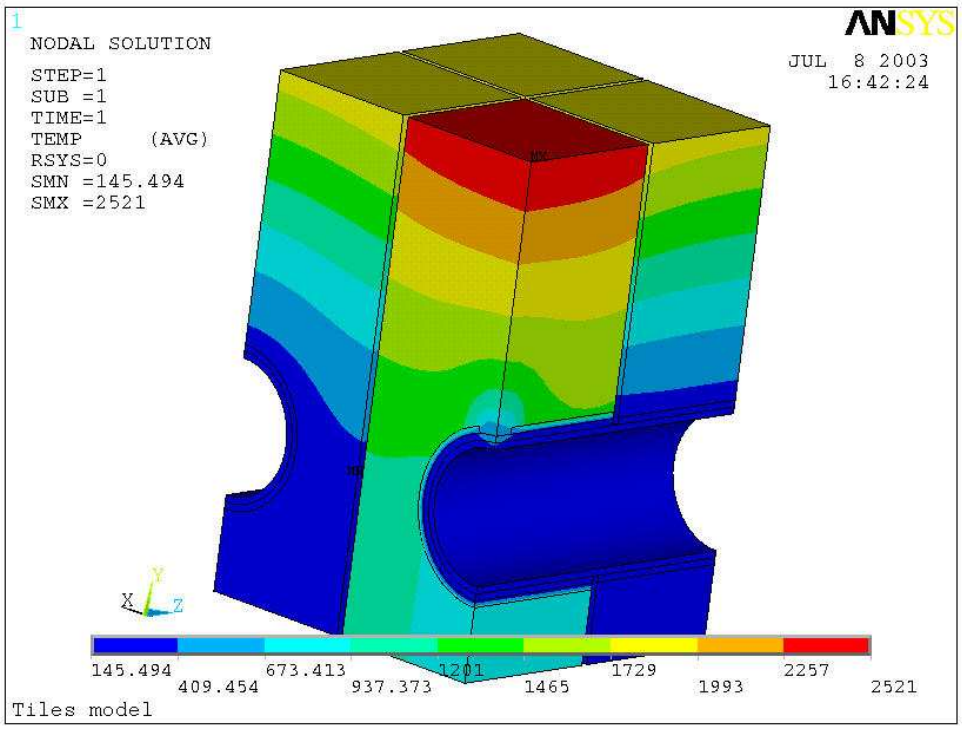

Fig. 4.3.5.3.2. Temperature distribution [°C] in the damaged tile when the thickness of the cooling pipe is 1 mm (0.5 mm in the pure Cu layer, 0.5 mm in the CuCrZr pipe).

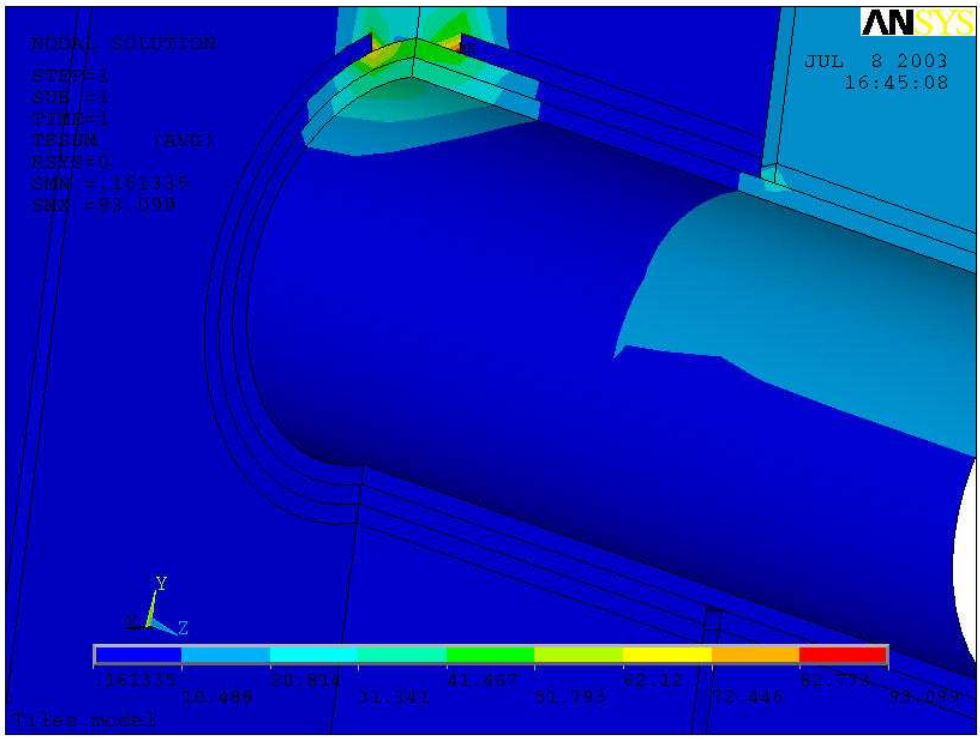

Fig. 4.3.5.3.3. Thermal flux distribution [MW/m^2] in the damaged tile when the thickness of the cooling pipe is 1 mm (0.5 mm in the pure Cu layer, 0.5 mm in the CuCrZr pipe).

The following pictures show the temperature distribution and the thermal flux distribution when the thickness of the pure copper tube is 1.5 mm and the thickness of the CuCrZr is 1.5 mm.

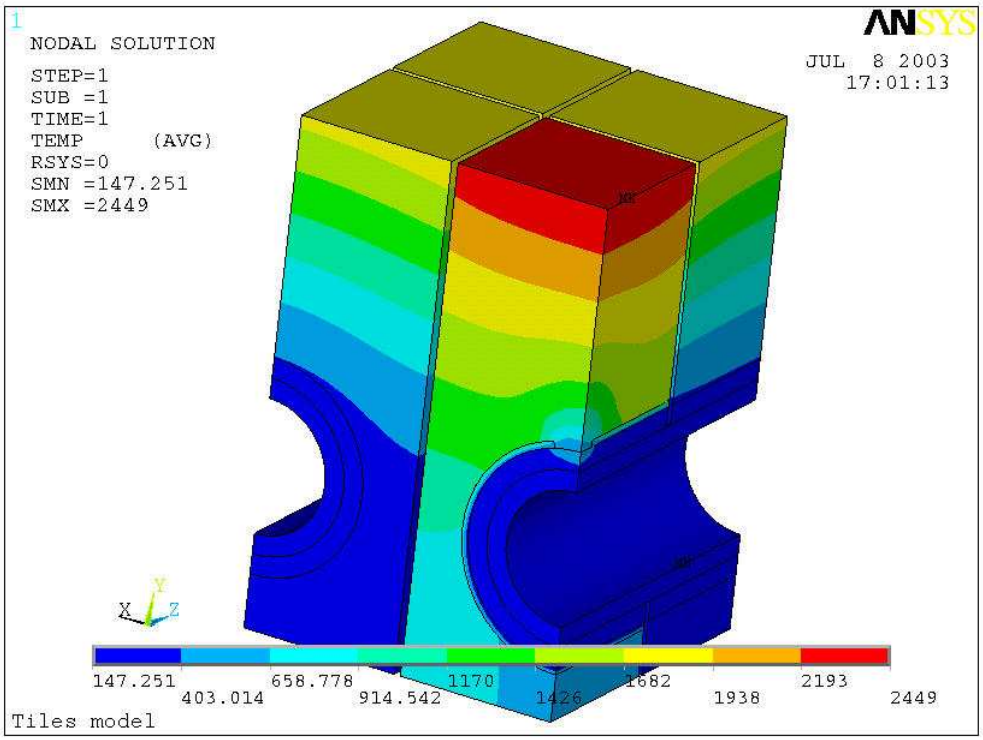

Fig. 4.3.5.3.4. Temperature distribution [°C] in the damaged tiles when the thicknesses of the cooling pipe is 3 mm (1.5 mm in the pure Cu layer, 1.5 mm in the CuCrZr pipe).

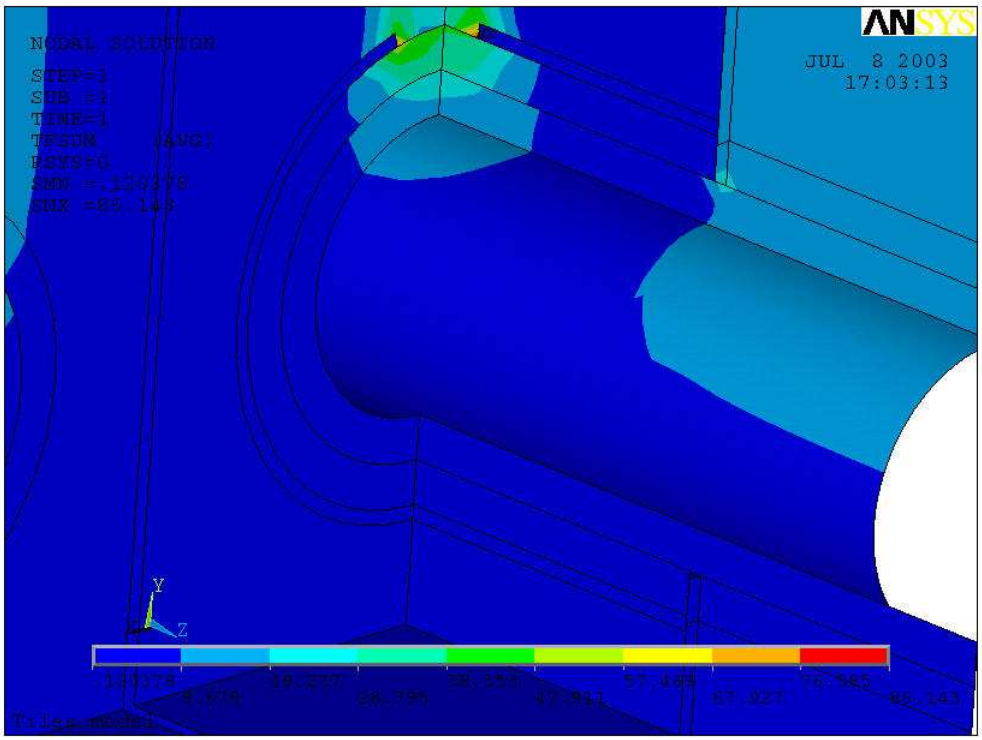

Fig. 4.3.5.3.5. Thermal flux distribution [MW/m^2] in the damaged tile when the thickness of the cooling pipe is 3 mm (1.5 mm in the pure Cu layer, 1.5 mm in the CuCrZr pipe).

4.3.6 Final considerations

It appears, even with a very limited contact between CFC and Cu tube, that the heat flux is redistributed in the Cu tube such that the burn-out limit of 35 MWm^{-2} is not reached when a heat flux of 10 MWm^{-2} is applied. The study showed that the worst case, from the CHF point of view, is when there is local attachment in the middle of the monoblock at the top of the tube (12 o'clock) nearest the irradiated surface (see figures Fig. 4.3.5.2.1 - Fig. 4.3.5.2.3). This is explained by the fact that the path from the irradiated surface to the cooling channel is shorter and the heat cannot be efficiently removed by radiation to the neighbouring tiles. However, the analysis shows that with a heat flux of 10 MWm^{-2} even with a contact of only 30° (a length of ≈ 3.5 mm) at 12 o'clock per 3 mm in axial direction the heat flux at the coolant interface is less than the CHF.
When the monoblock is damaged and it is attached to the cooloing pipe in the middle of the monoblock at the top of the tube (12 o'clock), the thicker the tube the lower the maximum value of the heat flux near the film. By increasing the wall thickness from 1 to 3 mm there is a significant reduction in peak WHF. However, increasing the tube thickness will increase residual manufacturing stresses. A limit of 2.5 mm (1 mm of pure copper and 1.5 mm of CuCrZr) has been suggested from the industry involved in this business.

4.4 SATIR test simulation to evaluate a detectable defect in the tile

4.4.1 General considerations

The aim of this chapter is to investigate whether or not the defects in the joints, that might prejudice normal operation of the machine, can be identified using SATIR technique.
A monoblock with different kind of defects has been analysed assuming a constant value of the heat transfer coefficient. The defects analysed are of 180° on the top and on the bottom, 90° on the top on the side and on the bottom and a defect of 45° all around the cooling channel and poloidaly fully extended. Some analyses have been done also with a poloidal extension of the defect ½ of the total length of the tile.
There are several parameters that can introduce errors in the measurement of the ΔT between the reference and the tested monoblock during SATIR test. An important factor is the variation in the thermal conductivity of the CFC. From previous analyses a ΔT of ≈ 6 °C has been found using the most extreme material property conditions (highest and lowest thermal conductivity) i.e. ± 3 °C on the value obtained using the average value of the thermal conductivity.

4.4.2 The model

The ANSYS models shown in fig.4.4.2.1 and 4.4.2.2 have been used to analyse the behaviour of the monoblock during the analyses described in the above paragraph. The

dimensions of these models (shown in fig 4.4.2.1) have been slightly modified and still will be modified. It is important to point out that the diameter as well as the thickness of the cooling channel has been increased respectively from 10 to 12 mm and from 1 to 1.5 mm. The height, the width and the depth of the monoblock are respectively 46, 28 and 20 mm. The cooling channel (CuCrZr in green) has an outer diameter of 15 mm and an inner diameter of 12 mm. The thickness of pure copper to join the Cu alloy to the CFC is now 1 mm instead than 0.5 mm. The distance between the irradiated surface and the cooling channel is 19.5 mm. The gap between adjacent monoblocks is 0.5 mm.

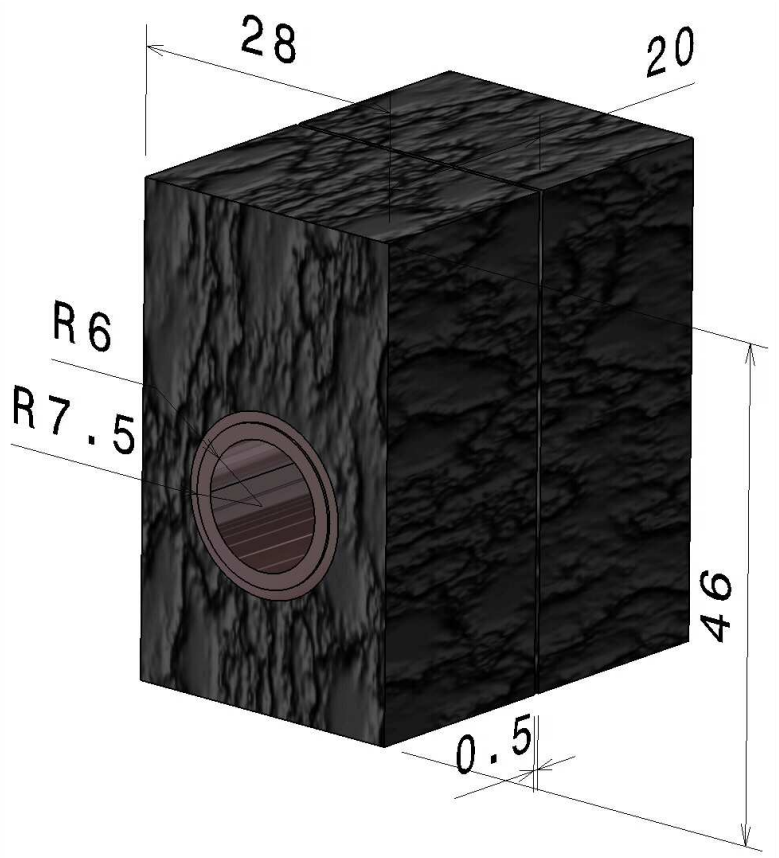

Fig. 4.4.2.1 Dimension of the monoblock

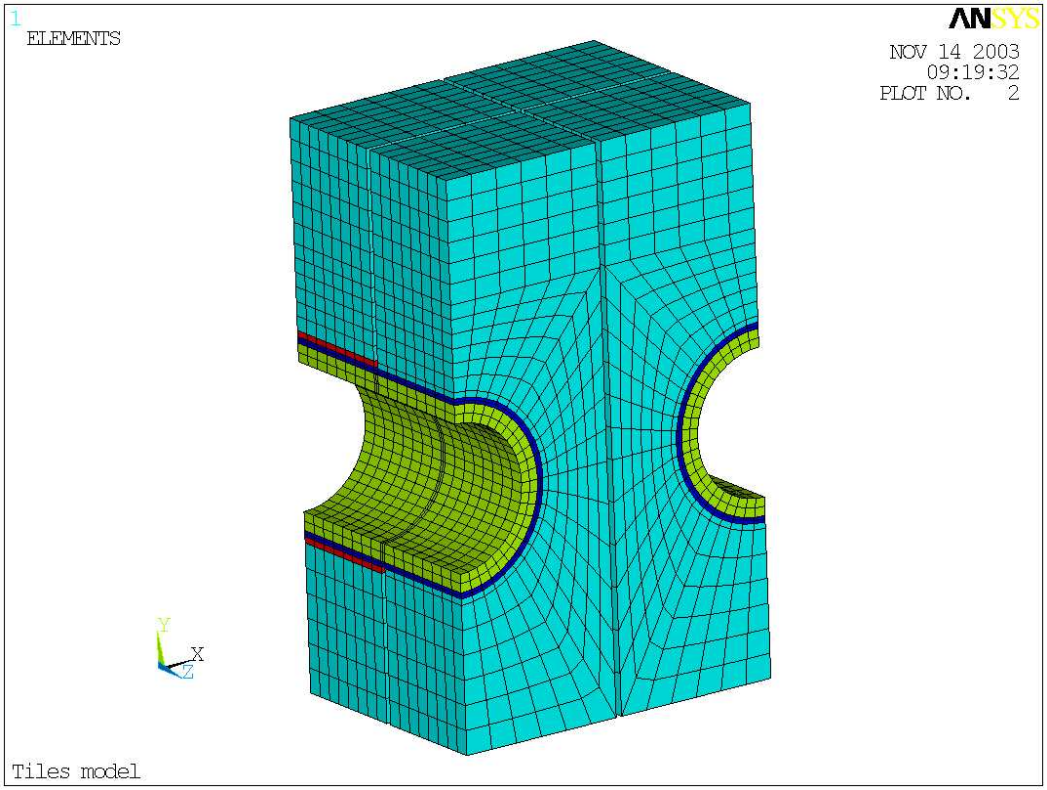

Fig. 4.4.2.2 3D FE Model of the monoblock to analyse symmetric defects

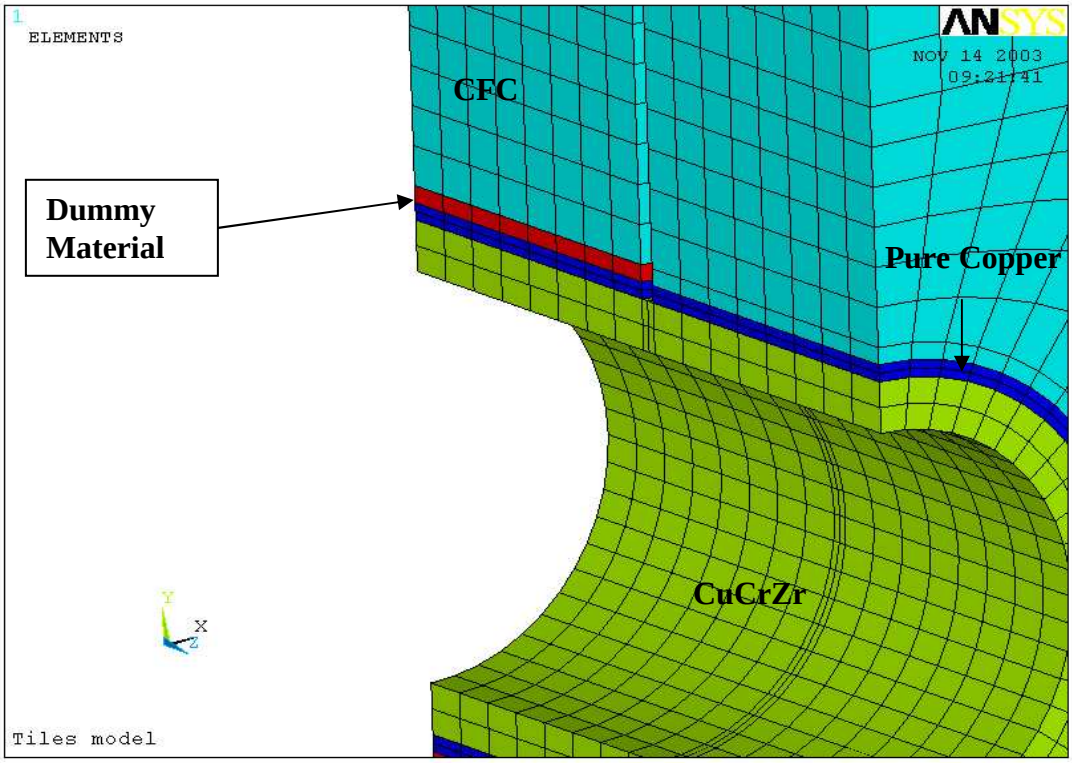

Fig. 4.4.2.3 Detailed 3D FE Model of the monoblock

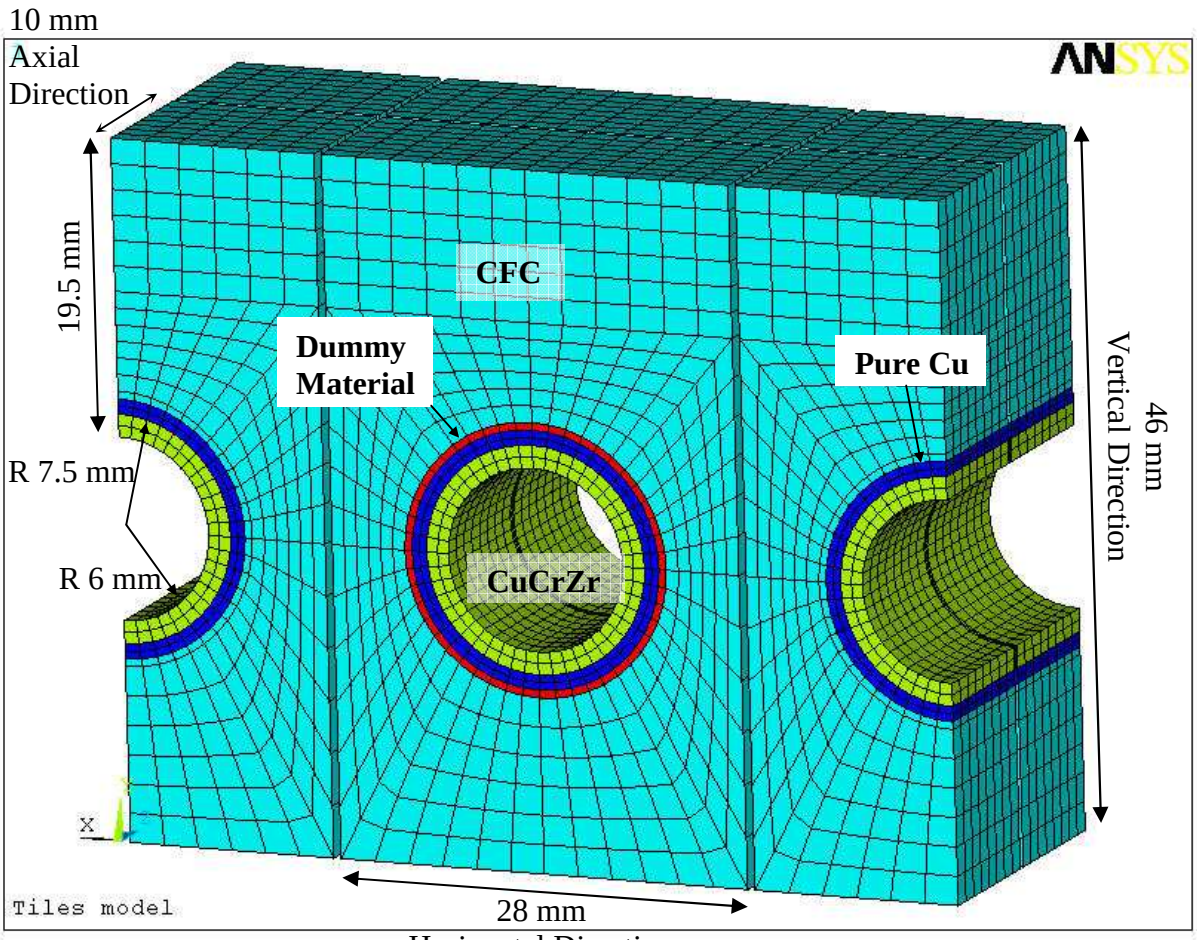

Fig. 4.4.2.4 3D FE Model of the monoblock to analyse asymmetric defects

4.4.3 The material properties

The materials used are **C**arbon **F**iber **C**omposite (CFC) for the tile, Oxygen Free Copper (OF Cu) for the layer between the cooling channel and the CFC, CuCrZr for the cooling tube and a "dummy" material implemented into the FE model to simulate detachment.
After a study of the database of measured values of the thermal conductivity, the minimum, temperature dependent material properties obtained from a batch have been used to carry out the analyses, these values are summarised in the tables 4.4.3.1, 4.4.3.2 and 4.4.3.3.
Note that the CFC is orthotropic and the value of the conductivity for 3500 °C is an extrapolation.

CFC SEP NB31	T=100 °C	T=800 °C	T=1500 °C	T=3500 °C
Thermal conductivity along horizontal direction [W/mm*K]	0.117	0.057	0.050	0.050
Thermal conductivity along vertical direction [W/mm*K]	0.279	0.135	0.115	0.080
Thermal conductivity along axial direction [W/mm*K]	0.105	0.055	0.046	0.045
Density [Kg/mm^3]	1.958e-6	-	-	-

Table 4.4.3.1 Material property of CFC SEP NB31 (previously called N312C)

CuCrZr copper	T=20 °C	T=200 °C	T=500 °C	T=700 °C
Thermal conductivity [W/mm*K]	0.320	0.320	0.320	0.320
Density [Kg/mm^3]	8.86e-6	-	-	-

Table 4.4.3.2 Material property of CuCrZr Copper

Pure Copper Oxygen free	T=20 °C	T=250 °C	T=500 °C	T=800 °C
Thermal conductivity [W/mm*K]	0.390	0.378	0.364	0.345
Density [Kg/mm^3]	8.95e-6	8.81e-6	8.67e-6	8.49e-6

Table 4.4.3.3 Material property of pure Copper Oxygen free

Degradation in the quality of the CFC-Cu joint has been modelled by changing the conductivity of some elements. In the FE model a "dummy" material (shown in red in fig. 4.4.2.3) with a low conductivity (see Table 4.4.3.4) has been used to simulate detachment. The "*High*" thermal conductivity of the dummy material corresponds to a well-attached monoblock. To simulate local detachment of the joint the thermal conductivity of the dummy material is set to "*Low*" (insulation).
For the "Low" conductivity a conservative value of 0.0013 $Wmm^{-1}K^{-1}$ has been chosen acting over a length of 0.5 mm. It comes from consideration about thermal contact resistivity (see chap. 4.3.3).

Temperature		100 °C	800 °C	1500 °C	3500 °C
Thermal conductivity *High (CFC-no detachment)* *Low*	 $Wmm^{-1}K^{-1}$ $Wmm^{-1}K^{-1}$	 .105÷.279 .0013	 .055÷.135 .0013	 .046÷.115 .0013	 .045÷.080 .0013
Density	$Kg\ mm^3$	1.958e-6	1.958e-6	1.958e-6	1.958e-6

Table 4.4.3.4 Material property of the dummy material.

4.4.4 Loading and boundary conditions

The SATIR test has been already described in chap. 4.2. The fig. 4.4.4.1 shows the scheme of the method.

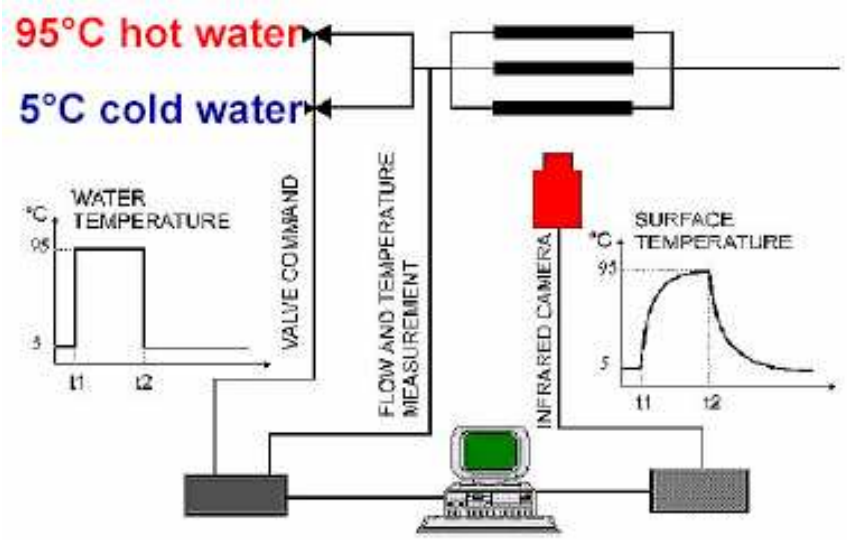

Fig. 4.4.4.1 Scheme of the SATIR test.

Cold water (5 °C) is sent to the monoblocks, suddenly the temperature of the water is increased to 95 °C, past a certain time the temperature of the water is decreased again to 5 °C. An infrared camera pointed on the monoblocks, read the variation of the surface temperature of the monoblocks. The behaviour of the surface temperatures of the tiles during the transient are compared with the same curve obtained for the reference tile. A difference during the ascending or descending curve between the reference and the tested tiles is considered as a defect in the tiles.
A quarter of a monoblock has been modeled with its 3 neighbouring monoblocks where possible. Hence, the "symmetric" model has 4 planes of symmetry, one per each lateral side. Figure 4.4.2.2 shows the model used.
For the SATIR test simulation, the heat comes from the cooling channel; a fixed heat transfer coefficient (=0.07934 MW/(m^2*K)) has been applied to the cooling channel. The emissivity of the CFC is 0.8 and the temperature of the surrounding environment has been fixed in 25 °C.

4.4.5 Results & discussions

An analysis of the tile has been done in order to establish the surface temperature values for the reference tile. Several points have been chosen in the reference tile, on the side and on the top and bottom surfaces, where the temperature of the monoblock is compared with the monoblock to test (see fig. 4.4.5.1). To avoid undesirable border effects the points chosen are not at the edges of the model.

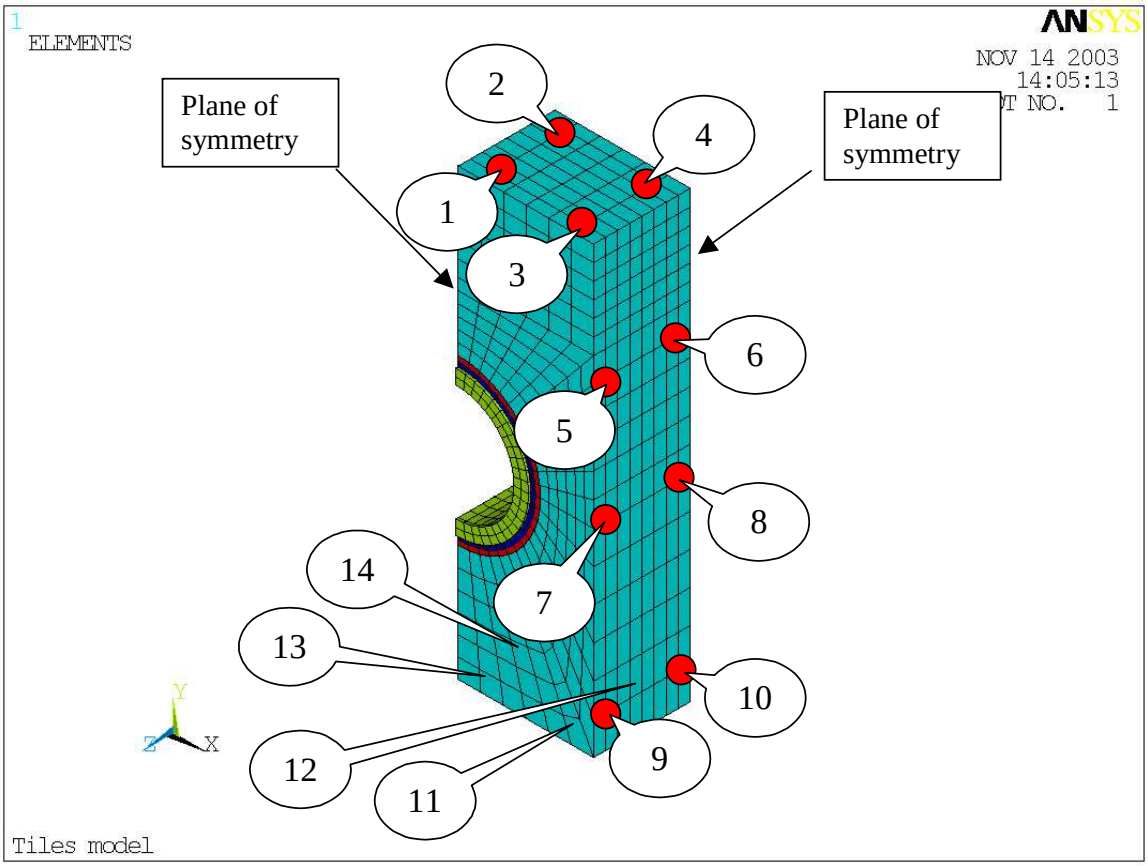

Fig. 4.4.5.1 Detection point where to compare the temperature.

The figures below report the behaviour, in term of temperature, of the 14 point of the reference tile function of the time when the temperature is switched from 5 to 95 °C (ascendant zone) and vice versa (descendent zone).

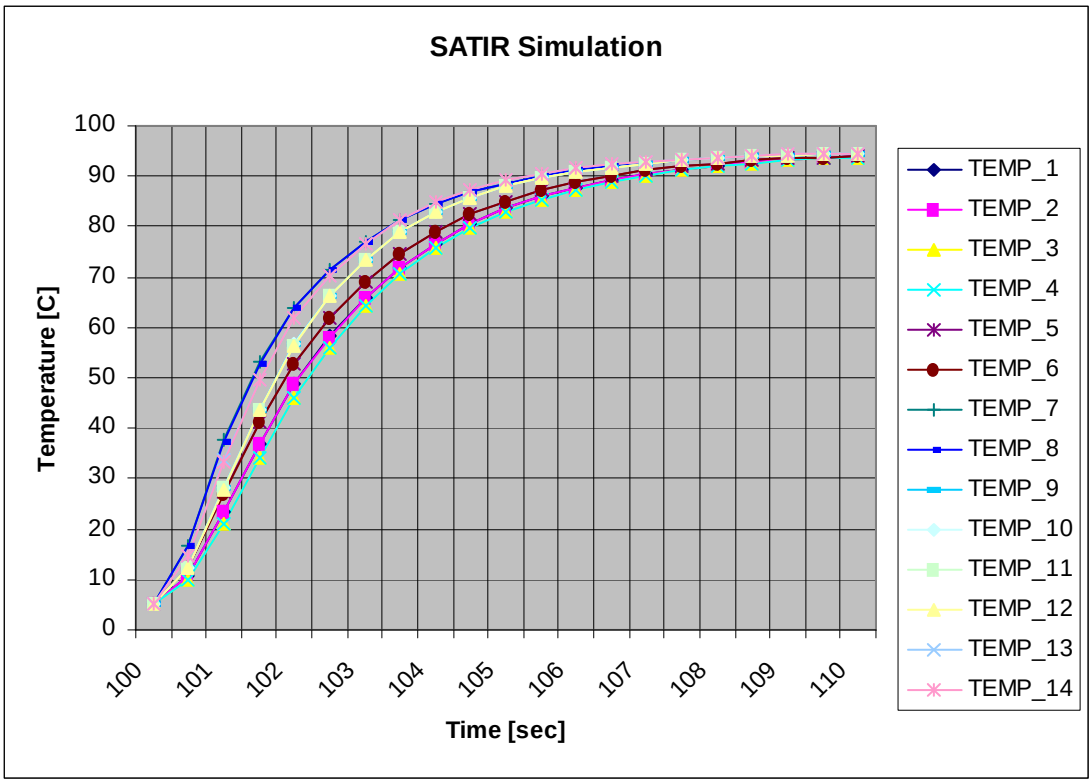

Fig. 4.4.5.2 Details of the ascendant zone of the 14 points of the reference tile

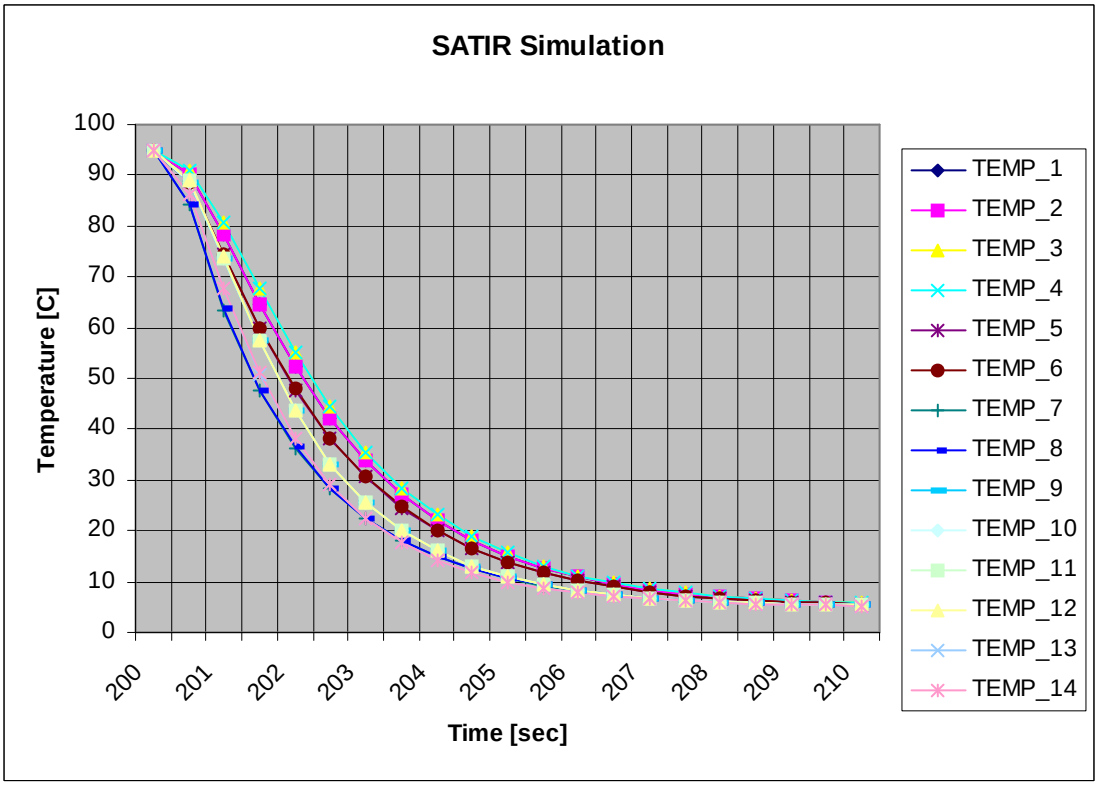

Fig. 4.4.5.3 Details of the descendent zone of the 14 points of the reference tile

The cases analysed are reported in the figures below:

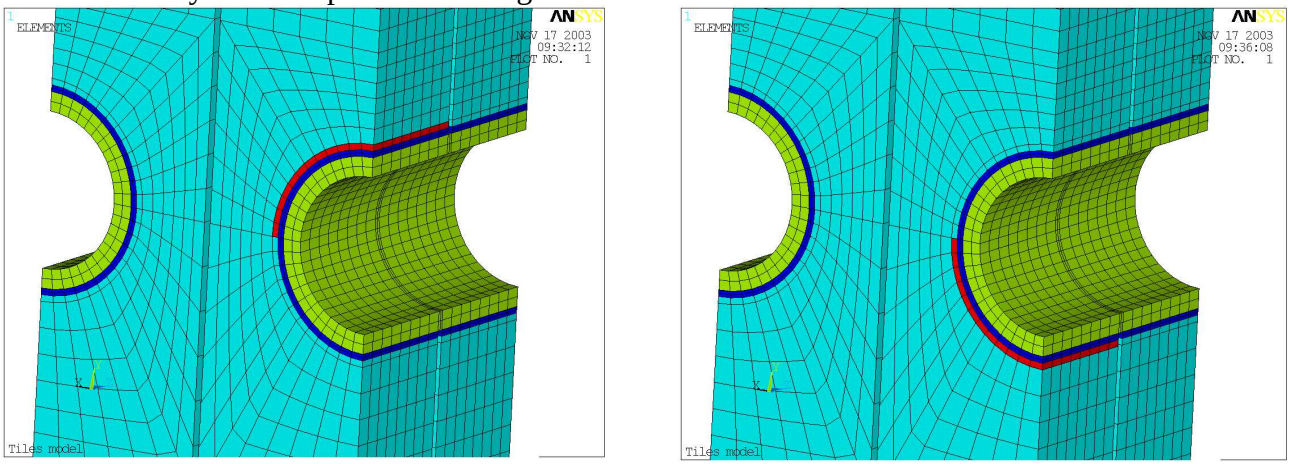

Fig. 4.4.5.4 Defect of 180° on the top and on the bottom (the defect is visible in red)

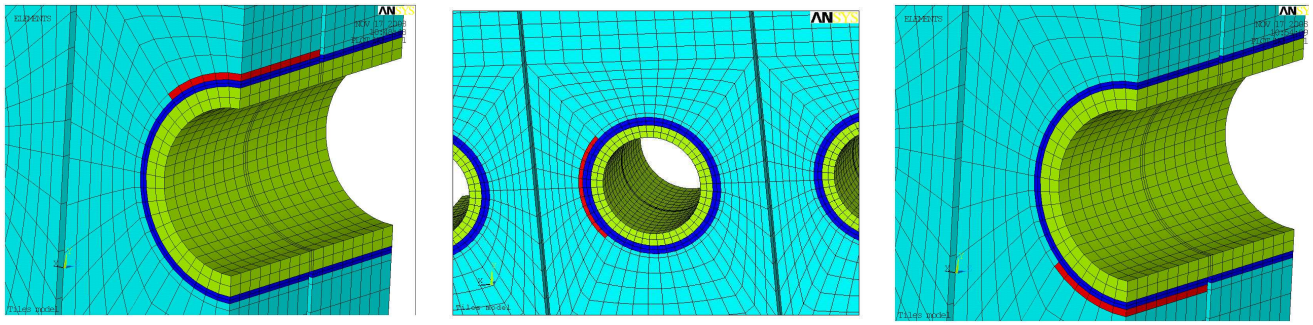

Fig. 4.4.5.5 Defect of 90° on the top, on the side and on the bottom (the defect is visible in red)

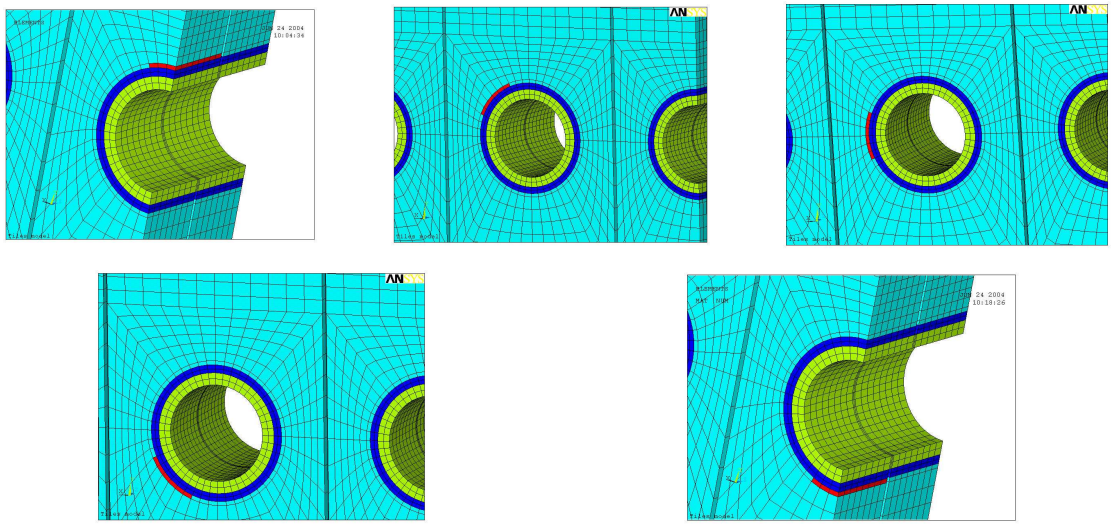

Fig. 4.4.5.6 Defect of 45° on the top, on the side and on the bottom (the defect is visible in red)

The defects are all along the axial direction. The table below report the maximum ΔT between the reference and the sample tile for the 14 points analysed. The table below contains only the descendant values of ΔT.

	Descendant zone Maximum Delta T [°C]													
Detection Point	1	2	3	4	5	6	7	8	9	10	11	12	13	14
Defect on 180° on top	**35**	**35**	33	33	30	30	15	15	5	5	5	5	3	3
Defect on 180° on bottom	2	2	3	3	5	5	16	16	31	31	32	32	**38**	**38**
Defect on 90° on top	**16**	**16**	13	13	10	10	3	3	1	1	1	1	0	0
Defect on 90° on side	2	2	5	5	10	10	**18**	**18**	9	9	8	8	3	3
Defect on 90° on bottom	0	0	0	0	1	1	3	3	10	10	11	11	**19**	**19**
Defect on 45° on top	**5**	**5**	3	3	2	2	1	1	0	0	0	0	0	0
Defect on 45° on upper side	3	3	5	5	**6**	**6**	3	3	1	1	0	0	0	0
Defect on 45° on middle side	1	1	1	1	3	3	**7**	**7**	2	2	2	2	1	1
Defect on 45° on lower side	0	0	0	0	1	1	3	3	**6**	**6**	**6**	**6**	4	4
Defect on 45° on bottom	0	0	0	0	0	0	0	0	2	2	2	2	**6**	**6**

Table 4.4.5.1. A summary of the results obtained in the simulation of SATIR method.

In the table above the maximum values are reported in bold.

4.4.6 Final considerations

The analyses carried out in this chapter will be useful to establish logic to set up reasonable acceptable criteria for SATIR testing of monoblock tiles. The analyses done on the simulation of the SATIR test shows a defect of 180° is certainly detectable. A defect of 90° is also detectable when the ΔT evidence of all flux exposed surfaces of the monoblock is taken into account. In terms of linear dimensions, a defect of 90° corresponds to a detachment of 11 mm around the cooling channel per 20 mm along the channel (practically the whole axial length of the monoblock). To detect a defect of 45° it is required a better accuracy. In fact a ΔT of 6-7 °C should be detectable to identify a defect of 45°. The defects studied in these analyses have been considered fully extended along poloidal direction. Some analyses have been done to check if a defect not fully extended along poloidal direction can be detected. The conclusion is that a defect with a poloidal extention of ½ of the total poloidal length can be detected with the same accuracy than a fully extended defect. This is due to the elevated number of points where the temperature of the sample is read and compared with the reference tile (see par. 4.4.5). Some other analyses have been done to check the influence on the ΔT having defects in poloidal adjacent monoblock. The results were that the detection of a defect in a tile is not influenced by the presence of a defect in the adjacent tile.

4.5 The impact of a defect on the behaviour of the tiles

4.5.1 General considerations

In this chapter has been repeated all the series of analysis done in the previous chapter with the scope to investigate the consequence of a defect in a monoblock. Considering that has never been observed a propagation of a crack, the main drive to choose the critical defect is the surface temperature and the Heat Flux on the surface of the cooling channel. In fact, the temperature must remain under certain value because the exponential increasing of the erosion of the CFC due to the temperature and the heat flux between the cooling channel and the water must stay below the Critical Heat Flux (CHF) to prevent burnout events.

4.5.2 The model

The ANSYS models used for this set of analyses is the same used in the previous chapter. For clearness, a brief description with figures will be repeated in this paragraph.
The figures 4.5.2.1 and 4.5.2.2 shown the FE model. The height, the width and the depth of the monoblock are respectively 46, 28 and 20 mm. The cooling channel (CuCrZr in green) has an outer diameter of 15 mm and an inner diameter of 12 mm. The thickness of pure copper to join the Cu alloy to the CFC is now 1 mm instead than 0.5 mm. The distance between the irradiated surface and the cooling channel is 19.5 mm. The gap between adjacent monoblocks is 0.5 mm.

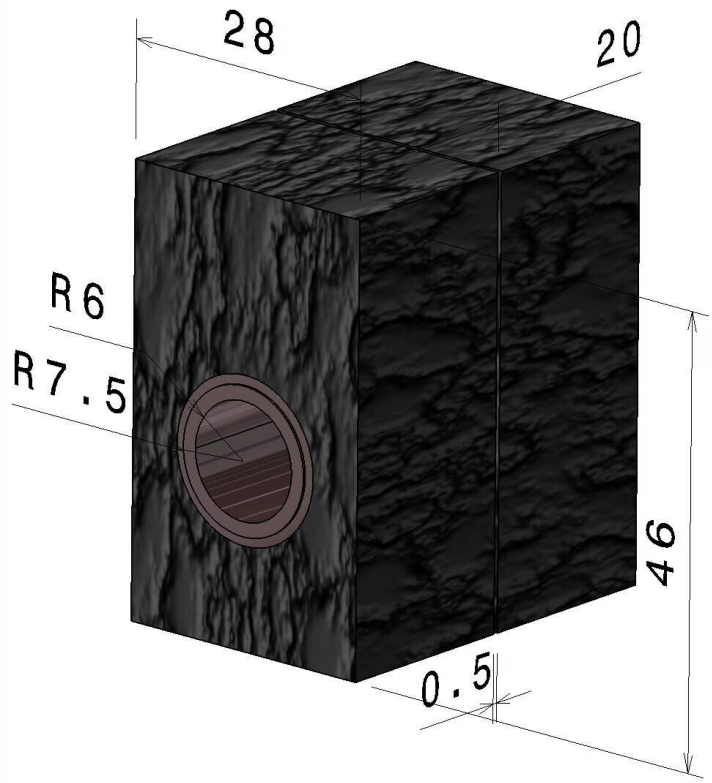

Fig. 4.5.2.1 Dimension of the monoblock

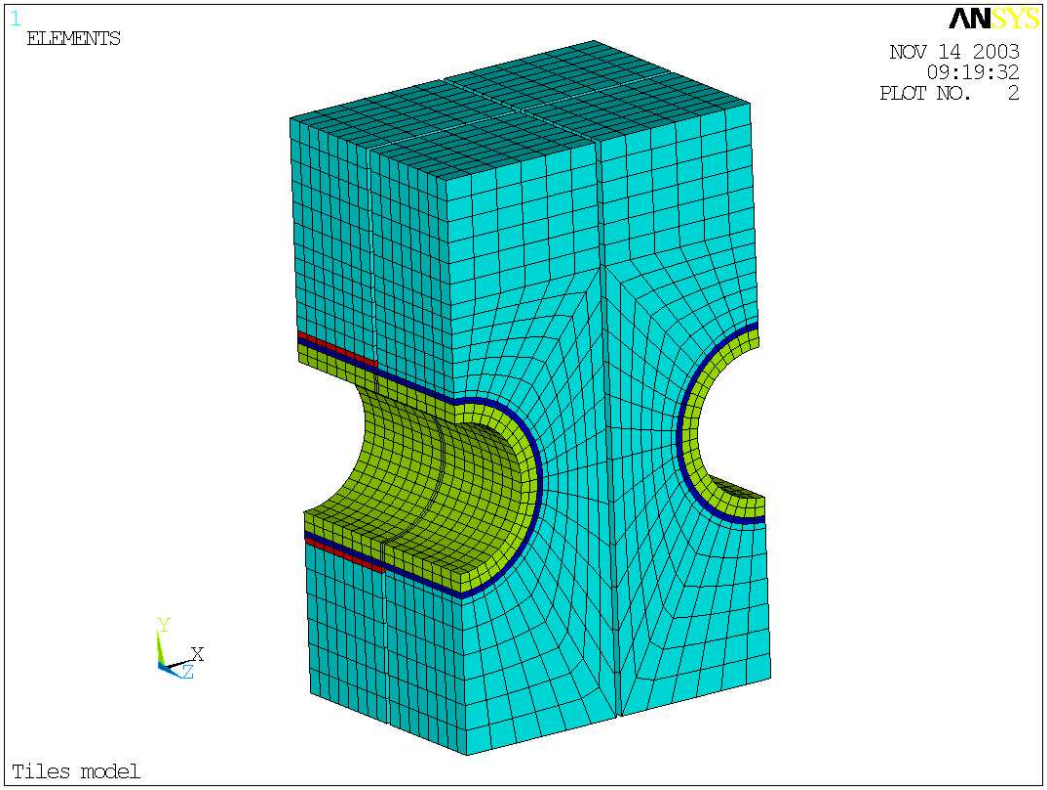

Fig. 4.5.2.2 3D FE Model of the monoblock to analyse symmetric defects

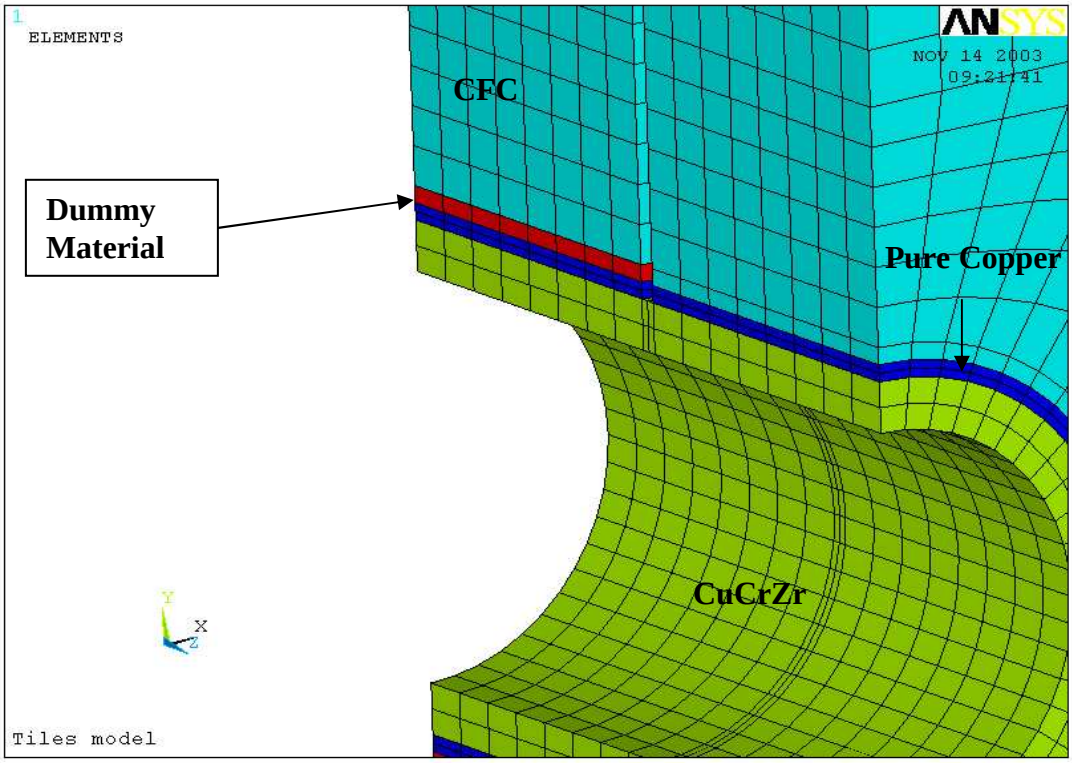

Fig. 4.5.2.3 Detailed 3D FE Model of the monoblock

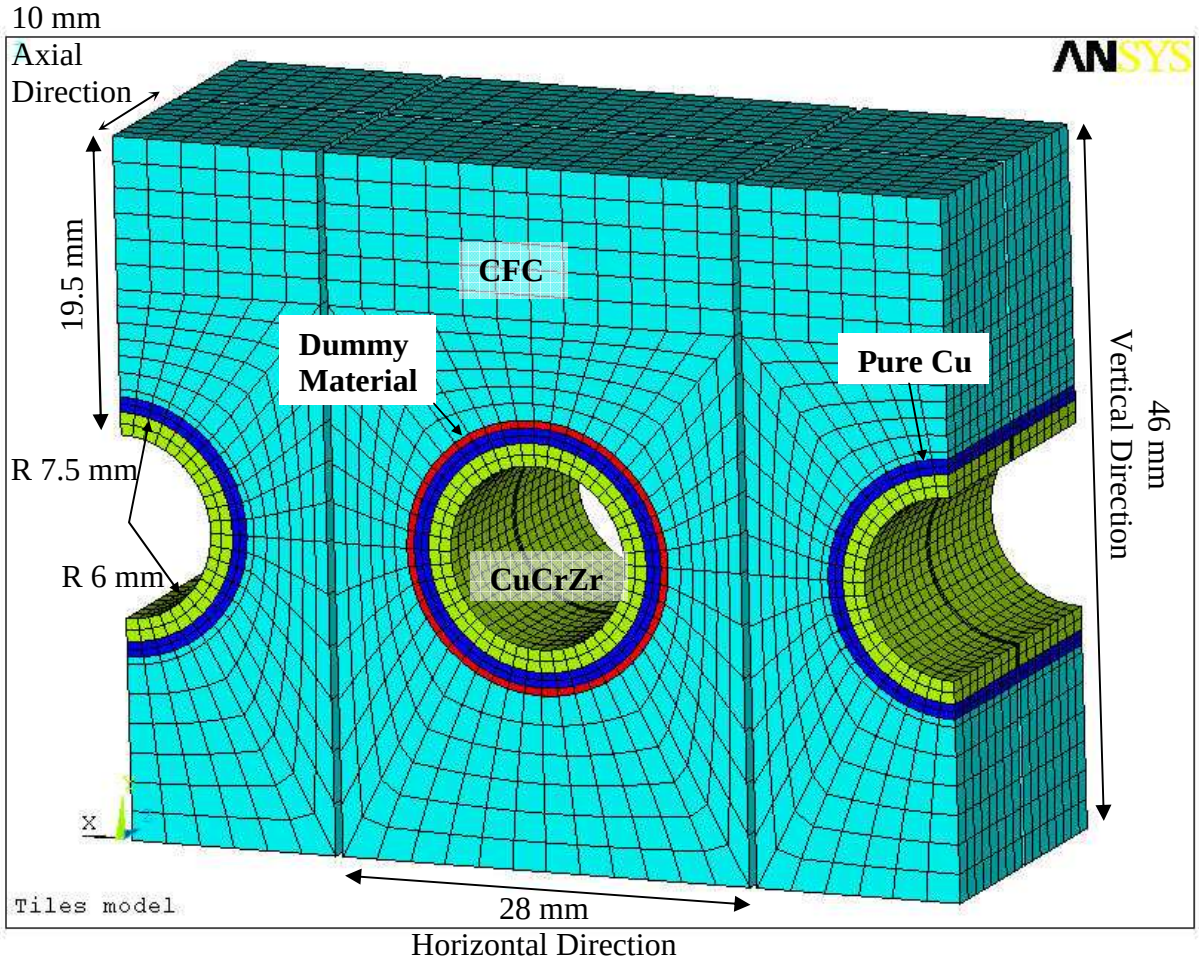

Fig. 4.5.2.4 3D FE Model of the monoblock to analyse asymmetric defects

4.5.3 The material properties

The material properties used for this set of analyses is the same used in the previous chapter. Briefly:

CFC SEP NB31	T=100 °C	T=800 °C	T=1500 °C	T=3500 °C
Thermal conductivity along horizontal direction [W/mm*K]	0.117	0.057	0.050	0.050
Thermal conductivity along vertical direction [W/mm*K]	0.279	0.135	0.115	0.080
Thermal conductivity along axial direction [W/mm*K]	0.105	0.055	0.046	0.045
Density [Kg/mm^3]	1.958e-6	-	-	-

Table 4.5.3.1 Material property of CFC SEP NB31 (previously called N312C)

CuCrZr copper	T=20 °C	T=200 °C	T=500 °C	T=700 °C
Thermal conductivity [W/mm*K]	0.320	0.320	0.320	0.320
Density [Kg/mm^3]	8.86e-6	-	-	-

Table 4.5.3.2 Material property of CuCrZr Copper

Pure Copper Oxygen free	T=20 °C	T=250 °C	T=500 °C	T=800 °C
Thermal conductivity [W/mm*K]	0.390	0.378	0.364	0.345
Density [Kg/mm^3]	8.95e-6	8.81e-6	8.67e-6	8.49e-6

Table 4.5.3.3 Material property of pure Copper Oxygen free

Temperature		100 °C	800 °C	1500 °C	3500 °C
Thermal conductivity *High (CFC-no detachment)* *Low*	 $Wmm^{-1}K^{-1}$ $Wmm^{-1}K^{-1}$	 .105÷.279 .0013	 .055÷.135 .0013	 .046÷.115 .0013	 .045÷.080 .0013
Density	$Kg\ mm^3$	1.958e-6	1.958e-6	1.958e-6	1.958e-6

Table 4.5.3.4 Material property of the dummy material.

4.5.4 Loading and boundary conditions

The heat, on the surfaces of the tile, is due to radiation and to the incident particle flux (see fig. 4.5.4.1).

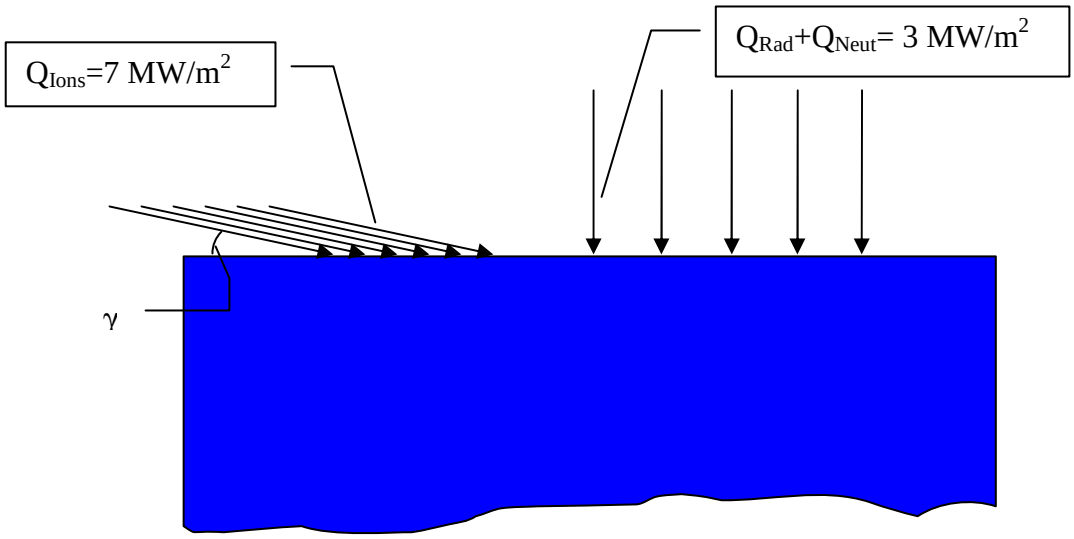

Fig. 4.5.4.1 Distribution of the heat on the surface of the tiles.

As shown in the above figure, the ion flux is not perpendicular to the surface of the tiles. The angle is 3° [8].
Considering as reference the **O**uter **V**ertical **T**arget (OVT) thas is the worst loaded Plasma Facing Component, the contribution due to the neutrals is almost zero (see fig 4.5.4.2). Therefore, it has been assumed that the power delivered to the surfaces of the tile, at the initial condition, is:

- 3 MW/m^2 due to radiation;

- 7 MW/m^2 due to ions;
- 0 MW/m^2 due to neutrals.

The total heat flux on the surface is 10 MWm^{-2}. This is considered the load during normal operation of the tiles. An off-normal condition will be also studied: 20 MWm^{-2} per 10 sec.

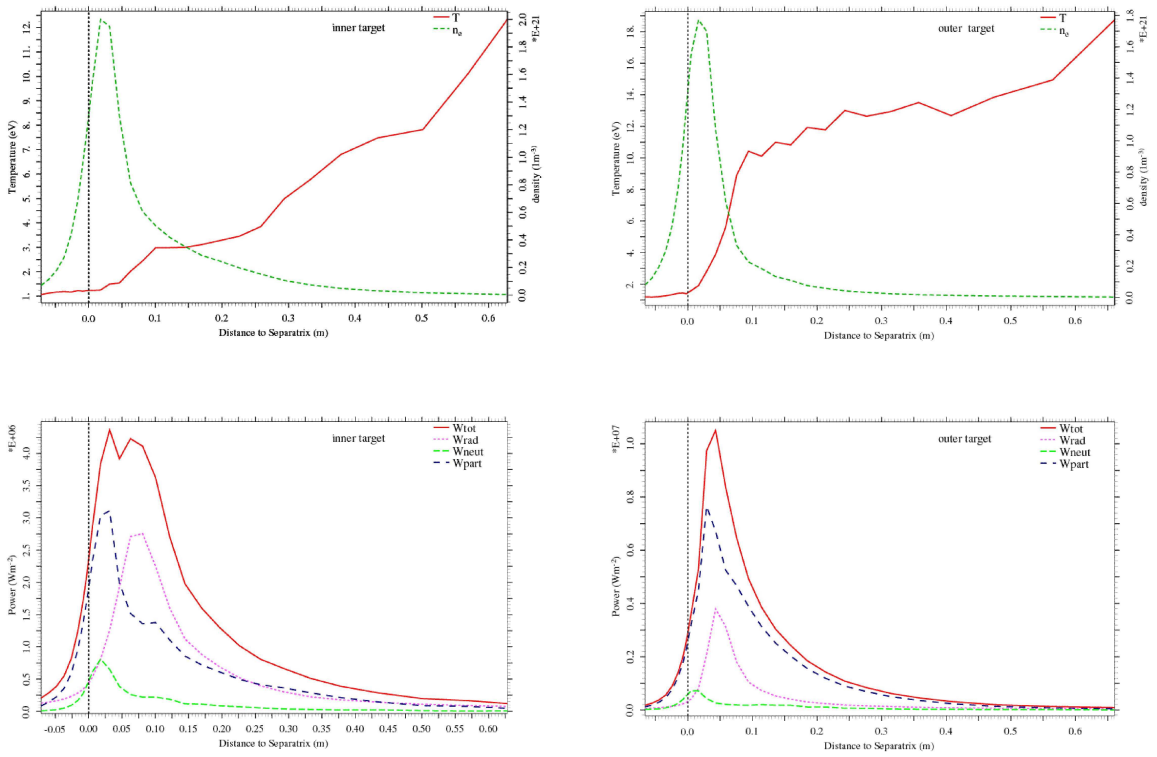

Fig. 4.5.4.2. Distribution of the power on the surface of the tiles (from B2-EIRENE code)[9].

A quarter of a monoblock has been modeled with its 3 neighbouring monoblocks where possible. Hence, the "symmetric" model has 4 planes of symmetry, one per each lateral side. Figure 4.5.2.2 shows the model used.

For normal operation, the heat is applied to the top of the surface; a convective heat transfer has been applied to the cooling channel and the heat transfer coefficient has been calculated (function of the temperature) using the EUPITER 4.2 code [10]. It is assumed that the tube includes a swirl tape, which acts as a turbulence promoter. The twist ratio of the tape is 2 (180° twist in 2 internal pipe diameters). Table 4.5.4.1 shows the input data used to find the heat transfer coefficient. Table 4.5.4.2 shows the output data of the EUPITER 4.2 code.

Geometry data	Flow inner diameter [mm]	Tape thickness average [mm]	Tape twist ratio	Surface roughness [mm]
	12	2	2	3e-3
	Pressure [MPa]	Temperature [°C]	Velocity [m/s]	
Inlet water conditions	3.8	120	9	

Table 4.5.4.1 Input data for the EUPITER 4.2 code

Temperature of the cooling Channel [°C]	Heat Transf. Coeff. [MW/(m^2*K)]		Temperature of the cooling Channel [°C]	Heat Transf. Coeff. [MW/(m^2*K)]
120	0.07934		309	0.13137
138	0.08058		311	0.13689
156	0.08165		313	0.14253
182	0.08293		315	0.14827
199	0.08362		318	0.15411
216	0.08420		320	0.16003
232	0.08470		322	0.16602
254	0.08523		324	0.17208
279	0.09082		325	0.17820
296	0.10784		327	0.18438
306	0.12599		328	0.18748

Table 4.5.4.2. Heat transfer coefficient function of temperature calculated by EUPITER 4.2.

The CHF calculated by EUPITER 4.2 is 35 MWm^{-2}.
Radiation between adjacent monoblocks is taken into account. A radiation heating condition has been implemented among the four modelled monoblocks. Moreover, radiation from the plasma facing top surface of the monoblock is also taken into account. The emissivity of the CFC is 0.8 and the temperature of the surrounding environment has been fixed at 550 °C. The analysis is conservative because it does not take into account the heat lost by evaporative cooling of the CFC although at this regime the amount of heat loss is very low.

4.5.5 Results & discussions

To verify, by comparison, the performance of the defective tile, an analysis has been carried out of a normal monoblock (without defect) under operational condition. The defects included in the monoblock are the same used in the previous chapter showed briefly in the figures below:

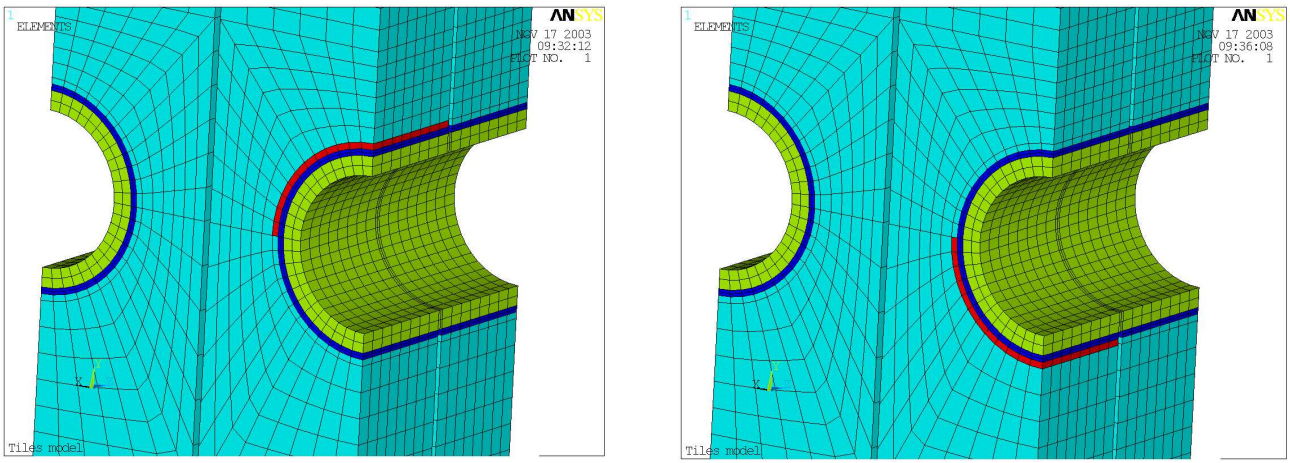

Fig. 4.5.5.1 Defect of 180° on the top and on the bottom (the defect is visible in red)

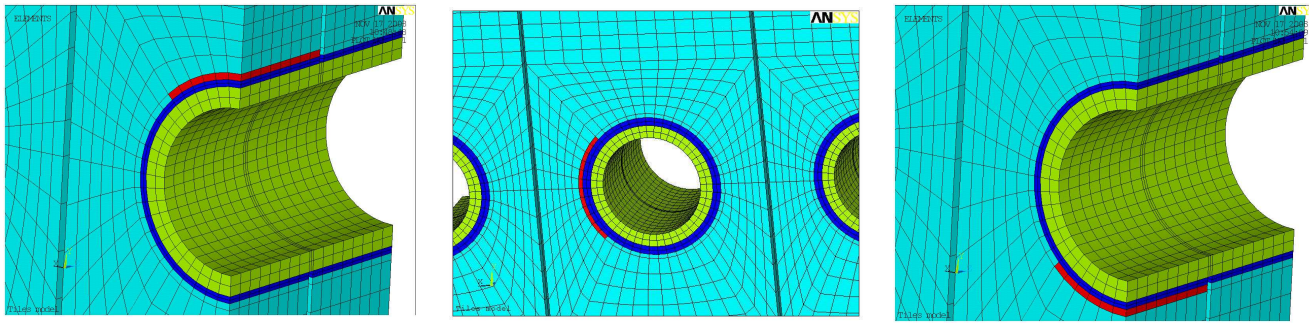

Fig. 4.5.5.2 Defect of 90° on the top, on the side and on the bottom (the defect is visible in red)

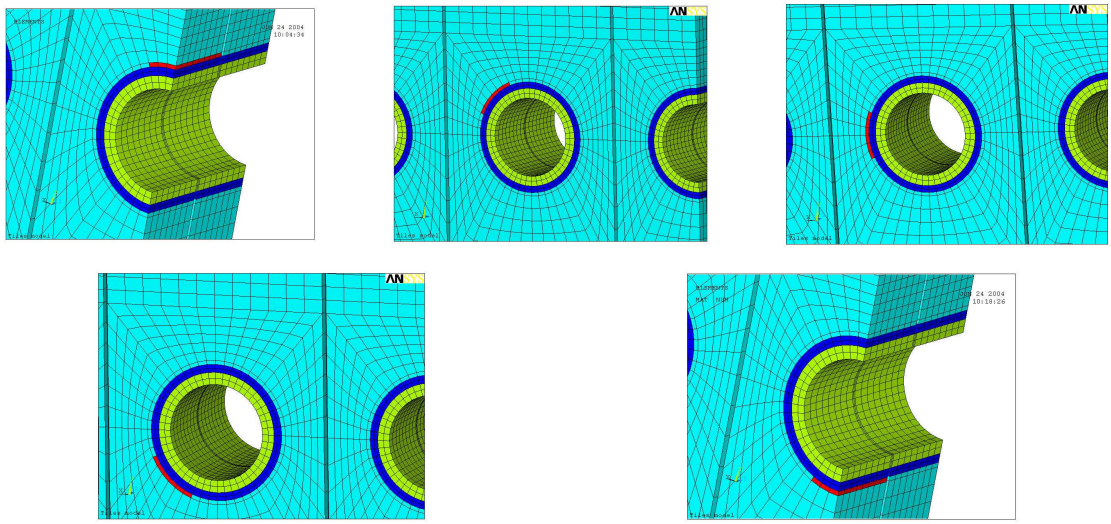

Fig. 4.5.5.3 Defect of 45° on the top, on the side and on the bottom (the defect is visible in red)

The figures below show the temperature and the heat flux distribution during normal operation (10 MWm^{-2} steady state) for the monoblock without defect and with the defect considered mentioned above.

During normal operations

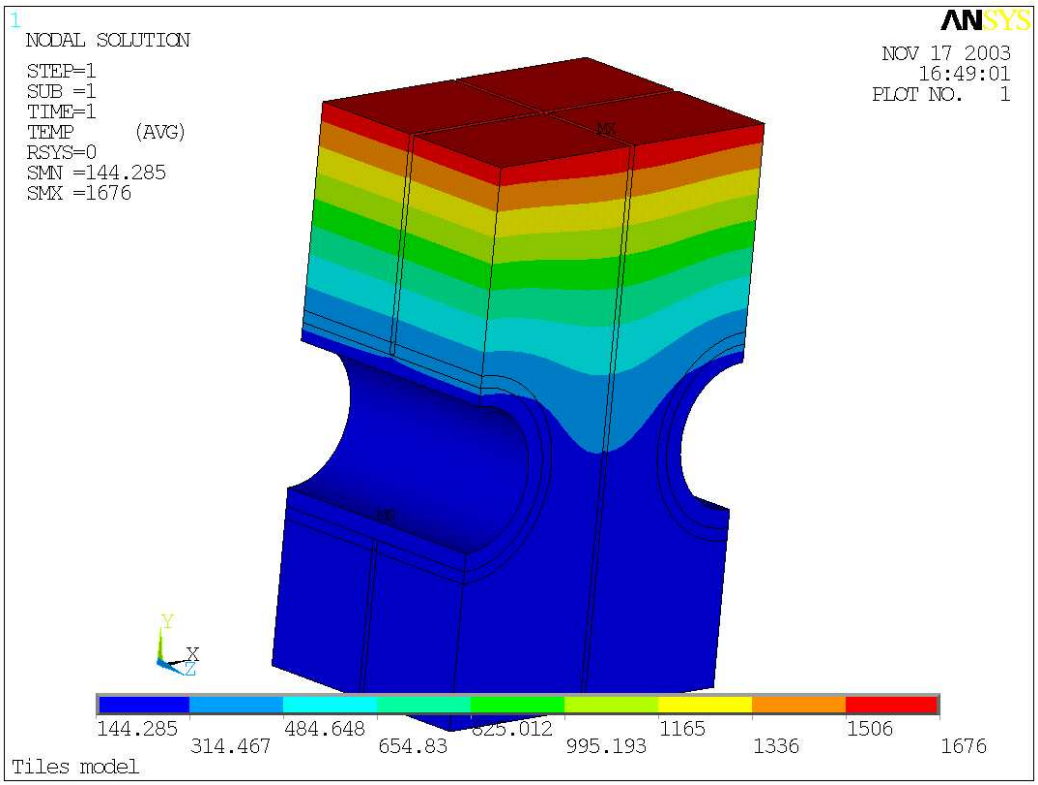

Fig. 4.5.5.4. Temperature distribution [°C] of the monoblock under normal operation.

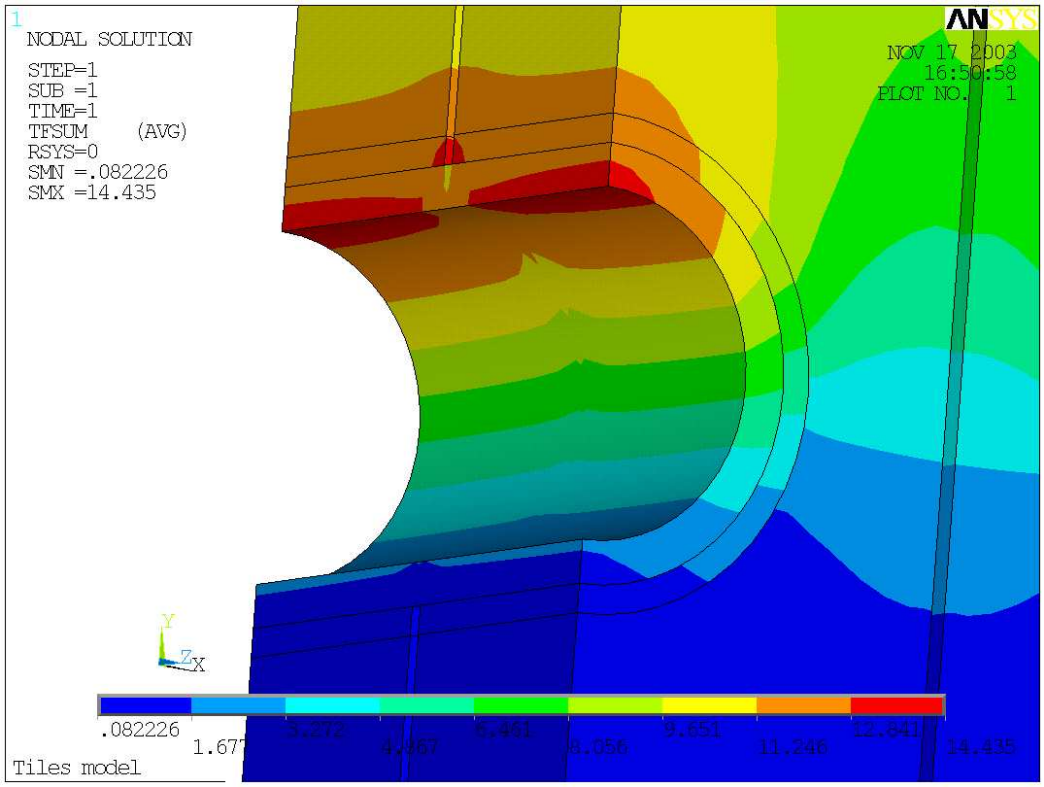

Fig. 4.5.5.5. Thermal flux distribution [MW/m^2] of the monoblock under normal operation.

From the analyses above the maximum surface temperature of the monoblock is ≈ 1670 °C, the sublimation point of the CFC is 2600 °C. Moreover, the maximum heat flux in the cooling channel is ≈ 14 MW/m^2, the CHF for this configuration is 35 MW/m^2.

A detachment of 180°

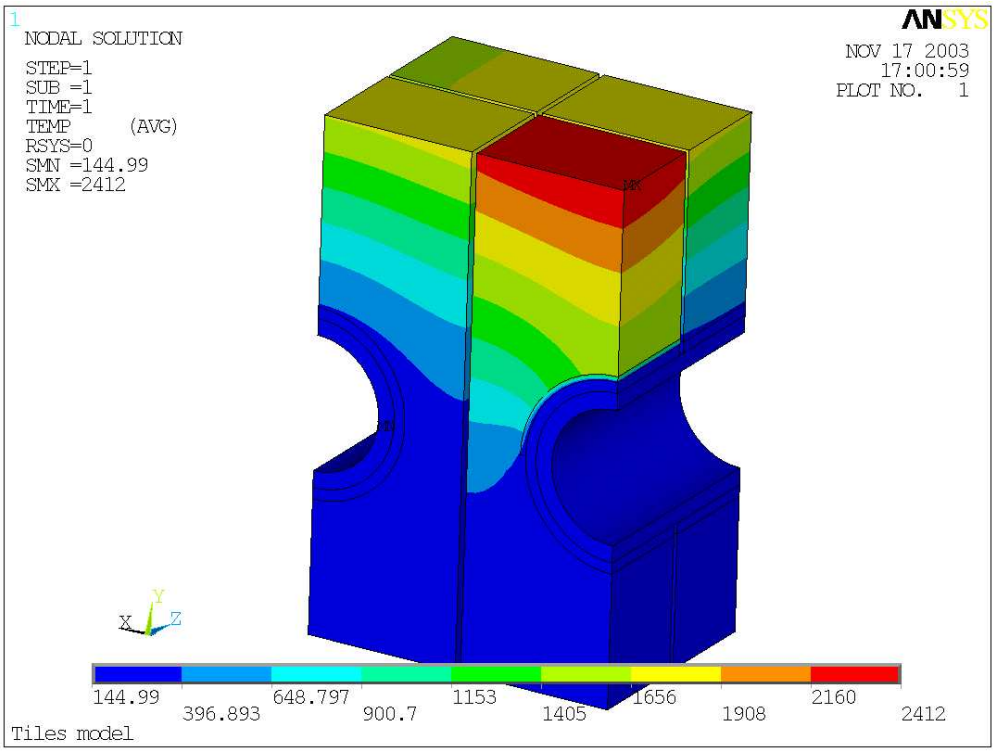

Fig. 4.5.5.6. Temperature distribution [°C] of the monoblock with a detachment of 180° from its cooling channel. The detachment is located on the top.

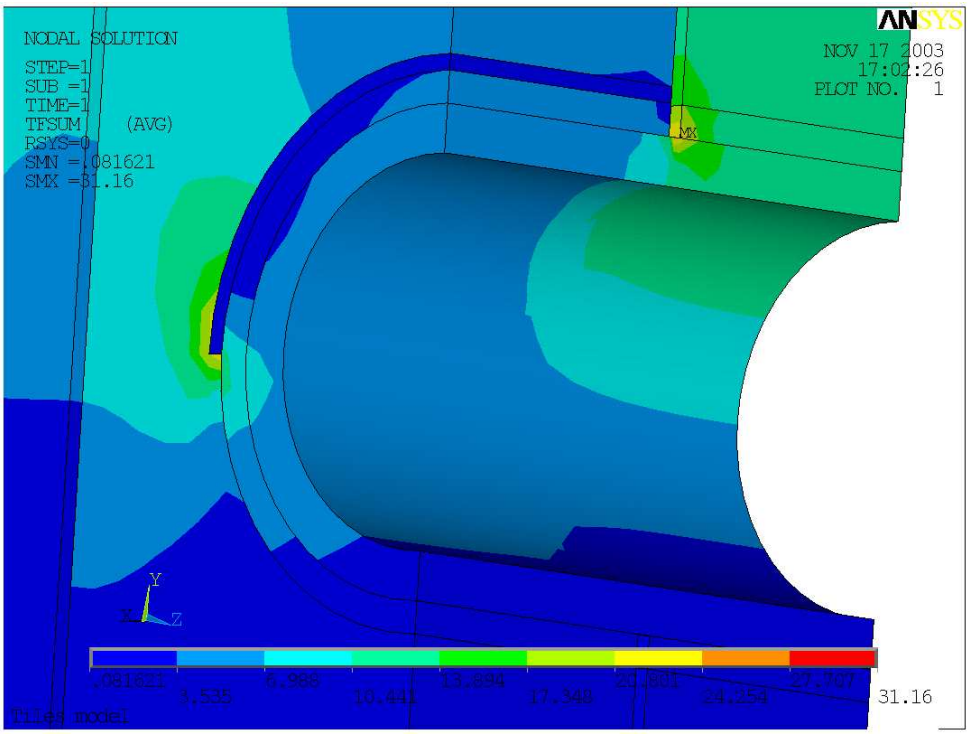

Fig. 4.5.5.7. Thermal flux distribution [MW/m^2] of the monoblock with a detachment of 180° from its cooling. The detachment is located on the top.

From the analyses above the maximum surface temperature of the monoblock when it is detached from its cooling channel on the top is ≈ 2410 °C. Moreover, the maximum heat flux in the cooling channel on the monoblock nearest to the defective monoblock is ≈ 14 MW/m^2, the CHF for this configuration is 35 MW/m^2. The maximum heat flux in the cooling channel of the defective monoblock is ≈ 7 MW/m^2.

The figures below show the temperature and the thermal flux distribution of the monoblock when the defect is located on the bottom of the cooling channel.

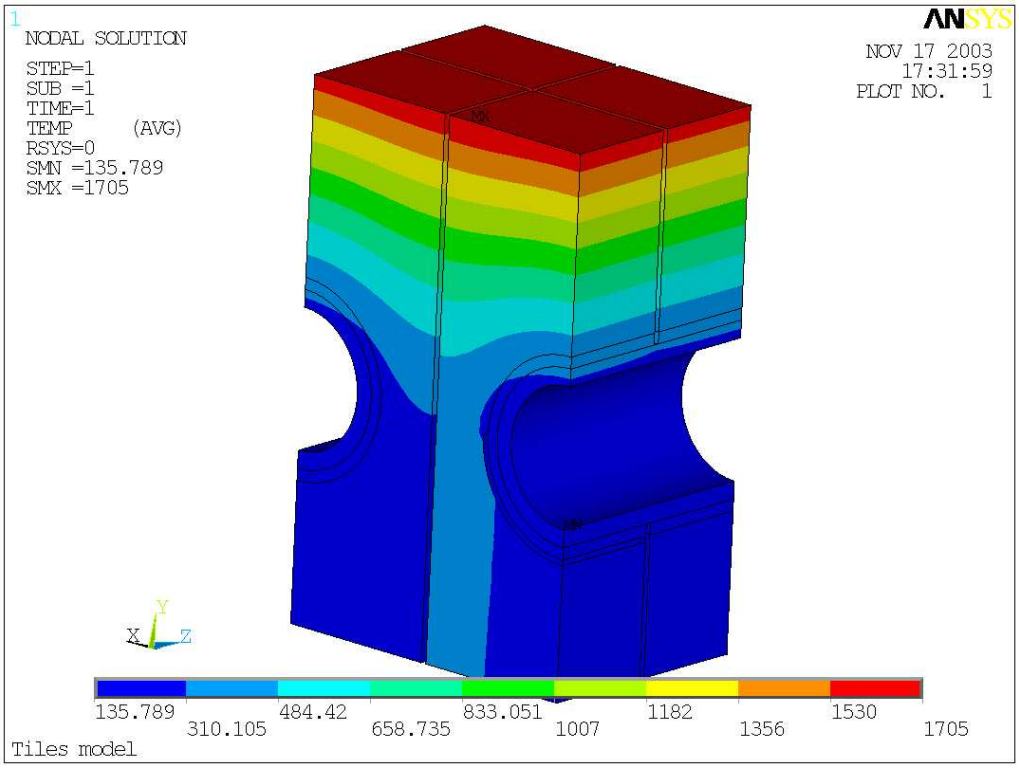

Fig. 4.5.5.8. Temperature distribution [°C] of the monoblock with a detachment of 180° from its cooling channel. The detachment is located on the bottom.

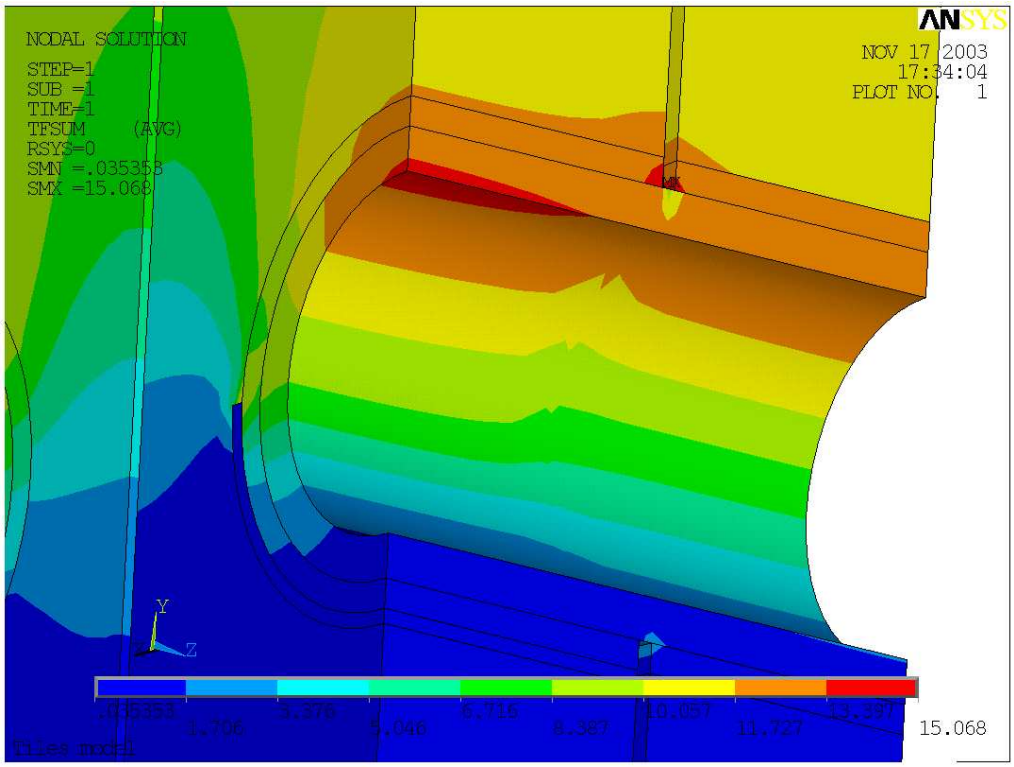

Fig. 4.5.5.9. Thermal flux distribution [MW/m^2] of the monoblock with a detachment of 180° from its cooling channel. The detachment is located on the bottom.

From the analyses above the maximum surface temperature of the monoblock when it is detached from its cooling channel on the bottom is ≈ 1710 °C. Moreover, the maximum heat flux in the cooling channel of the defect monoblock is ≈ 15 MW/m^2, the CHF for this configuration is 35 MW/m^2.

A detachment of 90°

The figures below show the temperature and the thermal flux distribution of the monoblock when the defect is located on the top of the cooling channel.

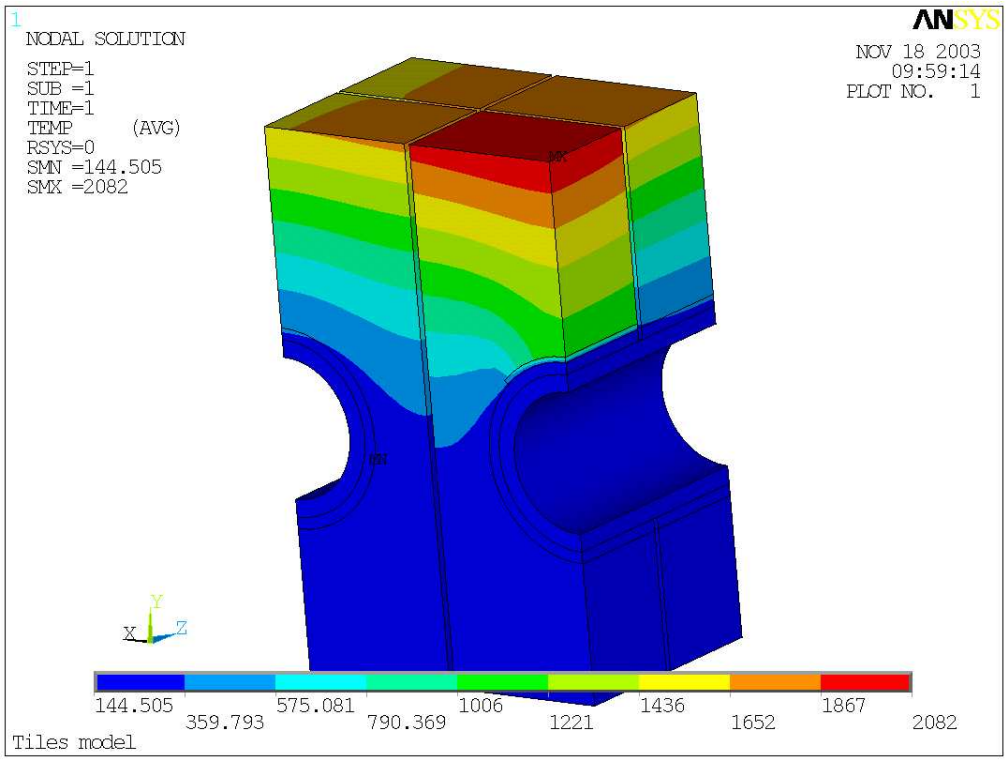

Fig. 4.5.5.10. Temperature distribution [°C] of the monoblock with a detachment of 90° from its cooling channel. The detachment is located on the top.

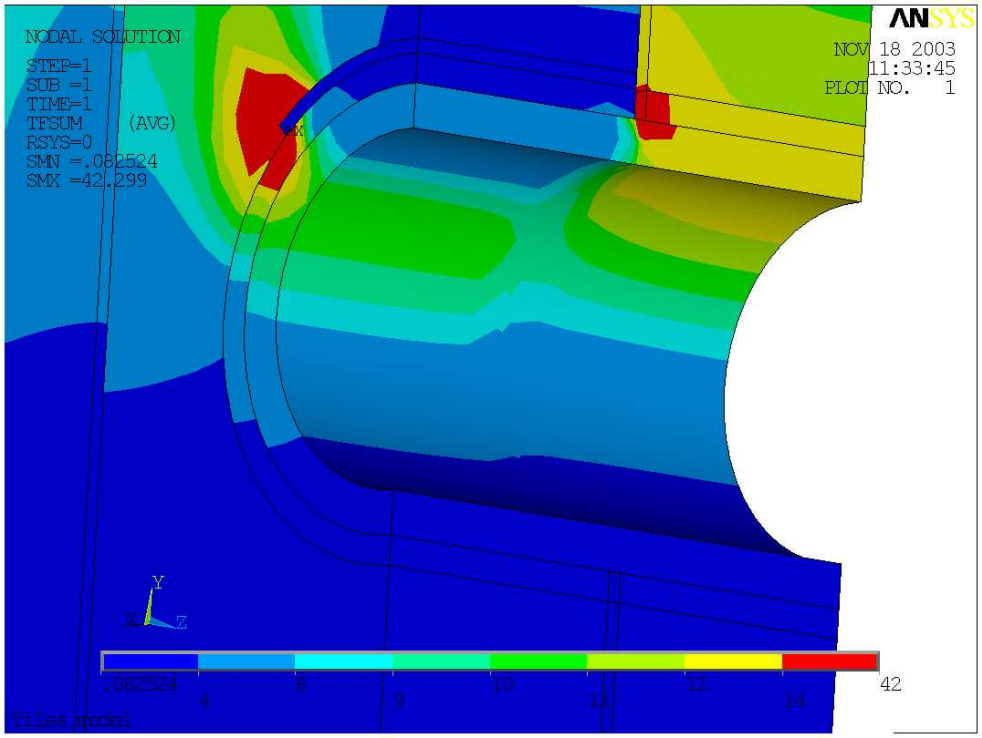

Fig. 4.5.5.11. Thermal flux distribution [MW/m^2] of the monoblock with a detachment of 90° from its cooling channel. The detachment is located on the top.

From the analyses above the maximum surface temperature of the monoblock when it is detached from its cooling channel on the top is ≈ 2080 °C. Moreover, the maximum heat flux in the cooling channel of the defective monoblock is ≈ 11 MW/m^2, the CHF for this configuration is 35 MW/m^2.
The figures below show the temperature and the thermal flux distribution of the monoblock when the defect is located on the side of the cooling channel.

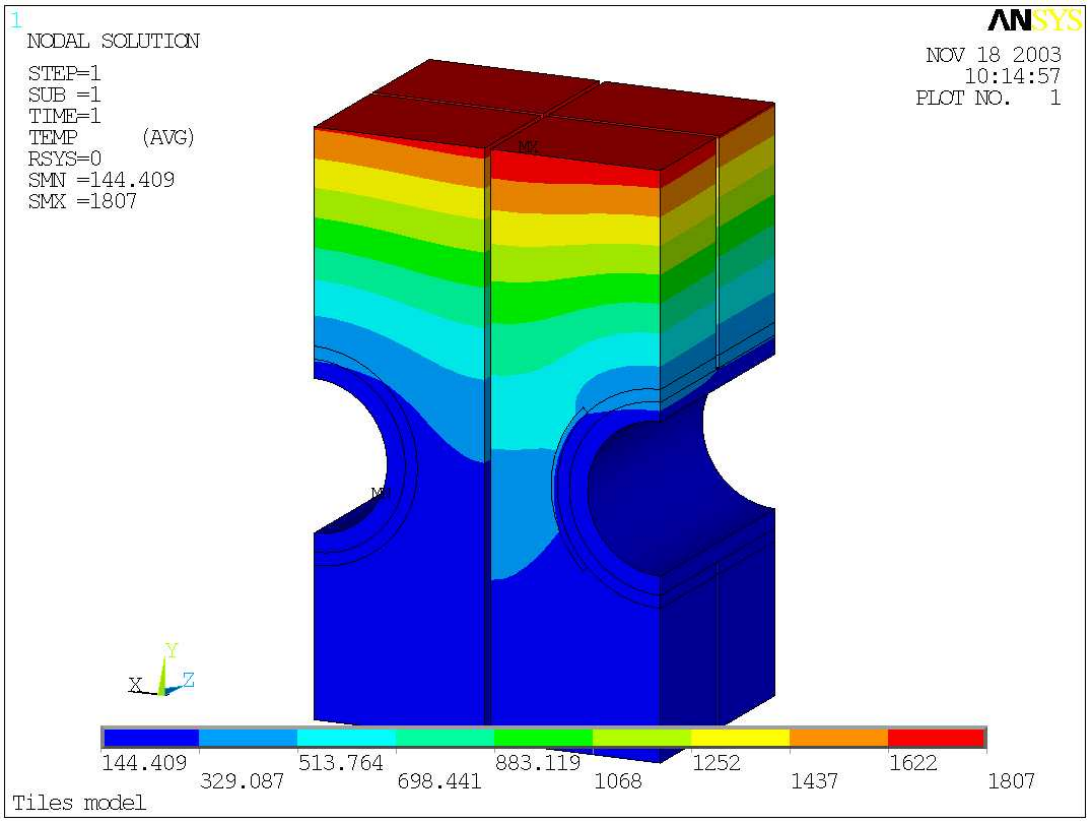

Fig. 4.5.5.12. Temperature distribution [°C] of the monoblock with a detachment of 90° from its cooling channel. The detachment is located on the side

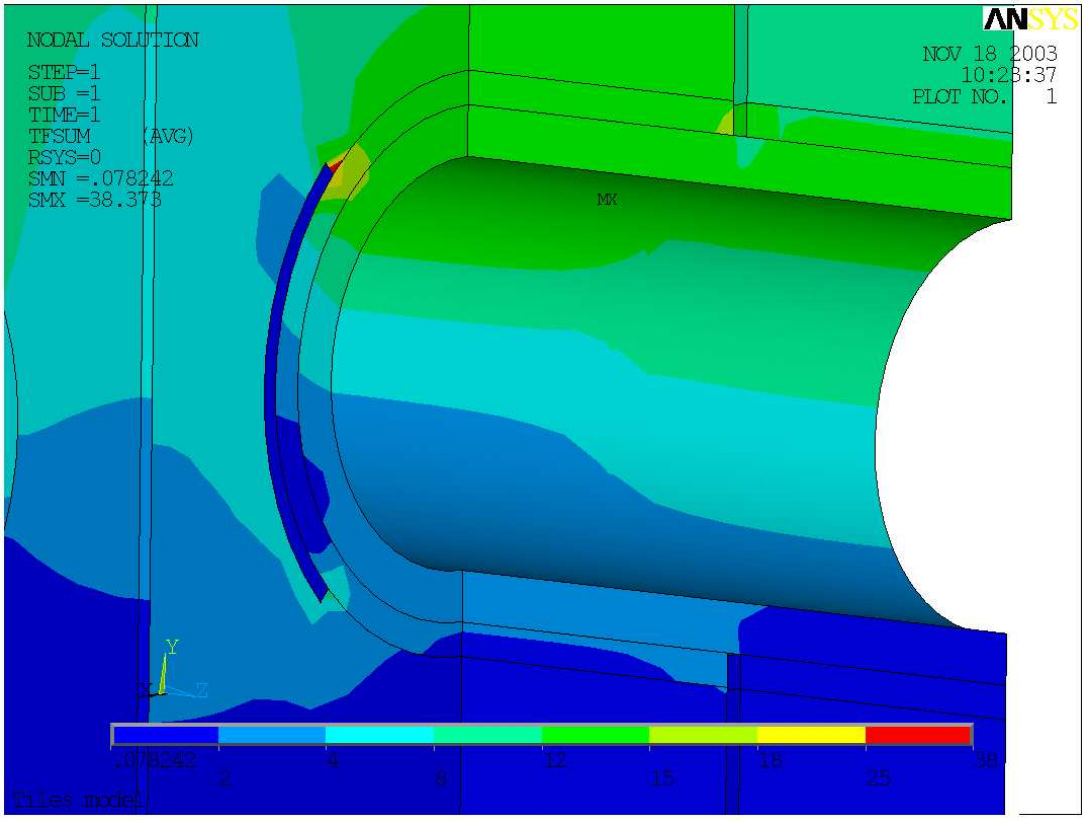

Fig. 4.5.5.13. Thermal flux distribution [MW/m^2] of the monoblock with a detachment of 90° from its cooling channel. The detachment is located on the side.

From the analyses above the maximum surface temperature of the monoblock when it is detached from its cooling channel on the side is ≈ 1807 °C. Moreover, the maximum heat flux in the cooling channel of the defective monoblock is ≈ 15 MW/m^2, the CHF for this configuration is 35 MW/m^2.

The figures below show the temperature and the thermal flux distribution of the monoblock when the defect is located on the bottom of the cooling channel.

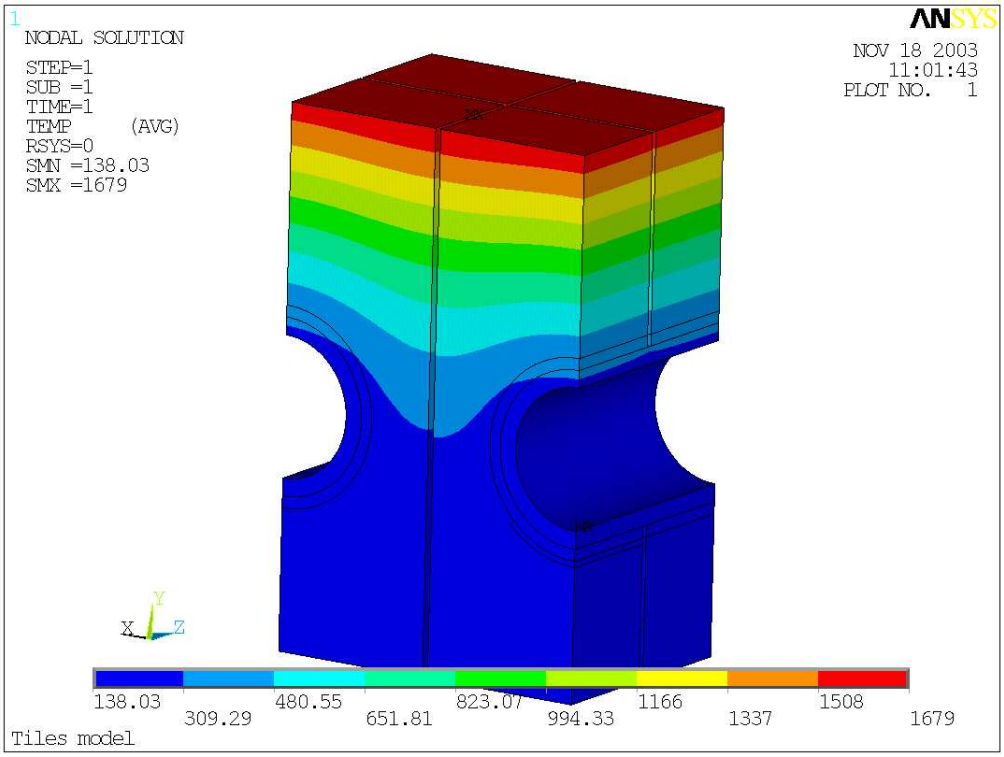

Fig. 4.5.5.14. Temperature distribution [°C] of the monoblock with a detachment of 90° from its cooling channel. The detachment is located on the bottom.

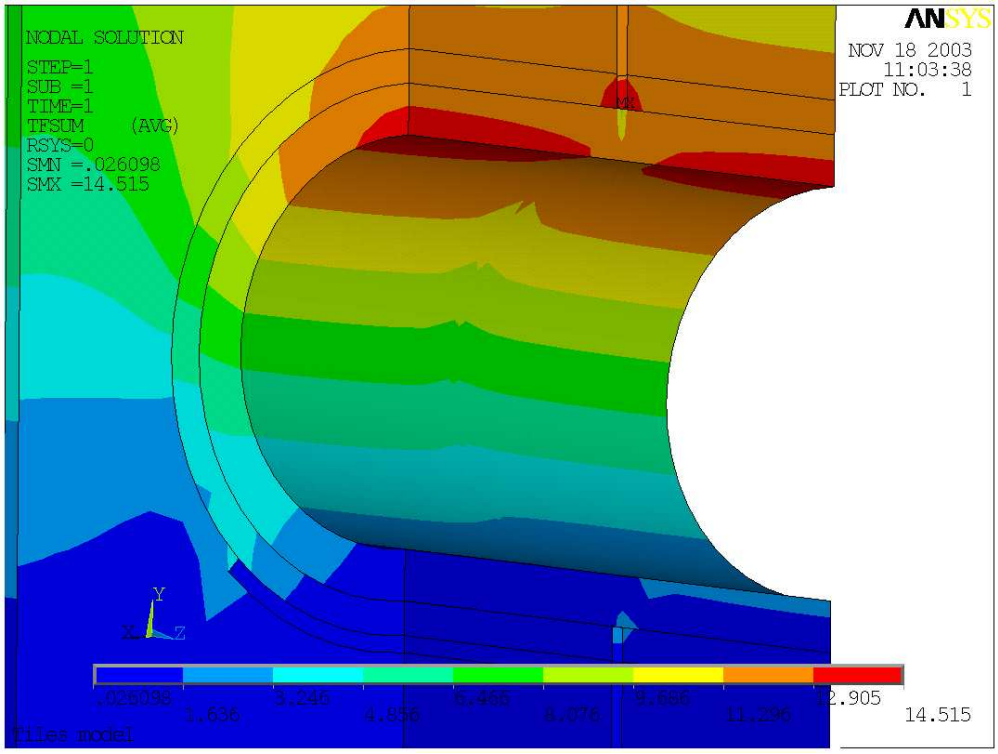

Fig. 4.5.5.15. Thermal flux distribution [MW/m^2] of the monoblock with a detachment of 90° from its cooling channel. The detachment is located on the bottom.

From the analyses above the maximum surface temperature of the monoblock when it is detached from its cooling channel on the bottom is ≈ 1680 °C. Moreover, the maximum heat flux in the cooling channel of the defective monoblock is ≈ 14 MW/m^2, the CHF for this configuration is 35 MW/m^2.

A detachment of 45 °

The figures below show the temperature and the thermal flux distribution of the monoblock when the defect is located on the top of the cooling channel.

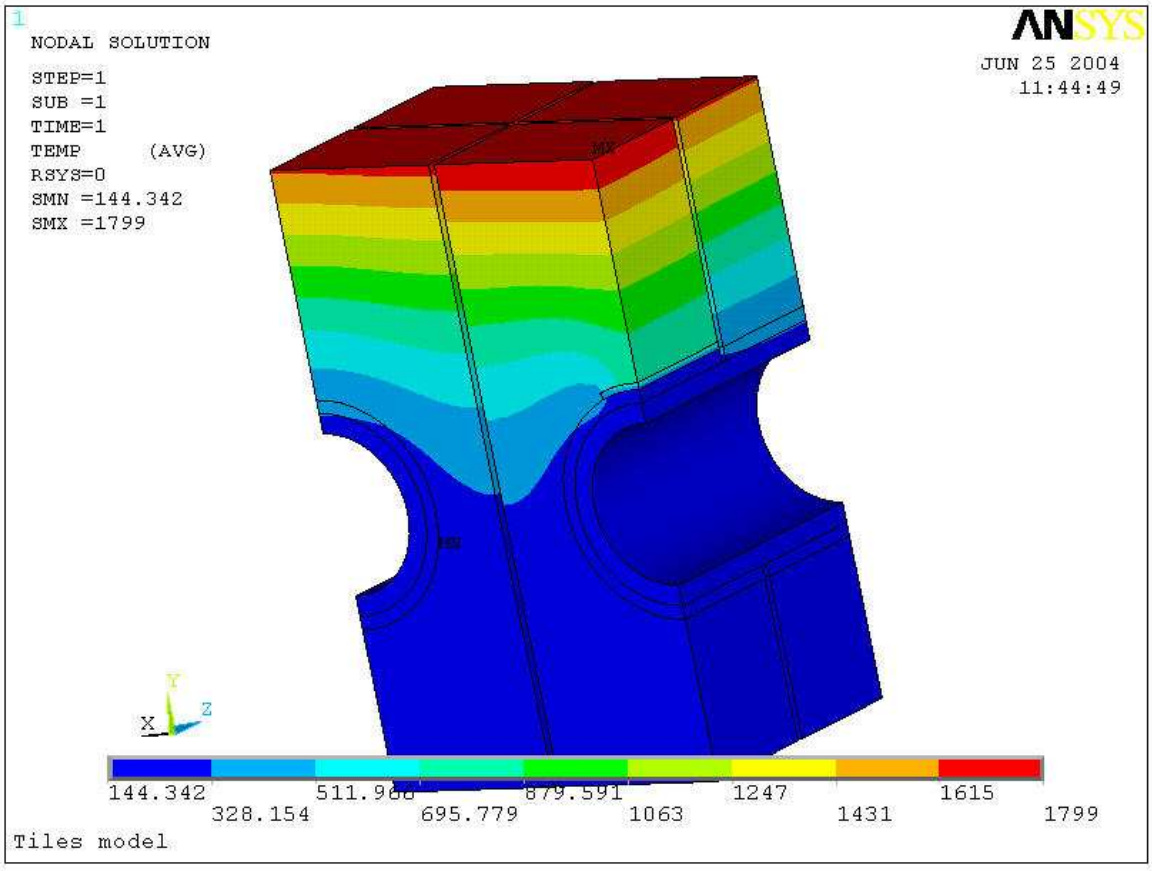

Fig. 4.5.5.16. Temperature distribution [°C] of the monoblock with a detachment of 45° from its cooling channel. The detachment is located on the top.

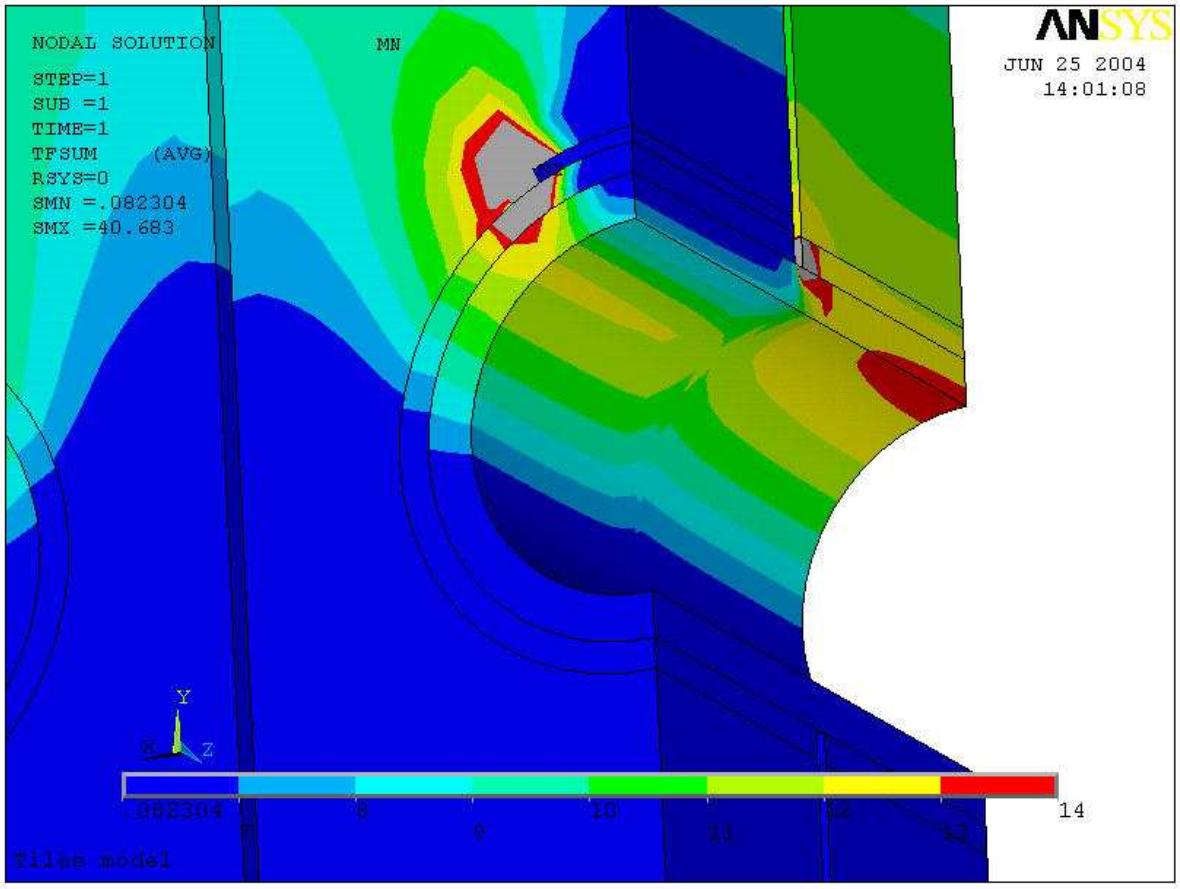

Fig. 4.5.5.17. Thermal flux distribution [MW/m^2] of the monoblock with a detachment of 45° from its cooling channel. The detachment is located on the top.

From the analyses above the maximum surface temperature of the monoblock when it is detached from its cooling channel on the top is ≈ 1799 °C. Moreover, the maximum heat flux in the cooling channel of the defective monoblock is ≈ 12 MW/m^2, the CHF for this configuration is 35 MW/m^2.

The figures below show the temperature and the thermal flux distribution of the monoblock when the defect is located on the upper side of the cooling channel.

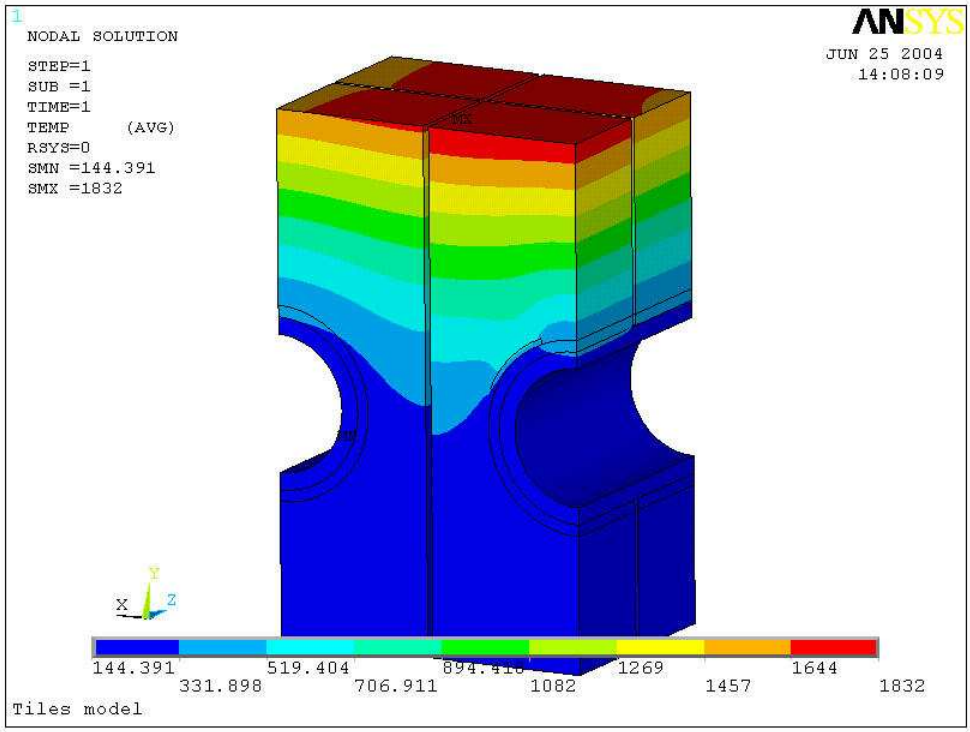

Fig. 4.5.5.18. Temperature distribution [°C] of the monoblock with a detachment of 45° from its cooling channel. The detachment is located on the upper side.

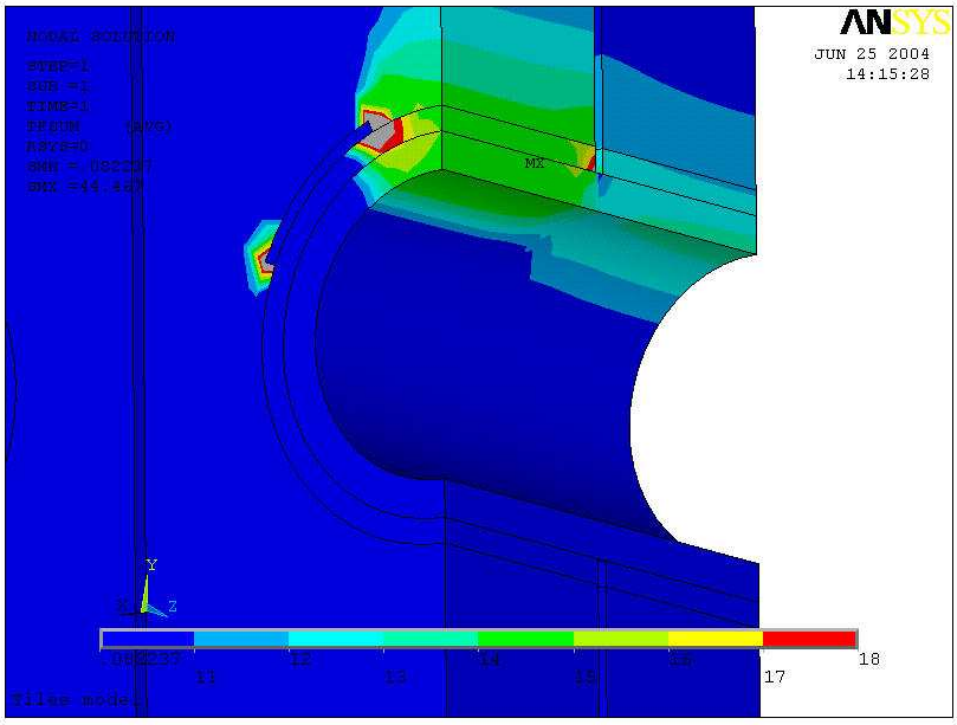

Fig. 4.5.5.19. Thermal flux distribution [MW/m^2] of the monoblock with a detachment of 45° from its cooling channel. The detachment is located on the upper side.

From the analyses above the maximum surface temperature of the monoblock when it is detached from its cooling channel on the upper side is ≈ 1832 °C. Moreover, the maximum heat flux in the cooling channel of the defective monoblock is ≈ 15 MW/m^2, the CHF for this configuration is 35 MW/m^2.
The figures below show the temperature and the thermal flux distribution of the monoblock when the defect is located on the side of the cooling channel.

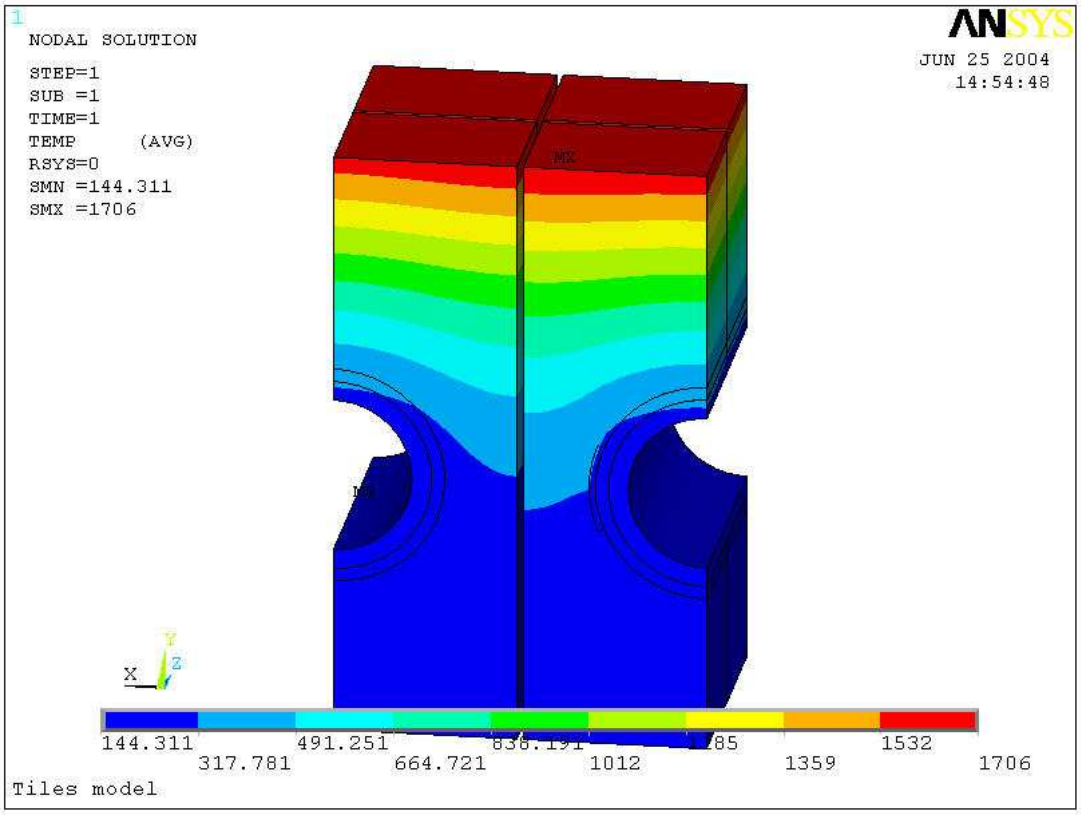

Fig. 4.5.5.20. Temperature distribution [°C] of the monoblock with a detachment of 45° from its cooling channel. The detachment is located on the side.

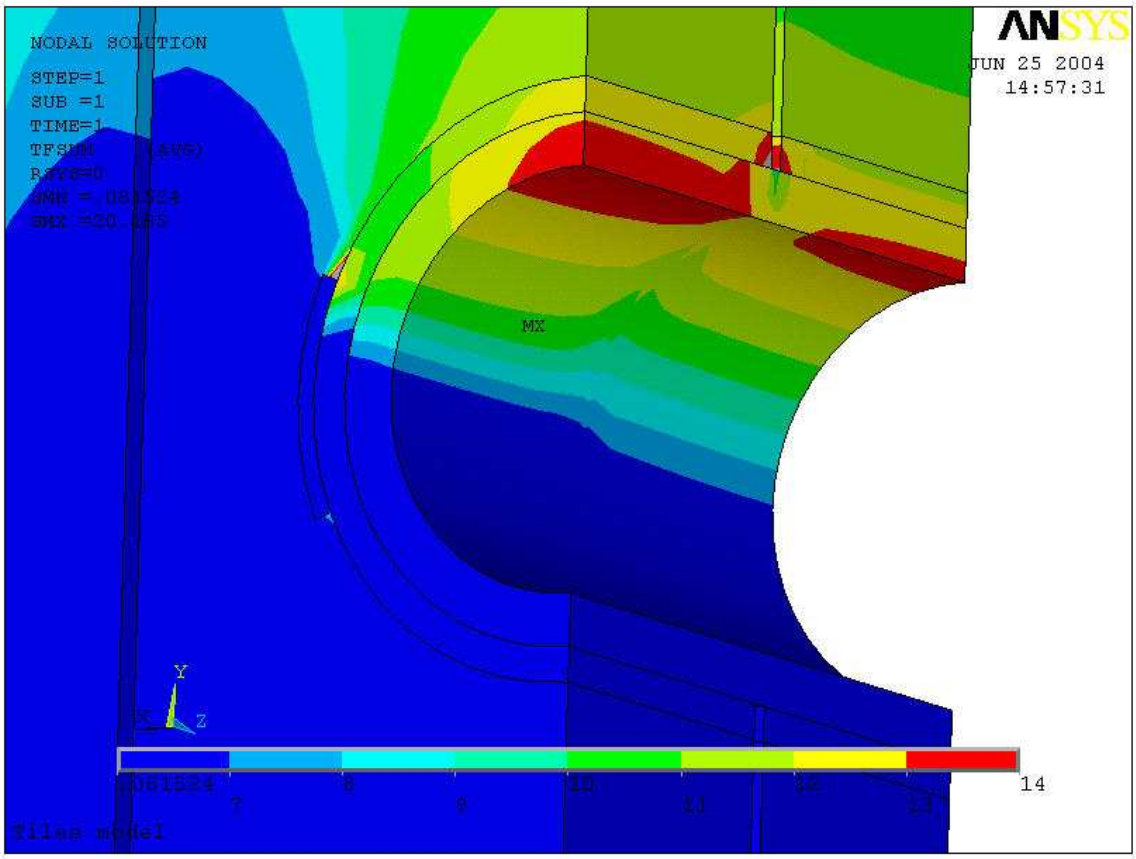

Fig. 4.5.5.21. Thermal flux distribution [MW/m^2] of the monoblock with a detachment of 45° from its cooling channel. The detachment is located on the side.

From the analyses above the maximum surface temperature of the monoblock when it is detached from its cooling channel on the side is ≈ 1706 °C. Moreover, the maximum heat flux in the cooling channel of the defective monoblock is ≈ 14 MW/m^2, the CHF for this configuration is 35 MW/m^2.

The figures below show the temperature and the thermal flux distribution of the monoblock when the defect is located on the bottom side of the cooling channel.

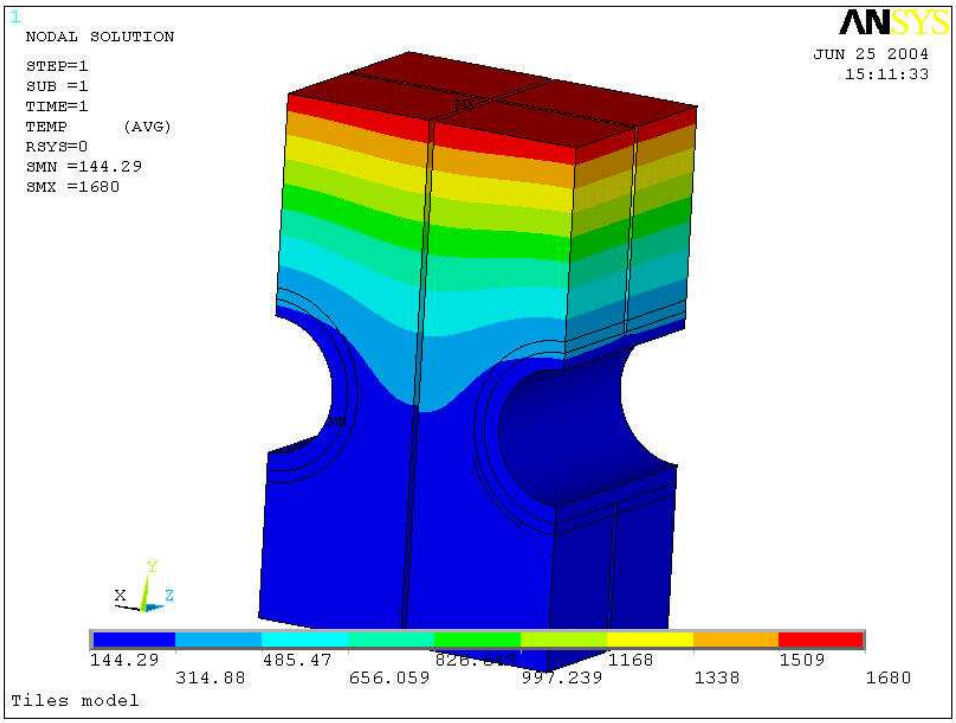

Fig. 4.5.5.22. Temperature distribution [°C] of the monoblock with a detachment of 45° from its cooling channel. The detachment is located on the bottom side.

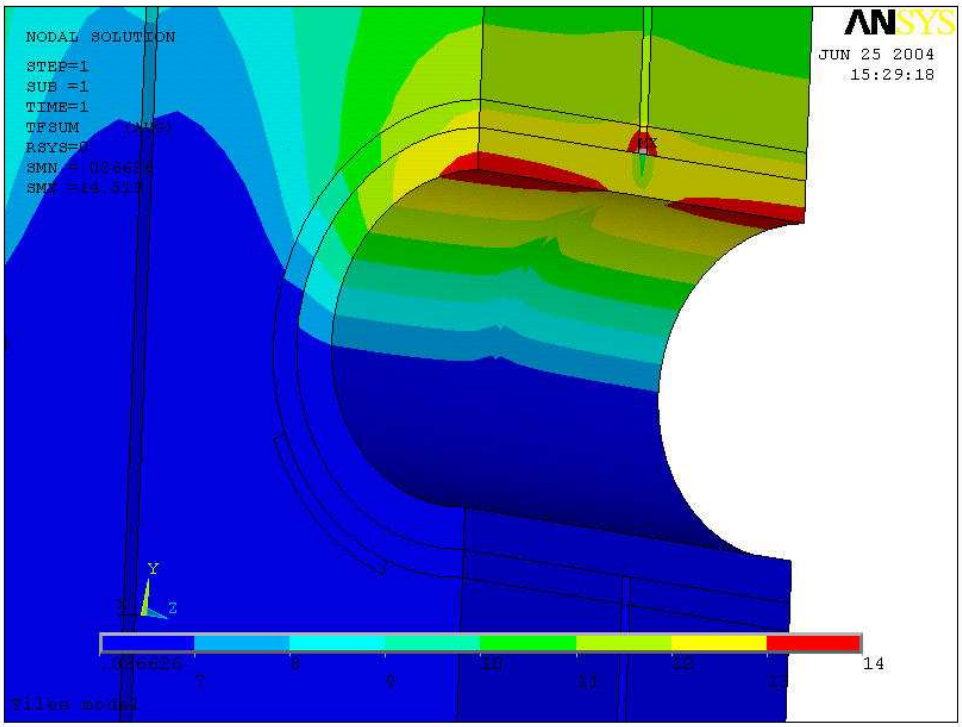

Fig. 4.5.5.23. Thermal flux distribution [MW/m^2] of the monoblock with a detachment of 45° from its cooling channel. The detachment is located on the bottom side.

From the analyses above the maximum surface temperature of the monoblock when it is detached from its cooling channel on the bottom side is ≈ 1680 °C. Moreover, the maximum heat flux in the cooling channel of the defective monoblock is ≈ 14 MW/m^2, the CHF for this configuration is 35 MW/m^2.
The figures below show the temperature and the thermal flux distribution of the monoblock when the defect is located on the bottom of the cooling channel.

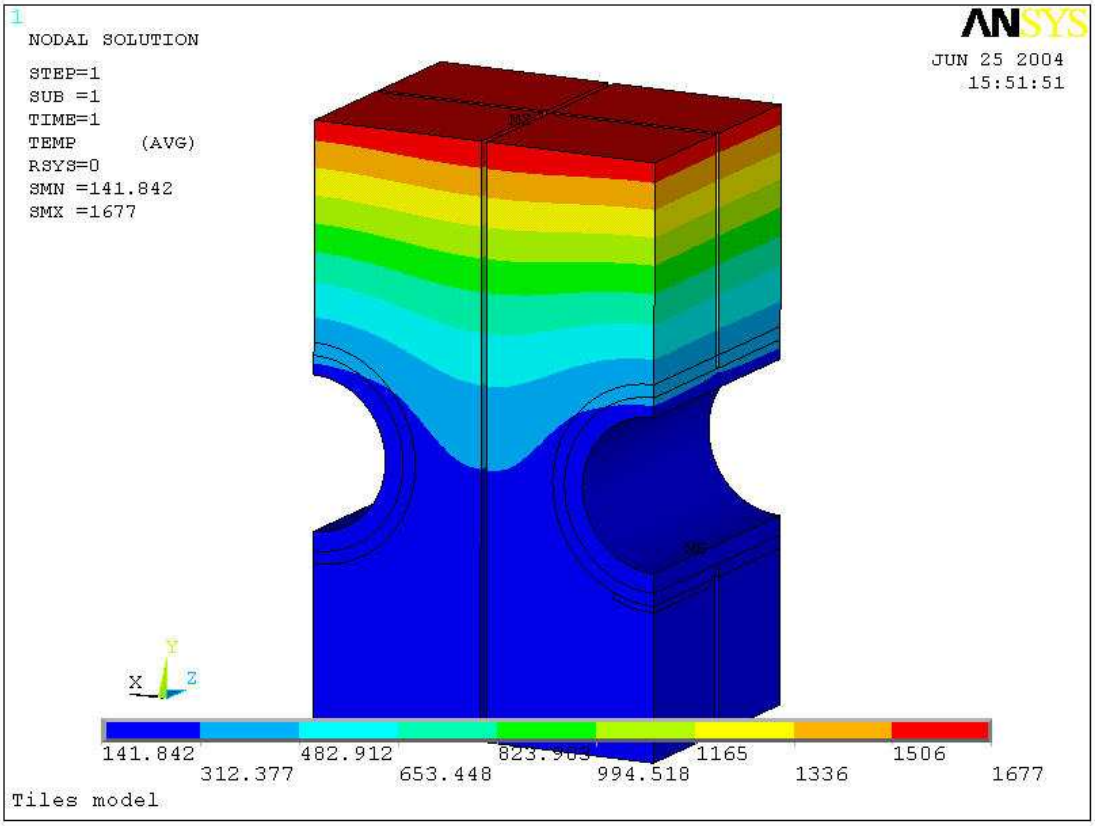

Fig. 4.5.5.24. Temperature distribution [°C] of the monoblock with a detachment of 45° from its cooling channel. The detachment is located on the bottom

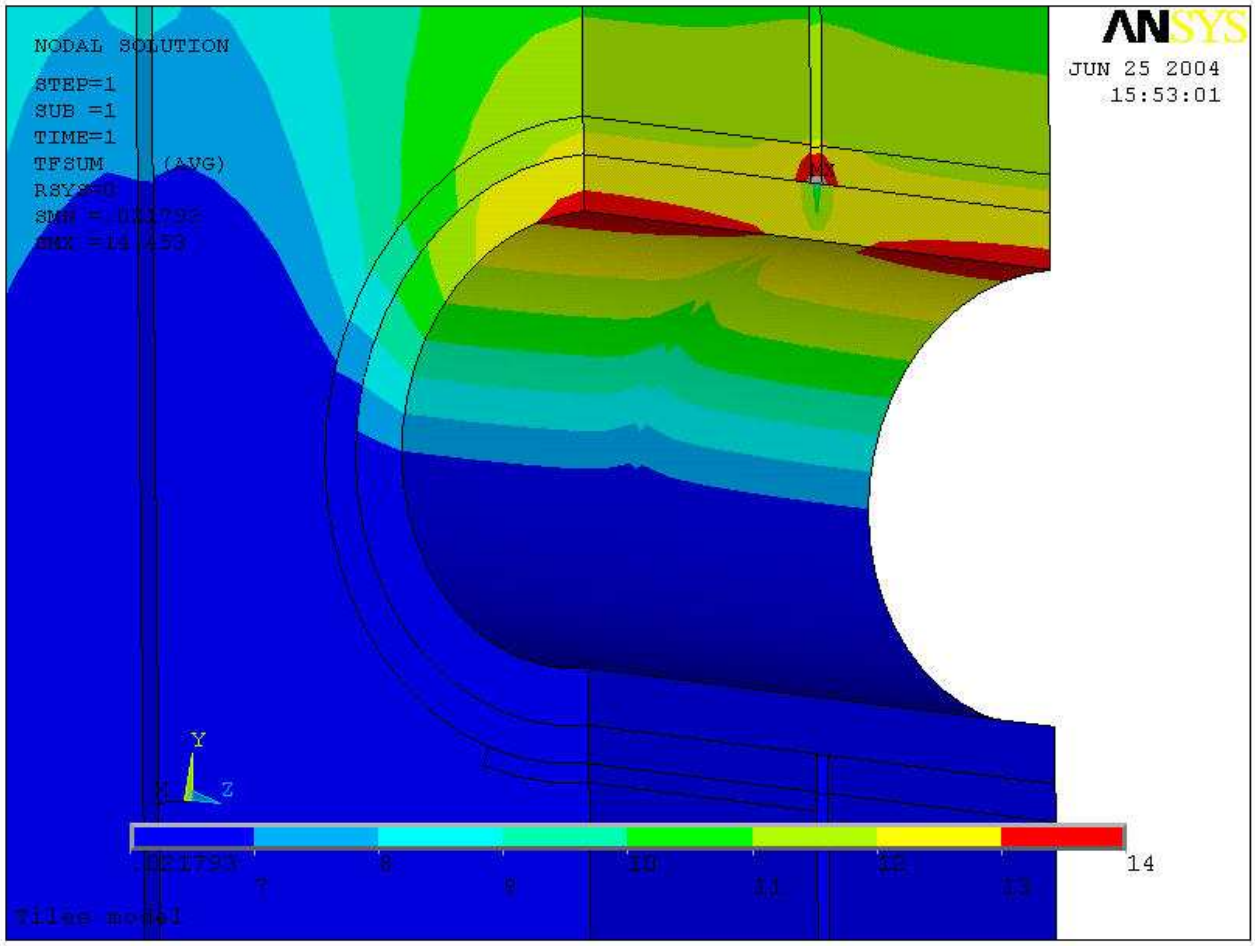

Fig. 4.5.5.25. Thermal flux distribution [MW/m^2] of the monoblock with a detachment of 45° from its cooling channel. The detachment is located on the bottom.

From the analyses above the maximum surface temperature of the monoblock when it is detached from its cooling channel on the bottom is ≈ 1680 °C. Moreover, the maximum heat flux in the cooling channel of the defective monoblock is ≈ 14 MW/m^2, the CHF for this configuration is 35 MW/m^2.

In the tables below are summarized the results obtained in this paragraphs using defect tiles under normal operation.

Reference tile		Defect tile, 180° detached			
		Top		Bottom	
Surf. Temp [°C]	Heat flux [MW/m^2]	Surf. Temp [°C]	Heat flux [MW/m^2]	Surf. Temp [°C]	Heat flux [MW/m^2]
1676	13	2412	7	1705	14

Table 4.5.5.1. A summary of the results obtained considering defects of 180°.

Reference tile		Defect tile, 90° detached					
		Top		Side		Bottom	
Surf. Temp [°C]	Heat flux [MW/m^2]	Surf. Temp [°C]	Heat flux [MW/m^2]	Surf. Temp [°C]	Heat flux [MW/m^2]	Surf. Temp [°C]	Heat flux [MW/m^2]
1676	13	2082	14	1783	16	1679	13

Table 4.5.5.2. A summary of the results obtained considering defects of 90°.

Reference tile		Defect tile, 45° detached									
		Top		Top-Side		Side		Bottom-side		Bottom	
Surf. Temp [°C]	Heat flux [MW/m^2]	Surf. Temp [°C]	Heat flux [MW/m^2]	Surf. Temp [°C]	Heat flux [MW/m^2]	Surf. Temp [°C]	Heat flux [MW/m^2]	Surf. Temp [°C]	Heat flux [MW/m^2]	Surf. Temp [°C]	Heat flux [MW/m^2]
1676	13	1799	12	1799	13	1701	13	1679	13	1677	13

Table 4.5.5.3. A summary of the results obtained considering defects of 45°.

Of course the well-attached monoblock, near to the defective monoblock, have an increased value of the wall thermal flux. However, they are always below the 15 MW/m^2.

4.5.6 Final considerations

It is clear, looking at the analyses, that the performances of a defective tile with a detachment of 45° or 90° are acceptable. When the detachment is of 180° the value of the heat flux is still acceptable but the value of the surface temperature reaches 2400 °C.
The performance obtained with a defective tile with a detachment of 90° and 45° is acceptable in term of CHF, the values of heat flux on the wall (Wall Heat Flux) between

the cooling channel and the water is always below 15 MW/m^2 against the 14 MW/m^2 of the well attached monoblock. The CHF for this configuration is 35 MW/m^2. The WHF rest below 35 MW/m^2 even for off-normal condition (20 MW/m^2 per 10 sec).
Of course the life of a detached tile will be reduced because the surface temperature will be higher. But it depends on the location of the defect. In fact, for a defect of 90° on the top of the joint the temperature of the surface directly irradiated from the plasma will increase (2082 °C against the 1679 °C of the well attached tile). If the defect of 90° is on the bottom of the cooling channel, then the performance of the defective tile is practically the same as a well-attached tile. Another fact to report is that a defect of 45° located on the top-side of the cooling channel is worst in term of temperature and wall thermal flux (1832 °C and 15 MW/m^2) than the same defect located on the top (1799 °C and 12 MW/m^2). This is true because the highest surface temperature is on the edges of the tiles then interrupting the thermal path between the edges and the cooling channel results in the highest possible surface temperature.
The assumption of a defect all along the axial direction is conservative in term of performance of the monoblock. Nevertheless, some analyses have been done with a defect not fully extended poloidally (see also the preliminary analyses in chap. 4.3) and with two adjacent defects located in poloidal adjacent tiles. The conclusions were that the worst condition in term of highest surface temperature and highest WHF are when the CFC is detached from the cooling channel all along the poloidal direction in one single tile.

4.6 The way adopted for the definition of the acceptance criteria for the CFC tiles

4.6.1 The logic behind the definition of the acceptance criteria

As already said above, in the divertor design there are ~$5x10^4$ CFC to Cu-tube monoblock joints subjected to high heat flux. NDE (**N**on **D**estructive **E**xamination) during the fabrication and before the installation are central to avoiding poor operation of the machine. In particular, it is expected that reliance will be placed on the SATIR method (infrared thermography) and the UltraSound techniques.
This chapter is on the definition of tentative acceptance criteria for the SATIR test. There must be a logic behind the definition of the acceptance criteria for the tiles installed in the machine.
The general idea is to proceed with a cut off value in terms of ΔT_{SATIR} in order to avoid the installation of monoblock that may generate operational problems. This means check every monoblock before the installations, if the monoblock analysed had a ΔT_{SATIR} higher than a certain value it would be rejected.
The idea of a cut-off value must be complementary to the definition of a statistical approach in order to ensure a good average component quality.
Here the statistical approach is used in a different way respect to the industry where it is used to check a series fabrication process. We are already relatively sure that we will not have problems during operation because a 100% check of every monoblock will be done. For the definition of the statistical approach a reference distribution of the achievable quality must be defined and the sample must be compared statistically with the defined

reference distribution. Then a procedure of decision could be established in order to decide if reject or not the poloidal element (a series of monoblock connected by the cooling channel, it can belong to the outer vertical target or to the inner vertical target).

4.6.2 Evaluation of the cut-off value of the acceptance criteria

From an engineering point of view two conditions can be defined:

- The surface temperature of the installed tiles during normal operation must stay below the 2000 °C.
- The wall heat flux of the cooling channel during normal operation must be less than 23 MWm-2.

The first assumption is based on the fact that increasing the temperature further increase the amount of CFC that is eroded and this might ultimately lead to operational problems ("plasma-poisoning"). The choice of 2000 °C is suggested since the sputtering yield may be almost the same as at 500°C (depending on the plasma condition, see fig. 4.6.2.1) a temperature that is commonly achieved some distance away from where the scrape-off layer intercepts the Vertical Target. The second assumption relates to the requirement to avoid a burnout condition. The wall CHF for the configuration actually used is 35 MWm^{-2} (i.e. the heat flux at the copper cooling tube to water interface), and hence a wall heat flux of 23 MWm^{-2} gives a safety factor of 1.5.

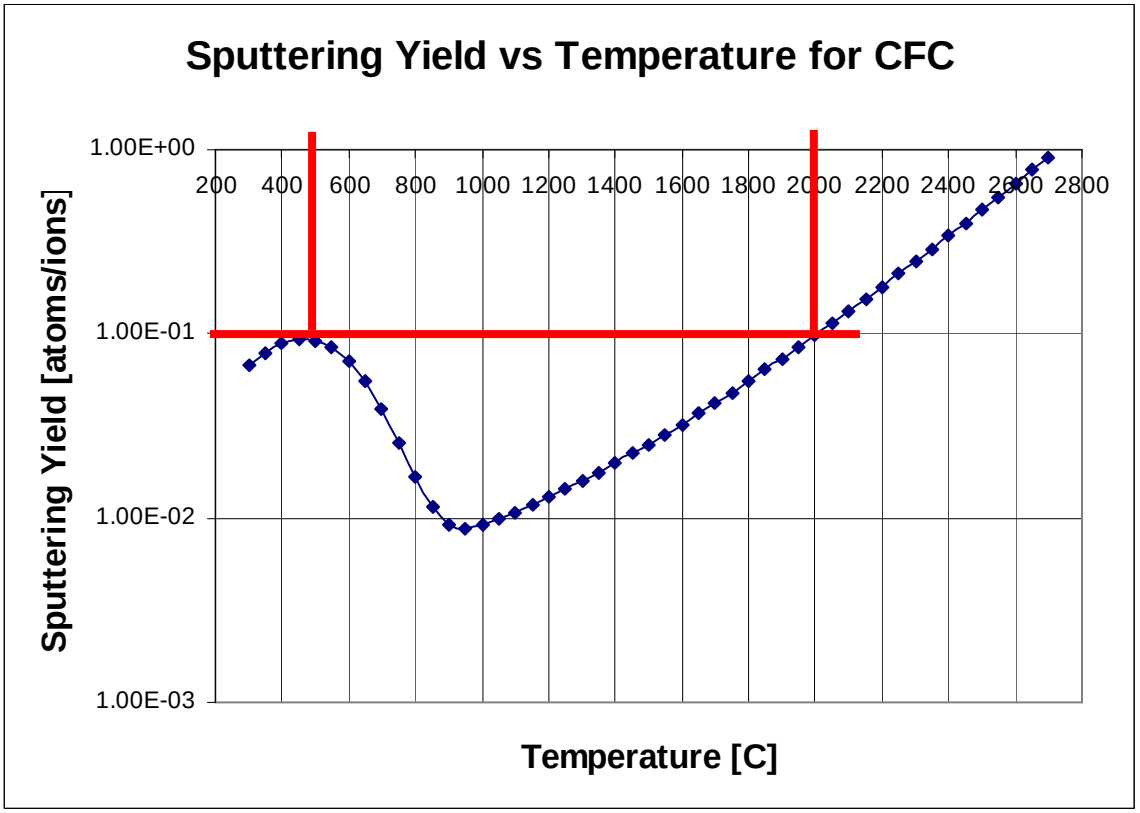

Fig. 4.6.2.1. Temperature dependence of the sputtering yield for CFC [12].

The associated defect to have a surface temperature of the tiles below 2000 °C can be obtained from the calculation done in the paragraph 4.5. The curve in fig 4.6.2.2 shows the steady state surface temperature of the monoblock as a function of defect dimension, for defects located on the top of the tube (centred at 12 o'clock).

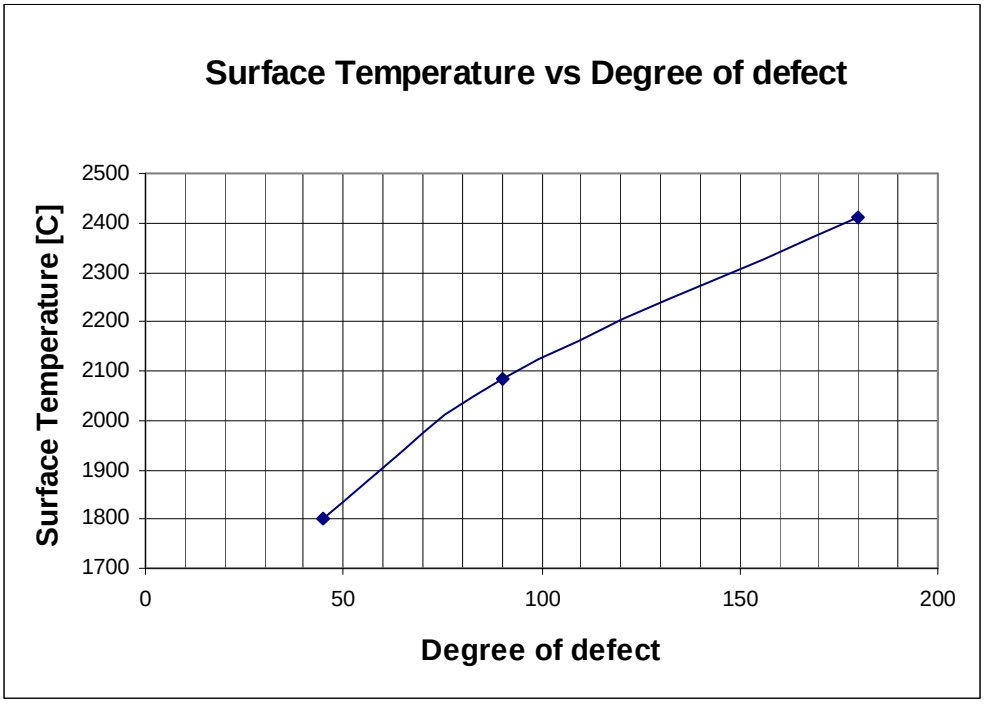

Fig. 4.6.2.2. Surface temperature of the tile as a function of the size of the defect when the centre of the defect is located at the top of the tube (at the applied heat flux side).

A defect of 60° produces a surface temperature of ≈ 1900°C. On the other hand a defect of 60°, with the assumption done in paragraph 4.4 corresponds to a ΔT_{SATIR} of 8 °C (see fig. 4.6.2.3).

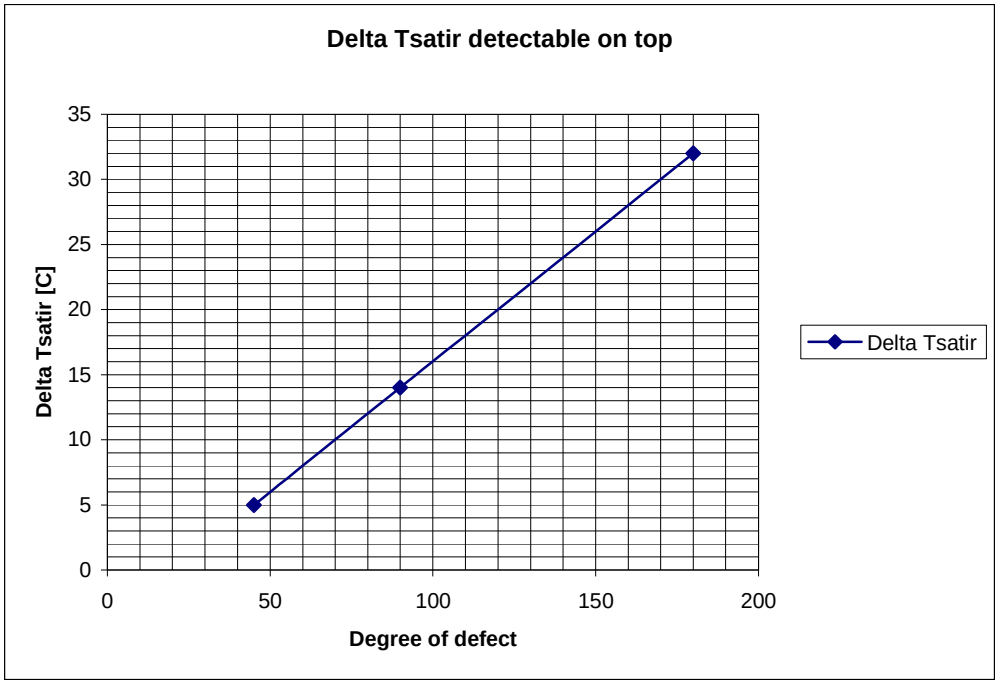

Fig. 4.6.2.3 ΔT_{SATIR} function of the amplitude of the defect located on the top of the monoblock.

Some other analysis have been done [13] in order to verify that the WHF during normal operation with a defect of 60° located on the top is below 23 MWm^{-2} and during off-normal transients (20 MWm^{-2} for 10 sec) is again below 23 MWm^{-2} (see the model used fig. 4.6.2.4).

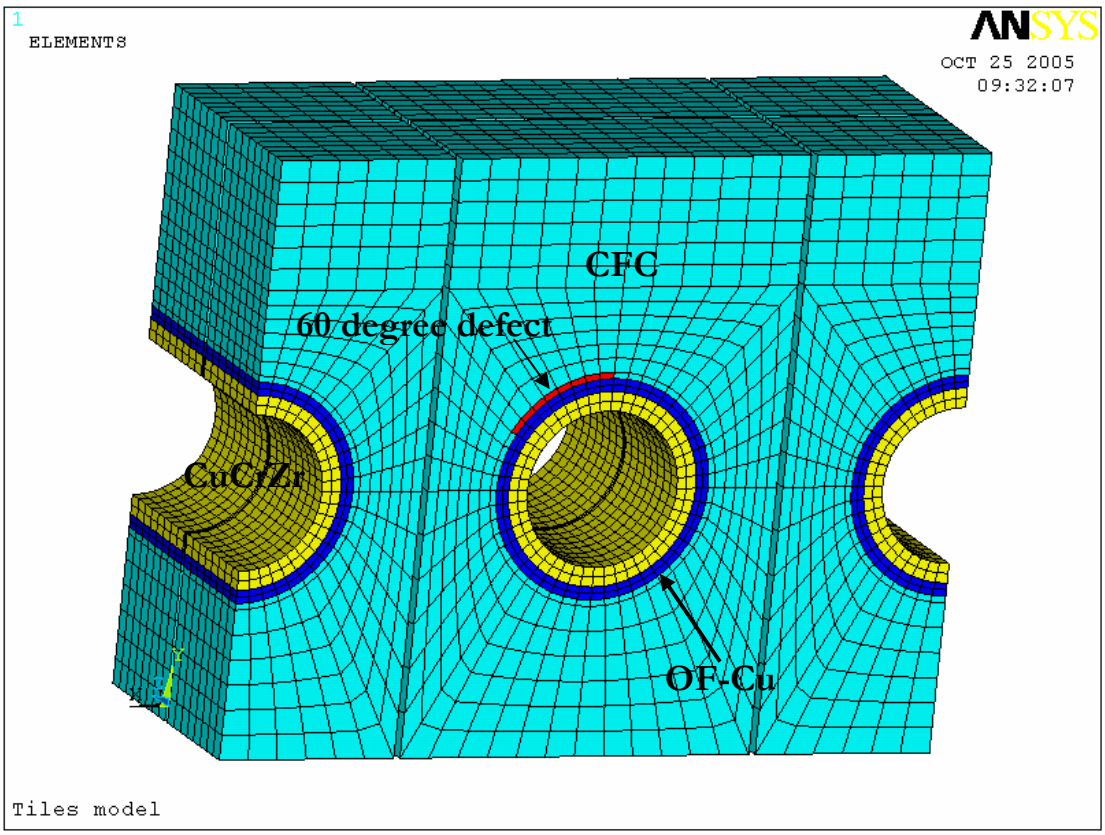

Fig. 4.6.2.4. The model used to study a 60° defect located on the top.

Therefore, a cut-off value of ΔT_{SATIR} = 8 °C can be used as tentative value to accept each tiles.
A variation of thermal conductivity for sure will influence the behaviour of the tiles in term of maximum surface temperature and maximum heat flux on the wall of the cooling channel. A study has been performed with a series of analyses, to verify the influence of the variation of the thermal conductivity in the surface temperature and in the WHF.
A new set of analyses using the same condition described in chap. 4.5 has been carried on for different defect and thermal conductivity. The considered kinds of defects are showed in fig. 4.6.2.5 (in red).

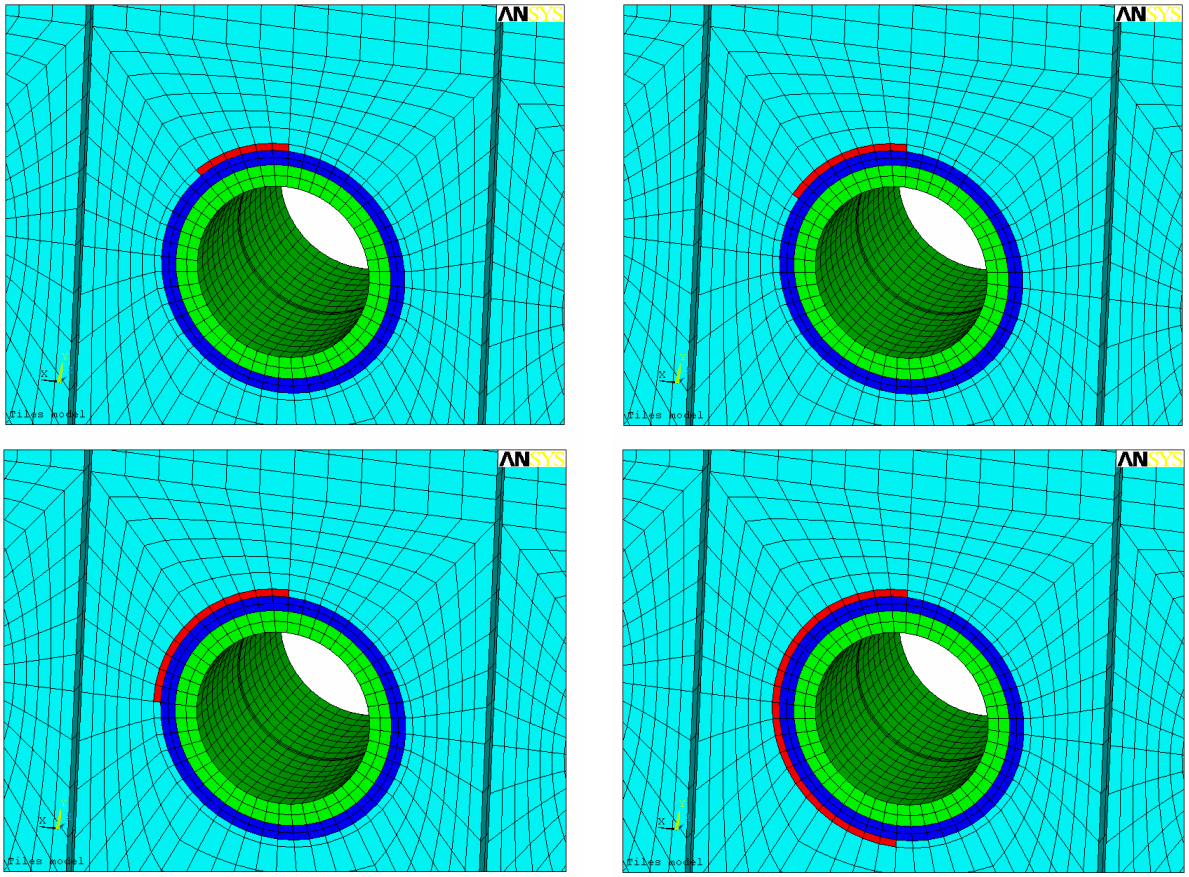

Fig. 4.6.2.5 The kind of defects considered for the assess of the influence of the thermal conductivity and the extension of the defect in the surface temperature and WHF of the tiles

The figures below show the tridimensional behaviour of the WHF and the surface temperature as function of the defect extension and the variation of thermal conductivity.

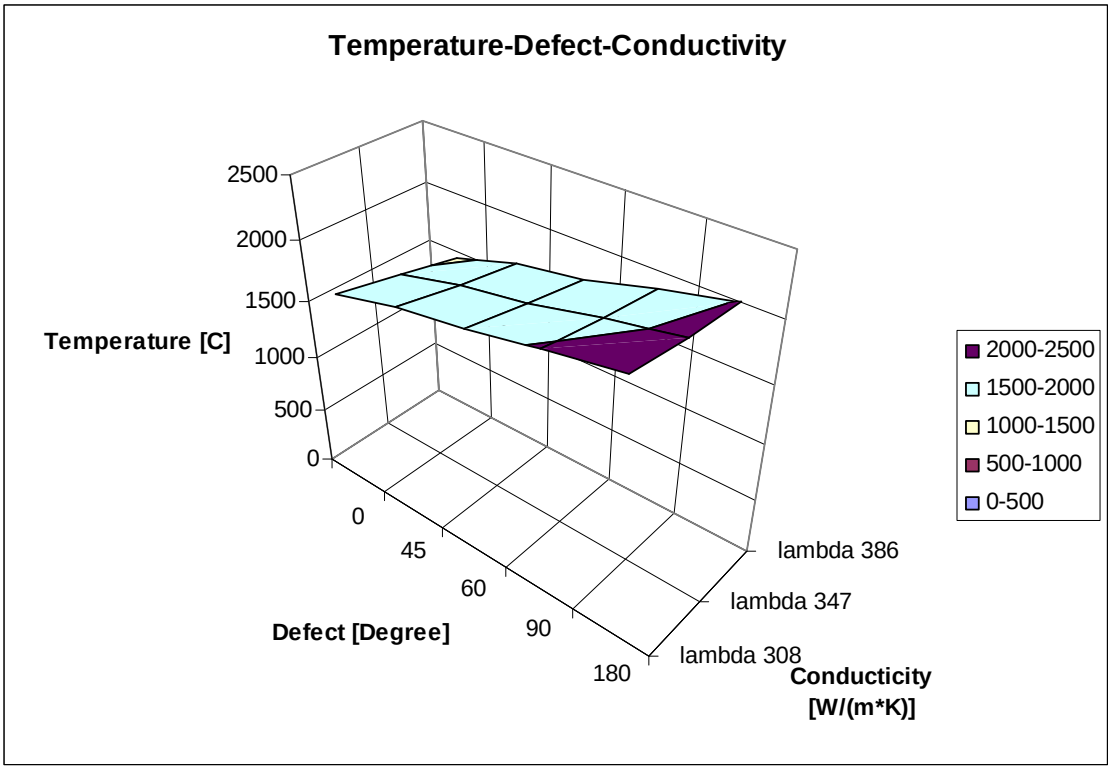

Fig. 4.6.2.6 The Surface temperature functions of the thermal conductivity and extension of the defect.

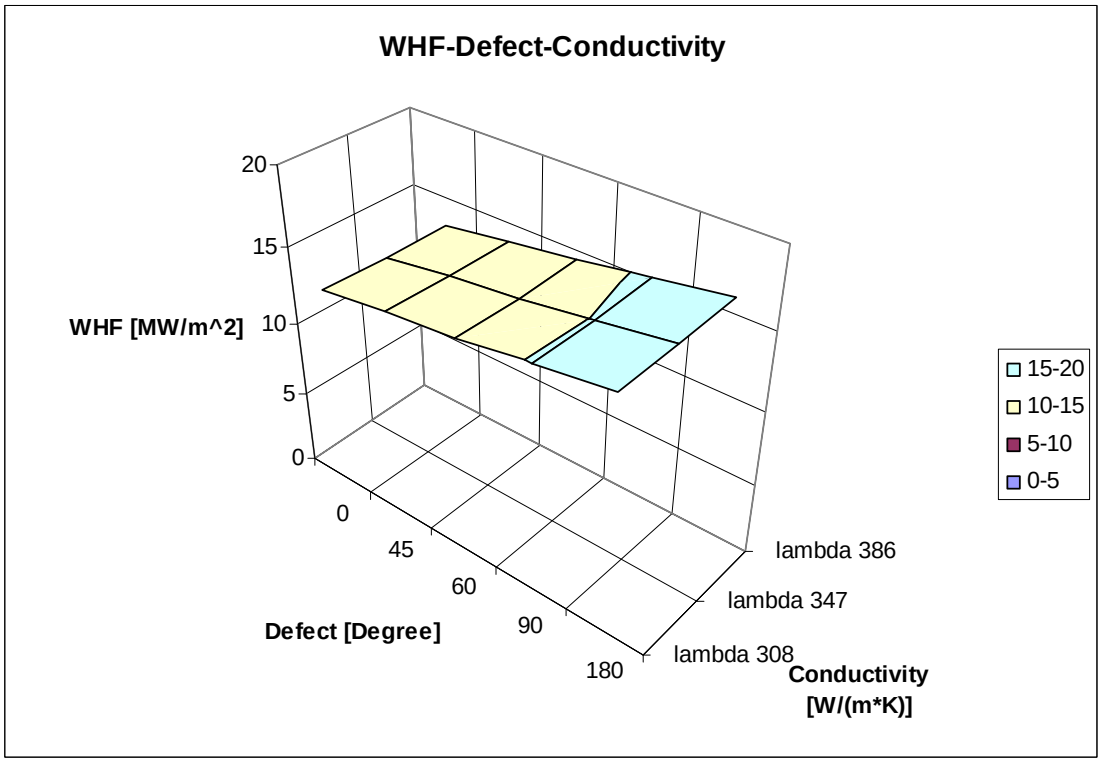

Fig. 4.6.2.7 The Wall Heat Flux functions of the thermal conductivity and extension of the defect.

To better understand the behaviour of the surface temperature and WHF function of the extension of the defect and the conductivity, just for example two bi-dimensional pictures have been extracted respectively from the figures 4.6.2.6 and 4.6.2.7 @ 2000 °C and @ 14 MW/m^2:

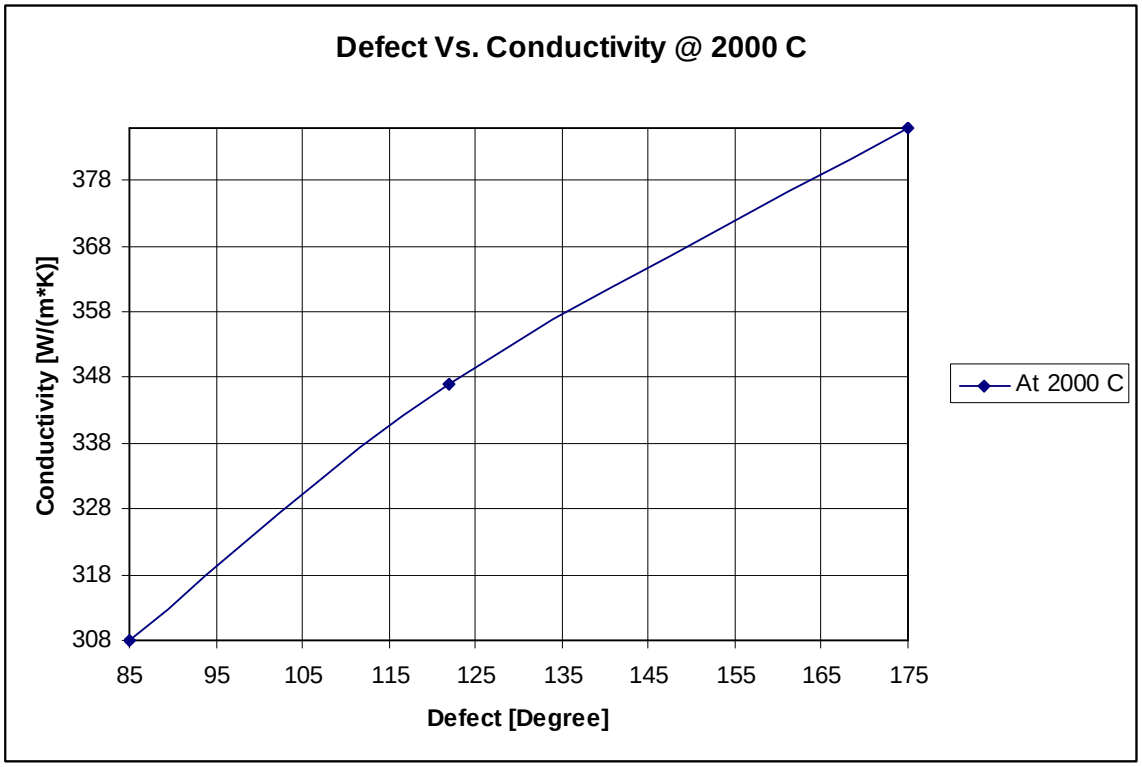

Fig. 4.6.2.8 2D figure extracted from figure 4.6.2.6 @ 2000 °C

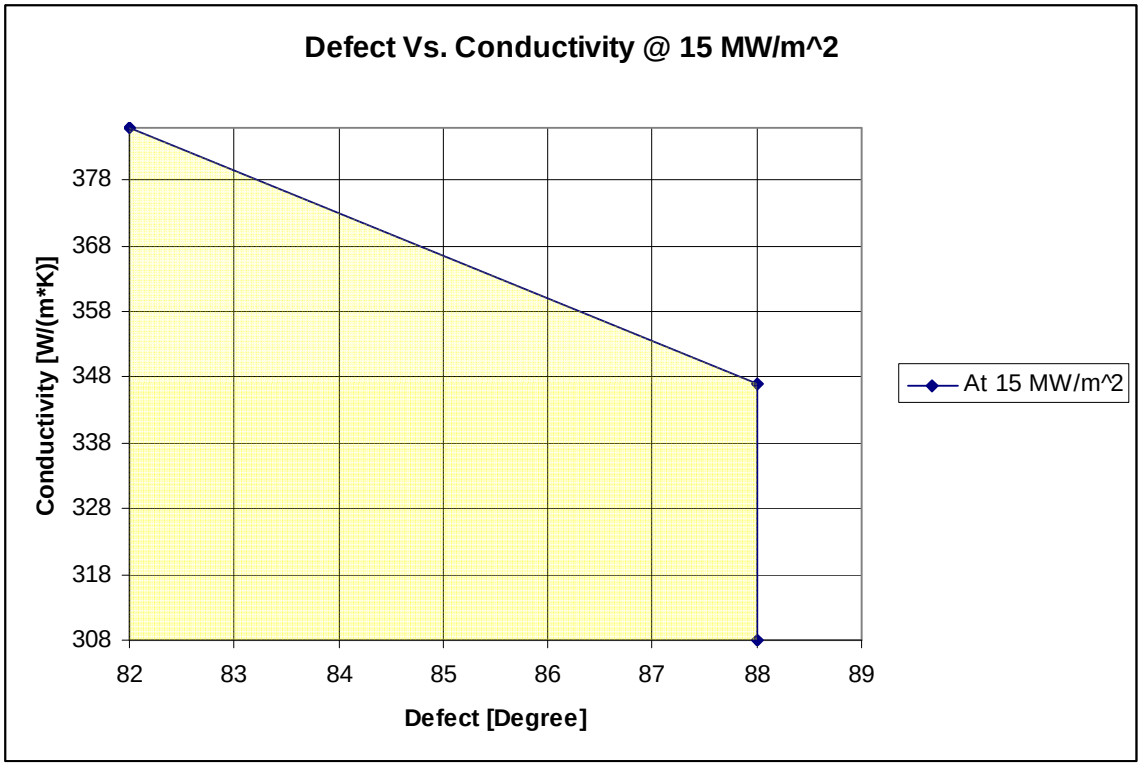

Fig. 4.6.2.9 2D figure extracted from figure 4.6.2.7 @ 15 MW/m^2.

The figure 4.6.2.8 shows that the variation of conductivity and/or the presence of a defect in the tiles gave an almost linear variation of the surface temperature. This means that the presence of a defect or an equivalent variation of thermal conductivity has the same effect in term of variation of surface temperature.

The figure 4.6.2.9 shows that the variation of conductivity and/or the presence of a defect in the tiles have a completely different effect in term of WHF (as we were expecting). The good new is that the influence of the variation of thermal conductivity in the WHF is very limited also with different condition (not showed here). In the figure 4.6.2.9 is showed, for example, that a big variation of thermal conductivity correspond to a few degree of defect (with a WHF of 15 MW/m^2) 6 degree from 82 to 88 degree.
When all the data will be fixed a curve like 4.6.2.9 could be used as curve of acceptance.
Looking fig. 4.6.2.9, a condition of acceptance could be defined: all the tiles that fall in the yellow region can be accepted and vice versa.

4.6.3 Evaluation of the reference distribution

The cut-off value, which avoids the likelihood of burnout, though suitable for an individual tile is not acceptable for the target as a whole, as there is a need to ensure a good average component quality, and avoid excessive erosion. The possible way to solve this kind of problems is a probabilistic approach. A reference distribution (representing the quality that we want to achieve) must be defined. Then the distribution obtained from testing the tiles with the SATIR method should be compared with the reference distribution. At the end a decision must be taken to accept or refuse the poloidal elements.

The best way to choose the reference distribution should be consider the real distribution involved in the process. It is possible to estimate that the final distribution is the sum of the distributions due to the main parameters that govern the whole process:

1) The variation of thermal conductivity in the CFC that in terms of ΔT_{SATIR} should have a mean value of 0 °C with a certain standard deviation.
2) The defect itself that might have a mean value of 2 °C (equivalent to a defect of 20°)

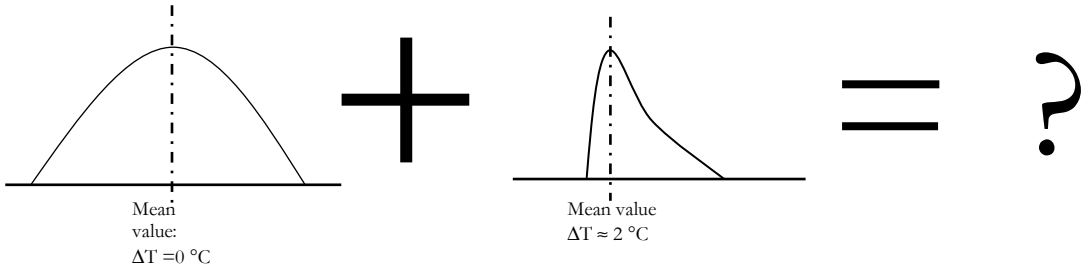

Fig. 4.6.3.1. The total distribution should be a combination of the two main parameters that govern the whole process: Variation of thermal conductivity and the presence of a defect.

At this point could be useful to see the situation of the existing mock-up doing a statistical study on the experimental data available. The fig. 4.6.3.2 shows a mock-up of the inner vertical target. The upper part is made by Tungsten, the lower part is CFC.

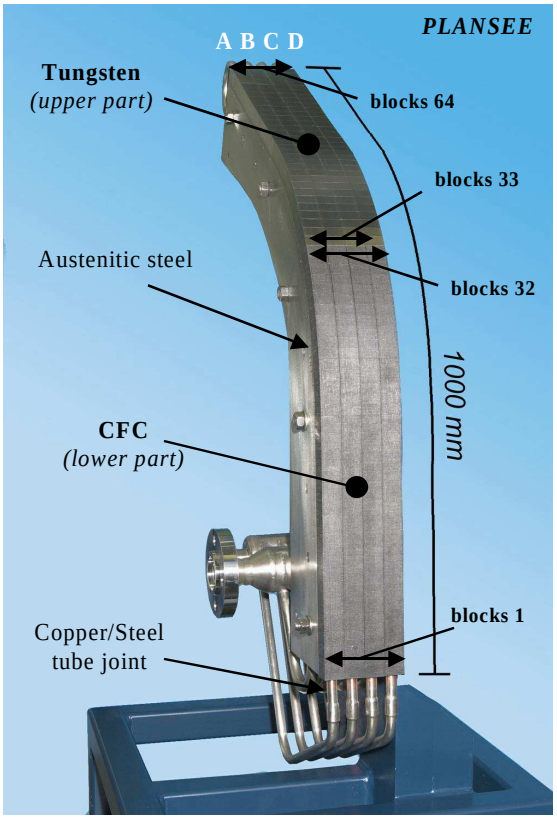

Fig. 4.6.3.2. European prototype with CFC & W armour.

In the figure are visible 4 poloidal elements i.e. 4 polodal strip with 32 monoblocks per each strip. On these 4 poloidal elements (A,B,C and D) has been performend a SATIR examination and for comparison a high flux test with the facility FE200 (electron beam). The results of this examination are shown in fig. 4.6.3.3.

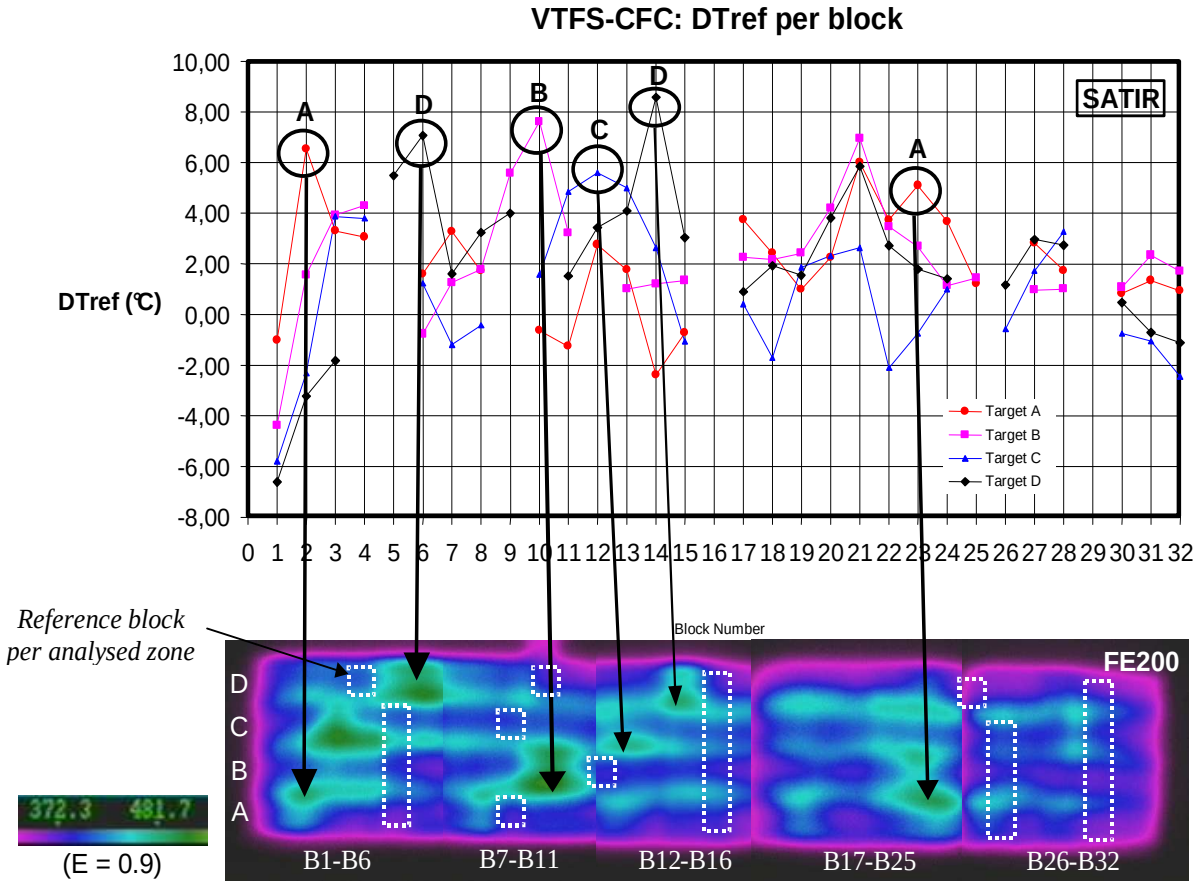

Fig. 4.6.3.3. Results of the SATIR test and high heat flux test.

In the poloidal element D has been found a monoblock with a $\Delta T_{SATIR} > 8$ °C then only the data of the poloidal elements A, B and C has been introduced in the graph of fig. 4.6.3.4. The figure below shows the frequency distribution of the number of tiles per each range of ΔT_{SATIR} (i.e. between 0 and 1 °C of ΔT_{SATIR} there are 6 monoblock belonging to the poloidal elements A, B and C).

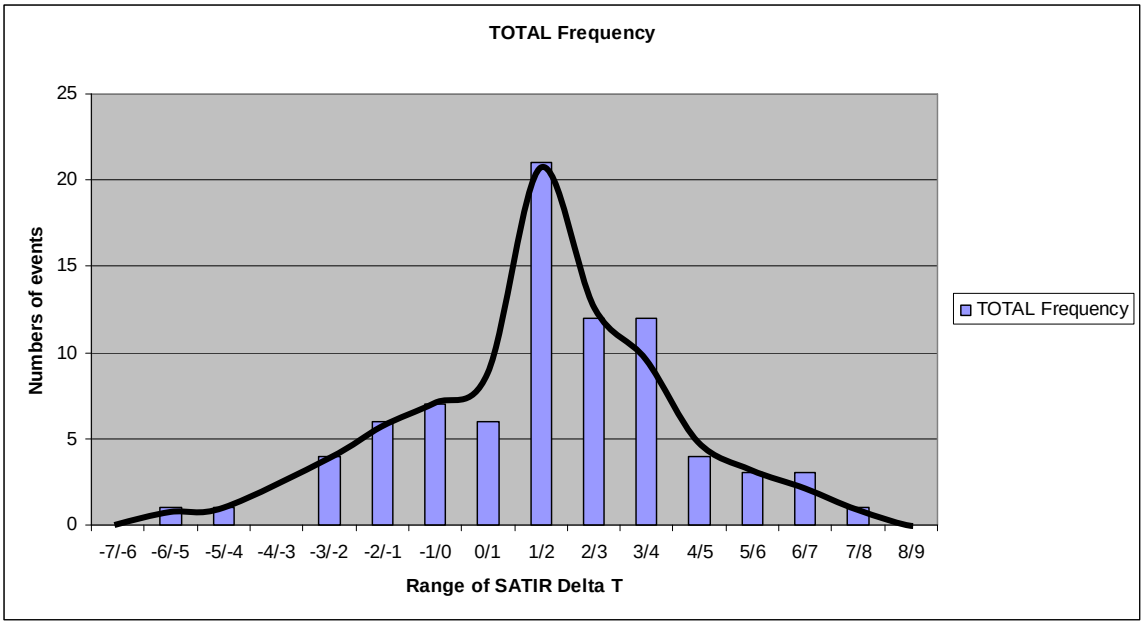

Fig. 4.6.3.4. Total distribution function of the ΔT_{SATIR}

Taking in mind the fig. 4.6.3.1, the fig. 4.6.3.4 represent the total distribution (the curve on the question mark). Therefore, it is possible to subtract from the total distribution the distribution relative to the uncertainty due to the thermal conductivity. This is easy to do because the distribution relative to the uncertainty of the thermal conductivity must be centered on $\Delta T_{SATIR}=0$, must be symmetric and the results of this subtraction can not have value of $\Delta T_{SATIR} < 0$. Then the fig. 4.6.3.5 is the distribution of the defect in the tiles (i.e. there are 17 monoblock that have a ΔT_{SATIR} between 1 and 2 °C)

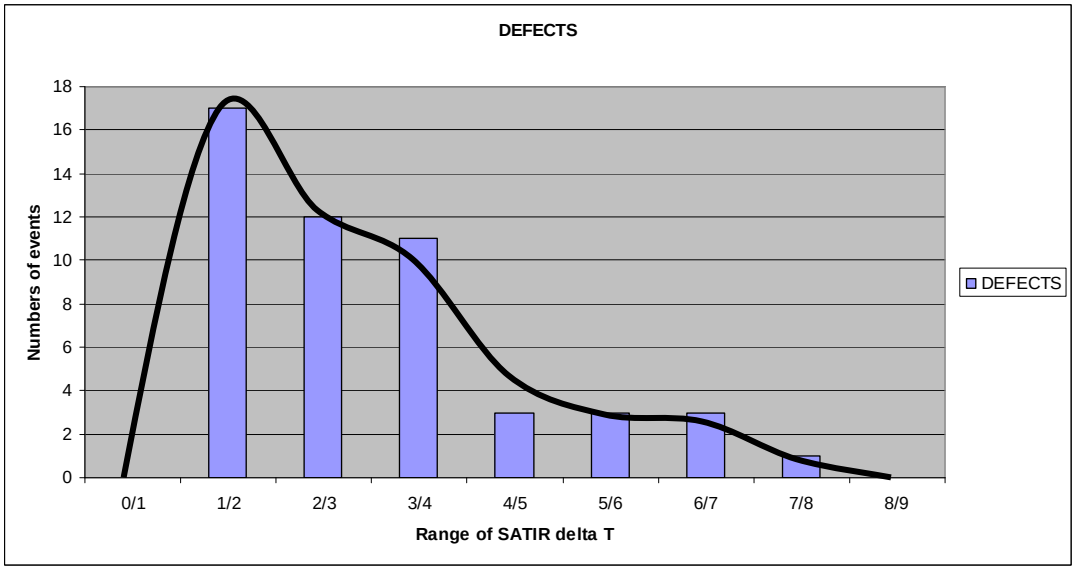

Fig. 4.6.3.5. Distribution function of the defect in the tiles.

The distribution of fig. 4.6.3.6 has the shape that we were thinking (compare with fig. 4.6.3.1). Using the medical commercial software MedCalc 7.5.0.0 a test of normality using the D'Agostino-Pearson approach has been done on the total distribution of the tiles. The results are reported in fig. 4.6.3.6.

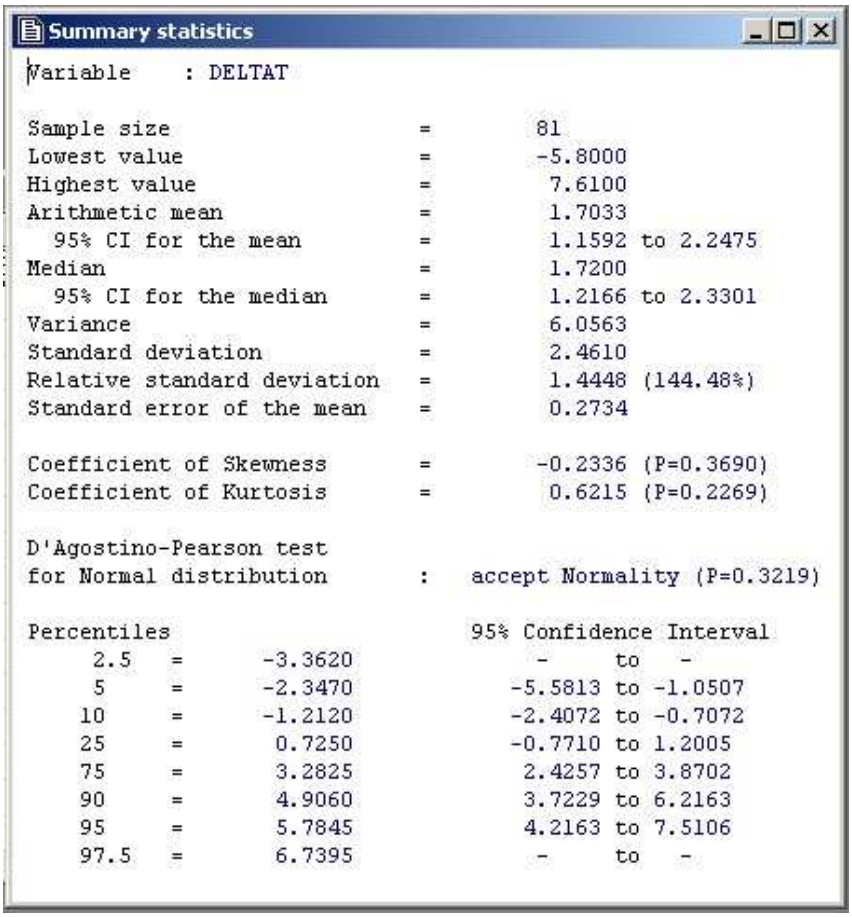

Summary statistics

Variable : DELTAT

Sample size	=	81	
Lowest value	=	-5.8000	
Highest value	=	7.6100	
Arithmetic mean	=	1.7033	
95% CI for the mean	=	1.1592	to 2.2475
Median	=	1.7200	
95% CI for the median	=	1.2166	to 2.3301
Variance	=	6.0563	
Standard deviation	=	2.4610	
Relative standard deviation	=	1.4448	(144.48%)
Standard error of the mean	=	0.2734	
Coefficient of Skewness	=	-0.2336	(P=0.3690)
Coefficient of Kurtosis	=	0.6215	(P=0.2269)

D'Agostino-Pearson test for Normal distribution : accept Normality (P=0.3219)

Percentiles			95% Confidence Interval		
2.5	=	-3.3620	-	to	-
5	=	-2.3470	-5.5813	to	-1.0507
10	=	-1.2120	-2.4072	to	-0.7072
25	=	0.7250	-0.7710	to	1.2005
75	=	3.2825	2.4257	to	3.8702
90	=	4.9060	3.7229	to	6.2163
95	=	5.7845	4.2163	to	7.5106
97.5	=	6.7395	-	to	-

Fig. 4.6.3.6. Summary of the normality test conducted on the total distribution.

It is important to show that in this case the total distribution can be considered a normal distribution (this assumption will simplify all future operations). This mean that the variation of thermal conductivity play the main role on the distribution of the value of ΔT_{SATIR} . From the summary of the statistical check of normality can be extracted other informations: the mean value of the distribution is 1.7 and the standard deviation is 2.46. Based on the standard deviation in the thermal conductivity and on the results obtained from the manipulation of the experimental data relative to the existing mock-ups the choice, as reference distribution, of a normal distribution with a mean value per batch of ΔT_{SATIR} = 2°C and with a standard deviation = 3°C seems reasonable as a compromise between ensuring good average component quality and manufacturing feasibility. This implies an average defect size equivalent to a 15-20° (2mm) circumferential crack over the entire length of a tile.

4.6.4 Rules of decision

The last problem is to decide if the sample belongs to the population i.e. to the reference distribution. Rules need to be established to allow the decision to be taken [14], [15]. The parameters α (error of first kind) and β (error of second kind) should form the basis for the contract decisions to be taken with industry. An explanation of the meaning of these two parameters can be made with a legal analogy reported in table 4.6.4.1.

- Hypothesis0: The accused is innocent – the sample belong to the population
- Hypothesis1: The accused is guilty – the sample doesn't belong to the population
- alfa = error of first kind (convict an innocent) – reject a good element
- beta = error of second kind (acquit a guilty) – accept a bad element
- The guilt must be proved without any reasonable doubt. A good element should not be rejected. Alfa should be as low as possible
- The guilty must be convicted. A bad element should not be accepted. Beta as low as possible.
- A low value of alfa means high value of beta and vice versa.
- Theoretically to have alfa = 0 you should release all the accused $\Rightarrow$ beta = 1 (i.e. accept all elements).
- Theoretically to have beta = 0 you should acquit all the accused $\Rightarrow$ alfa = 1 (i.e. reject all elements).
- The only way to minimise alfa and beta is to increase the investigation to ensure a good decision is taken - increase the sample analysed.

Table. 4.6.4.1. Legal analogy to explain the meaning of alfa (error of first kind) and beta (error of second kind)

The application of the procedure to our case can be summarized in the table below:

Hypothesis:

H0: $\bar{x} = \mu$

The mean value of the sample is equal to the mean value of the population (the reference distribution). The sample belongs to the population.

H1: $\bar{x} > \mu$

The mean value of the sample is higher than the mean value of the population (the reference distribution). The sample doesn't belong to the population.

Data:

Mean value of the reference distribution = 2 °C

Standard deviation of the reference distribution = 3 °C

Sample analysed = 32 units (one CFC strip; for the outboard target is 40 units)

Table 4.6.4.2. Application of the rule of decision to our situation.

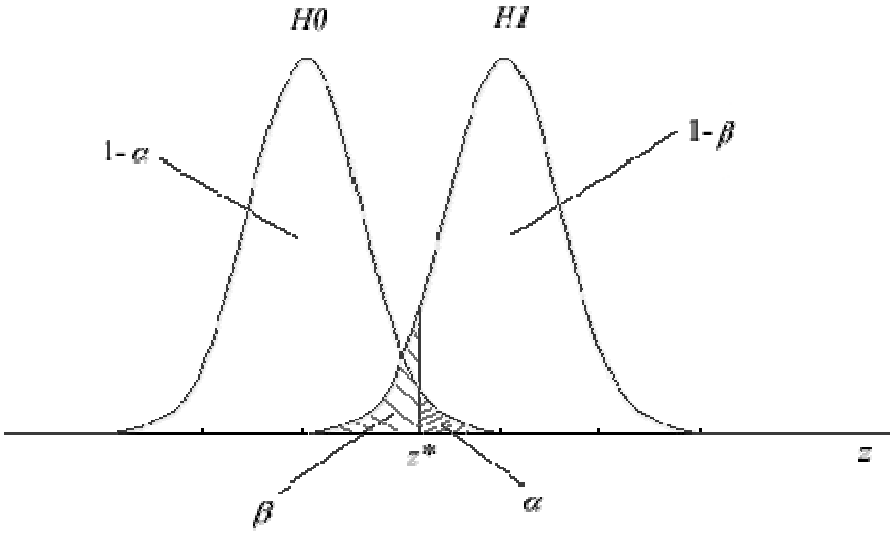

Fig. 4.6.4.1. Meaning of alfa and beta related to the hypothesis

Then:

Alfa is the probability to reject H0 when it is true. The probability to reject a good element! A good element is an element that has a mean $\Delta T_{SATIR} \leq 2$ °C.

Beta is the probability to accept H0 when it is false and H1 is true. The probability to accept a bad element! A bad element is an element that has a mean $\Delta T_{SATIR} > 2$ °C.

Fixing alfa to 1% it is possible to find beta relative to our problem with the "operative curve" (see fig. 4.6.4.1.).

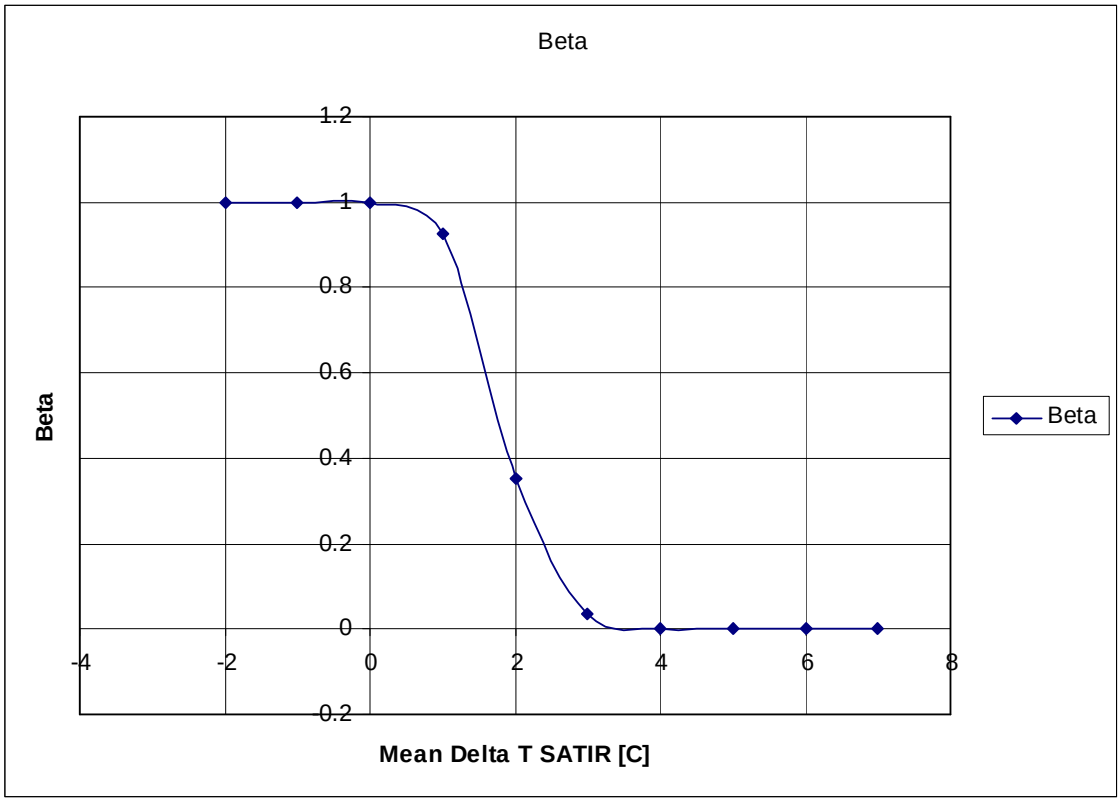

Fig. 4.6.4.2. Operative curve relative to ours problem

The probability to reject a good element is 1% (alfa) when we reject all the samples that have a ΔT_{SATIR} mean >3.3 °C. This can be calculated with the formula:

$$z = \frac{\overline{x} - \mu}{\sigma / \sqrt{n}}$$

Where:

$\overline{x}$ is the mean value of the batch;

μ is the mean value of the population (2 °C);

σ is the standard deviation of the population (3 °C),

n is the number of monoblocks per poloidal elements (32).

z is 1.88 (the normalised value for a level of confidence for 99 % of a Gaussian distribution with one tail).

3.3 °C correspond to the normalized value of 1.88

The probability to accept a "bad" element (beta) when it has a ΔT_{SATIR} means value > 2 °C. For example: the probability to accept an element with a ΔT_{SATIR} mean value of 3 °C instead than 2 °C are ≈ 1.4 % (see figure 4.6.4.2). Moreover, the probability to accept an element with a ΔT_{SATIR} mean value of 4 °C instead than 2 °C are ≈ 0%.

4.7 An example of the adopted procedure

It could be useful to summarize with an example the procedure of acceptance of the monoblocks and the poloidal elements.

Using the following data:

- Alfa = 0.01
- Mean value of the reference distribution = 2 °C
- Standard deviation of the reference distribution = 3 °C
- Cut off value = 8 °C
- Sample analysed = 32 units, one CFC strip (40 units for the external side)

ΔT_{BLOCK} is the maximum ΔT_{SATIR} of each individual monoblock

ΔT_{MEAN} is the mean ΔT_{SATIR} of a strip of monoblocks on a poloidal element.

The procedure can be described with the flow chart of fig. 4.7.1.

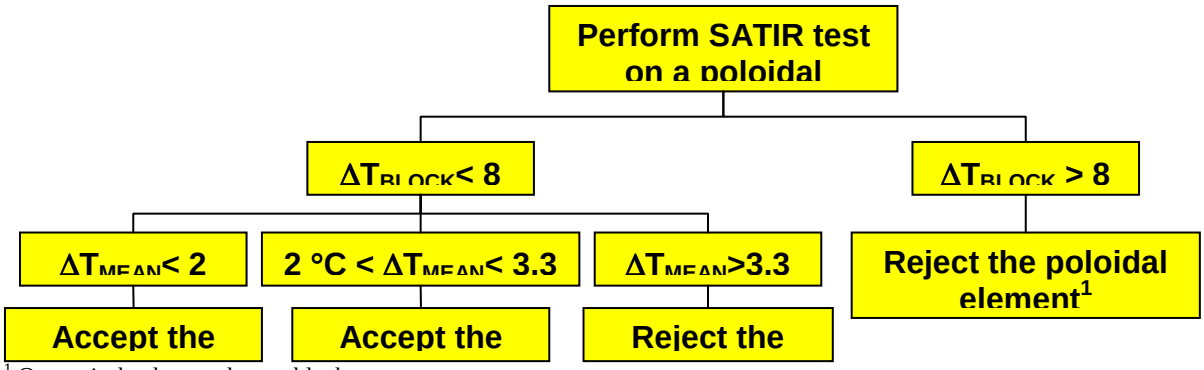

[1] Or repair the damaged monoblock

[2] May happen that the real mean value of the poloidal element is < 2 °C

[3] There is a probability β between 35 % and 1 % that the real mean value of the poloidal element is between 2 and 3.3 °C

[4] There is a 1 % probability α that a good poloidal element is rejected.

Fig. 4.7.1 Flow chart of a possible procedure to accept or reject monoblocks and poloidal elements in the machine

4.8 Final considerations

In order that the monoblock armour can operate without risk of burnout and without releasing excessive amounts of carbon the following tentative acceptance limits are proposed for the CFC monoblock armour subjected to the SATIR test:

- each tile shall have a $\Delta T_{SATIR} \leq 8°C$,

and after passing this first test

- each batch shall belong to a normal distribution with a mean $\Delta T_{SATIR} = 2°C$ and a standard deviation = 3°C.

A batch could include 80-40 monoblock tiles of two or one outer VT poloidal element or the 64-32 tiles of two inboard elements. The proposed values are based on using CFC with a room temperature thermal conductivity $\geq 350 Wm^{-1}K^{-1}$ and a standard deviation of 18 $Wm^{-1}K^{-1}$. The practicality of using these postulated values is to be tested during the R&D programme currently under way in the EU, on completion of which the values of acceptance levels can be finally set. In particular, ITER and EFDA (European Fusion Development Agreement) are working with CFC manufacturers in an attempt to reduce the standard deviation of the CFC thermal conductivity. The values are also tentative in that they have been developed based on start-of-life performance of the armour and future studies using the tools that have been developed during this thesis (see chap. 5) will take into account of the predicted performance as the armour is eroded away.

5. The erosion of the CFC tiles in the ITER divertor

5.1 Background

5.1.1 General considerations

The detailed analysis of the erosive phenomena of the material of the first wall is fundamental for the studies of the possible configuration during the normal operation as well as for the evaluation of the life of the components. The evaluation of the speed of erosion of the CFC (Carbon Fibre Composite) tiles of the divertor is very important to evaluate the longevity of those components.
The idea is to develop a user-friendly software, inside a commercial and certificate finite element code like ANSYS, able to evaluate the evolution of the erosion in the CFC tiles of the divertor.
The program developed can take into account the shadow effect of a tile on its ions bombarded neighbour as well as a detachment of the monoblock from its cooling channel.

5.1.2 Fundamental process on proton-carbon interaction at high temperature

The interaction of energetic hydrogen ions with graphite and carbon compounds and the induced dominant mechanism of erosion have been hugely studied for the use of these materials as plasma facing wall in the fusion devices Tokamak [17-36]. These interaction lead to several physico-chemical processes that can result in a high sputtering yield and to hydrocarbons and carbon atoms emission and give to graphite a special behavior, compared to metals. In fact, contrary to the metals for which the sputtering yield does not depend on target temperature, the graphite shows a steady increase of the yield above 1500 K.
When graphite is irradiated by hydrogen ions, at high temperature, it may be sputtered due to three processes:

- the physical sputtering, which implies collisional processes and is characterized by C_1 emission [17-22];
- the chemical sputtering, which is due to a chemical affinity between the implanted particles and the target material and come to molecules formation [18], [21-24];
- the thermal sublimation and the radiation enhanced sublimation (RES): the thermal sublimation dominates for temperature above 2000 K and consists essentially of the emission of C_1, C_2 and C_3 clusters. The RES is peculiar to graphite and carbon materials and is characterized by only mono-atomic carbon emission [21], [22], [26-29].

5.1.2.1 The physical sputtering

The physical sputtering occurs for all materials, independently of the chemical nature of the projectile and target atoms and of the temperature. It results from a nuclear energy transfer of the projectile to the target atoms, leading to atomic displacements, thus causing lattice damages and sputtering. The surface atoms are ejected if they have received a sufficient kinetic energy to overcome the surface binding energy Es of the solid.
The interaction of energetic particles, the collisional and physical processes, especially the physical interaction of graphite with H^+ ions, have been well developed in the last 30 years by numerous authors [17-22].
The physical sputtering yield at normal incidence can be described by the Bohdansky formula [21] and [36] which gives a good agreement with experimental data in the keV region.

$$Y_{PHY}(E) = Q \cdot Sn(E) \cdot \left[1 - \left(\frac{E_{TH}}{E_0}\right)^{\frac{2}{3}}\right] \cdot \left(1 - \frac{E_{TH}}{E_0}\right)^2$$

Where:
Q is a fitting parameter [atoms/ions];
Sn(E) is the function for the energy dependence of the energy deposited in elastic collision (stopping power);
E_{TH} is the energy threshold [eV];
E_0 is the energy of incident particles [eV].
The *Sn(E)* function can be approximated by the relation based on the Thomas–Fermi potential:

$$Sn(E) = 0.5 \cdot \frac{\ln\left(1 + 1.2288 \frac{E_0}{E_{TF}}\right)}{\frac{E_0}{E_{TF}} + 0.1728 \cdot \sqrt{\frac{E_0}{E_{TF}}} + 0.008 \cdot \left(\frac{E_0}{E_{TF}}\right)^{0.1504}}$$

A non-perpendicular angle of incidence enhances the sputtering yield. Its angular dependence is well described by the Yamamura formula [21] and [36].

$$Y_{PHY}(\theta) = Y_{PHY}(\theta = 0) * (\cos\theta)^{-f} \, e^{\left[f\left(1 - \cos\theta^{-1}\right) * \cos\theta_{OPT}\right]}$$

Where:
θ is the angle of incidence;
f and θ_{opt} are used as fitting parameters.
The different parameters for proton incident on carbon foils are given in [35] and [36]. Figures 5.1.2.1.1 and 5.1.2.1.2 give the comparison of the energy and angular

dependencies of the physical sputtering yield obtained with the Bohdansky formula and with the TRIDYN code.

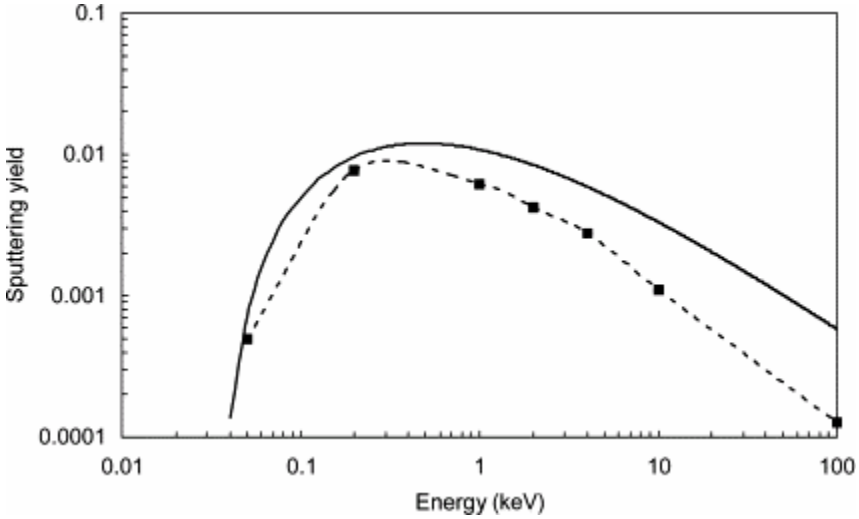

Fig. 5.1.2.1.1. Dependence of the physical sputtering yield of graphite on incident energy for hydrogen ions at normal incidence, calculated with TRIDYN (points and dotted line) and with the Bohdansky formula (continuous line).

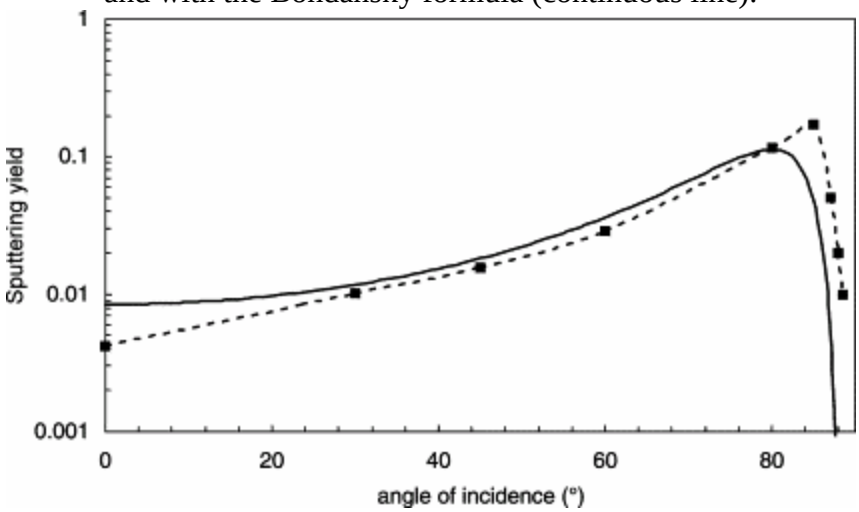

Fig. 5.1.2.1.2. Dependence of the physical sputtering yield of graphite on the angle of incidence for hydrogen ions (2 keV) calculated with TRIDYN (points and dotted line) and with the Yamamura formula (continuous line).

The TRIDYN code that has been developed by Möller et al. [20] is a dynamic version of the TRIM code [37] that has been used to check and set-up the program developed during this thesis. It takes into account the composition changes in real time due to the deposition of the projectiles and the collisional transport. It can thus simulate the fluence dependent phenomena like sputtering and reflection, and allows to obtain accurate results in good agreement with experimental data.
Both these codes are MonteCarlo codes based on the binary collision approximation, assuming that the target is amorphous. They are well described in [19], [20].

5.1.2.2 The chemical sputtering

The chemical reactions between hydrogen ions and graphite are complex and lead to the emission of hydrocarbons [18], [21], [22], [24], [25], [34] and [35]. We actually have a good overview of the main chemical mechanisms for temperature less than 1000 K.
After a collision sequence, the ions penetrate at a depth of about a few hundred nanometers and are implanted in the graphite, diffuse in the bulk material and get trapped. Finally, the hydrogen will react with carbon atoms or recombine with implanted hydrogen atoms at the end of their range. These reactions lead to the emission of hydrocarbons (such as CH_4, C_2H_x, CH_3 radicals and heavier hydrocarbons) and H_2 molecules.
Wittmann and Küppers [34] and Roth [35] have explained the chemical erosion and the hydrogenation at the surface of carbon materials according to an atomistic process: their models deal with a change of the hybridization (from sp^2 to sp^3) due to incident H atoms.
Three processes determine the chemical erosion of carbon under low energy hydrogen bombardment:
(1) The reaction of thermalised ions within the implanted surface proceeds via the hydrogenation of carbon atoms to CH_3–C complexes. At temperatures above 400 K CH_3 radicals can be released while at temperatures above 600 K recombinative hydrogen release (H_2) starts to reduce the chemical erosion yield. This thermal chemical erosion was elucidated in detail by Küppers et al. [58], [38] and was described analytically by Roth and García-Rosales [59]. For the thermal reaction no dependence on the hydrogen isotope was observed.
(2) The thermal reaction is enhanced by radiation damage introduced in the material which provides open bonds for hydrogen attachment. Damage is created by kinetic energy transfer from incident ions to lattice atoms and is, therefore, responsible for the dependence of the chemical erosion yield on hydrogen isotope. This yield enhancement is characterized by a threshold energy for damage production, E_{dam}. The basic thermal reaction below the threshold for damage production depends strongly on the crystalline perfection of the carbon material with maximum yields between 10^{-3} for well annealed pyrolytic graphite and 10^{-1} for amorphous a-C:D layers [39]. At energies where radiation damage amorphises the graphite lattice, the strong dependence on the material structure disappears [40].
(3) At low surface temperatures all available carbon atoms are essentially hydrated but no thermal release of hydrocarbons occurs. However, hydrocarbon radicals are bound to the surface with much smaller binding energy (≈1 eV) than carbon surface atoms in their regular lattice environment (7.4 eV). This leads to an ion induced desorption of hydrocarbon radicals which can be described in a manner analogous to physical sputtering using a threshold energy, E_{des}, in the low eV range.
The investigation and description of these processes has been performed for thermal hydrogen atom or ion fluxes of the order of 10^{18}–10^{20} m^{-2} s^{-1}. The thermal reaction cycle predicts a pronounced shift of the temperature, T_{max}, where the maximum yield occurs towards higher temperatures with increasing ion flux, while the maximum yield itself decreases only slightly. This temperature shift with ion flux is well reproduced in the experimental data [41]. However at fluxes above 10^{21} m^{-2} s^{-1} as reached in plasma simulators or under tokamak conditions, the temperature of maximum yield does not

exceed 900 K. At these elevated temperatures, the thermodynamic equilibrium of H/C system shifts from CH_4-formation to H_2 release [42] and the erosion yield is expected to decrease with ion flux. Additionally, annealing of radiation damage will result in lower reactivity of the carbon material.
The combination of these three effects is given by the formula:

$$Y_{CHEM}(E,\Phi) = Y_{surf} + Y_{THERM} + D * Y_{THERM} * Y_{DAM}$$

where *D* is a parameter depending on the hydrogen isotope.
For a more detailed explanation of this formula see chap. 5.3.3.7.

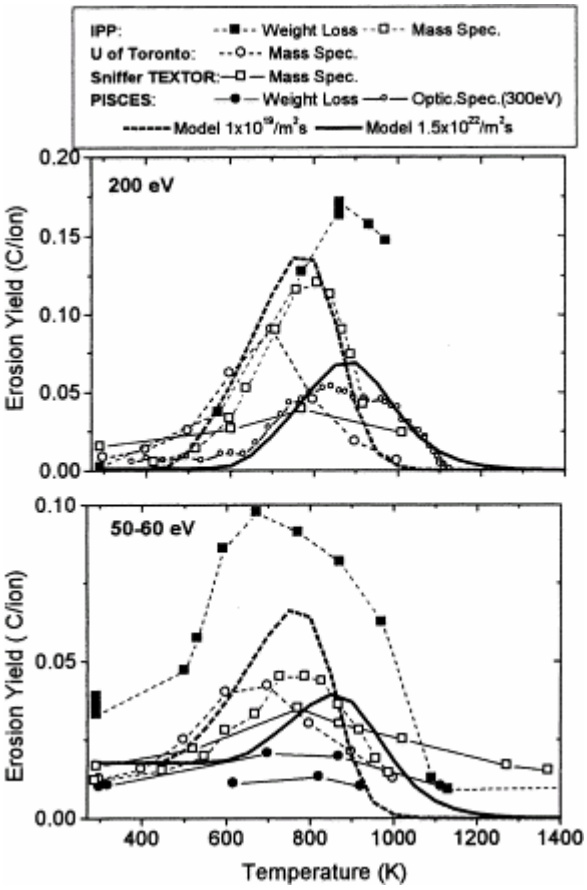

Fig. 5.1.2.2.1. Comparison of experimental data for the temperature dependence of the chemical erosion of carbon under deuterium bombardment with the analytic model suggested by Roth. Data for ion fluxes around 10^{19} m^{-2} s^{-1} (ion beam experiments): dashed lines; high flux data around 1.5×10^{22} m^{-2} s^{-1} from plasma experiments: solid lines. Note that physical sputtering has been subtracted from weight loss data.

The figure 5.1.2.2.1 show a comparison of some experimental data with the model suggested by Roth. The fact that emitted hydrocarbon radicals partly stick to the vessel surfaces rather than being hydrated to volatile saturated hydrocarbons may explain the

experimental discrepancies between erosion yields determined by weight loss and by residual gas mass spectrometry.

5.1.2.3 Sublimation of graphite

In our temperature range and in the high vacuum of the chamber, graphite will loose mass by sublimation. We can thus assume that the effects of recondensation on the surface are unimportant and that the equilibrium vapor pressure for each carbon species is equal to their partial pressure. The rate of vaporization for each carbon species i is given by the Langmuir–Knudsen equation. The total rate of vaporization thus writes:

$$\dot{m}_i(T) = \sum_{i=1}^{n} \alpha_i P_i(T) \left(\frac{M_i}{2\pi RT} \right)^{1/2}$$

where $\dot{m}_i$ is the mass loss rate (g m^{-2} s^{-1}) of species i, α_i the vaporization coefficient, P_i the equilibrium vapor pressure, M_i the molecular weight, T the temperature, and R the universal gas constant.
The above equation allows us to calculate the mass loss rates for each the carbon species C_1 through C_5 and the total mass loss rate as a function of temperature. The results are plotted in figure 5.1.2.3.1. In the temperature range from 1800 to 2400 K, the most important species are C_1, C_2 and C_3. The mass loss rates and so the carbon species flux increase drastically with temperature, by a factor of 10 for each 100 K step. This steep increase thus requires to control very accurately the temperature of the material.

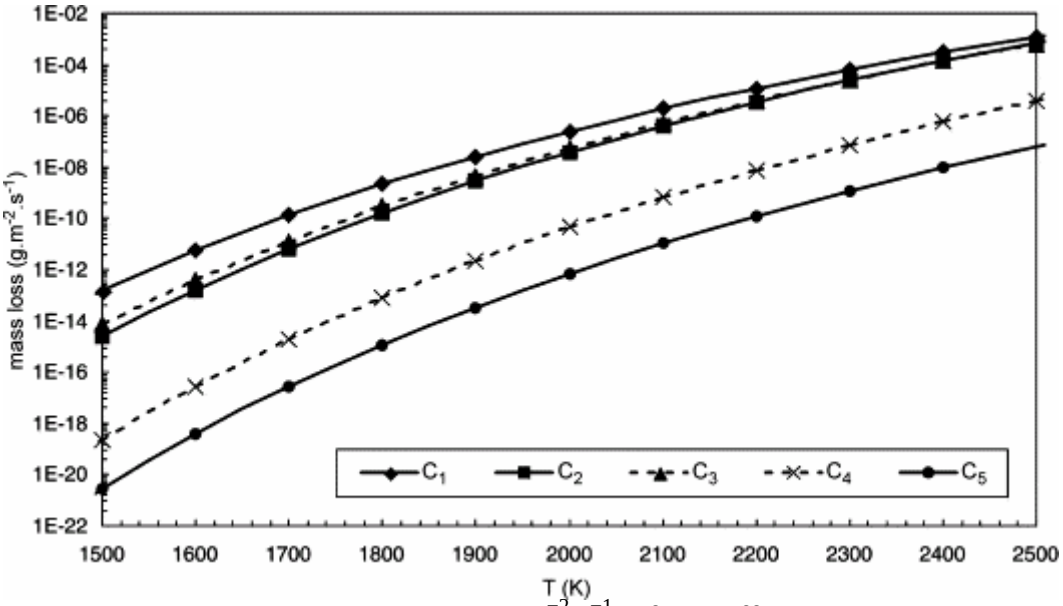

Fig. 5.1.2.3.1. Calculated mass loss rate (g m^{-2} s^{-1}) of the different carbon species C_1 to C_5 due to graphite sublimation versus temperature.

5.1.2.4 The RES (Radiation Enhanced Sublimation)

For temperatures above 1500 K, the erosion of graphite is dominated by sublimation. Above that temperature, there is another erosion process peculiar to graphite called RES [26-29]. This last effect has only been observed for graphite and is characterized by a steady increase of the sputtering yield with temperature. The RES is not a chemical process since it occurs for hydrogen as well as for inert ions like He or Ar. The sputtering yield due to the RES does not depend on the chemical nature of the incident ions. The temperature dependence of this sputtering yield Y_{RES} is exponential:

$$Y_{RES} = Y_0 e^{\left(-\frac{E_{RES}}{k_B T}\right)}$$

where E_{RES} is the activation energy which varies between 0.75 and 0.85 eV, for hydrogen, k_B the Boltzmann constant, and Y_0 an experimental factor. E_{RES} remains stable for fluxes located between 10^{17} and 10^{19} ions m^{-2} s^{-1} and increases slightly with stronger flux (10^{22} ions m^{-2} s^{-1}). With high incident energy, E_{RES} decreases to reach values of about 0.55 eV.

The RES process consists of the emission of mono-atomic carbon with thermal energies and an isotropic angular distribution. This process can be explained using a collisional model: when incident ions collide the carbon atoms, part of their energy is transferred to the atoms of the network which are dislodged out of their lattice site towards an interstitial position. The interstitial atoms have a large mobility throughout the basal plane and diffuse towards the surface. They can also recombine with vacant sites or agglomerate to form clusters. The interstitial atoms that reached the surface are slightly related to this surface by a Van der Waals force and escape thermically very easily from the material.

5.2 Analytical simulation of the plasma machining phenomena

5.2.1 General considerations

In the ITER divertor the vertical targets that intercept the plasma scrape-off-layer (SOL) are subjected to intense heat flux. If the SOL were intercepted at normal incidence the heat flux would be ~140 MWm^{-2}. However, the targets are inclined so that the heat flux is ~10MWm^{-2}, making water cooling of the target feasible and reducing target erosion so as to provide an acceptable armour lifetime. Each target is armoured with two armour materials. CFC in the region of the SOL strike point, because it ablates rather than melts making it suitable for plasma transients. Tungsten on the upper part of the target where tungsten's low sputter-yield will mean there will be virtually no erosion during normal operation. This paragraph concentrates on CFC armour, and in particular, the armour at the strike point where the heat flux is most intense.

In the divertor design there are ~$5x10^4$ CFC to Cu-tube monoblock joints subjected to high heat flux. A large R&D has focused on developing repeatable and reliable joints, and robust and relatively homogeneous CFC material. Extensive NDE of the joints will be carried out, but this NDE is complicated by the geometry and by the nature of the

materials and processes used in manufacture. Hence, a few defects are likely to escape detection and be installed in the divertor. The consequences of such defects and those that might grow during operation are addressed in this note making some assumption on how the effect of these defects can be mitigated.
Two mechanisms are proposed that will mitigate the effect of a defective tile(s) on the performance of the vertical target:

- reduction in the conducted[1] heat flux to the target due to modification of the surface profile through enhanced surface erosion;
- reduction in the heat flux radiated to the tile due to a reduced view of the plasma due to erosion.

The erosion rate of the CFC is a function of both the surface temperature and the particle flux. At the strike point the majority of the heat in the SOL, ~ 70%, is brought by the particle flux that follows the field lines which intercept the target at a glancing angle (~2 to 3°), and the remaining 30% is a diffuse source radiated from the divertor channel. For cases with impaired (or zero) contact between the CFC and the heat sink tube, the CFC surface temperature will be higher and for a given particle flux there will be enhanced surface erosion. A defective tile will be eroded so as to present a more acute angle to the ion particle flux. The resulting angle should be such that the erosion rate, the product of particle flux and surface temperature, is the same as that of the defect free neighbouring tiles. The poorer the joint the more acute the angle to the ion flux. Thus, this mechanism should adjust the surface profile of the target to give uniform erosion of the surface in the region of the strike point regardless of joint quality.

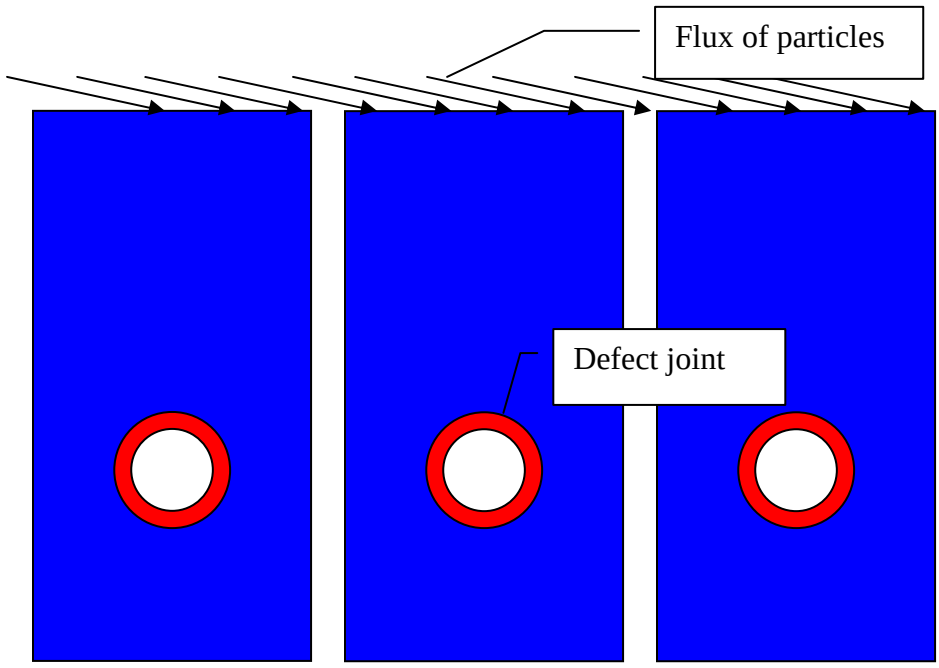

Fig. 5.2.1.1 Schema of the tiles exposed to a stream of particles

[1] The conducted heat flux is the heat due to the stream of the particles that impact the tiles with a certain angle.

The studies carried on in this chapter have the preliminary scope to try to predict the behaviour of a defect tiles under normal steady state and transient conditions. A more detailed study will be conducted in the next chapter where a program to take into account the erosion process has been developed. Moreover, it has been proved for the start-of-live condition under normal operation by analyses [56] and experiments [57] that the cascade failures[2] effect has not been observed.
Two cases will be studied:

1. poor thermal path to the coolant due to partial failure in the CFC-Cu joint or defects in the CFC leading to enhanced surface erosion of the CFC. This case will be simulated introducing a lower value of thermal conductivity all around the cooling channel using a dummy material (see paragraph 5.2.3);
2. complete failure of CFC-Cu joint, but the tile remains in place protecting the cooling tube. This case will be simulated introducing a very low value of thermal conductivity all around the cooling channel using a dummy material (see paragraph 5.2.3);

5.2.2 The model

The ANSYS model shown in fig.5.2.2.1 has been used to analyse the effect of the detachment of the copper tube (in red) from the body of the tile body. The conductivity of the elements of the model (in deep blue with a thickness of 0.5 mm) is changed in order to simulate the detachment between the cooling channel and the tile. The dimensions used to model the monoblock are indicated in the figure. The height and the width of the monoblock are respectively 38 and 24 mm. The cooling channel has an outer diameter of 12 mm and an inner diameter of 10 mm. The distance between the irradiated surface and the cooling channel is 20 mm. The gap between adjacent monoblocks is 0.5 mm.

[2] The cascade failure effect is when a defect tile is ejected or completely eroded then the thermal flux on the neighbours tiles is suddenly doubled then it can fail and so on giving a catastrophic domino effect.

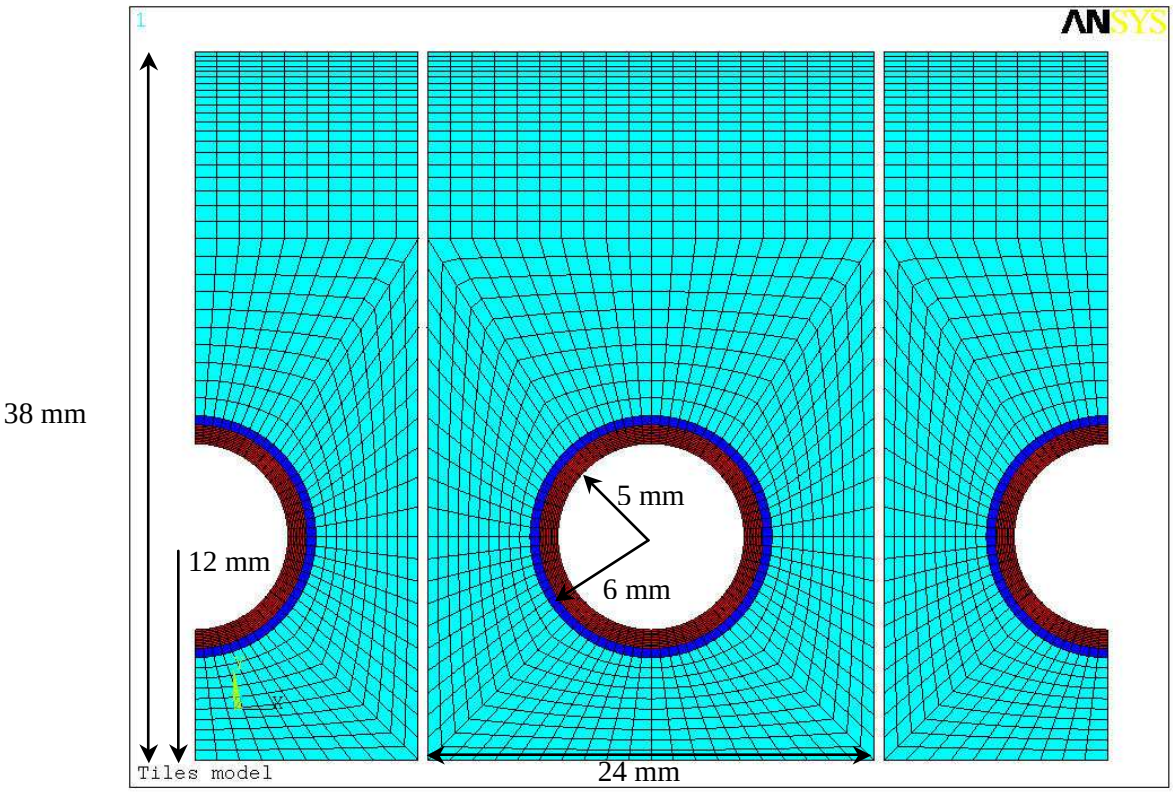

Fig. 5.2.2.1 Finite Element model of the tile of the PFC.

5.2.3 The material properties

The materials used are **C**arbon **F**iber **C**omposite (CFC) for the tile, Oxygen Free Copper (OF Cu) for the cooling tube and a "dummy" material implemented into the FE model to simulate detachment or the poor thermal path. The cooling channel in the monoblock has two layers. The external layer is OF Cu, the internal layer of the tube is CuCrZr. To simplify the analysis, it has been assumed that both layers of the cooling channel are OF Cu, the thermal material properties of the CuCrZr and OF Cu being very similar.
The properties of the dummy material come from consideration on the reliability of the monoblock.
Temperature dependent material properties have been used and are summarised in the tables 5.2.3.1, 5.2.3.2 and 5.2.3.3.

CFC SEP NB31	T=100 °C	T=800 °C	T=1500 °C	T=3500 °C
Thermal conductivity along horizontal direction [W/mm*K]	0.117	0.058	0.055	0.050
Thermal conductivity along vertical direction [W/mm*K]	0.283	0.154	0.136	0.100
Density [Kg/mm^3]	1.958e-6	-	-	-

Table 5.2.3.1. Material property of CFC SEP NB31 (previously called N312C)

Pure Copper Oxygen free	T=27 °C	T=327 °C	T=527 °C	T=927 °C
Thermal conductivity [W/mm*K]	0.398	0.383	0.371	0.342
Density [Kg/mm^3]	8.88e-6	8.78e-6	8.68e-6	8.46e-6

Table 5.2.3.2 Material property of OF Copper

In the FE model a "dummy" material (shown in blue in fig. 5.2.2.1) with an intermediate or a low conductivity (see Table 5.2.3.3) have been used respectively to simulate joint degradation (case 1) or full detachment (case 2).
In the first analyses reported below, an intermediate value of thermal conductivity was found which when applied around the entire circumference of the joint gives a transient response or thermal lag of the surface temperature of the tile that can easily be detected by thermographic NDE (SATIR [43]).
In the second analysis a very low thermal conductivity has been used in order to simulate a complete detachement of the cooling channel from the monoblock.
Degradation in the quality of the CFC-Cu joint has been modelled by changing the conductivity of the element. The thickness of the elements defined as dummy material is 0.5 mm.

Temperature		100 °C	800 °C	1500 °C	3500 °C
Thermal conductivity					
High	$Wmm^{-1}K^{-1}$	.117÷.283	.058÷.154	.055÷.136	.050÷.100
Intermediate	$Wmm^{-1}K^{-1}$	.02	.02	.02	.02
Low	$Wmm^{-1}K^{-1}$	.0013	.0013	.0013	.0013
Density	$Kg\ mm^3$	1.958e-6	1.958e-6	1.958e-6	1.958e-6

Table 5.2.3.3 Material property of the dummy material.

5.2.4 Loading and boundary conditions

The heat, on the surfaces of the tile, is due to radiation and to the flux of the incidence particle (see fig. 5.2.4.1).

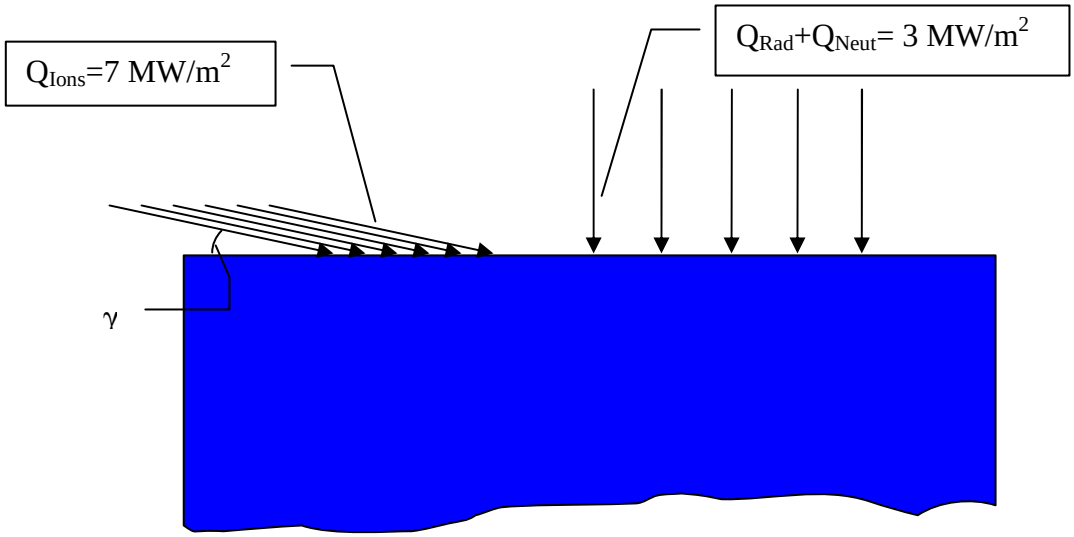

Fig. 5.2.4.1 Distribution of the heat on the surface of the tiles.

As showed on the above figure, the flux of the ions is not perpendicular to the surface of the tiles. We can suppose that this angle, at the initial condition for the attached tiles, is γ=3 degree [8].

Considering as reference the **O**uter **V**ertical **T**arget (OVT), the contribution due to the neutrals is almost zero (see fig 5.2.4.2). Therefore, it has been assumed that the power delivered to the surfaces of the tile, at the initial condition, is:

- 3 MW/m^2 due to radiation;
- 7 MW/m^2 due to ions;
- 0 MW/m^2 due to neutrals.

The total heat flux on the surface is 10 MWm^{-2}.

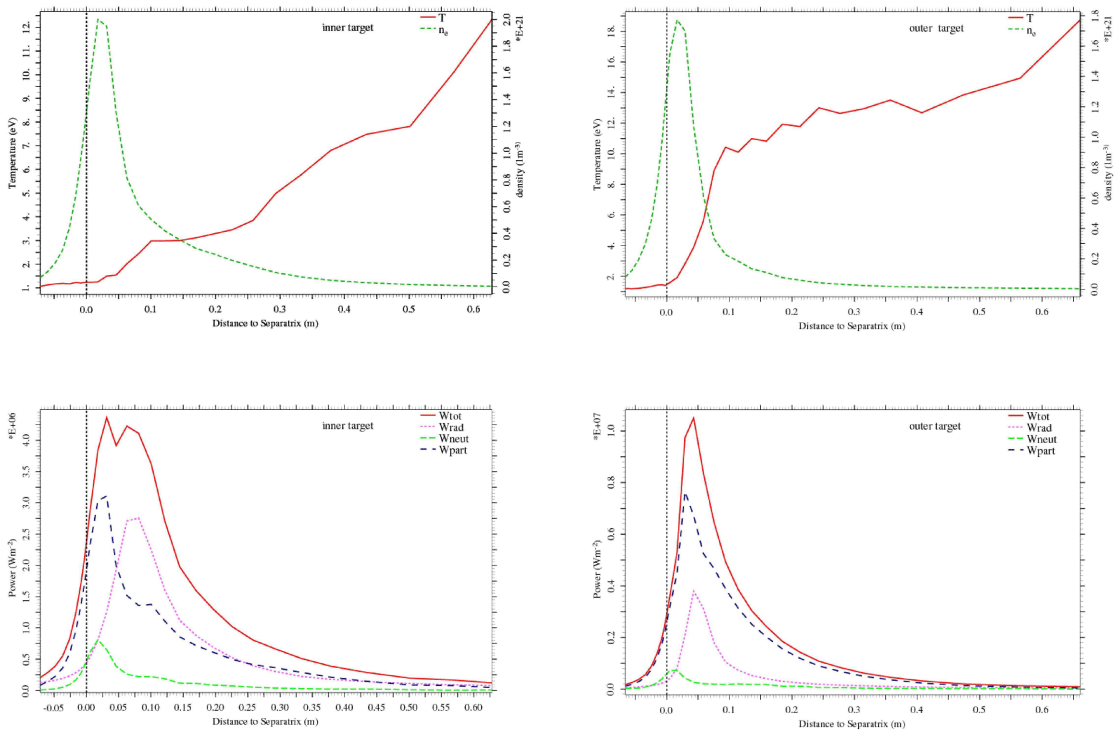

Fig. 5.2.4.2. Distribution of the power on the surface of the tiles (from B2-EIRENE code)[9].

The monoblock is symmetric but some loads may be asymmetric, hence a full monoblock sandwiched between two half monoblocks has been modelled. Figure 5.2.2.1 show the model used. Heat transfer convection has been applied to the cooling channel and the heat transfer coefficient has been calculated (function of the wall temperature) by the code EUPITER 4.2 [10]. The table 5.2.4.1 shows the heat transfer coefficient function of the wall temperature of the cooling channel used for this analysis.

Temperature [°C]	Heat Transf. Coeff. [MW/(m^2*K)]		Temperature [°C]	Heat Transf. Coeff. [MW/(m^2*K)]
120	0.10069		319	0.16940
140	0.10225		321	0.17708
159	0.10356		324	0.18472
178	0.10462		326	0.19251
197	0.10548		329	0.20043
215	0.10618		331	0.20847
234	0.10675		334	0.21661
252	0.10720		336	0.22486
264	0.10772		338	0.23321
282	0.11371		340	0.24163
301	0.13347		342	0.25015

Table 5.2.4.1 Heat transfer coefficient function of temperature calculated by EUPITER 4.2.

Radiation between adjacent monoblocks is taken into account. A radiation heating condition between the three modelled monoblock has been implemented. Moreover, radiation from the plasma facing top surface of the monoblock is also taken into account. The emissivity of the CFC is 0.8 and the temperature of the surrounding environment has been fixed to 550 °C. To take into account the radiation in the "poloidal" direction to poloidally adjacent monoblocks an emissivity of 1.6 instead of 0.8 has been used.
The detachment of the cooling channel from the monoblock has been considered using a dummy material with a very low thermal conductivity (see paragraph 5.2.3).
The analysis is conservative because it does not take into account the heat lost by evaporative cooling of the CFC.

5.2.5 Results & discussions

5.2.5.1 Nominal case for well-attached tile

A preliminary analysis to verify the loading and boundary options in normal condition has been carried out. The fig. 5.2.5.1.1 shows the distribution of the temperature and fig. 5.2.5.1.2 the heat flux distribution for the steady-state condition with nominal load described in the previous paragraphs and without detachment of the cooling channel.

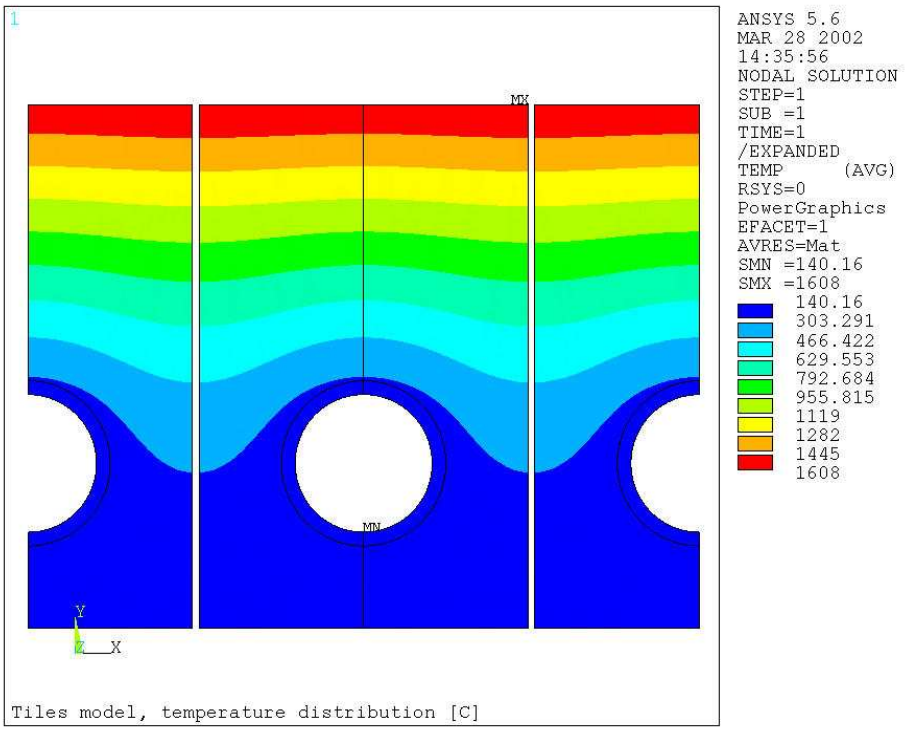

Fig. 5.2.5.1.1 Temperature distribution [°C] in nominal condition.

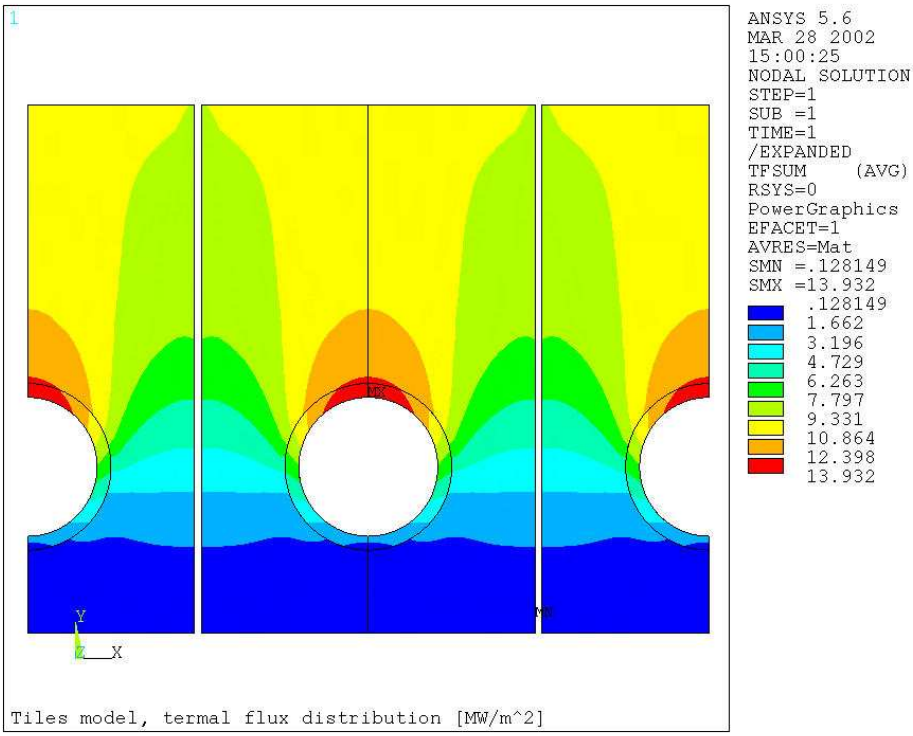

Fig 5.2.5.1.2 Thermal flux distribution [MW/m^2] in nominal condition.

5.2.5.2 CASE 1: Poor thermal path (intermediate conductivity)

This paragraph refers to case 1 as defined above. The analysis considers the erosion of the well-attached tile and the defective tile. It could be assumed that after initial modification of the surface profile the two tiles (defect and well-attached) erode at the same rate. The calculation takes into account that the sputtering yield is a function of both particle flux and surface temperature. The surface temperature of the defective tile is higher than that of its well-attached neighbour, but the particle flux to the defective tile is less. This is because the angle to the SOL is more acute, i.e. the tile surface is eroded at an angle α to the SOL (see fig.5.2.5.2.1). Note this also reduces the conducted heat flux to the tile. The calculation establishes the angle at which the tile must be eroded for its erosion rate to be the same as its well-attached neighbour. Of course the particle and heat flux avoided by the defective tile is redistributed over the adjacent downstream tiles. Fig. 5.2.5.2.2 shows the temperature distribution and figure 5.2.5.2.3 shows the thermal flux distribution.

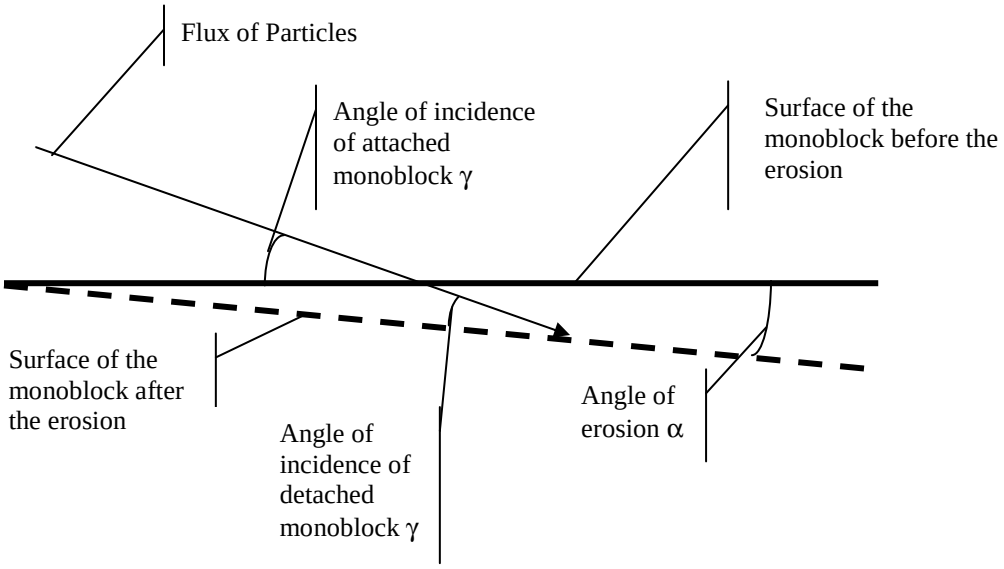

Fig. 5.2.5.2.1. Configuration of the surface of the detached tile (continuos line before erosion; dotted line after erosion).

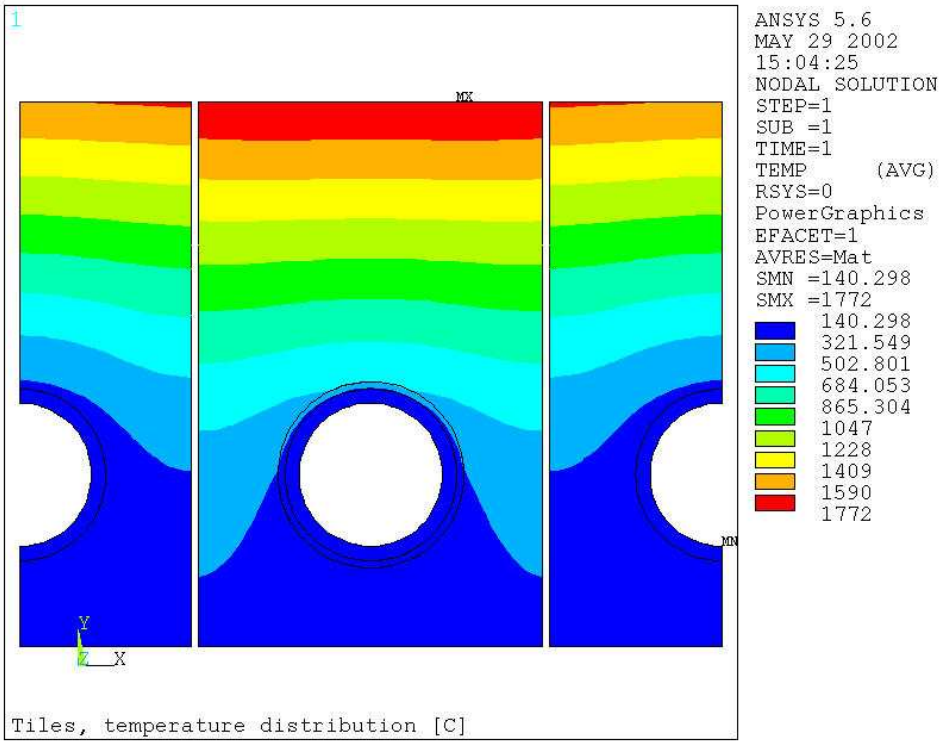

Fig. 5.2.5.2.2 Temperature distribution [°C] for the case of poor thermal path (intermediate conductivity).

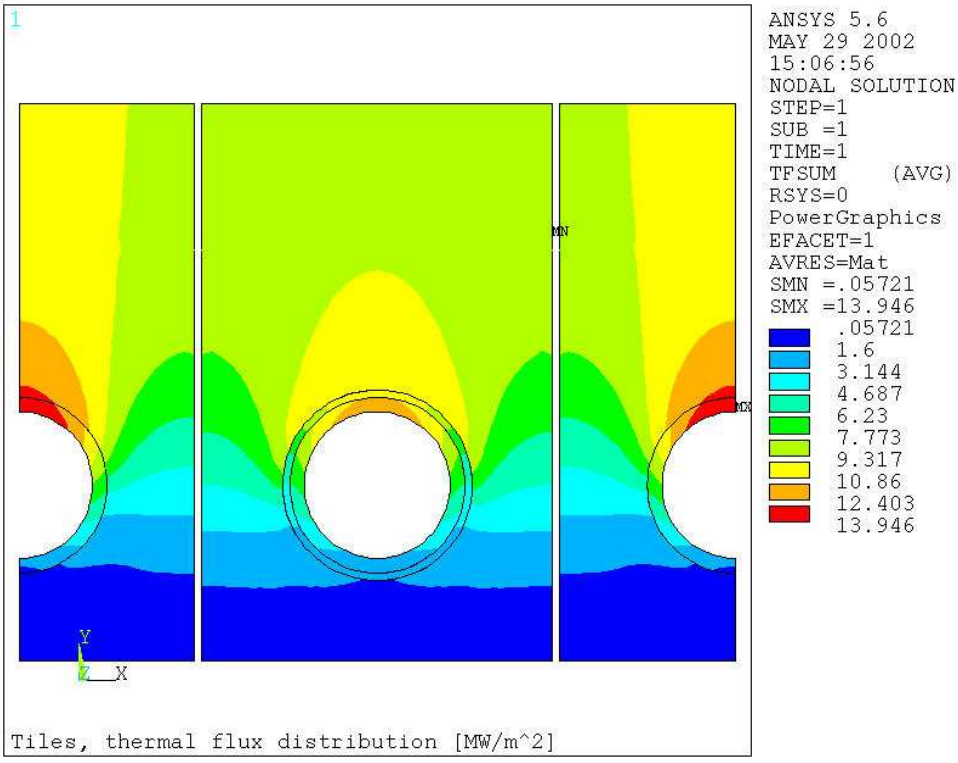

Fig. 5.2.5.2.3 Thermal flux distribution [MW/m^2] for the case of poor thermal path (intermediate conductivity).

The erosion rate is:

$$\delta = \Gamma_{Particles} \cdot Y(T)$$

where :
$\Gamma_{Particles}$ is the flux of the incidence particles [Particles/(m^2 sec)];
Y(T) is the yield sputtering function of the temperature [atoms/ions].
The particles are ions and neutrals, so:

$$\delta = (\Gamma_{Ions} + \Gamma_{Neutrals}) \cdot Y(T)$$

Assuming that the erosion rate is the same for the attached and detached tiles:

$$\delta_{ATTACHED} = \delta_{DETACHED}$$

This means:

$$\left[(\Gamma_{Ions} + \Gamma_{Neutrals}) \cdot Y(T)\right]_{ATTACHED} = \left[(\Gamma_{Ions} + \Gamma_{Neutrals}) \cdot Y(T)\right]_{DETACHED}$$

The flux of incidence ions is also:

$$\Gamma_{Ions} = f \cdot \Gamma_{Neutrals}$$
$$\Gamma_{Ions} = n \cdot c_S \cdot \sin\gamma$$

Where:
f is a constant parameter;
n is the density [ions/m^3];
c_S is the ion acoustic speed at the target plate [m/sec];
γ is the angle of incidence.

Supposing that the density and the ion acoustic speed are constant and approximating the angle with its sine, with some simplifications it can be written that:

$$\left[\gamma \cdot Y(T)\right]_{ATTACHED} = \left[\gamma \cdot Y(T)\right]_{DETACHED}$$

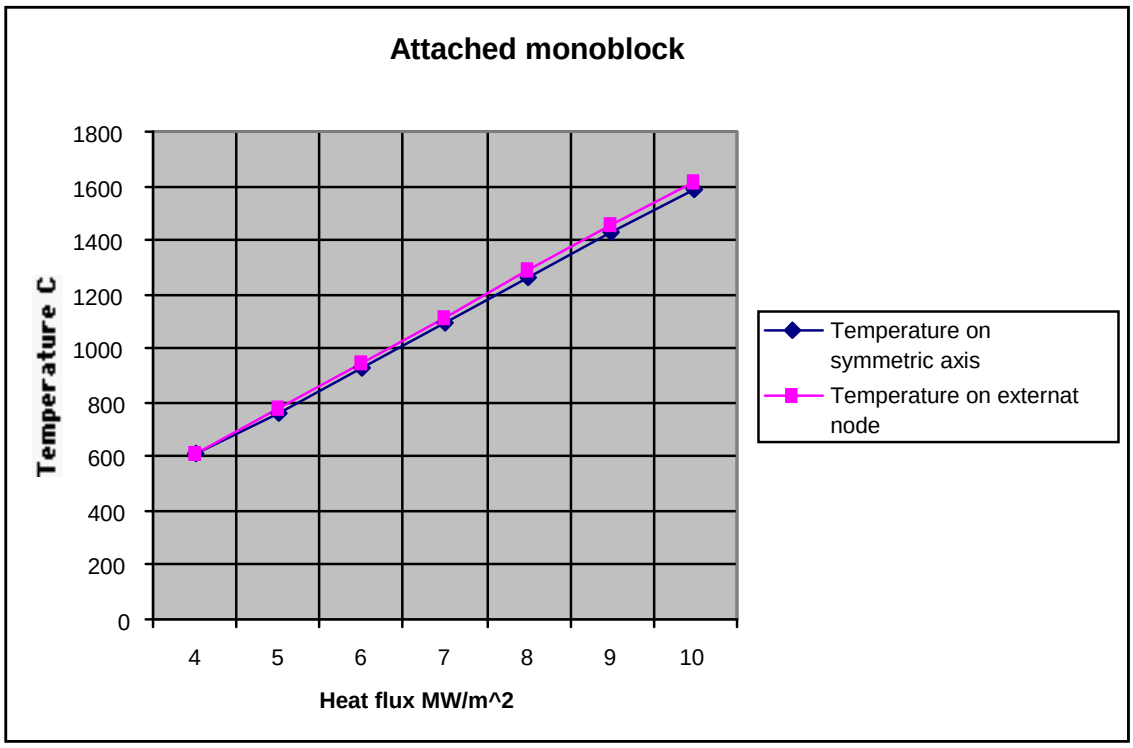

Fig. 5.2.5.2.4 Variation of the temperature of the well-attached tile versus surface heat flux

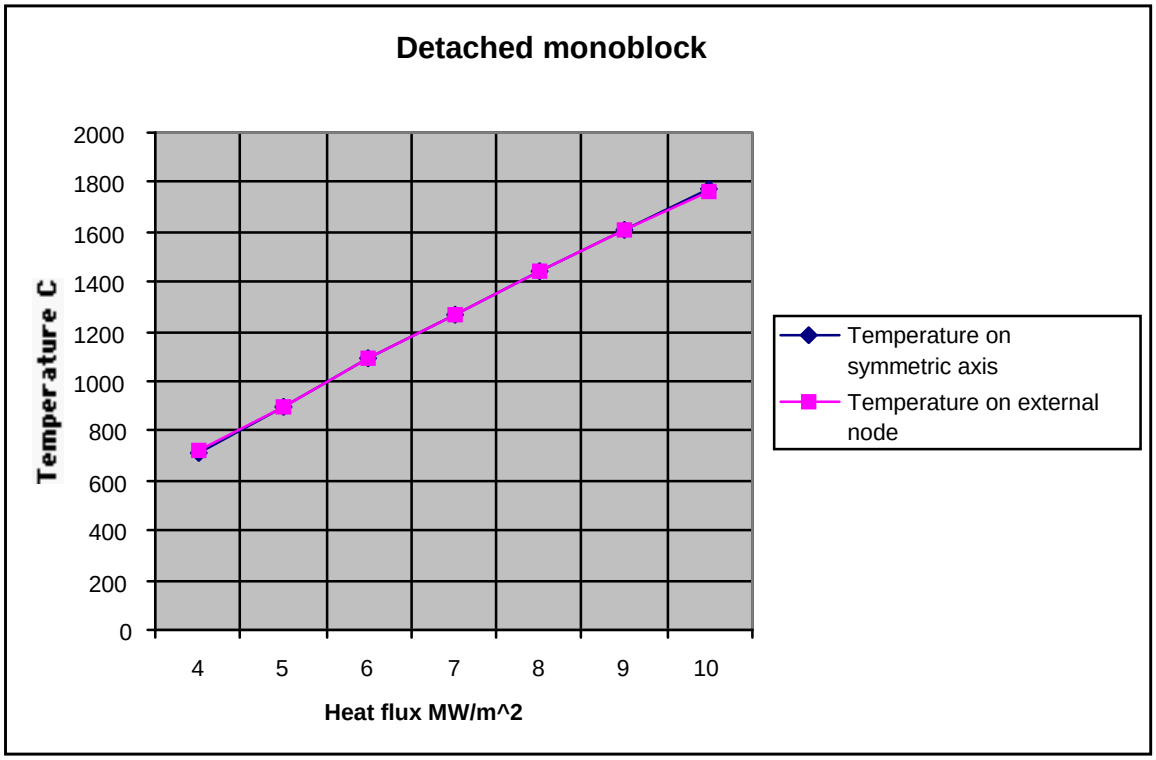

Fig. 5.2.5.2.5 Variation of the temperature of the defective tile versus the surface heat flux.

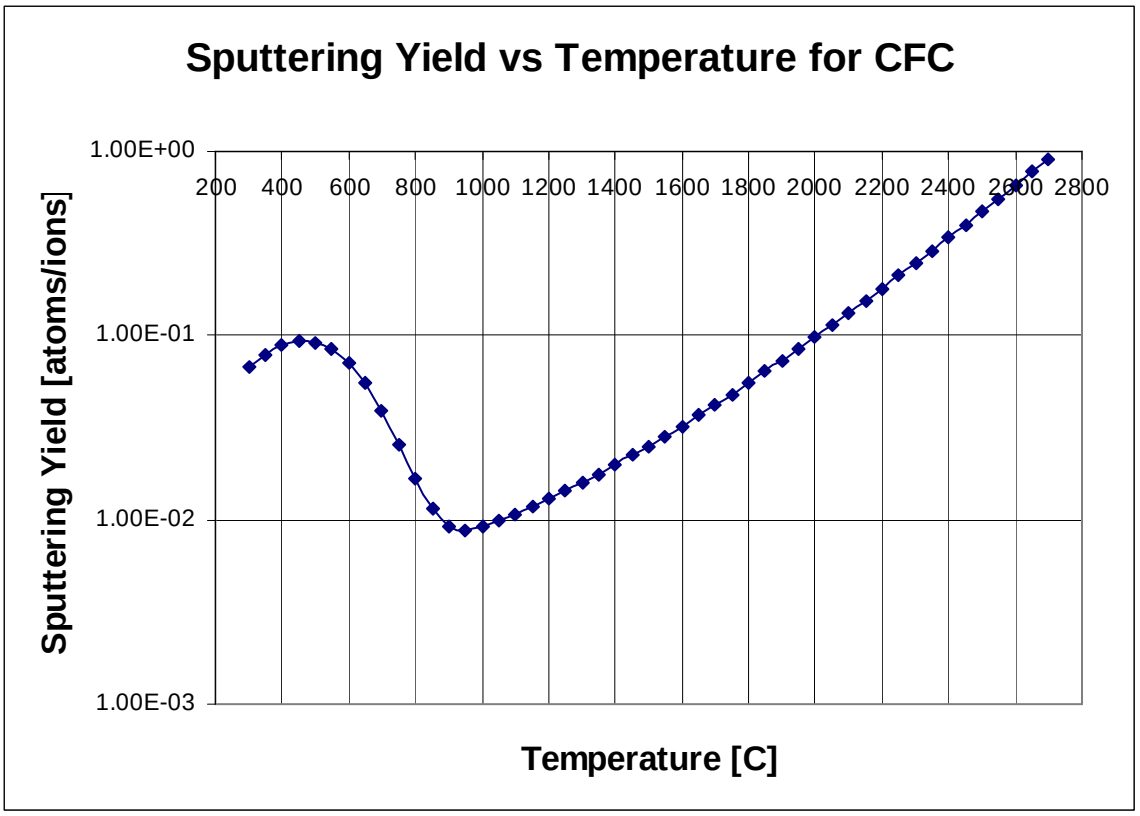

Figure 5.2.5.2.6. Temperature dependence of the sputtering yield for CFC [44].

Using an iterative procedure, the equations above, the diagram in fig. 5.2.5.2.6 and the diagrams in figs. 5.2.5.2.4 and 5.2.5.2.5 the angle of erosion, α, is found where the temperature dependent product of sputter yield and particle flux is the same for the two surfaces. Note that the heat flux to the tile radiated from the plasma is the same for the defective and well-attached tile, and only the conducted fraction varies.

	20 mm CFC	
	Attached	Detached
γ angle of incidence [degree]	3°	2.6°÷2.7°
α angle of "erosion" [degree]	0°	0.3°÷0.4°
Q_{Tot} heat on the surface [MW/m^2]	10	9.0÷9.3
Q_{Rad} heat on the surface [MW/m^2]	3	3
Q_{Cond} heat on the surface [MW/m^2]	7	6.0÷6.3
Maximum temperature on the surface [°C]	1616	1612÷1665

Table 5.2.5.2.1. Table of relevant values when the tile remains attached to the cooling channel through a poor thermal path (intermediate conductivity).

From Table 5.2.5.2.1 the heat flux conducted to the surface is reduced by 12%, from 7 to a mean of 6.15 MWm^{-2}.

5.2.5.3 CASE 2: Complete failure of the connection of the CFC to the cooling channel (low conductivity)

This step calculates the resulting eroded angle of a detached monoblock (i.e. very low conduction of the CFC to the cooling channel) such that the erosion rate is similar to that of its defect-free neighbouring tiles. In this case for normal operation the temperature of the heated surface is higher than for cases with partially attached monoblocks, hence the sputtering yield is higher. Fig. 5.2.5.3.1 shows the temperature distribution and figure 5.2.5.3.2 the vector plot of the thermal flux.

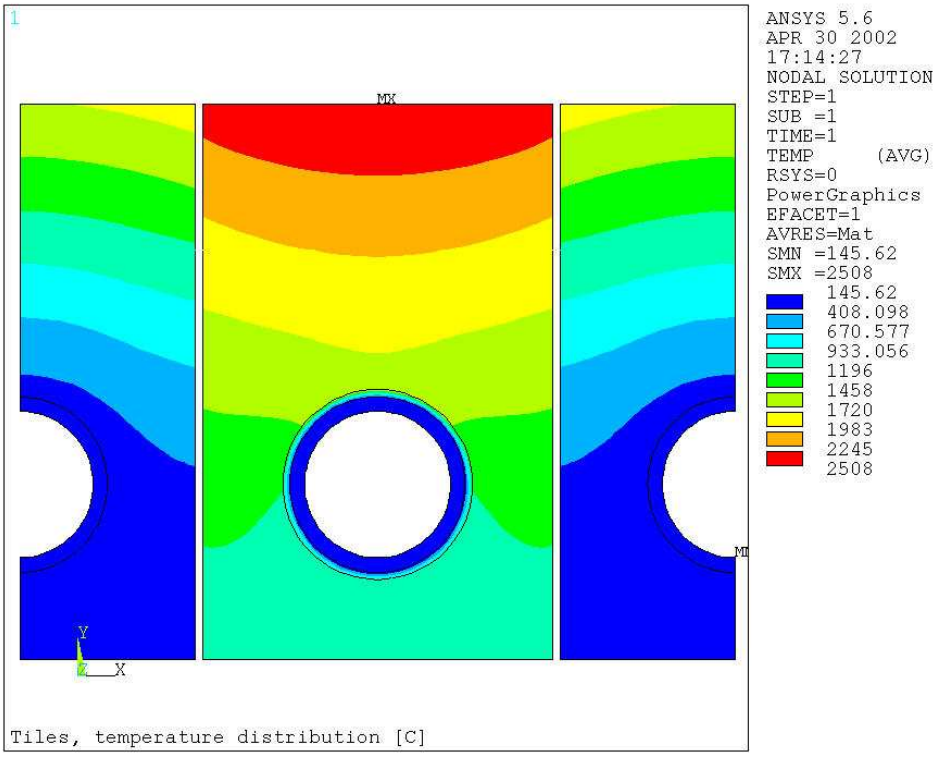

Fig. 5.2.5.3.1. Temperature distribution [°C] with the tile completely detached (low conductivity) from the cooling channel.

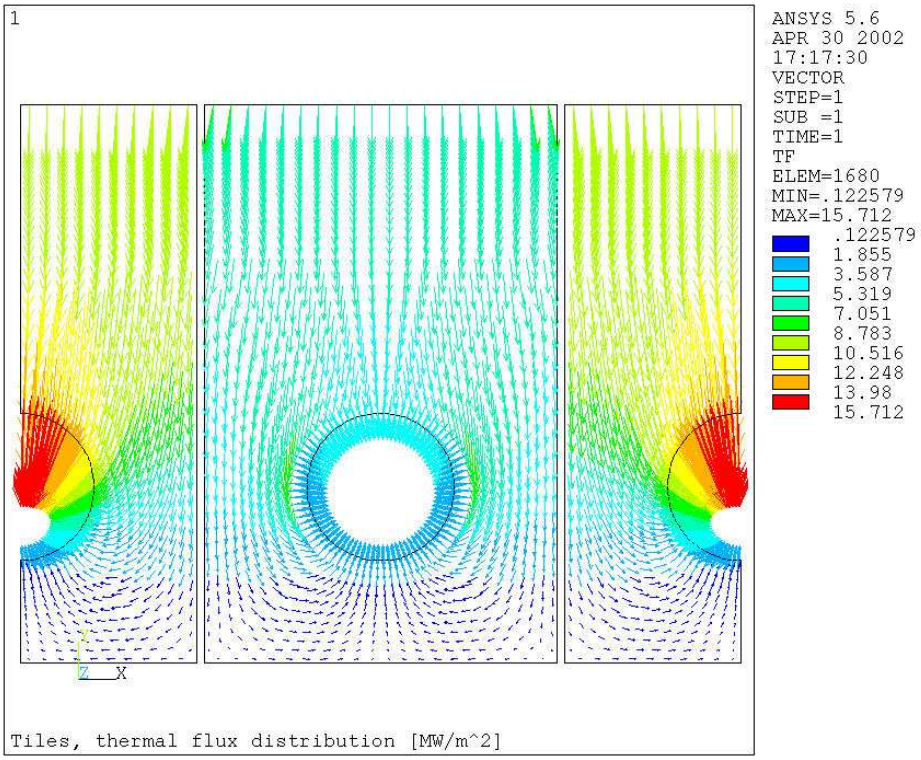

Fig. 5.2.5.3.2. Thermal flux distribution [MW/m^2] with the tile completely detached (low conductivity) from the cooling channel.

The heat load is distributed to the neighbouring tiles by radiation.
Following the same procedure used for the partial detachment of the cooling channel (see paragraph. 5.2.5.2) and using the figures 5.2.5.3.3 and 5.2.5.3.4 it is possible to find the erosion angle for this case (see table 5.2.5.3.1).

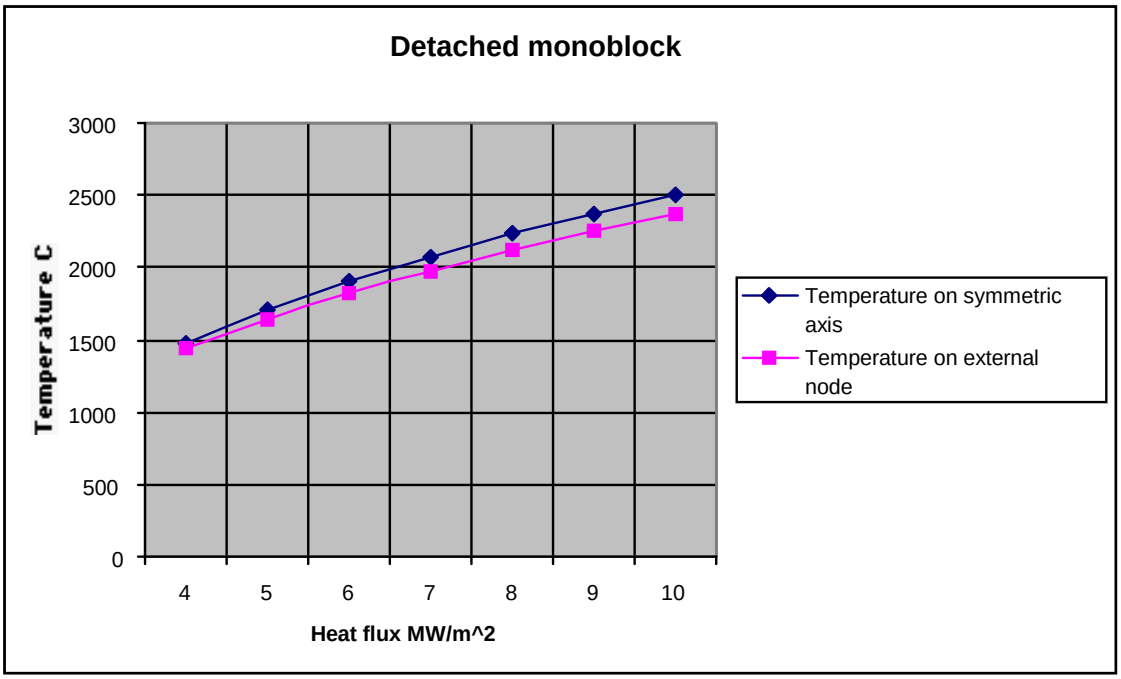

Fig. 5.2.5.3.3 Variation of the temperature on the detached tile versus the heat flux applied on the surface.

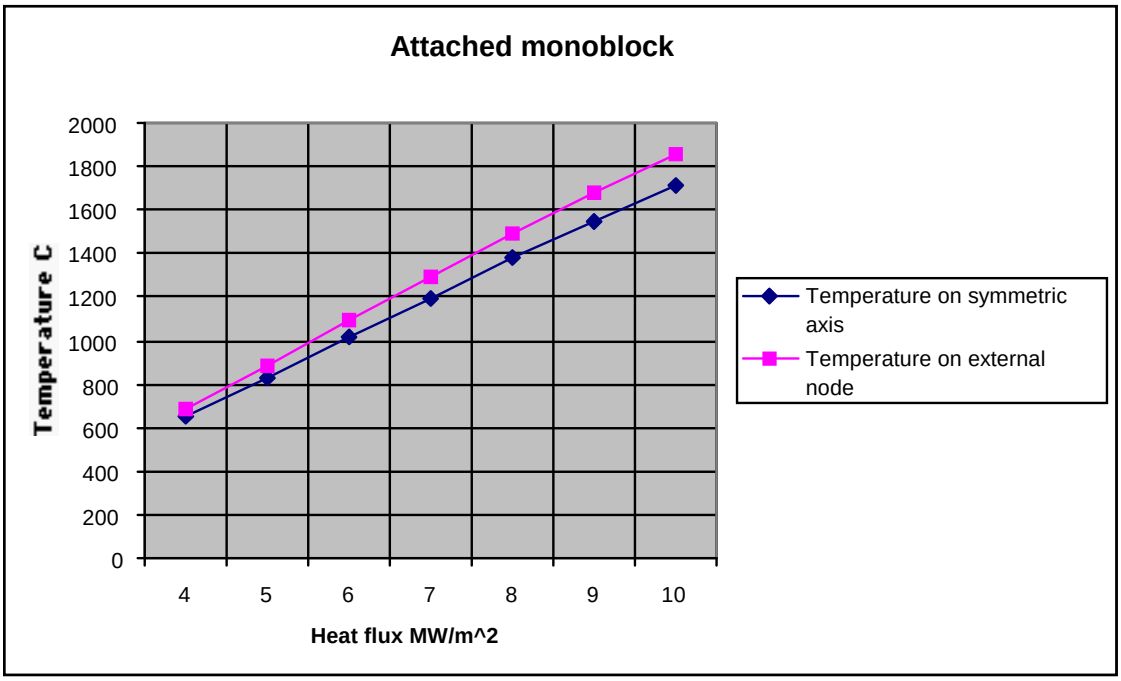

Fig. 5.2.5.3.4 Variation of the temperature on the attached tile versus the heat flux applied on the surface.

	20 mm CFC	
	Attached	Detached
γ angle of incidence [degree]	3°	1.4°÷1.5°
α angle of "erosion" [degree]	0°	1.5°÷1.6°
Q_{Tot} heat on the surface [MW/m^2]	10	6.3÷6.5
Q_{Rad} heat on the surface [MW/m^2]	3	3
Q_{Cond} heat on the surface [MW/m^2]	7	3.3÷3.5
Maximum temperature on the surface [°C]	1851	1943÷1987

Table 5.2.5.3.1 Table of relevant values for a tile completely detached (low conductivity) from the cooling channel.

Hence in this case, during nominal operation, the conducted heat flux to the detached tile is reduced to a mean of 3.4 MWm^{-2}, and the total heat flux to 6.4 MWm^{-2}.

5.2.6 Experimental available data

Some experiments as well as some numerical calculation have been conducted by CEA [57] and Efremov Institute [56] about the possibility of the cascade failure effect.
Using an ion beams, an experiment has been conducted in collaboration with the CEA on the possibility of cascade failure effect in flat tiles cooled with hypervapotron.

Fig. 5.2.6.1 The internal structure of the tiles.

The hypervapotron is a particular geometry (see fig above) of the cooling channel in order to promote turbulence flow to increase heat transfer coefficient.

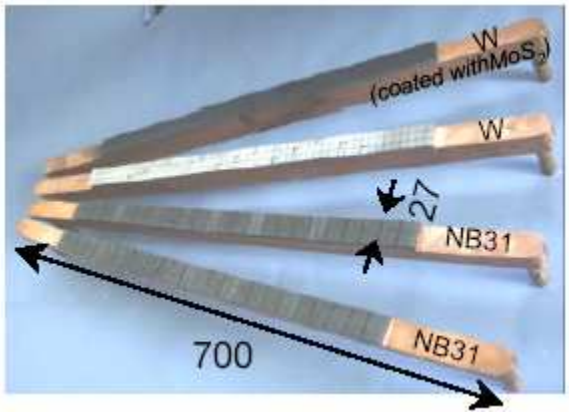

Fig. 5.2.6.2. A picture of the tiles tested.

The experiment has been conducted loading the tiles with 500 shots of 10 MW/m^2 with a duration of 10 sec per shot and with a single shot of 10 MW/m^2 per 1000 sec. To simulate the cascade failure some tiles have been machined to expose the neighbour tile to the double of the power (see fig. 5.2.6.3).

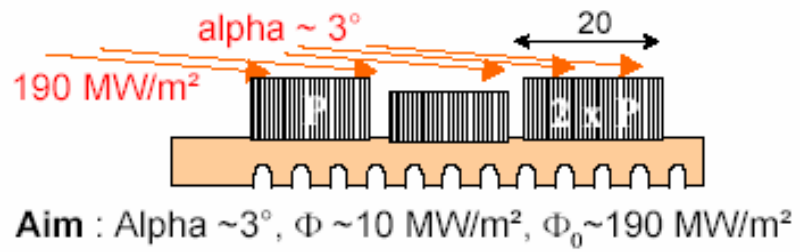

Fig. 5.2.6.3. Schema of the machined tile in order to expose the neighbour tile to the double of the power.

The picture below shows the erosion on the more exposed tiles. In these conditions no cascade failure has been observed.

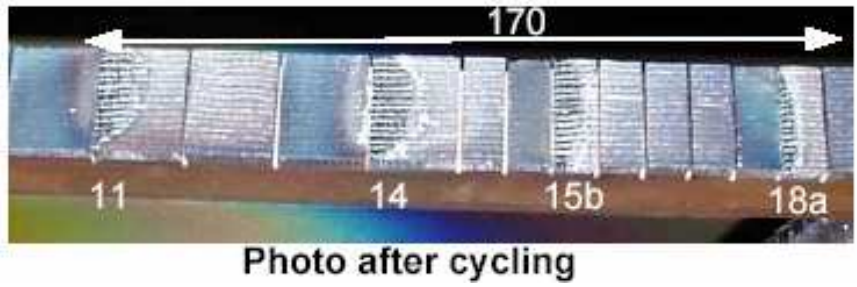

Fig. 5.2.6.4. Picture of the tiles after cycling. No cascade failure effects.

Some analyses have been conducted by the Efremov Institute with a code developed by themselves.

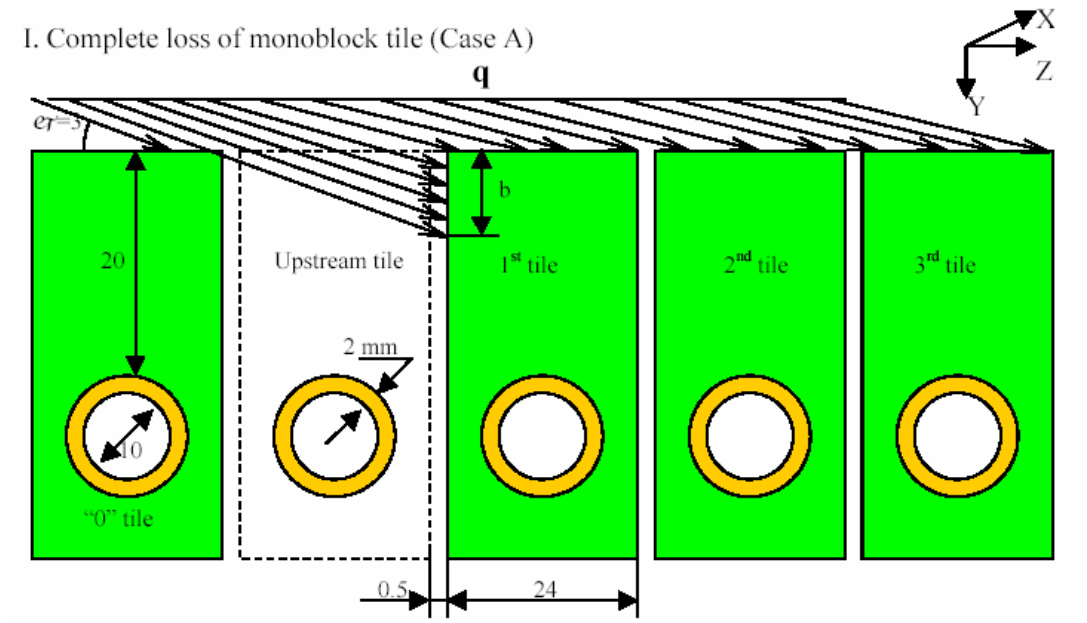

Fig. 5.2.6.5. The assumption of the calculation done by the Russian is a complete loss of a monoblock.

They developed a 2D FE code called ORION. They have simulated a complete loss of a monoblock loading the tiles with 10 shots of 400 sec (390 sec @ 10 MW/m^2 and 10 sec @ 20 MW/m^2). The result profile of the 1st tile is shown in fig. 5.2.6.6.

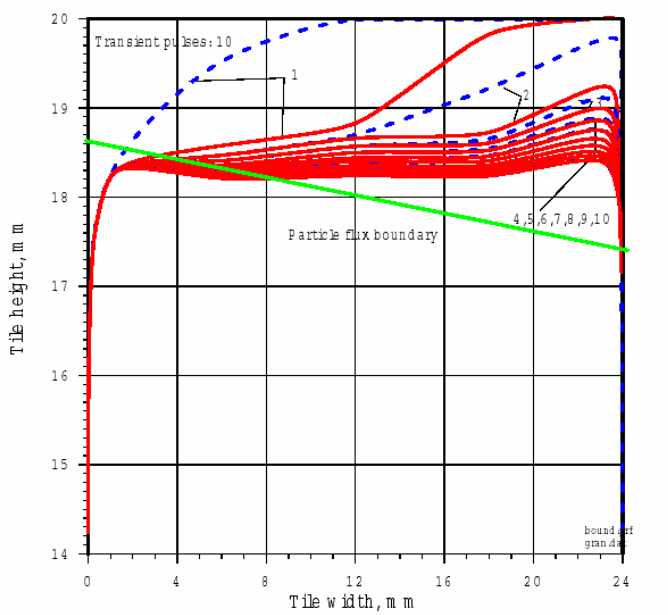

Fig. 5.2.6.6. The evolution of the profile of the 1st tile during the shots. The green line represents the maximum inclination that the stream of particle can achieve due to the lack of the "upstream tile".

5.3 A software to evaluate the erosion on the CFC tiles of the divertor

5.3.1 General considerations

The detailed analysis of the erosive phenomena of the material of the first wall is fundamental for the studies of the possible configuration during the normal operation as well as for the evaluation of the life of the components. The evaluation of the speed of erosion of the CFC (Carbon Fibre Composite) tiles is very important to evaluate the longevity of those components. The code will be used also to understand and fix the conditions of the acceptance criteria (see chap. 4).
The idea is to develop a software, inside a commercial and certificate finite element code like ANSYS, able to evaluate the evolution of the erosion in the CFC tiles of the divertor taking into account the shadow effect that each tile exercise to other tiles and the possible presence of a defect in the joint between the cooling channel and the monoblock.
The software developed is able to calculate the amount of erosion [g] of the two tiles modelled as well as the profile. Although the mathematical model used to simulate the phenomena implemented in the code are well know and fully validated, the code has been validated also comparing some results with experimental data within a collaboration with the CEA Cadarache (see chapter 5.4).
The erosion of the carbon exposed to a flux of particles is a very complex process. Here the word "erosion" will be used to indicate a loss of material from a surface of carbon. In the software developed, it has been considered 3 different kind of erosion (the word "erosion" here is used generically to indicate a loss of material from a surface of carbon). The first is the sublimation of the carbon. In fact, at high temperature and low pressure the carbon sublimate, going from a solid state to a gaseous state. The second is the physical erosion. When particles hit a surface, they put away a certain amount of material. The third is the chemical erosion. The hydrogen has a strong chemical affinity with carbon, when hydrogen atoms (or isotopes of hydrogen) impacts carbon atoms may trigger some chemical reaction to form cluster of CH_x that are pulled out from the surface.

5.3.2 The finite element code

The picture below shows the 2D finite element model used in the software. A lot of parameters, also geometric parameters, could be changed. The figure below shows the default configuration.
Referring to the figure 5.3.2.1 it is possible to recognise in purple the cooling channel, in red the pure copper 1 mm thick used to join the CuCrZr to the CFC. In the software has been implemented the possibility to simulate a detachment between the cooling channel and the CFC.
The position and circumferential length of the defect is simulated by using a low thermal conductivity [45] in individual elements (0.5 mm thick) that form a ring around the cooling tube. Moreover, on the surface of the tiles, layers (2 mm thick) of very small elements are used in order to better simulate the erosion of the CFC. It is possible also to reduce this region to 0.5 mm achieving a surface element thickness of 2.6 μm.

In the default configuration the dimension of the monoblock (in mm) are visible in the figure 5.3.2.2. Moreover, the gap between monoblock in toroidal direction has been assumed 0.5 mm.

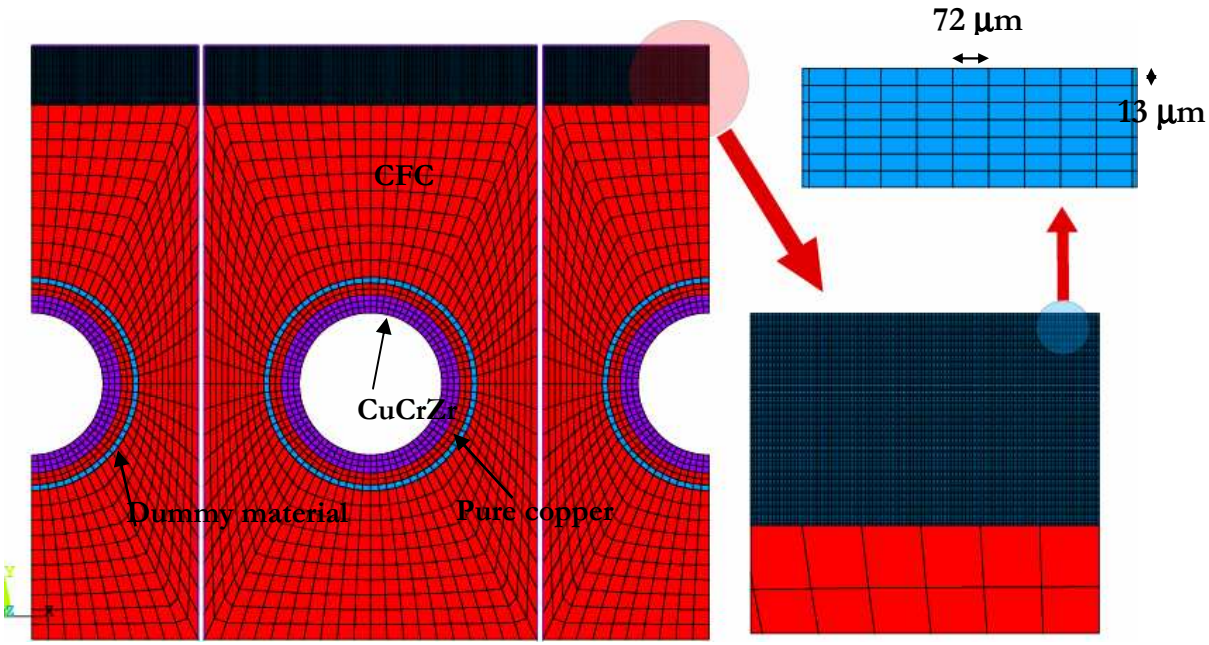

Fig. 5.3.2.1. The finite element model used in the software.

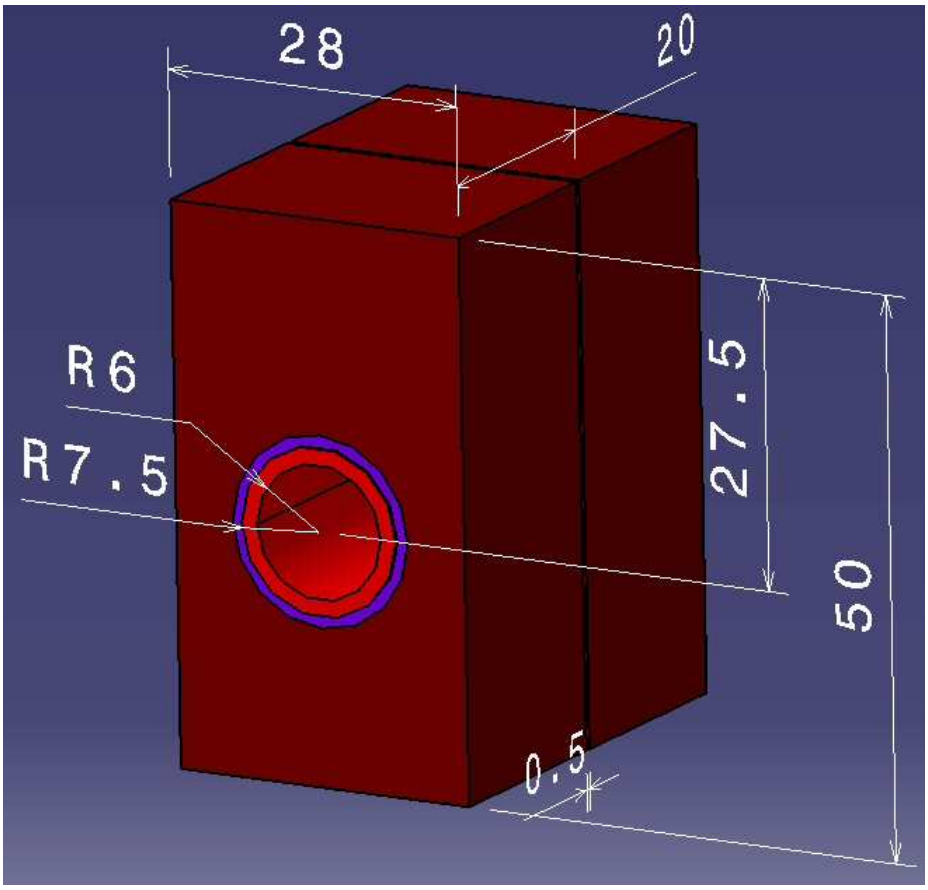

Fig. 5.3.2.2. The default dimension of the monoblock [mm].

In the software to model the tiles have been used 3 kinds of elements:

1) Plane55 a 2D element to simulate the materials involved in the processes
2) Link32 to simulate the radiation and as dummy elements to simulate the evolution of the profile.
3) Matrix50 the so called super element to simulate the radiation.

The software contains 5 material properties:

1) Carbon Fiber Composite 1D NB31
2) Carbon Fiber Composite 2D Dunlop
3) Oxigen Free Pure copper, to join the cooling channel to the CFC
4) CuCrZr, for the cooling channel
5) Dummy material, to simulate detachment between the cooling channel and the CFC

The table below summarizes the material properties used for the above mentioned materials.

CFC 1D NB31	**T=100 °C**	**T=800 °C**	**T=1500 °C**	**T=3500 °C**
Thermal conductivity along horizontal direction [W/(mm*K)]	0.105	0.058	0.055	0.050
Thermal conductivity along vertical direction [W/(mm*K)]	0.283	0.154	0.136	0.100
Specific heat [J/(Kg*K)]	880	1820	2150	2150
Density [Kg/mm^3]	1.958e-6	-	-	-
CFC 2D Dunlop	**T=100 °C**	**T=800 °C**	**T=1500 °C**	**T=3000 °C**
Thermal conductivity along horizontal direction [W/(mm*K)]	0.311	0.141	0.091	0.040
Thermal conductivity along vertical direction [W/(mm*K)]	0.311	0.141	0.091	0.040
Specific heat [J/(Kg*K)]	970	1797	1991	1991
Density [Kg/mm^3]	1.9e-6	-	-	-
OF Pure copper	**T=27 °C**	**T=327 °C**	**T=727 °C**	**T=927 °C**
Thermal conductivity [W/(mm*K)]	0.398	0.383	0.357	0.342
Specific heat [J/(Kg*K)]	386	425	471	492
Density [Kg/mm^3]	8.88e-6	0.78e-6	8.59e-6	8.46e-6
CuCrZr	**T=100 °C**	**T=300 °C**	**T=500 °C**	**T=700 °C**
Thermal conductivity [W/(mm*K)]	0.365	0.351	0.357	0.350
Specific heat [J/(Kg*K)]	396.88	417.09	437.93	459.38
Density [Kg/mm^3]	8.86e-6	-	-	-
Dummy Material	**T=100 °C**	**T=500 °C**	**T=1500 °C**	**T=3500 °C**
Thermal conductivity [W/(mm*K)]	0.0013	0.0013	0.0013	0.0013
Specific heat [J/(Kg*K)]	880	1570	2150	2150
Density [Kg/mm^3]	1.958e-6	-	-	-

Table 5.3.2.1. Material properties

Moreover it is possible to use different material property for the tiles in the middle and the two adjacent tiles.
The tiles are symmetric respect to their vertical axis but are loaded in a cyclic way. The effect of an asymmetric detachment of the cooling channel from the CFC monoblock will be studied. Hence, as shown in the fig. 5.3.2.1, one tile plus 2 half tiles have been used to implement the phenomena involved in the processes of erosion. The 2 half tiles are coupled with cyclic condition (coupling the node on the left tiles with the correspondence node on the right tile), see fig.5.3.2.3.

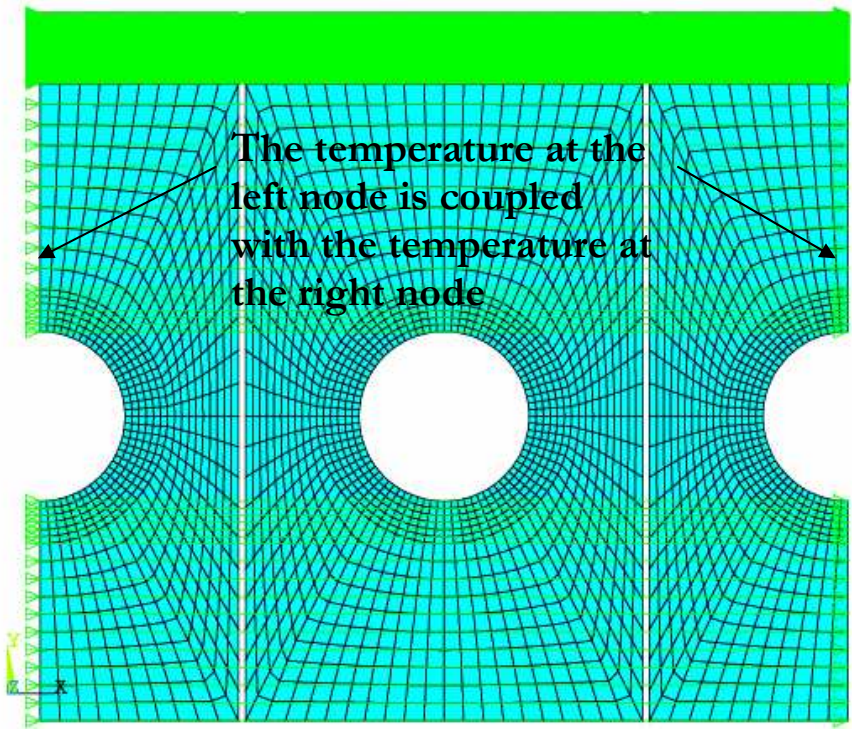

Fig.5.3.2.3. Coupling condition to simulate the cycling loads.

A zone of fine mesh has been coupled with a zone of coarse mesh in order to increase the performance having the fine mesh only where it is needed, see fig. 5.3.2.4.

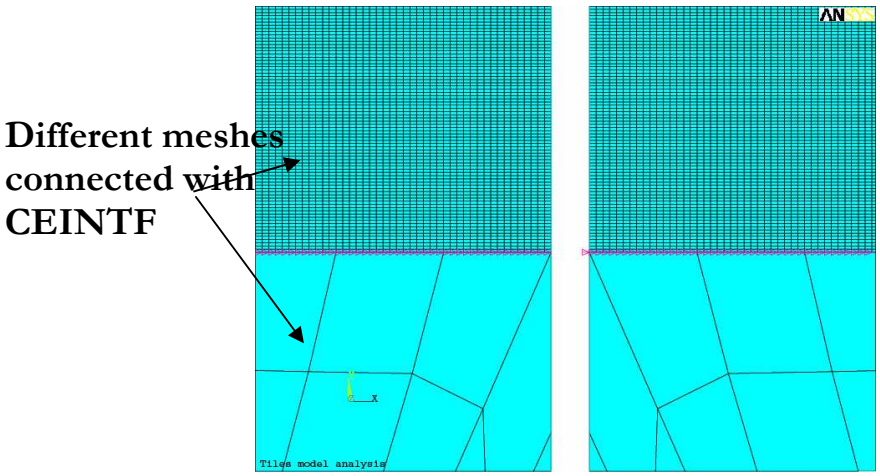

Fig. 5.3.2.4. Connection of a fine mesh zone with a coarse mesh zone.

5.3.3 The phenomena included in the code

The table below summarizes the phenomena that have been implemented in the software.

Phenomena	**Consequence**
Radiation	• Cooling
Convection function of Twall and Twater	• Cooling
Load (heat flux) as a function of the position	• Asymmetry and self shadowing
Sublimation	• Cooling • Loss of material
Physical erosion	• Loss of material
Chemical erosion	• Loss of material

Table 2.2.1 The phenomena and the consequence included in the software.

Some simplifications have been made in order to make the problems involved in the erosion of the CFC easier:

- The code does not consider the contribution due to neutral particles.
- The code does not consider the contribution due to self sputtering.
- The incoming flux in the gaps might be more complex than just the geometrical shadowing effect (sheath effect, neutrals and so on).
- The code does not consider the contribution due to RES (Radiation enhance sublimation).

Due to calculations made with Monte Carlo code, considering the working condition of ITER and discussions with erosion experts, at this stage and for the main purpose of the code it has been decided that the above effects can be neglected.

5.3.3.1 The radiation

In the software developed has been included the possibility to exchange heat by radiation. This possibility must be taken into account mainly for two reasons:

1) Because the very high temperature that can be achieved during off normal operation;
2) Because the tiles are in the void and radiation to the environment, in case of detachment of the cooling channel, can became the main way to exchange heat.

The tiles can loss heat by radiation to the environment as well as they can exchange heat to each other. This second possibility will be very useful when will be studied the effect of a defect in the joint between the cooling channel and the CFC.
The implementation in ANSYS has been done surrounding the lateral radiation surface with element link32, using the super-element Matrix50 and using the TABLE functions how is described in the manual [46].

5.3.3.2 The convection

The exchange of heat by convection with the cooling channel is the main way to remove the heat from the monoblock. The values of the film coefficient function of the temperature of the wall and water have been calculated with the code Thermprop 5.0 (previously called EUPITER) [10]. The fig.5.3.3.2.1 shows the cooling channel with the convection condition applied on it. The problem of the dependency of the heat transfer coefficient on T_{wall} and T_{water} has been implemented in ANSYS with the TABLE functions.
The tables 5.3.3.2.1 and 5.3.3.2.2 contains the input data used in the Thermprop code in order to evaluate respectively the film coefficient for the normal operation and for the SATIR test.

Geometry data	Flow inner diameter [mm]	Tape thickness average [mm]	Tape twist ratio	Surface roughness [mm]
	12	1.65	2	$3e^{-3}$
	Pressure [MPa]	Temperature [°C]	Velocity [m/s]	
Inlet water conditions	3.8	100-140	9	

Table 5.3.3.2.1 Input data used in the Thermprop code to evaluate the film coefficient for normal operation.

Geometry data	Flow inner diameter [mm]	Tape thickness average [mm]	Tape twist ratio	Surface roughness [mm]
	12	none	none	$3e^{-3}$
	Pressure [MPa]	Temperature [°C]	Velocity [m/s]	
Inlet water conditions	1	5-95	12	

Table 5.3.3.2.2 Input data used in the Thermprop code to evaluate the film coefficient for SATIR test.

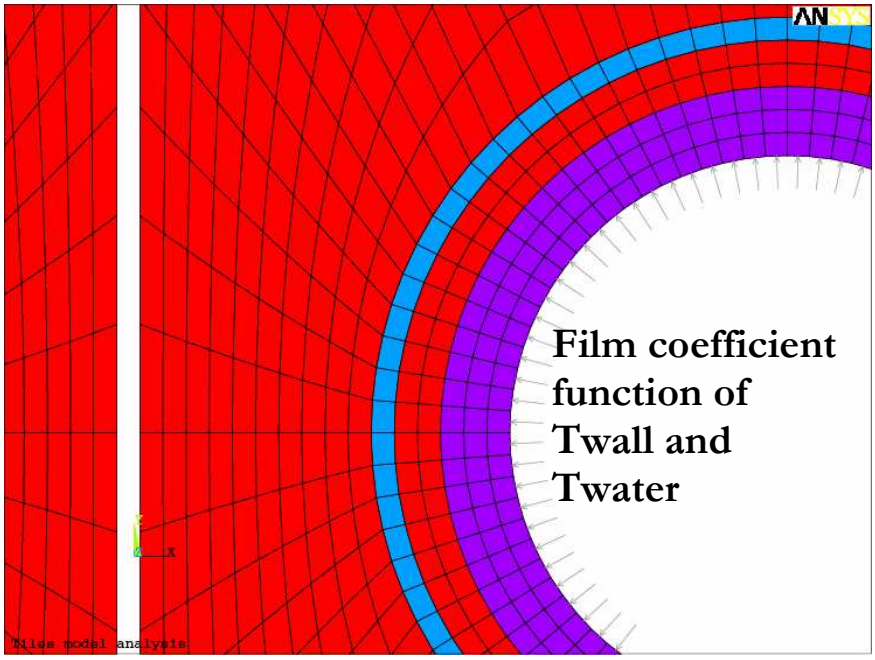

Fig. 5.3.3.2.1 The convection condition applied on the cooling channel.

5.3.3.3 Load conditions –Normal and off-normal operations

During normal operation the heat is transferred from the plasma to the first wall by radiation and conduction of particles. The main amount of heat is transferred by conduction from the charged particles that impact the surface of the tiles with a certain angle. The heat transferred from these particles to the surface of the tiles is function of the angle of impact.
Because of the glancing angle of incidence of the particles on the first wall (typically 3° [8]) leading edges and shadowed areas need to be considered. This aspect has been implemented in ANSYS using 3 different kinds of loads.
The figure 5.3.3.3.1 refers to a sublimation calculation with an incident load power of 20 MW/m^2 for 30 sec, it shows the three possible kinds of loads considered.

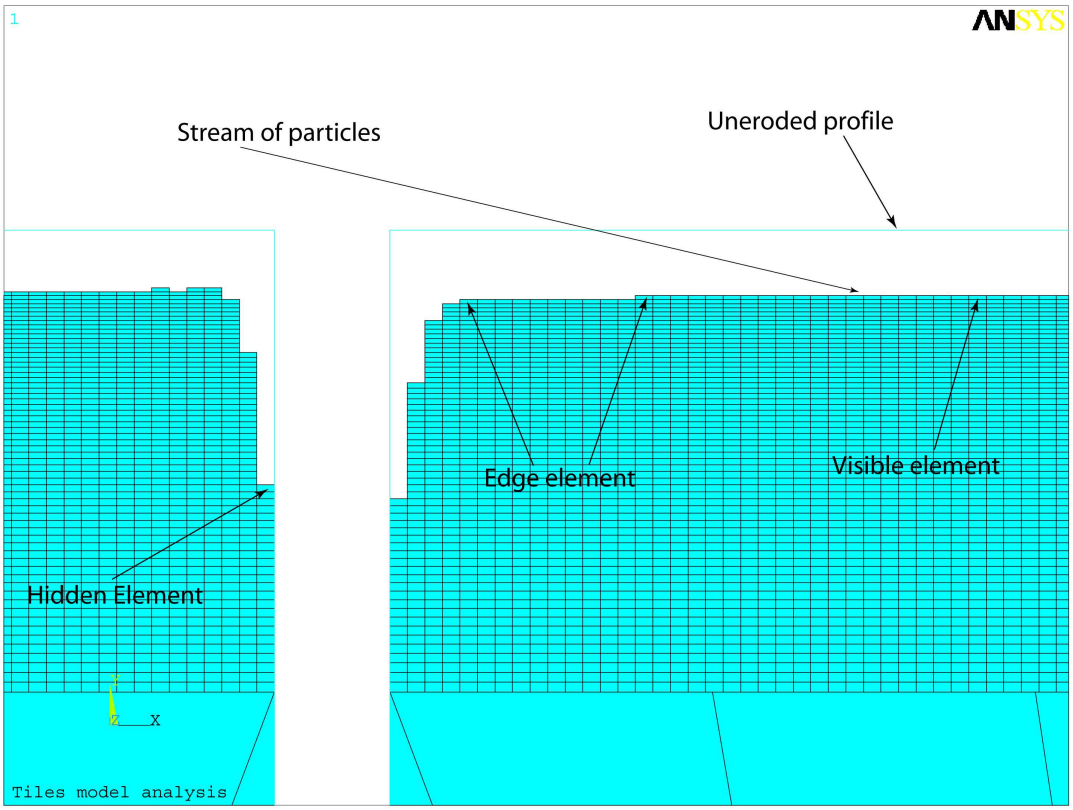

Fig. 5.3.3.3.1 The three possible kinds of load considered.

1) **The visible elements:** Looking the fig. 5.3.3.3.1, the particles come from the left and hit the surface of the tile with an angle of 3°. The load on the surface elements is due to the radiation from the plasma + the conduction of the particles that impacts the surface. The loads have been calculated using the code B2-EIRENE [9] on the OVT (Outer Vertical Target) where the scrape off layer hit the surface of the vertical target. During normal operation the contribution of the irradiation is 3 MWm^{-2}. The contribution due to the ions is 7 MWm^{-2}. The contribution due to the neutrals is 0. Hence, the total load on the surface is 10 MWm^{-2}, 70% due to the particles and 30% due to the radiation from the plasma.
2) **The hidden elements:** May happen that a group of element or the neighbours tile put in shadow some other elements. If such events happen, the elements in shadow are loaded only by radiation from the plasma. Hence, during normal operation such elements are loaded with 3 MWm^{-2}.
3) **The visible elements with exposed edge:** May happen that some elements are exposed to the flux of particles coming from the plasma with an angle of 87°. Because the energy transferred from these particle to the surface of the tiles depends on the angle of incidence [8] for normal operation the edge of the tiles exposed to the plasma particles with an angle of 87° are loaded with $7/\sin(3°) = 133.7$ MWm^{-2}.

At the begin of the analysis, when the tiles are still not eroded at all, the element with exposed edge are those element on the left edge of the tiles (if the particles comes from the left see fig. 5.3.3.3.1). The fig. 5.3.3.3.2 shows that for a poloidal gap between adjacent tiles of 0.5 mm, the exposed tiles on the right is loaded for an extension of ≈ μm 26. This suggest that the vertical length of the elements involved in the calculation in that position should be 26 μm or its multiple (13, 8.6, 6.5, 2.6 etc).

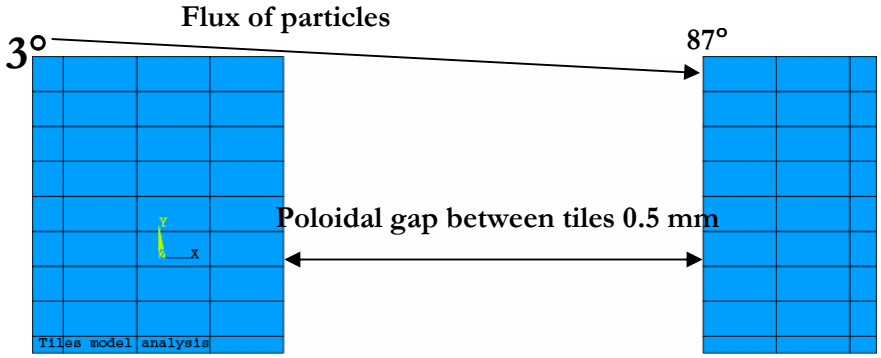

Fig. 5.3.3.3.2. The region of the gap between adjacent tiles.

5.3.3.4 Load conditions – The SATIR test

The software give the possibility also to simulate the SATIR test. The SATIR test is a thermographic NDT. Cold water (5 °C) is sent to the monoblocks, the temperature of the water is suddenly switched to 95 °C, after a pause the temperature is decreased again to 5 °C. An infrared camera aimed at the monoblocks, monitors the variation of the surface temperature of the monoblocks. The behaviour of the surface temperatures of the tiles during the transient are compared with the same curve obtained for the reference tile. A difference during the ascending or descending curve between the reference and the tested tiles is an indication of a defect in the tile.

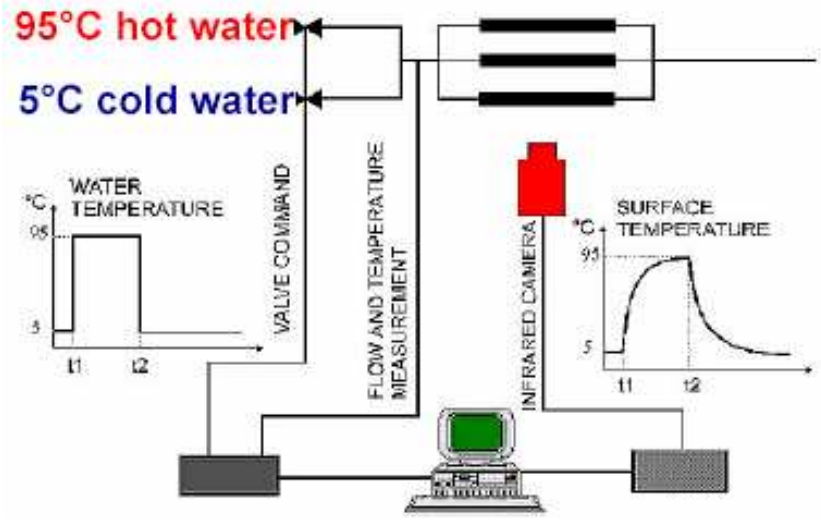

Fig. 5.3.3.4.1 Scheme of the SATIR test.

5.3.3.5 The sublimation

The software has the possibility to simulate the lost of material by sublimation in order to evaluate the evolution of the profile. The sublimation implemented in the code considers implicitly the non equilibrium condition. During sublimation, in equilibrium conditions, there are a certain amounts of particles that sublimate from the surface equal to the amount of particles that condensate on the surface. The vapor pressure during equilibrium leads the amount of particles that condensate on the surface. Our working conditions are completely different from equilibrium conditions. The cryopump continuously pump away particles from the surface hence (conservatively) there are no particles that condensate on the surface of the tiles. The amount of particles that sublimate from the surface depend on the surface temperature and because the cooling of the surface depend on the amount of particles that leave the surface, there will be an equilibrium temperature (depending on the load) when the increase of temperature due to the load is compensate by the sublimation cooling due to the sublimation of the particles. In other words, the condition of equilibrium are achieved not as a balance of ions sublimate versus ions condensate but are function of the temperature of the surface that is the main parameter that govern the "expulsion" of the ions from the heated surface. Hence an equilibrium temperature is achieved function of the thermal load applied on the surface of the tile.
Therefore, in the software the sublimation has two consequences, lost of material and cooling of the surface.
The ratio of the mass sublimated [50] is:

$$\dot{m}_{subli} = 1/4 * n * v$$

Where:
n is the density of the gas [atoms/mm^3];
v is the speed of the atoms in the gas.
The formula above can be written [50]:

$$\dot{m}_{subli} = \frac{2.6*10^{18}}{\sqrt{MT[K]}} 10^{B-A/T[K]} \left[\frac{atoms}{mm^2 \sec} \right]$$

Where:
M is atomic mass of the material (for carbon M=12 UMA);
T [K] is the temperature in Kelvin.
A, B are parameter to describe the behaviour of the vapour pressure for the material considered [51], [52] (for carbon considering the combination of three species C_1, C_2, C_3, A=40181, B=14.80).
The amount of heat lost by sublimation [53] is:

$$q''_{subli} = \dot{m}_{subli} * h$$

Where:
q''_{subli} is the amount of heat lost by "evaporative cooling" [W/m^2];
$\dot{m}_{subli}$ is the ratio of the mass sublimated as [Kg/(m^2*sec)];
h is the latent heat [J/Kg] of the carbon.
The figures 5.3.3.5.1 and 5.3.3.5.2 shows respectively the ratio of mass sublimated function of the surface temperature and the heat lost by evaporative cooling from the surface of the tiles.

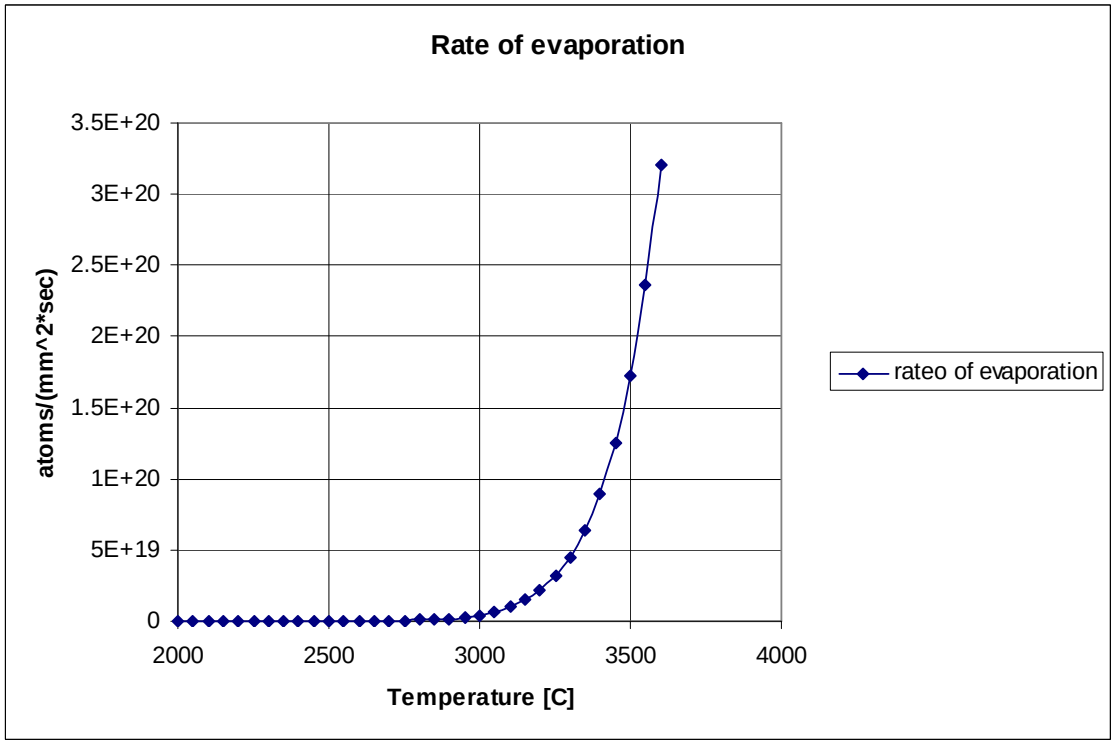

Fig. 5.3.3.5.1 Ratio of mass sublimated function of the temperature.

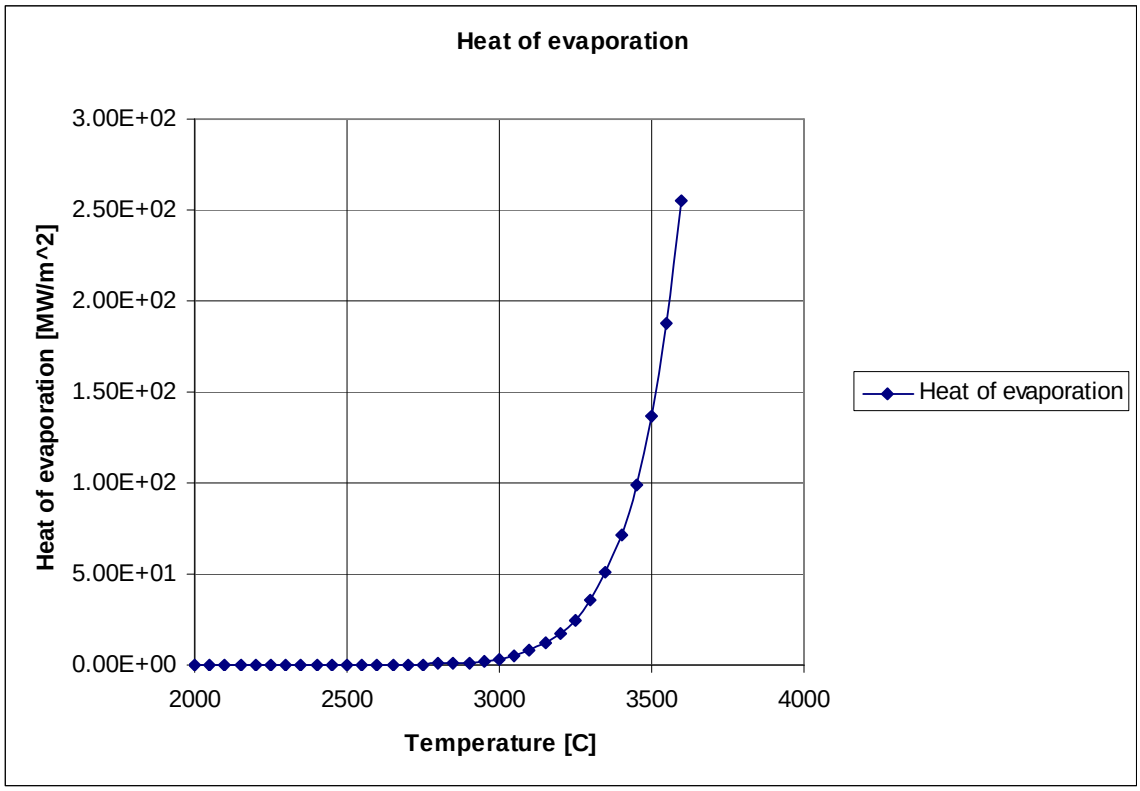

Fig. 5.3.3.5.2. Heat lost by evaporative cooling function of the temperature.

It is clear, looking the figures above, that the sublimation process start to be significant when the surface temperature is between 2500-3000 °C.
The software solves numerically the integral, reported below, for each element able to sublimate (i.e. the external elements of the tiles exposed to the plasma):

$$\delta_{subli} = \int_{t_{expo}}^{t_{kill}} A \cdot \dot{m}_{subli} dt$$

Where:
δ_{subli} is the amount of material lost [g];
t_{kill}, t_{expo} is the period of exposure of the considered element [sec];
A is the area where the material can sublimate [mm^2].
If the amounts of material sublimated calculated in an element exceed the amounts of the material in the element itself, that element is killed.

5.3.3.6 The physical erosion

The software has the possibility to simulate the lost of material by physical erosion. When a flux of particles hit a surface there will be some particles on the surface that will be scattered away. The amount of particles removed from the surface will depend on the binding lead and on the energy of the incident particles. As incident particles has been considered only the contribution due to the ions neglecting the contributions due to the neutral. The ratio of the particles eroded is given by:

$$\dot{m}_{Phy} = \Gamma_{Particles} \cdot Y_{PHY}(E)$$

Where:
$\Gamma_{Particles}$ is the flux of the incidence particles (ions) [Particles/(m^2 sec)];
$Y_{PHY}(E)$ is the sputtering yield as a function of the energy of the incidence particles [atoms/ions].
The sputtering yield due to the physical erosion can be calculated using two way:
a) with the formulation developed by Bohdansky [48];
b) with a formula derived from experimental data valid for the ITER working conditions tested with the Monte Carlo code TRIM [37].
For what concern the Bohdansky formula:

$$Y_{PHY}(E) = Q \cdot Sn(E) \cdot \left[1 - \left(\frac{E_{TH}}{E_0}\right)^{\frac{2}{3}}\right] \cdot \left(1 - \frac{E_{TH}}{E_0}\right)^2$$

Where:
Q is a fitting parameter [atoms/ions];
$Sn(E)$ is the function for the energy dependence of the energy deposited in elastic collision (stopping power);
E_{TH} is the energy threshold [eV];
E_0 is the energy of incident particles [eV].
The $Sn(E)$ function is given by:

$$Sn(E) = 0.5 \cdot \frac{\ln\left(1+1.2288\frac{E_0}{E_{TF}}\right)}{\frac{E_0}{E_{TF}} + 0.1728 \cdot \sqrt{\frac{E_0}{E_{TF}}} + 0.008 \cdot \left(\frac{E_0}{E_{TF}}\right)^{0.1504}}$$

Where:
E_0 is the energy of incident particles [eV];
E_{TF} is the Thomas-Fermi potential function of the atomic mass of the projectile and target particles [eV].
The formula for the Physical sputtering yield is valid for flux of particle perpendicular to the target. A lot of formulas are available to take into account the angle of the incident particles with the target. In the software has been introduced a parameter in order to take into account the variation of the sputtering yield due to the angle of incidence of the particles.
The fig. 5.3.3.6.1 shows the sputtering yield due to the physical erosion function of the energy of the incident particles using the Bohdansky formula. The figure show also the difference when the incident particles are deuterium or carbon ions (this last case is referred to self-sputtering).

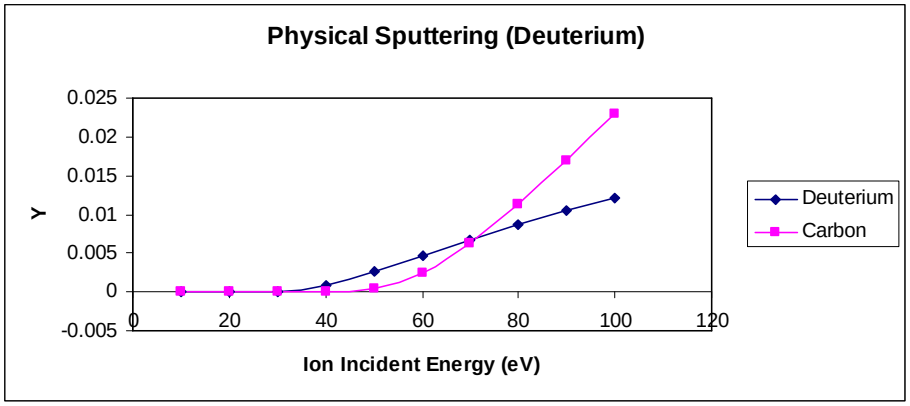

Fig. 5.3.3.6.1 Physical sputtering yield function of the energy of the incident particles.

Unfortunately, the Bohdansky formula doesn't take into account that the ions that impact the surface of the tiles have an energy spectrum (the Bohdansky formula is valid only for monoenergetic ions). Using some experimental data [49] and some data calculated with the Monte Carlo code TRIM [37] has been built a curve where the physical sputtering yield is function of the ions temperature (see fig. 5.3.3.6.2).

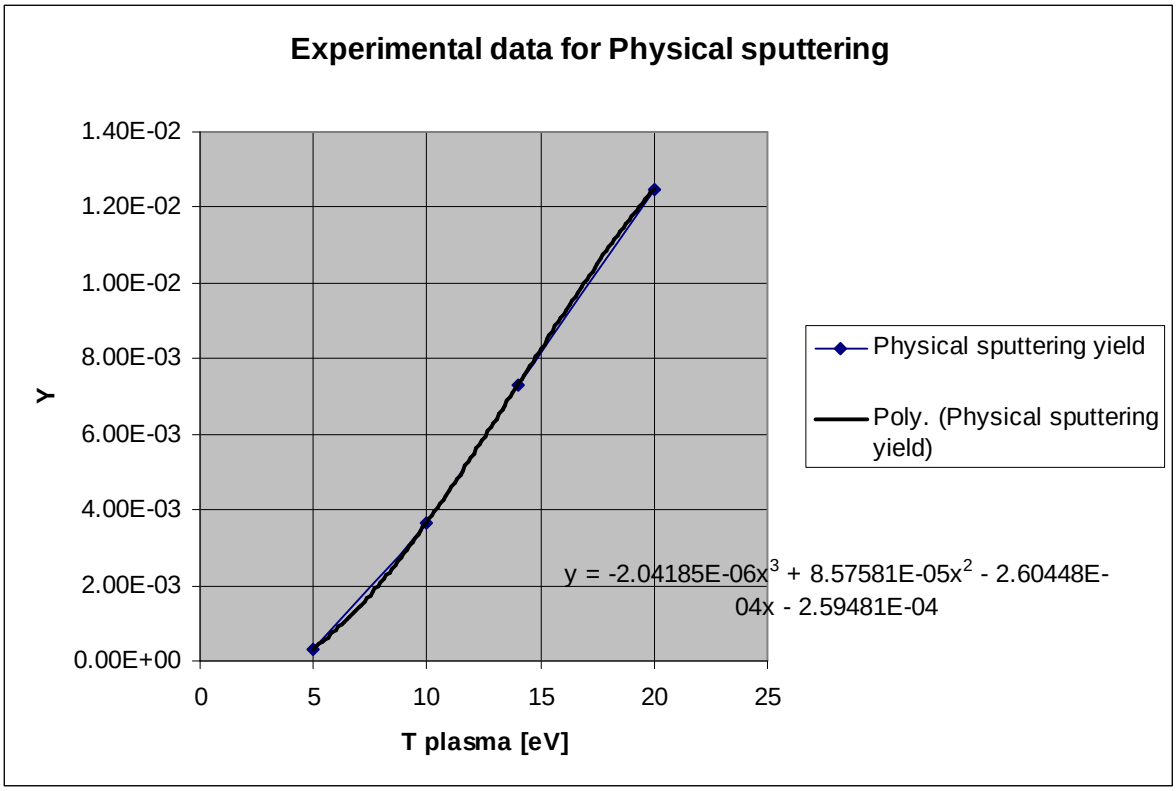

Fig. 5.3.3.6.2 Physical sputtering yield functions of the ions temperature obtained interpolating experimental data.

These data are valid for condition typical for ITER and for temperature of the ions among 5 and 20 eV. (1 eV = 11600 K).
The software solves numerically the integral below, for each element able to erode (i.e. the elements exposed to the stream of particles coming from the plasma):

$$\delta_{Phy} = \dot{m}_{Phy} \int_{t_{expo}}^{t_{kill}} A \cdot dt$$

Where:
δ_{Phy} is the amount of material lost [g];
A is the area where the incidence particles hit the target [mm^2];
t_{kill}, t_{expo} is the period of exposure of the considered element [sec];
If the amount of material eroded calculated in an element exceed the amount of the material in the element itself, that element is killed.

5.3.3.7 The chemical erosion

The software has the possibility to evaluate the chemical erosion of the tiles. The chemical erosion is a particular kind of erosion that happen because the chemical affinity of the target and projectile materials. In fact may happen that some particles of hydrogen (deuterium or tritium) chemically react with the target of carbon giving molecules of CH_x. The main contribution is due to the ionized isotopes of hydrogen. To be more precise, studies of Roth [54] recognize 3 different kinds of chemical erosion:

1) The surface process happen at low surface temperature, the available carbon atoms are essentially hydrated but no thermal release of hydrocarbons occurs. However, hydrocarbon radicals are bound to the surface with much smaller binding energy (≈ 1 eV) than carbon surface atoms in their regular lattice environment (7.4 eV). This lead to an ion induced desorption of hydrocarbon radicals which can be described in a manner analogous to physical sputtering using a threshold energy in the low eV range.
2) The thermal activated process. At temperature above 400 K CH_3 radicals can be released while at temperature above 600 K reconbinative hydrogen release (H_2) start to reduce the chemical erosion yield.
3) The thermal reaction described above is enhanced by radiation damage introduced in the material which provides open bonds for hydrogen attachment. This yield enhancement is characterized by threshold energy for damage production.

Moreover, the contributions of the phenomena described above may change depending by the hybrid state of Carbon atoms (sp^x).
The model developed by Roth [55]:

$$Y1_{surf} = C_{surf} * \frac{\left(2*10^{-32}*\phi + e^{-1.865*\frac{11604}{T}}\right)}{\left[2*10^{-32}*\phi + \left(1+\frac{2*10^{29}}{\phi}*e^{-1.8*\frac{11604}{T}}\right)*e^{-1.865*\frac{11604}{T}}\right]} * Z_{aux}$$

$$Y2_{surf} = C_{surf} * \frac{\left(2*10^{-32}*\phi + e^{-1.7*\frac{11604}{T}}\right)}{\left[2*10^{-32}*\phi + \left(1+\frac{2*10^{29}}{\phi}*e^{-1.8*\frac{11604}{T}}\right)*e^{-1.7*\frac{11604}{T}}\right]} * Z_{aux}$$

$$Y3_{surf} = C_{surf} * \frac{\left(2*10^{-32}*\phi + e^{-1.535*\frac{11604}{T}}\right)}{\left[2*10^{-32}*\phi + \left(1+\frac{2*10^{29}}{\phi}*e^{-1.8*\frac{11604}{T}}\right)*e^{-1.535*\frac{11604}{T}}\right]} * Z_{aux}$$

$$Y4_{surf} = C_{surf} * \frac{\left(2*10^{-32}*\phi + e^{-1.38*\frac{11604}{T}}\right)}{\left[2*10^{-32}*\phi + \left(1+\frac{2*10^{29}}{\phi}*e^{-1.8*\frac{11604}{T}}\right)*e^{-1.38*\frac{11604}{T}}\right]} * Z_{aux}$$

$$Y5_{surf} = C_{surf} * \frac{\left(2*10^{-32}*\phi + e^{-1.26*\frac{11604}{T}}\right)}{\left[2*10^{-32}*\phi + \left(1+\frac{2*10^{29}}{\phi}*e^{-1.8*\frac{11604}{T}}\right)*e^{-1.26*\frac{11604}{T}}\right]} * Z_{aux}$$

Where:
Yn_{surf} are the contribution to the total chemical sputtering yield due to the surface process [atoms/particles];
ϕ is the flux of particle incident on the surface of the tiles (ions) [particles/(m^2*sec)];
T is the surface temperature of the tiles [K];
C_{surf} and Z_{aux} are parameters for the calculation of the sputtering yield due to the surface process:

$$C_{surf} = \left[\frac{1}{1+\left(1.67*10^{-22}*\phi\right)^{0.54}*\left(1+3*10^{7}*e^{-1.6*\frac{11604}{T}}\right)}\right]$$

$$Z_{aux} = Q * Sn(E)\frac{\left[1-\left(\frac{E_{THS}}{E_0}\right)^{\frac{2}{3}}\right]*\left(1-\frac{E_{THS}}{E_0}\right)^{2}}{\left(1+e^{\frac{E_0-65}{40}}\right)}$$

Where:
$Sn(E)$ is the stopping power (already used for the physical sputtering yield);
Q is a fitting parameter (already used for the physical sputtering yield);
E_{THS} and E_0 are respectively the threshold energy for the surface process and the energy of the incident particles [eV].
The contribution of the thermal activated process is:

$$Y1_{THERM} = C_{surf} * \frac{\left(2*10^{-32}*\phi + e^{-1.865*\frac{11604}{T}}\right)}{\left[2*10^{-32}*\phi + \left(1+\frac{2*10^{29}}{\phi}*e^{-1.8*\frac{11604}{T}}\right)*e^{-1.865*\frac{11604}{T}}\right]} * 0.033 * \frac{e^{-1.865*\frac{11604}{T}}}{2*10^{-32}*\phi + e^{-1.865*\frac{11604}{T}}}$$

$$Y2_{THERM} = C_{surf} * \frac{\left(2*10^{-32}*\phi + e^{-1.7*\frac{11604}{T}}\right)}{\left[2*10^{-32}*\phi + \left(1+\frac{2*10^{29}}{\phi}*e^{-1.8*\frac{11604}{T}}\right)*e^{-1.7*\frac{11604}{T}}\right]} * 0.033 * \frac{e^{-1.7*\frac{11604}{T}}}{2*10^{-32}*\phi + e^{-1.7*\frac{11604}{T}}}$$

$$Y3_{THERM} = C_{surf} * \frac{\left(2*10^{-32}*\phi + e^{-1.535*\frac{11604}{T}}\right)}{\left[2*10^{-32}*\phi + \left(1+\frac{2*10^{29}}{\phi}*e^{-1.8*\frac{11604}{T}}\right)*e^{-1.535*\frac{11604}{T}}\right]} * 0.033 * \frac{e^{-1.535*\frac{11604}{T}}}{2*10^{-32}*\phi + e^{-1.535*\frac{11604}{T}}}$$

$$Y4_{THERM} = C_{surf} * \frac{\left(2*10^{-32}*\phi + e^{-1.38*\frac{11604}{T}}\right)}{\left[2*10^{-32}*\phi + \left(1+\frac{2*10^{29}}{\phi}*e^{-1.8*\frac{11604}{T}}\right)*e^{-1.38*\frac{11604}{T}}\right]} * 0.033 * \frac{e^{-1.38*\frac{11604}{T}}}{2*10^{-32}*\phi + e^{-1.38*\frac{11604}{T}}}$$

$$Y5_{THERM} = C_{surf} * \frac{\left(2*10^{-32}*\phi + e^{-1.26*\frac{11604}{T}}\right)}{\left[2*10^{-32}*\phi + \left(1+\frac{2*10^{29}}{\phi}*e^{-1.8*\frac{11604}{T}}\right)*e^{-1.26*\frac{11604}{T}}\right]} * 0.033 * \frac{e^{-1.26*\frac{11604}{T}}}{2*10^{-32}*\phi + e^{-1.26*\frac{11604}{T}}}$$

Where:
Yn_{therm} are the contribution to the total chemical sputtering yield due to the thermal activated process [atoms/particles];
ϕ is the flux of particle incident on the surface of the tiles [particles/(m^2*sec)];
T is the surface temperature of the tiles [K];
C_{surf} is the same parameter used for the surface process (see above).
The so called "Damage enhancement" phenomenon is considered with the following model:

$$Y_{DAM} = Q * Sn(E) * \left[1 - \left(\frac{E_{THD}}{E_0}\right)^{\frac{2}{3}}\right] * \left(1 - \frac{E_{THD}}{E_0}\right)^2$$

Where:
$Sn(E)$ is the stopping power (already used for the physical sputtering yield);
Q is a fitting parameter (already used for the physical sputtering yield);
E_{THD} and E_0 are respectively the threshold energy for the damage effect and the energy of the incident particles [eV].
The contribution to the total chemical sputtering yield due to the processes considered is:

$$Y1_{CHEM} = Y1_{surf} + Y1_{THERM} + 125 * Y1_{THERM} * Y_{DAM}$$

$$Y2_{CHEM} = Y2_{surf} + Y2_{THERM} + 125 * Y2_{THERM} * Y_{DAM}$$

$$Y3_{CHEM} = Y3_{surf} + Y3_{THERM} + 125 * Y3_{THERM} * Y_{DAM}$$

$$Y4_{CHEM} = Y4_{surf} + Y4_{THERM} + 125 * Y4_{THERM} * Y_{DAM}$$

$$Y5_{CHEM} = Y5_{surf} + Y5_{THERM} + 125 * Y5_{THERM} * Y_{DAM}$$

And finally:

$$Y_{CHEM} = \frac{Y1_{CHEM} + Y2_{CHEM} + Y3_{CHEM}}{4.5} + \frac{Y4_{CHEM} + Y5_{CHEM}}{9}$$

The ratio of the particles eroded by chemical erosion is:

$$\dot{m}_{Che} = \Gamma_{Particles} \cdot Y_{CHE}(E,T)$$

Where:
$\Gamma_{Particles}$ is the flux of the incidence particles [Particles/(m2 sec)];
$Y_{CHE}(E,T)$ is the sputtering yield as a function of the energy of the incidence particles and the surface temperature [atoms/ions].
The figures 5.3.3.7.1 and 5.3.3.7.2 show respectively the chemical sputtering yield function of the surface temperature and of the particles flux for incident particles of 10 eV and the sputtering yield function of the surface temperature and the energy of the incident particles for a flux of 1e24 [Particles/(m^2*sec)].

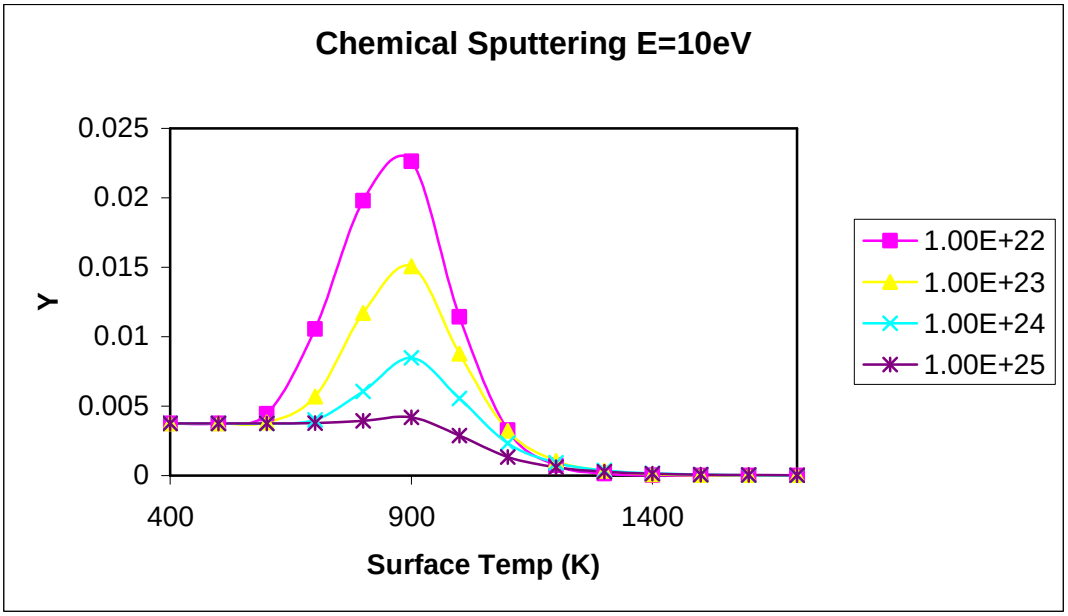

Fig. 5.3.3.7.1 Chemical sputtering yield function of the surface temperature and flux particles for incidence particles of 10 eV.

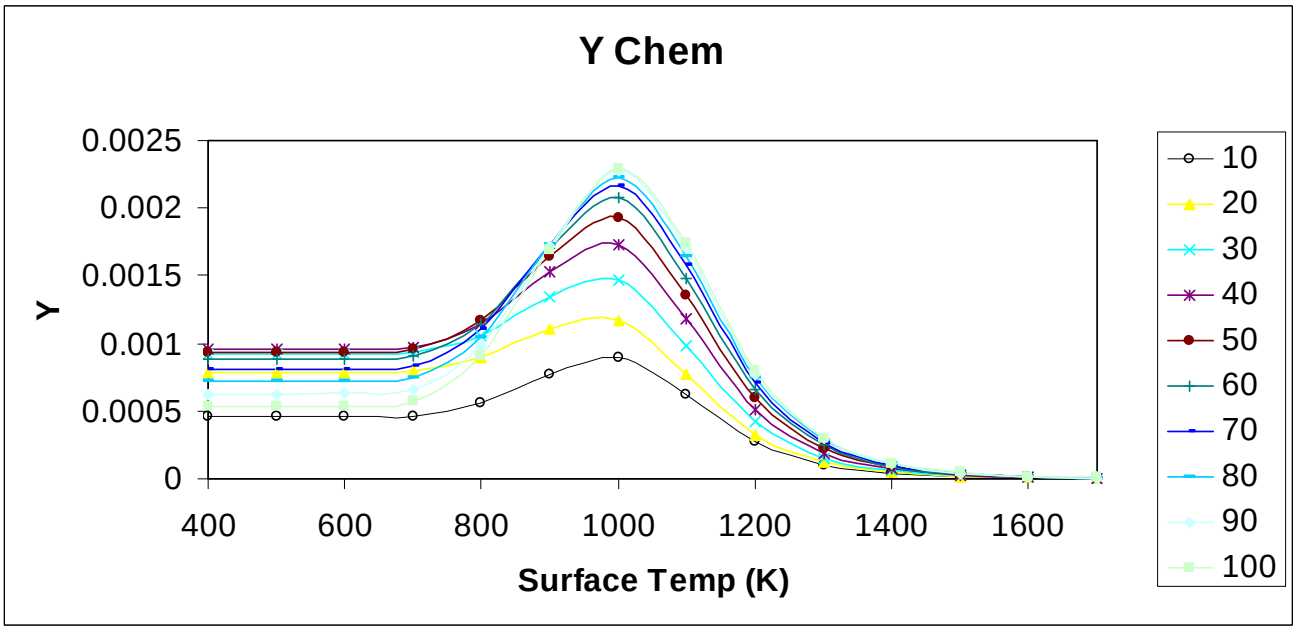

Fig. 5.3.3.7.2 Chemical sputtering yield function of the surface temperature and the energy of the incidence particles for a flux of 1e24 [Particles/(m^2*sec)].

The software solves numerically the integral, reported below, for each element able to erode (i.e. the elements exposed to the stream of particles coming from the plasma):

$$\delta_{Che} = \int_{t_{expo}}^{t_{kill}} A \cdot \dot{m}_{Che} dt$$

Where:
δ_{Che} is the amount of material lost [g];
t_{kill}, t_{expo} is the period of exposure of the considered element [sec];
A is the area where the material is hit from the particles [m^2].
If the amount of material eroded calculated in an element exceed the amount of the material in the element itself, that element is killed.

5.3.4 Description of the structure of the code

The software is made by 26 subroutines and 8 macro. Below is shown the flow diagram of the code.

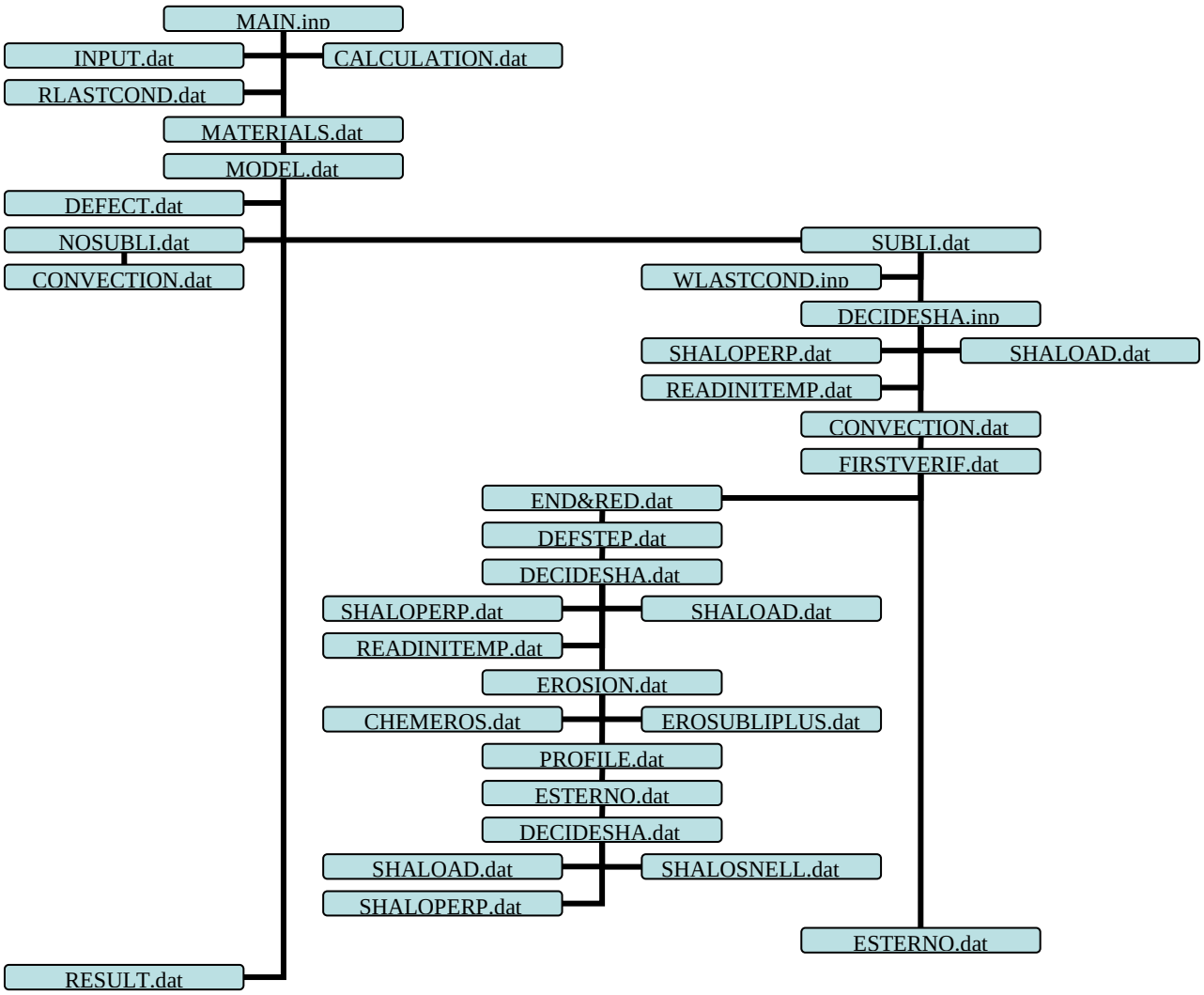

Fig.5.3.4.1 Flow diagram of the software.

The software may solve different kind of problem related to the monoblock:

1) steady state analysis

2) transient analysis
    a. SATIR simulation
    b. Normal operation
    c. Erosion

These problems can be solved varying a lot of parameters. It is also possible to include a defect in the junction between the cooling channel and the CFC.
The following table will describe briefly each subroutine of the code:

Name	Description
MAIN.inp	It contains the main structure of the code. All the procedure starts from this routine.
RESTART.inp	This routine is used in case of erosion when an analysis has been stopped and the user wants to restart the analysis starting from the point where it has been stopped.
INPUT.dat	There is the possibility to insert the input parameters using an input file. Hence, this file contains the input parameter of the case analysed.
CALCULATION.dat	In case of erosion this subroutine is called to calculate some useful values in order to solve the problem of the chemical and physical erosion.
RLASTCOND.dat	In case of erosion it is possible to extend the analysis doing several loadstep changing load conditions. This routine read the data from a previous analysis and it write this condition in a temporary file. These conditions are used then as starting point of the new analysis. This process will be further better explained.
MATERIALS.dat	This routine contains the material properties as well as the table used to setup convection and load function of the surface temperature.
MODEL.dat	This routine generates the geometry and the finite element model using the geometric parameters collected previously.
DEFECT.dat	There is the possibility to include a defect in the junction between the cooling channel and the CFC.
NOSUBLI.dat	This routine manages the case without erosion.
SUBLI.dat	This routine manages the case with erosion.
CONVECTION.dat	This routine applies the convection loads on the cooling channel.
WLASTCOND.dat	In case of erosion it is possible to extend the analysis doing several loadstep changing load conditions. This routine read the last condition written in the previous analysis (see routine RLASTCOND.dat) and include this condition in the new analysis changing for example the eroded profile of the surface of the tiles. These conditions are used then as starting point of the new analysis. This process will be further better explained.
SHALOAD.dat	This routine applies the heat flux loads on the surface following the logic explained in the chap. 2.2.3.
READINITEMP.dat	It is possible to start from a distribution of temperature instead

	that from a constant temperature. This routine read the initial condition considered from a file generated with a macro called "zmaketempfile.mac".
FIRSTVERIF.dat	This routine verifies if some elements have been eroded in the analysed case. If it is true the control of the erosion is given to the subroutine "END&RED.dat".
END&RED.dat	This routine manages the erosion.
DEFSTEP.dat	This routine find the time till the erosion is absent allowing the code to do a faster normal transient analysis up to that point. This routine tries also to find a tentative initial timestep to be used in the erosion.
EROSION.dat	This routine find and kill the element to be eroded with the different concept used to make it (sublimation, physical erosion and chemical erosion).
CHEMEROS.dat	This routine is complementary with "EROSION.dat" in case of chemical erosion. It calculates all the derived parameters in order to estimate the amount of material eroded by chemical erosion.
EROSUBLIPLUS.dat	This routine is complementary with "EROSION.dat" in case of physical and chemical erosion. It take care of the possible erosion by sublimation of element not exposed to plasma during analysis of physical and/or chemical erosion.
PROFILE.dat	This routine change the profile of tiles in case the routine "EROSION.dat' killed some elements. Update the profile is useful in order to be able to apply the loads function of the position (see chap. 2.2.3.).
ESTERNO.dat	This routine save the model and clean the memory in order to avoid using the page.file. This routine contains also a parameter, called "permesso", that if set up on 0 stop the procedure of erosion and exit from ANSYS (during a batch job) in a "clean" way, saving the results obtained till then.
DECIDESHA.dat	This routine decides which procedure to use to apply the loads function of the position following the logic explained in the chap. 2.2.3. In fact there are two routine to apply the heat flux on the surface, "SHALOAD.dat" and "SHALOSNELL.dat". The first one is the "standard" procedure the second one is a faster procedure used only in certain case when element near the edge of the tiles have not been eroded.
SHALOSNELL.dat	This routine applies the heat flux loads on the surface following the logic explained in the chap. 2.2.3 but using an algorithm faster that the one used in the routine "SHALOAD.dat". Unfortunately this algorithm is not always usable.
SHALOPERP.dat	This routine apply the heat flux loads on the surface of the tile in a perpendicular way without follow the logic explained in the chap 2.2.3.
RESULT.dat	This routine is used to plot some results at the end of the job like temperature distribution etc… The subroutine is called only if the

	job has been done using the graphical interface. This routine is not called in case of batch job.

Table 5.3.4.1 Description of the 26 subroutine of the software developed.

The following table will describe briefly the 8 macro part of the program.

Name	Description
RUN.bat	This script is used to launch an analysis in batch mode.
RUNRESTART.bat	This script is used to restart an analysis previously interrupted with the subroutine “ESTERNO.dat” (see manual in appendix A).
ZSTARTFROMBATCH.mac	This script is used to resume from ansys an analysis already done and to plot on the screen the distribution of the temperature of the last timestep calculated (see manual in appendix A)
ZEROSIONVSTIME.mac	This script is used to plot and calculate the amount of erosion [g] function of the time relative to the two tiles modelled. This macro write a file: 1) “erosion.data” where the four columns represent the time [sec] and the erosion [g] of the 2 half and the middle monoblock.
ZCHEMCOEF.mac	This macro is used to calculate the chemical sputtering yield on the surface of the central monoblock. The script generate two files: 1) “chesputtemp.data” where the first column represents the time [sec] and the others 4 columns represents the surface temperature of the central monoblock on the left corner on the middle (2 values) and on the right corner. 2) “chesputtime.data” where the first column represents the time [sec] and the other 4 columns represents the surface chemical sputtering yield of the central monoblock on the left corner, on the middle (2 values) and on the right corner (see manual in appendix A)
ZMAKETEMPFILE.mac	Macro to write the distribution of the temperature of the timestep in the current analysis. This macro write the distribution of the temperature in a file “inittemp.data” in order to start another analysis using as starting point the temperature distribution recorded in the file “inittemp.data” (see manual in appendix A)
ZWRITETIMECHECK.mac	This script is used to write in a file the vector “timecheck” in order to verify the goodness of the analysis. The macro generate the file “timecheck.data” where in the column are written the values of the vector “timecheck” and is calculated the average time that represents the error

	introduced in the calculation (see manual in appendix A).
ZPROTEMP.mac	This script is used to write the temperature profile [°C], for a certain time, of the left, middle and right tile. The macro generate the files “tempprofleft%number of substep requested%.data, tempprofmiddle%number of substep requested%.data and tempprofright%number of substep requested%.data” that contain four columns: The first column contains the nodes where the temperature has been read; the second column contains the coordinate X of the node where the temperature has been read; the third column contains the coordinate Y of the node where the temperature has been read; the fourth column contains the temperature [°C] of the corresponding node;

Table 5.3.4.2 Description of the 8 macro developed.

There are some restrictions using the code:

1) The database of the material properties contains 5 materials but could be extended.
2) The database for the film coefficient function of the water bulk temperature is valid for range of water temperature 100-140 °C for normal operation and 5-100 °C for SATIR test. Moreover, the database is valid for the conditions showed in the tables 5.3.3.2.1 and 5.3.3.2.2.
3) The generic transient analysis can be done with a maximum of 5 loadstep.
4) The erosion transient analysis can be done only with 1 loadstep with the load applied in a step way. Other loadstep can be added to the solution running again the procedure (see APPENDIX A).
5) An erosion transient analysis takes into account that the particles loads come with a glazing angle of 3° or perpendicular to the surface. All the other kind of analyses consider the heat loads coming only from the top without taking into account the logic explained in chap. 5.3.3.3.
6) The geometry can be modified taking into account that the modification of some parameters, like the internal diameter of the cooling channel, can interfere with some other fixed data, like the film coefficient database.

When the erosion is taking into account, the code behaves in a different particular way described in APPENDIX A, as well as the input parameter can have different meaning.

When the erosion is taking into account the code can do only one timestep. Strictly speaking, the code does a lot of time step to achieve the final time imposed from the user. In fact, ANSYS give back the control to the user only at the end of timestep and not among substeps. Because during erosion analyses the code must check the level of erosion there is an algorithm that establishes the delta time to use between loadstep. This algorithm calculates the timestep for the next loadstep considering what happened in the previous loadstep. The best setting for the timestep is to achieve a ratio between the amounts of material to erode and the amounts of the material in the maximum eroded element equal to 1. This goal is achieved by the algorithm above mentioned and the ratio described above is stored in the vector “timecheck”. Hence, to perform a good analysis or to understand the accuracy of the analysis, the vector “timecheck” should be checked in order to verify that the values inside the vector are less or as close as possible to 1.

5.4 Validation of the code

5.4.1 General considerations

Although the phenomena implemented in the code are very complex, there are a lot scientists that tried to describe, with mathematical model, the single phenomena involved in the erosion of the CFC. The mathematical models used in the program are very well validated (see references) then, it has been demonstrated that the results of the code correspond with the mathematical model of each phenomena.
Where applicable, the program results have been compared also with experimental results. It should be mentioned that the validation of the code has been conducted within collaboration with the CEA Cadarache.
It has been also checked the reliability of the code changing the timestep and the mesh. In fact, the main parameters that govern the calculation process are the dimension of the elements (mesh) and the timestep adopted. Several tests have been done checking the code with different mesh and with different timestep. To carry out these tests, the code has been set up to calculate only the erosion due to the sublimation process. The figure 5.4.1.1 shows the erosion due to sublimation of a tile loaded with 20 MW/m^2 function of the thickness of the mesh. The thicknesses labeled veryfine, fine and coarse correspond respectively to 8.5, 13 and 26 μm.

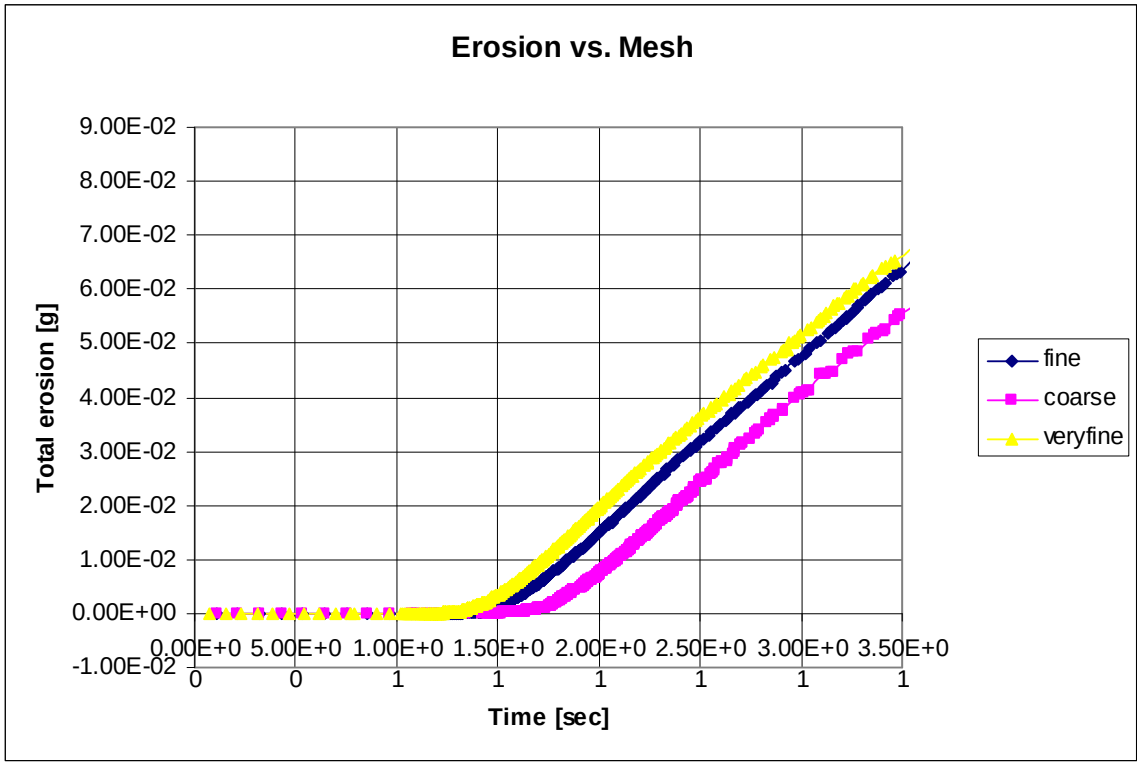

Fig. 5.4.1.1 The erosion of a tile loaded with 20 MW/m^2 due to sublimation versus the dimension of the mesh (veryfine = 8.5 μm thick, fine = 13 μm thick, coarse 26 μm thick).

From the picture above it seems that the code is achieving an asymptote increasing the thickness of the mesh. As confirmation the figure below has been done to verify that at certain time the erosion, refining the mesh, is achieving an asymptote.

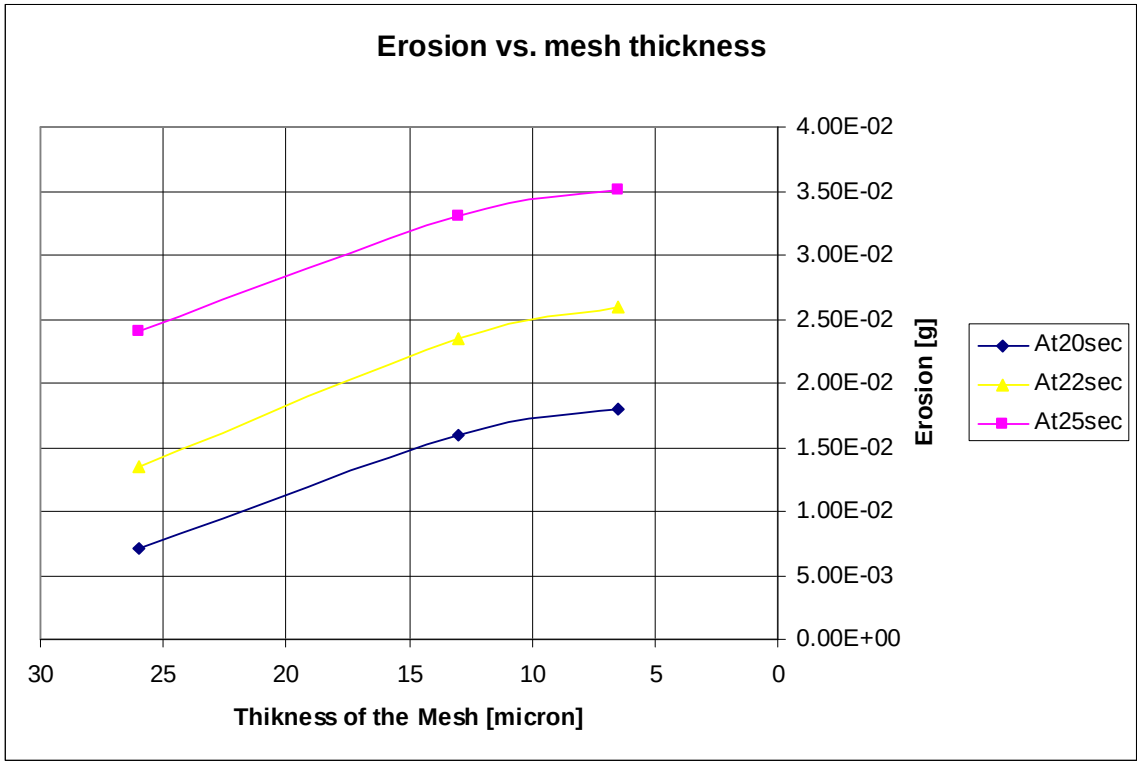

Fig. 5.4.1.2. At different time the behaviour of the code is to achieve an asymptote refining the mesh.

The same kind of test has been conducted with the timestep instead that with the dimension of the elements. The figure below show the erosion due to sublimation of a tile loaded with 20 MW/m^2 function of the timestep used during calculation. . The timestep labeled 1e-3 refer to a fixed timestep of 1 msec, 1e-2 refer to a fixed timestep of 10 msec, the label algorithm refer to a time modified every timestep following the algorithm explained in paragraph 5.3.4.

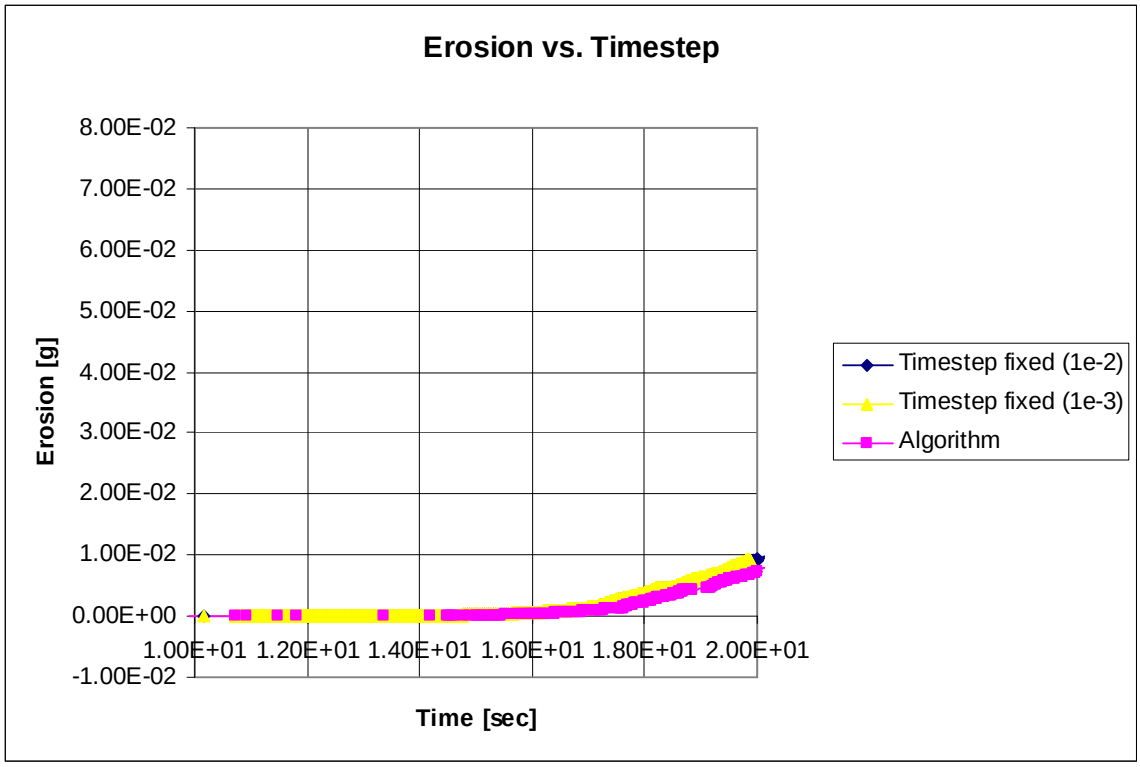

Fig. 5.4.1.3 The erosion of a tile loaded with 20 MW/m^2 due to sublimation versus the time used for the timestep (timestep fixed 1e-3 = 1 msec, timestep fixed 1e-2 = 10 msec, algorithm = time variable governed by the algorithm presented in paragraph 5.3.4).

From the picture above it seems that the code gives very similar results using short timestep. A curve has been built to try to better understand the behavior of the erosion versus the timestep adopted. The fig. below shows a comparison at different time of the erosion using different timestep. For 1 and 10 msec the result of the erosion is practically the same (the values horizontally aligned), using the algorithm, then with a variable timestep, there is a discrepancy of about 10 %. Therefore, the algorithm introduces an error but makes the calculation very fast (about 10 time faster). However, the error introduced can be monitored as explained in paragraph 5.3.4.

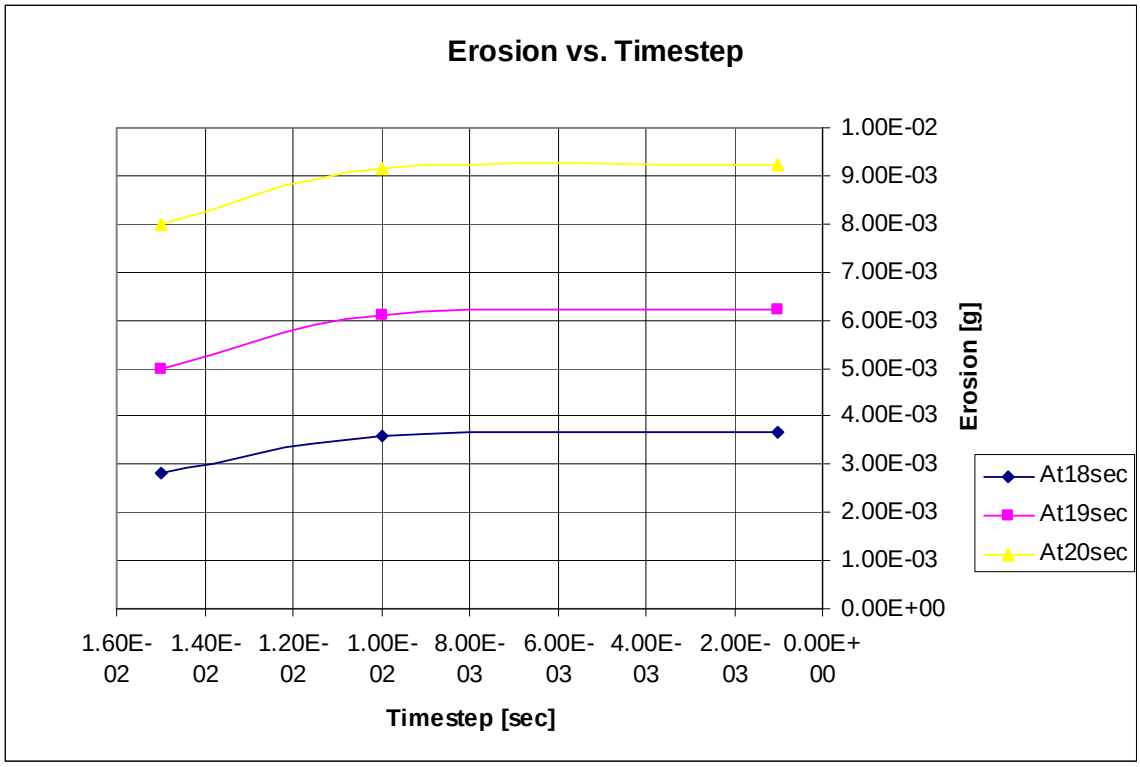

Fig. 5.4.1.4 The code achieve an asymptote using a timestep shorter and shorter. The algorithm adopted give good results.

5.4.2 Validation of Physical erosion

The figure below shows a comparison among Ansys calculation, the Bohdansky's formula and TRIM calculation to check the physical sputtering yield. It has been assumed a flux of deuterium ions with an energy of 200 eV perpendicular to the surface.

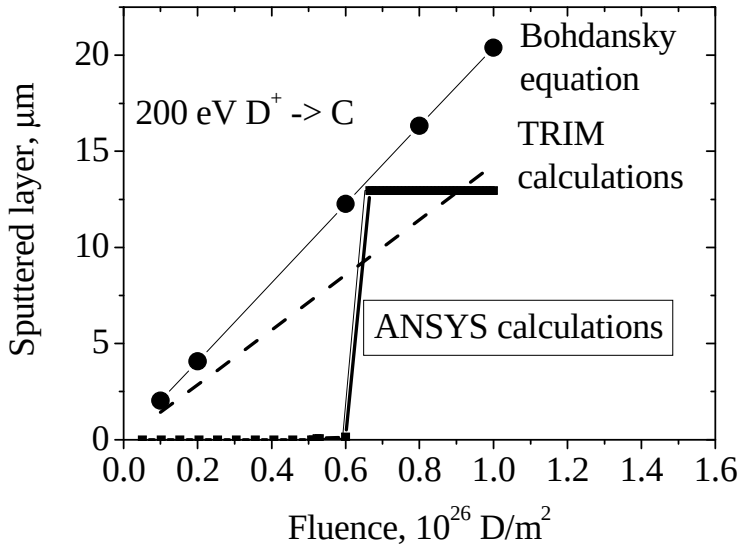

Fig. 5.4.2.1 Comparison among Bohdasky model, Ansys calculation and TRIM calculation for a monoenergetic flux of deuterium ions.

The figure above shows a good agreement between the Bohdansky formula and the Ansys calculation, considering that a FE model works with element with a certain dimension (the model is discrete not continued). The above calculation shows a comparison using elements with a thickness of 13 μm. The ansys code underestimates the erosion of 13 μm.

During the validation of the program, it has been recognised that the mathematical model developed by Bohdansky to describe the physical erosion of the CFC overestimate the erosion. The Bohdansky model assumes to use a stream of monoenergetic particles. In reality there is an energetic spectrum.

To overcame this problem, it has been decided to made some calculations for different configuration with the Monte Carlo code TRIM [37] and to use the results of the Monte Carlo code to made an empirical formula that give the physical sputtering yield function of the plasma temperature.

Therefore, the program has been tested with typical parameter of ITER. The fig. below shows a comparison, for different plasma temperature, of Ansys calculation and TRIM calculation.

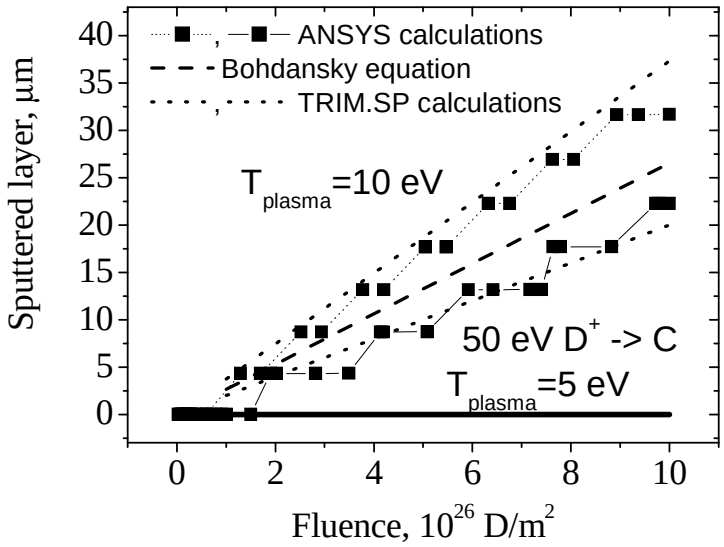

Fig. 5.4.2.3 Comparison among Bohdasky model, Ansys calculation and TRIM calculation for typical ITER conditions.

There is a good agreement between the calculation done with the Monte Carlo code and with Ansys.

5.4.3 Validation of chemical erosion

The chemical erosion has been tested comparing the results of the Roth model [54] with the results of the ANSYS program developed.
As shown in fig. 5.4.3.1 there is a good agreement between the Roth model and the results obtained with the Ansys code.

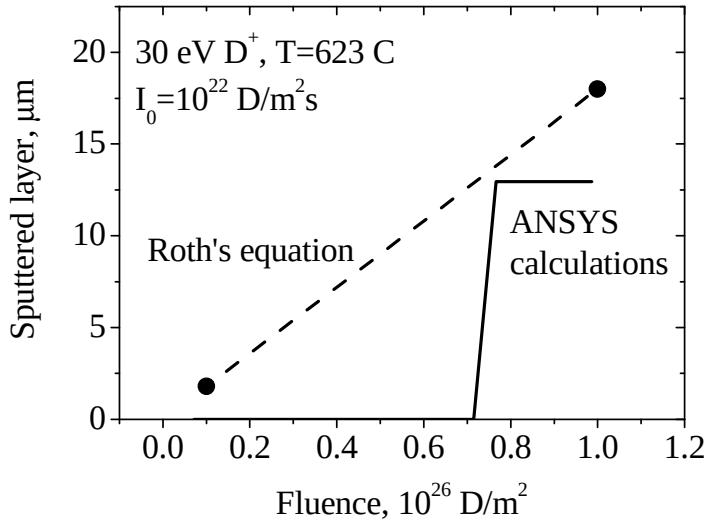

Fig. 5.4.3.1 Comparison among Roth model and Ansys calculation.

As for the physical erosion, the Ansys program proceeds with step of the dimension of the thickness of the elements involved in the erosion process (13 μm for the above example).

5.4.4 Validation of sublimation

Less effort has been used to validate the sublimation because at the first stage the code will be used mainly to simulate chemical and physical erosion. However, the validation of the sublimation has been conducted comparing the erosion obtained in a laser facility [61] with the erosion obtained with Ansys calculation and with another code PHEMOBRID [60]. The fig. 5.4.4.1 shows the erosion obtained experimentally, with PHEMOBRID and with Ansys. PHEMOBRID overestimate the erosion while the ANSYS code underestimate the erosion but generally, considering the uncertainly a margin of a 10 % can be considered a good result. The different behaviour of the erosion curve between Ansys and PHEMOBRID has not been deeply investigated. However, it is reasonable expecting a change of the slope of the curve due to the exponential behaviour of the erosion function of the temperature (see fig. 5.3.3.5.1).

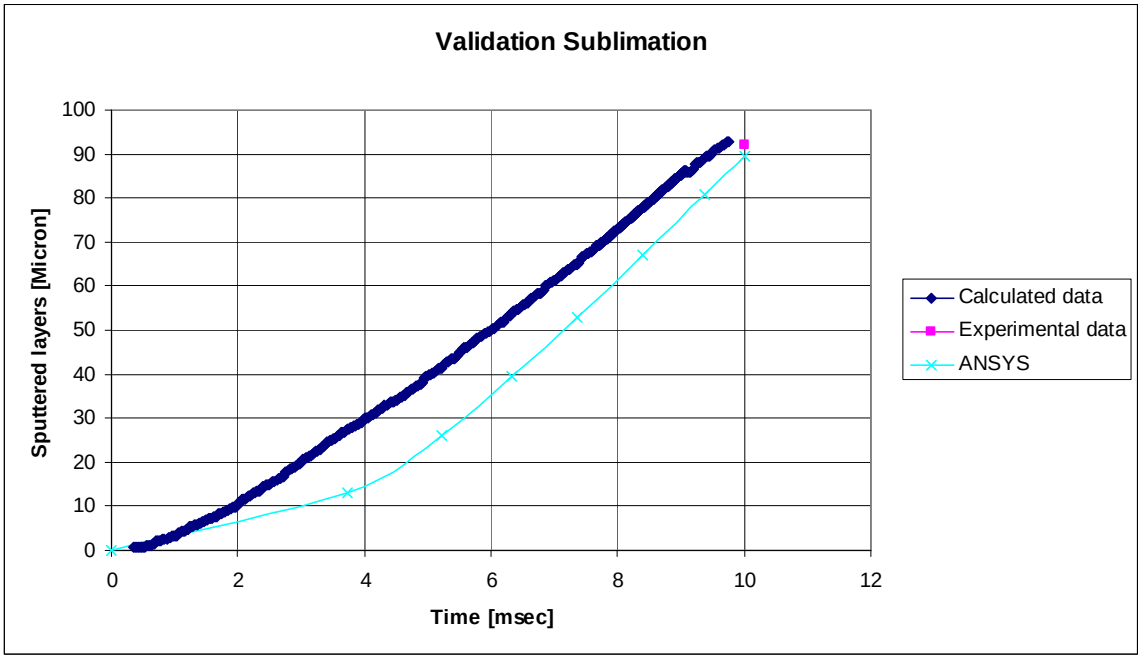

Fig. 5.4.4.1 Comparison between the erosion calculated with an ad hoc code, with ANSYS and the erosion observed experimentally.

5.5. Final considerations

The erosion of the CFC is a complex topic. The work done during this Ph.D. about the erosion has been aimed to better understand the processes involved in ITER and to have a flexible and reliable tool. In the first part of this chapter has been investigated the so

called cascade failure effect. With experimental test and with some calculation has been seen that the possibility that this kind of event take place for the ITER condition are exceptional.
In the second part has been presented the code developed inside Ansys in APDL language. The aim of this work is to have a flexible, reliable and easy to use tool to evaluate as a first approximation the behaviour of tiles exposed to a stream of particles. Through modelling tiles with defective joints, these studies will also be useful to establish the acceptance criteria for the tiles. It is still on going some calculations using the code developed to set up the acceptance criteria for ITER.

6. Conclusion

Referring to the main topics of this work the targets have been achieved.
A methodology and a possible approach to the problem of set up the acceptance criteria for the tiles of CFC (Carbon Fibre Composite) of the divertor at the start of life of the ITER machine has been suggested as well as it has been developed a user-friendly software, inside a commercial, certificated and very well documented finite element code like ANSYS, able to evaluate as a first approximation the behaviour of tiles exposed to a stream of particles.
For what concern the acceptance criteria for the tiles, in order that the monoblock armour can operate without risk of burnout and without releasing excessive amounts of carbon the following tentative acceptance limits are proposed for the CFC monoblock armour subjected to the SATIR test:

- each tile shall have a $\Delta T_{SATIR} \leq 8°C$,

and after passing this first test

- each batch shall belong to a normal distribution with a mean $\Delta T_{SATIR} = 2°C$ and a standard deviation = 3°C.

A batch will include the 80 monoblock tiles of two outer VT poloidal element or the 60 tiles of two inboard elements. The proposed values are based on the assumption that CFC material of the plasma facing component has a room temperature thermal conductivity $\geq 350 Wm^{-1}K^{-1}$ and a standard deviation of 18 $Wm^{-1}K^{-1}$. The practicality of using these postulated values is to be tested during the R&D programme currently under way as part of an ITER R&D supported by EU, at the completion of which the values of acceptance levels can be finally set. In particular, ITER and EFDA are working with CFC manufacturers in an attempt to reduce the standard deviation of the CFC thermal conductivity. The values are also tentative in that they have been developed based on start-of-life performance of the armour and future studies will take into account of the predicted performance as the armour is eroded away.
For what concern the developed code to evaluate as a first approximation the behaviour of tiles exposed to a stream of particles, through modelling tiles with defective joints, these studies will also be useful to establish the acceptance criteria for the tiles. The software developed is able to calculate the amount of erosion [g] of two adjacent tiles as well as the evolving profile. Some simplifications have been made in order to make the problems involved in the erosion of the CFC easier:

- The code does not consider the contribution due to neutral particles.
- The code does not consider the contribution due to self sputtering.
- The incoming flux in the gaps might be more complex than just the geometrical shadowing effect (sheath effect, neutrals and so on).
- The code does not consider the contribution due to RES.

Due to calculations made with Monte Carlo code, considering the working condition of ITER and discussions with erosion experts, at this stage and for the main purpose of the code it has been decided that the above effects can be neglected.

REFERENCES

- [1] DRG1 Annex Physics Basis IDoMs No GAO GDRG 2 00-12-19 W0.6.
- [2] Materials Assessment Report, G 74 MA 10 01-07-11 W 0.2, section 3.3.
- [3] G. Vieider, et al; European Development of Prototypes for ITER High Heat Flux Components, ISFNT-5, Rome, 1999.
- [4] Escourbiac L-5 Meeting Naka 2003
- [5] 45 Non-destructive testing of actively cooled plasma facing components by means of thermal transient excitation and infrared imaging, R. Mitteau et al., Fus. Tech. & Des. Proc. 19th SOFT Lisbon 1996, pp 443-446.
- [6] J. P. Holman "Heat Transfer".McGraw-Hill 1981. pp 48 – 52.
- [7] E. D'Agata Internal document "Critical Heat Flux on the PFC Tiles on the ITER Divertor" IDoms G 17 139 03-11-11 W0.1
- [8] S. Chiocchio. "Comparison of peak flux onto the divertor targets for several ITER FDR Plasmas". Garching (1997).
- [9] G. Federici, P. Andrew, P. Barabaschi, J. Brooks, R. Doerner, A. Geier, A. Herrmann, J. Nucl. Mater. 11-22, (2003), pp. 313-316
- [10] M. Merola, U. Mszanowski, J. Schlosser, I. Smid. "EUPITER: The European Thermohydraulic Package for Plasma-Facing Components". Proceed of the ITER Thermal-hydraulic Technical Meeting on High Heat Flux Cooling, 23-25 September 1996, JET, Abingdon, UK.
- [11] Development of an original active thermography method adapted to ITER plasma facing components control Fusion Engineering and Design, vol. 75-79, p. 401-405 (2005)
  A. Durocher, N. Vignal, F. Escourbiac, J.L. Farjon, J. Schlosser, F. Cismondi
- [12] E. D'Agata, S. Grigoriev, G. Federici, C. Ibbott, A. Makhankov, V. Tanchuk, R. Tivey, Fusion Engineering and Design 66-68 (2003), pp. 329-334
- [13] E. D'Agata, R. Tivey, Fusion Engineering and Design 75-79 (2005), pp.441-445
- [14] NIST/SEMATECH e-Handbook of Statistical Methods, http://www.itl.nist.gov/div898/handbook/, date.
- [15] M.R. Spiegel "Probabilita' e statistica" ETAS libri (1979), pp 155-258
- [16], Data from M.Merola, Euromat 2005- Prague, 4-9 September 2005
- [17] R. Behrisch, et al., Sputtering by Ion Bombardment, Vol. I, Topics in Applied Physics, No. 47, Springer, Berlin, 1981.
- [18] R. Behrisch, et al., Sputtering by Ion Bombardment, Vol. II, Topics in Applied Physics, No. 52, Springer, Berlin, 1983.
- [19] W. Eckstein, Computer Simulation of Ion–solid Interactions, Springer Series in Materials Science, Vol. 10, Springer, Berlin, 1991.
- [20] W. Möller, W. Eckstein and J.P. Biersack, TRIDYN — binary collision simulation of atomic collisions and dynamic composition changes in solids. Comput. Phys. Commun. 51 (1988), pp. 355–368.

- [21] J. Roth, E. Vietzke, A.A. Haasz, Erosion of graphite due to particle impact, Atomic Plasma–Material Interact, Data For Fusion (Suppl. to Nucl. Fusion) 1 (1991) 63–78.
- [22] V. Philipps, Plasma wall interaction and its control by wall conditioning. Trans. Fusion Technol. 33 (1998), pp. 261–272.
- [23] A.A. Haasz, P. Franzen, J.W. Davis, S. Chiu and C.S. Pitcher, Two-region model for hydrogen trapping in and release from graphite. J. Appl. Phys. 77 (1995), pp. 66–85.
- [24] J. Roth and C. Garcia-Rosales, Analytic description of the chemical erosion of graphite by hydrogen ions. Nucl. Fusion 36 12 (1996), pp. 1647–1659.
- [25] M. Balooch and D.R. Olander, Reactions of modulated molecular beam with pyrolytic graphite. III. Hydrogen. J. Chem. Phys. 63 11 (1975), pp. 4772–4786.
- [26] J. Roth, J. Bohdansky and K.L. Wilson, Erosion of carbon due to bombardment with energetic ions at temperatures up to 2000 K. J. Nucl. Mater. 111/112 (1982), pp. 775–780.
- [27] J. Roth and W. Möller, Mechanism of enhanced sputtering of carbon at temperatures above 1200°C. Nucl. Instr. Meth. Phys. Res. B 7/8 (1985), pp. 788–792.
- [28] V. Philipps, E. Vietzke and H. Trinkaus, Radiation enhanced sublimation of carbon and carbon related materials. J. Nucl. Mater. 179–181 (1991), pp. 25–33.
- [29] Y. Ueda, K. Shiota, Y. Kitamura, Y. Ohtsuka, M. Isobe and M. Nishikawa, Detailed study of radiation enhanced sublimation of graphite under high flux beam irradiation. Fusion Eng. Des. 41 (1998), pp. 55–61.
- [30] M. Küstner, W. Eckstein, V. Dose and J. Roth, The influence of surface roughness on the angular dependence of the sputter yield. Nucl. Instr. Meth. Phys. Res. B 145 (1998), pp. 320–331.
- [31] M. Nishikawa, High flux dependence of erosion and retention in beam experiments and its significance to fusion systems. Fusion Eng. Des. 41 (1998), pp. 47–53.
- [32] Y. Yamamura, Computer studies of reemission and depth profiles for helium on molybdenum. Nucl. Instr. Meth. Phys. Res. B 28 (1987), pp. 17–26.
- [33] T. Kenmotsu, T. Kawamura, L. Zhijie, T. Ono and Y. Yamamura, Simulation studies on sputtering and reflection from compound materials at elevated temperatures. J. Nucl. Mater. 266–269 (1999), pp. 557–560.
- [34] M. Wittmann and J. Küppers, A model of hydrogen impact induced chemical erosion of carbon based on elementary reaction steps. J. Nucl. Mater. 227 (1996), pp. 186–194.
- [35] J. Roth, Chemical erosion of carbon based materials in fusion devices. J. Nucl. Mater. 266–269 (1999), pp. 51–57.
- [36] W. Eckstein, C. Garcia-Rosales, J. Roth, W. Ottenberger, Sputtering Data, Internal Report (Max-Planck-Institut für Plasmaphysik) IPP 9/82, February 1993.
- [37] J.P. Biersack and L.G. Haggmark, A Monte Carlo computer program for the transport ions in amorphous targets. Nucl. Instr. Meth. B 174 (1980), pp. 257–269.
- [38] M. Wittmann and J. Küppers. J. Nucl. Mater. 227 (1996), p. 186.

- [39] E. Vietzke, K. Flaskamp, V. Philipps, G. Esser, P. Wienhold, J. Winter, J. Nucl. Mater. 145–147 (1987) 443
- [40] R. Yamada, K. Nakamura, K. Sone and M. Saidoh. J. Nucl. Mater. 95 (1980), p. 278.
- [41] J. Roth, J. Bohdansky, K. Wilson, J. Nucl. Mater. 111/112 (1982) 775
- [42] J. Roth, in: R. Behrisch (Ed.), Sputtering by Particle Bombardment, vol. II, Springer, Berlin, 1983
- [43] R. Mitteau et al., Proceeding of the 19th on Fusion Technology, Lisbon, 1996, pg. 443-446.
- [44] J. Roth, E. Vietzke, A. A. Haasz. Nucl. Fusion Suppl. 1, 63 (1991).
- [45] E. D'Agata Internal document "3D analyses on the Critical Heat Flux on the PFC Tiles on the ITER Divertor" Idoms: G 17 MD 140 03-11-11 W0.1
- [46] ANSYS manual "Thermal analysis"
- [47] A.S. Kukushkin, H.D. Pacher, V. Kotov, D. Reiter, D. Coster and G.W. Pacher "Effect of neutral Transport on ITER Divertor performance"; Nucl. Fusion 45 (2005) 608–616
- [48] J. Bohdansky, A universal relation for the sputtering yield of monatomic solids at normal ion incidence, Nucl. Inst. and Meth., B 2:587, (1984).
- [49] W. Eckstein, "Calculated sputtering reflection and range values" IPP 9/132, 2002.
- [50] R. V. Stuart, Vacuum Technology, Thin Films and Sputtering, Academic press a subsidiary of Harcourt Brace Jovanovich Publisher (1983), pp. 1-131.
- [51] J. L. Margrave, The Characterization of High Temperature Vapors, John Wiley & Sons, New York, (1967).
- [52] R. Hultgren, R. L. Orr, P. D. Anderson, K. K. Kelley, Selected Values of Thermodynamic Properties of Metals and Alloy, John Wiley & Sons, New York, 1963 rev. 1972.
- [53] F. P. Incropera, D. P. De Witt. "Fundamental of Heat and Mass Transfer". J. Wiley & Sons 1990, pp. 355-364
- [54] J. Roth, Impurity generation, Journal of nuclear materials, 103 & 104 (1981), pp. 291-304.
- [55] J. Roth, "Chemical erosion of carbon based materials in fusion device, Journal of fusion materials, 266-269 (1999), pp. 51-57.
- [56] S. Grigoriev, A. Lipko, A. Makhankov, S. Sytchevskiy, V. Tanchuk "Divertor. Vertical Target. Failure Mode Analysis" internal document Number: ITER_D_23KUKC
- [57] Escourbiac F. et al "Experimental simulation of cascade failure effect on tungsten and CFC flat tile armoured high heat flux components" to appear in Fusion Eng. Des.
- [58] A. Horn, A. Schenck, J. Biener, B. Winter, C. Lutterloh, M. Wittmann, J. Küppers, Chem. Phys. Lett. 231 (1994) 193.
- [59] M. Wittmann and J. Küppers, J. Nuclear Material. 227 (1996) 186.
- [60] B.N. Bazylev, Y. Koza, I.S. Landman, J. Linke, S.E. Pestchanyi, H. Wuerz, Physica Scripta, T111 (2004) 213

- [61] J. G. van der Laan, H. Th Klippel, G. J. Kraaij, R.C.L.van der Stad, J. Linke, M. Akiba. “Effects of short pulse hight heat fluxes on carbon base plasma facing materials fot ITER” J. Nucl. Mater., vol. 196-198 pp. 612-617 (1992).

APPENDIX A

The manual of the code

This appendix contains a manual of the developed code. The first part has been dedicated to the procedure to follow to carry on an analysis, the second part has been dedicated to the explanation of the input parameters and the third and last part is about trick and tips to solve problems with the code.

The procedure to carry on an analysis

The code has been developed in an ANSYS environment, which means that to run the code a version of ANSYS (from 8.0) must be installed in the computer. Moreover, the version installed must be able to treat nonlinear thermal problem which means that at least a "mechanical license" or a license that include it must be used.
The analyses can be done in batch or interactively. When the interactively procedure has been chosen the user has the possibility to select between insert the input via GUI (Graphic User Interface) or via input file.
Below the sequence of action in order to start to use the code via GUI:

1) Open Ansys in the directory containing the files of the code.
2) Go to the File menu of ANSYS and select "File Read Input From"
3) Select the file "main.inp"
4) A series of windows will ask to introduce the input parameters…

Below the sequence of action in order to start to use the code in batch mode:

1) Open the file "input.dat" that contains the input parameters and set up the desired parameters.
2) Launch the file "run.bat" the code will start using the parameter set in the "input.dat" file.

The run of the code will produce mainly 4 files:

Dot_pro.db is the ansys database containing the geometry, boundary conditions, etc.. in binay format.
Dot_pro.rth is the ansys result file containing all the results obtained from the analysis.
Dot_pro.sub is an ansys file containing information about the superelement used to solve the radiation problem.
Ouput.out is the output file containing all the warning and all the operation performed from the code in order to solve the problem.

It is possible start an analysis with a distribution of temperature rather than a constant temperature everywhere in the tiles. Of course the temperature distribution must be read from a previous solution using the same amount and the same numeration of elements. A macro has been developed (called "zmaketempfile.mac") in order to write a file (called "inittemp.data") with the information about the distribution of the temperature. Below the sequence of actions to set up an initial temperature distribution:

1) resume an analysis where to get the initial distribution of temperature
2) go to the File menu of ANSYS and select "File Read Input From"
3) select the file "zmaketempfile.mac"
4) a file called "inittemp.data" will be generated in the working directory
5) exit from Ansys and setup the parameter inittemp=1 in the input file (see manual below)

6) follow the normal procedure (see above) to do an analysis with the code.

If an analysis of erosion is carried on, as we said above, there is a limitation in term of loadstep. It will be a transient analysis only with one timestep. At the end of this timestep is possible add another timestep with the use of the parameter "res=1" see below. The new timestep will be added taking the last condition from the previous analysis. Hence, to perform an analysis adding a timestep the results of the previous analysis must be present in the directory. That means that the files "dot_prog.db" and "dot_prog.rth" relative to the previous analysis will be read and renamed respectively to "pre1.db" and "pre1.rth".

An analysis of erosion may go on also for hours and/or days (depending on the analysis and on the computer performance) hence it has been included in the code the possibility to stop the analysis and check what is going on. This special procedure is very important because will allow to stop the analysis in a "clean" way and to restart the analysis from that point.

Below the sequence of actions in order to stop an analysis:

1) edit the file "esterno.inp"
2) set up the parameter permesso =0 (note that a row with an exclamation point is considered as comment line. Hence, it is sufficient to remove the exclamation point in the row "permesso=0")
3) save the file, exit and wait.

Below the sequence of actions in order to restart an analysis interrupted with the file "esterno.inp".

1) edit the file "esterno.inp";
2) replace the exclamation point removed before in the line "permesso=0" (see above)
3) if the user want to continue in batch mode, lunch the file "restart.bat"
4) if the user want to continue in interactively mode
    a. open Ansys in the directory containing the files of the code
    b. go to the File menu of ANSYS and select "File Read Input From"
    c. select the file "restart.inp";

In order to see the results of an erosion analysis, some useful macro has been included. Below the procedure to see directly the last converged solution:

1) Open Ansys in the directory containing the solutions files.
2) Go to the File menu of ANSYS and select "File Read Input From"
3) Select the file "zstartfrombatch.mac"
4) The results, in term of temperature distribution and eroded profile, of the last converged solution will be plotted on the screen.

Another macro has been developed in order to establish the total amount of erosion [grams] function of the time. Below the procedure to get the erosion related to the two tiles modelled function of the time:

1) Open Ansys in the directory containing the solutions files.
2) Go to the File menu of ANSYS and select "File Read Input From"
3) Select the file "zstartfrombatch.mac"
4) Go again to the File menu of ANSYS and select "File Read Input From"
5) Select the file "zerosionvstime.mac"
6) The results in term of a curve of erosion [g] function of the time [sec] for the tile in the middle will be plotted on the screen. Moreover, a file (called

"erosion.data") containing the time and the corresponding amount of erosion for the left, middle and right tiles will be generated in the working directory.

Another macro has been developed in order to get the chemical sputtering yield and the corresponding surface temperature in some location of the central monoblock:

1) Open Ansys in the directory containing the solutions files.
2) Go to the File menu of ANSYS and select "File Read Input From"
3) Select the file "zstartfrombatch.mac"
4) Go again to the File menu of ANSYS and select "File Read Input From"
5) Select the file "zchemcoef.mac".
6) A window will appear asking the deltatime [sec] at which the code should write the results. For example: choosing 5 sec the code will write results from begin to the end using step of 5 seconds.
7) A window will appear asking till when [sec] the code should write data. For example: choosing 20 sec the code will write results from begin till 20 sec using step defined in the previous question.
8) Two files will be generated: the first one (called "chesputtemp.data") contains the time considered and the surface temperature, relative to that time, of the central monoblock calculated on the left, on the middle (2 values) and on the right corner (4 columns). The second one (called "chesputtime.data") contains the time considered and the chemical sputtering yield, relative to that time, of the central monoblock calculated on the left, on the middle (2 values) and on the right corner (4 columns).

Another macro has been developed in order to get the temperature profile of the monoblocks at a certain time:

1) Open Ansys in the directory containing the solutions files.
2) Go to the File menu of ANSYS and select "File Read Input From"
3) Select the file "zstartfrombatch.mac"
4) Go again to the File menu of ANSYS and select "File Read Input From"
5) Select the file "zprotemp.mac".
6) A window will appear asking the corresponding loadstep number relative to the time the user wants to check. For example: choosing 14 the code will write results relative to the 14^{th} loadstep that will correspond to a certain time.
7) 3 files with 4 columns called "tempprofleft(middle or right)%number of substep requested%.data" will be generated: The first column contains the nodes where the temperature has been calculated; the second column contains the coordinate X of the node where the temperature has been read; the third column contains the coordinate Y of the node where the temperature has been read; the fourth column contains the temperature [°C] of the corresponding node.

The input parameters

The table below explains the meaning of the parameter to insert as input to the code. Where is not indicated the parameter is a number (integer or real).

Parameter	Possible values	Descriptions
fil	0 or 1	0 means that the input parameters will be read from GUI, 1 means that the input parameters will be read from input file.
wout	0 or 1	0 means that the output file (containing warning, and the status of the operations) will be write in the output windows of ANSYS. 1 means that the output file will be write in a file called "output.out".
Mtile	25, 35, 45	The number introduced here represents a label to call the material that must be used for the central monoblock. Actually is possible to chose between three materials CFC NB31 (label 25); CFC Dunlop concept (label 35); a user defined material (label 45) to be inserted in the file "material.dat".
Mtilelat	25, 35, 45	The number introduced here represents a label to call the material that must be used for the lateral monoblocks. Actually is possible to chose between three materials CFC NB31 (label 25); CFC Dunlop concept (label 35); a user defined material (label 45) to be inserted in the file "material.dat".
MCC	90	The number introduced here represents a label to call the material that must be used for the cooling channel. Actually there is only one material: CuCrZr (label 90)
Msup	80	The number introduced here represents a label to call the material that must be used to join the cooling channel to the monoblock. Actually there is only one material: Oxigen Free Pure copper (label 80)
emiss	-	The emissivity of the material of the monoblock (typically for the CFC 0.8-0.9).
H	-	The total height of the monoblock [mm].
W	-	The width of the monoblock [mm].
T	-	The distance between the bottom surface of the tile and the centre of the cooling channel [mm].
INFRA	-	Toroidal Gap between two adjacent tiles [mm].
DECI1	0 or 1	0 means that the film coefficient will be function of the wall temperature. 1 means that the film coefficient will be fix.
film	-	IF DECI1=1 THEN: The fixed value of the film coefficient

		[MW/(m^2*K)]
D	-	Diameter of the tube of the material to join the cooling channel to the monoblock [mm]
CU	-	External diameter of the cooling channel [mm]
IN	-	Internal diameter of the cooling channel [mm]
ana	0 or1	0 means that the code will solve a Normal Operation analysis where the heat comes from the surface of the monoblock. 1 means that the code will solve a SATIR analysis where the heat comes from the cooling channel.
Tra	0 or 1	0 means that the code will do a steady state analysis. 1 means that the code will do a transient analysis. To solve an erosion analysis the user must select a transient analysis.
evap	0 or 1	IF Tra=1 THEN: 0 means that the code will do a transient analysis not considering the erosion due to the sublimation of the CFC. 1 means that the code will do a transient analysis including the erosion due to the sublimation of the CFC.
loa	0 or 1	IF Tra=1 and evap=1 THEN: 0 means that the particles are inclined and the heat flux loads will follow the criteria described in the chap. 2.2.3.1. 1 means that the particles are perpendicular to the surface of the monoblock.
res	0 or 1	IF Tra=1 and evap=1 THEN: 0 means that the code will start a new analysis. 1 means that the code will continue an analysis taking the starting point prom a previous analysis present in the directory
fine	0,1 or 2	IF Tra=1 and evap=1 THEN: 0 means that the code will use a very fine mesh in the region of the erosion (2.6 μm x 72 μm) and the region of erosion is reduced to a thickness of 0.5 mm instead of 2 mm. 1 means that the code will use a fine mesh in the region of the erosion (13 μm x 72 μm). 2 means that the code will use a coarse mesh in the region of the erosion (26 μm x 145 μm).
Rdepossub	0-100	IF Tra=1 and evap=1 THEN: The number represents the amount of material redeposited by sublimation in percent. It means that using 0 all the material sublimated go away, using 100 all the material sublimated condensate and return on the surface.
phy	0 or 1	IF Tra=1 and evap=1 THEN:

		0 means that the code will not consider the contribution to the total erosion due to the physical erosion. 1 means that the code will include the contribution to the total erosion due to the physical erosion.
bod	0 or 1	IF Tra=1, evap=1 and phy=1 THEN: Decide if use calculate the physical sputtering yield using bohdansky formula [1] or the experimental data [0].
che	0 or 1	IF Tra=1 and evap=1 THEN: 0 means that the code will not consider the contribution to the total erosion due to the chemical erosion. 1 means that the code will include the contribution to the total erosion due to the chemical erosion.
parflux	-	IF Tra=1 and evap=1 and (phy=1 or che=1) THEN: The flux of particles incident on the surface (ions) [particles/(m^2sec)]
Ezero	-	IF Tra=1, evap=1, phy=1 and bod=1 THEN: The energy of the incident particles [eV].
Eft	-	IF Tra=1, evap=1, phy=1 and bod=1 THEN: The Thomas-Fermi potential [eV] (for deuterium Etf=447 eV)
Qc	-	IF Tra=1, evap=1, phy=1 and bod=1 THEN: Parameter function of the nature of the incidence particles and target (i.e. Deuterium-Carbon Qc=0.1 [atoms/ions])
Ethre	-	IF Tra=1, evap=1, phy=1 and bod=1 THEN: The threshold energy for the physical sputtering yield problem [eV]
tplasma	5-20	IF Tra=1, evap=1, phy=1 and bod=0 THEN: The temperature of the ions in [eV]. (1 eV = 11600 K).
tetafac	-	IF Tra=1 and evap=1 and phy=1 THEN: This is a multiplication factor to take into account that the Bohdansky model is related to incident particles perpendicular to the target. i.e.1 means that the sputtering yield is due to perpendicular particles.
Rdeposphy	0-100	IF Tra=1 and evap=1 and phy=1 THEN: The number represents the amount of material redeposited by physical erosion in percent. It means that using 0 all the material physically eroded go away, using 100 all the material physically eroded condensate and return on the

		surface.
Ezero	-	IF Tra=1, evap=1, che,1, (phy=0 or bod=0) THEN: The energy of the incident particles [eV].
Eft	-	IF Tra=1, evap=1, che,1, (phy=0 or bod=0) THEN: The Thomas-Fermi potential [eV] (for deuterium Etf=447 eV)
Qc	-	IF Tra=1, evap=1, che,1, (phy=0 or bod=0) THEN: Parameter function of the nature of the incidence particles and target (i.e. Deuterium-Carbon Qc=0.1 [atoms/ions])
Ethredam	-	IF Tra=1 and evap=1 and che=1 THEN: The threshold energy for the damage production (chemical sputtering yield problem) [eV]
Ethresurf	-	IF Tra=1 and evap=1 and che=1 THEN: The threshold energy for the surface process (chemical sputtering yield problem) [eV]
Rdeposche	0-100	IF Tra=1 and evap=1 and che=1 THEN: The number represents the amount of material redeposited by chemical erosion in percent. It means that using 0 all the material chemically eroded go away, using 100 all the material chemically eroded condensate and return on the surface
tempo(1)	-	IF Tra=1 and evap=1 THEN: The end of the timestep to analyse in seconds.
Hea(1)	-	IF Tra=1 and evap=1 THEN: The total surface loads comprehensive of irradiation contribute + conductive contribute [MW/m^2]
subtempo(1)	-	IF Tra=1 and evap=1 THEN: This is the maximum value [sec] of the substep in case of erosion. This value is modified during the calculation by an algorithm which chose the best timestep in order to kill only the elements that must be killed. (see chap 2.3.1)
Twater(1)	-	IF Tra=1 and evap=1 THEN: Water bulk temperature [°C]
NTS	1-5	IF Tra=1 and evap=0 THEN: For transient analysis without consider the erosion (evap=0) the user can define a maximum of 5 timestep.
Tempo(i)	-	IF Tra=1 and evap=0 THEN: Depending on the number of timestep defined (NTS value) the user must insert the duration of the timestep of the i^{th} value.
rampa(i)	0 or 1	IF Tra=1 and evap=0 THEN:

		Depending on the number of timestep defined (NTS value) the user must insert the behaviour of the load (0 ramped, 1 stepped) of the i^{th} timestep.
Hea(i)	-	IF Tra=1 and evap=0 THEN: Depending on the number of timestep defined (NTS value) the user must insert the heat flux of the i^{th} timestep [MW/m^2].
subtempo(i)	-	IF Tra=1 and evap=0 THEN: Depending on the number of timestep defined (NTS value) the user must insert the number of substep for the i^{th} timestep. Note: if subtempo(i)=0 the code will choose automatically the number of substep for the i^{th} timestep.
Twater(i)	-	IF Tra=1 and evap=0 THEN: Depending on the number of timestep defined (NTS value) the user must insert the water temperature of the i^{th} timestep [°C].
Heat	-	IF Tra=0 THEN: In case of steady state analysis (Tra=0), the heat flux that load the surface of the tiles [MW/m^2].
Twat	-	IF Tra=0 THEN: In case of steady state analysis (Tra=0), the water bulk temperature [°C].
initemp	0 or 1	0 means that the initial temperature distribution is constant. 1 means that the initial temperature distribution must me read from a file.
T0	-	IF initemp=0 THEN: The initial temperature of the tiles [°C].
Tspace	-	The temperature of the surround environment (for the calculation of the heat by irradiation) [°C].
meshsize	-	The number of element around the cooling channel. It's better don't touch this parameter and left the default value of 80
DECI2	0 or 1	0 means that not will be included a defect between the cooling channel and the monoblock (on the monoblock side). 1 means that a defect will be included between the cooling channel and the monoblock (on the monoblock side).
dife	-	IF DECI2=1 THEN: The extension of the defect in degree.
posi	-	IF DECI2=1 THEN: The position of the centre of the defect in degree. The origin is located on the top side of the cooling channel at 12.00 o'clock. A positive value is considered clockwise and vice versa. (i.e. posi=90 means 3.00 o'clock).

Mdummy	1 or 400	IF DECI2=1 THEN: The material to be used to simulate detachment. Mdummy=1 means no elements where the defect is located just a hole.

Tricks and Tips

Below some tricks and tips in order to use the code in a better way:

1) At the end of an erosion analysis, or also during the analysis stopping it. It is better to check the values of the vector "timecheck" this numbers should be less or as much as possible equal to 1.
2) At a certain point during an erosion analysis, may happen that the erosion process make the thickness of the fine element very small or, even worst, certain zones of the fine mesh has been eroded exposing the coarse mesh to the heat flux load. The results related with this conditions should not been considered reliable.
3) Doing an erosion analysis, it is possible to increase in the code the region finely meshed. Actually this zone is 2 mm thick when the parameter *fine* = 1 or 2 and 0.5 mm when *fine* = 0. In the routine "main.inp" there is a parameter "SUBDIST" that represent the thickness of this zone. Change it carefully !!.

AKNOWLEDGEMENTS

The extensive work performed during this thesis has been possible thanks to the help of some people that with their competence and commitment have helped me. First of all I would like to thanks my supervisors Prof. L. Bertini and Eng. G. Sannazzaro for their patience and dedication. The ITER International team and EFDA (European Fusion Development Agreement) group especially the people involved in the design, research and development of the divertor namely Eng. R. Tivey, Dr. M. Merola, Dr. G. Federici and Dr. C. Lowry. The CEA Cadarache, group of Fusion studies, for their collaboration, especially Dr. J. Schlosser and Dr. O. Ogorodnikova.